

# **Molecular Dynamics Simulation Studies on Behaviour of Water and Aqueous Solutions of Uranyl Ions in Bulk and Nanoporous Materials**

*By*

**MANISH CHOPRA**

**(CHEM01201204003)**

**Bhabha Atomic Research Centre, Mumbai**

*A thesis submitted to the  
Board of Studies in Chemical Sciences*

*In partial fulfillment of requirements  
for the Degree of*

**DOCTOR OF PHILOSOPHY**  
*of*  
**HOMI BHABHA NATIONAL INSTITUTE**



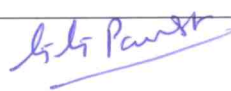
**June, 2018**

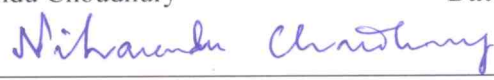


# Homi Bhabha National Institute<sup>1</sup>

## Recommendations of the Viva Voce Committee


As members of the Viva Voce Committee, we certify that we have read the dissertation prepared by Manish Chopra entitled “**Molecular Dynamics Simulation Studies on Behaviour of Water and Aqueous Solutions of Uranyl Ions in Bulk and Nanoporous Materials**” and recommend that it may be accepted as fulfilling the thesis requirement for the award of Degree of Doctor of Philosophy.


Chairman - Dr. G. G. Pandit  Date: 6/6/2018

Guide / Convener – Dr. Niharendu Choudhury  Date: 06/06/18

Examiner - Prof. Pratim Kumar Chattaraj  Date: 6. 6. 18.

Member 1- Dr. A. K. Samanta  Date: 06-06-18

Member 2- Dr. C. N. Patra  Date: 06/06/18

Member 3- Dr. K. R. S. Chandrakumar  Date: 06/06/2018

Final approval and acceptance of this thesis is contingent upon the candidate's submission of the final copies of the thesis to HBNI.

I/We hereby certify that I/we have read this thesis prepared under my/our direction and recommend that it may be accepted as fulfilling the thesis requirement.

Date: 06/06/2018

Place: Mumbai

  
Guide: Dr. Niharendu Choudhury

<sup>1</sup> This page is to be included only for final submission after successful completion of viva voce.





## **STATEMENT BY AUTHOR**

This dissertation has been submitted in partial fulfillment of requirements for an advanced degree at Homi Bhabha National Institute (HBNI) and is deposited in the Library to be made available to borrowers under rules of the HBNI.

Brief quotations from this dissertation are allowable without special permission, provided that accurate acknowledgement of source is made. Requests for permission for extended quotation from or reproduction of this manuscript in whole or in part may be granted by the Competent Authority of HBNI when in his or her judgment the proposed use of the material is in the interests of scholarship. In all other instances, however, permission must be obtained from the author.

Manish Chopra



## **DECLARATION**

I, hereby declare that the investigation presented in the thesis has been carried out by me. The work is original and has not been submitted earlier as a whole or in part for a degree / diploma at this or any other Institution / University.

Manish Chopra



## List of Publications arising from the thesis

### Journal

1. “Comparison of structure and dynamics of polar and nonpolar fluids through carbon nanotubes”, M. Chopra and N. Choudhury, *J. Phys. Chem. C*, **2013**, *117*, 18398-18405.
2. “Effect of uranyl ion concentration on structure and dynamics of aqueous uranyl solution: A molecular dynamics simulation study”, M. Chopra and N. Choudhury, *J. Phys. Chem. B*, **2014**, *118*, 14373-14381.
3. “Molecular dynamics simulation study of distribution and dynamics of aqueous solutions of uranyl ions: the effect of varying temperature and concentration”, M. Chopra and N. Choudhury, *Phys. Chem. Chem. Phys.*, **2015**, *17*, 27840-27850.
4. “Structural and dynamical aspects of uranyl ions in supercritical water: A molecular dynamics simulation study”, M. Chopra and N. Choudhury, *J. Mol. Liq.*, **2016**, *224*, 599-606.
5. “Molecular dynamics simulation study of hydration of uranyl nitrate in supercritical water: Dissecting the effect of uranyl ion concentration from solvent density”, M. Chopra and N. Choudhury, *Chem. Phys.*, **2017**, *495*, 48-58.

### Under preparation

1. “Adsorption of Uranyl Ions from its Aqueous Solution by Functionalized Carbon Nanotubes: A Molecular Dynamics Simulation Study”, M. Chopra and N. Choudhury, *J. Phys. Chem. C*, **2018**.

## Conferences

1. “Molecular dynamics simulation study of behaviour of fluids in and around carbon nanotubes: Effect of nanotube diameter and fluid polarity”, M. Chopra and N. Choudhury, *Proceedings of 4<sup>th</sup> Interdisciplinary Symposium on Materials Chemistry*, **2012**, pp: 260.
2. “Distribution of polar and non-polar solvent in and around carbon nanotube”, M. Chopra, N. Choudhury, R. N. Nair and V. D. Puranik, *Souvenir of National Conference on Material Science*, **2012**, pp: 12.
3. “Effect of confinements on the structure and dynamics of water in and around carbon nanotubes”, M. Chopra and N. Choudhury, *Proceedings of DAE-BRNS Eleventh Biennial Trombay Symposium on Radiation & Photochemistry*, **2012**, pp: 439.
4. “How does fluids with different polarity behave in carbon nanotubes?”, M. Chopra and N. Choudhury, *Proceedings of DAE-BRNS Symposium on Current Trends in Theoretical Chemistry*, **2013**, pp: 160.
5. “Transport of polar and non-polar solvents through a carbon nanotube”, M. Chopra, R. Phatak and N. Choudhury, *AIP Conf. Proc.*, **2013**, 1512, 562-563.
6. “Orientational order and dynamics of water in bulk and in aqueous solutions of uranyl ions”, M. Chopra and N. Choudhury, *Proceedings of DAE-BRNS Symposium on Multiscale Modeling of Materials and Devices*, **2014**, pp: 120.
7. “Structure and dynamics of aqueous solution of uranyl ions”, M. Chopra and N. Choudhury, *AIP Conf. Proc.*, **2014**, 1591, 164-166.
8. “Concentration Dependence of the Structure and Dynamics of Aqueous Solution of Uranyl Ions”, M. Chopra and N. Choudhury, *Presented in Fourteenth Theoretical Chemistry Symposium*, **2014**.

9. “Fluids in Nanochannels and Nanopores: As Envisaged through Molecular Dynamics Simulations”, M. Chopra and N. Choudhury, *Proceedings of DAE-BRNS sponsored theme meeting on applications of molecular modeling in separation processes*, **2015**, pp:17.
10. “Effect of Uranyl Ion Concentration and Temperature on the Solvation Shell Structure and Diffusivity of Various Species in Aqueous Uranyl Solution: A Molecular Dynamics Simulation Study”, M. Chopra and N. Choudhury, *Proceedings of Indo-UK Workshop on Modelling and Simulation of Safety and Materials for Nuclear Applications*, **2015**.

Manish Chopra





*Dedicated*  
*To*  
*My Parents*



## ACKNOWLEDGEMENTS

I would like to express my sincere gratitude to my advisor Dr. Niharendu Choudhury for providing me the opportunity to work under his valuable guidance. His inspiration, motivation and constant encouragement throughout this study has made this thesis possible. Specially, I want to acknowledge his patience to bear with me for long breaks during the course of this work when I used to be unavailable because of other official commitments.

I would also like to thank Dr. Alok Kumar Samanta, Theoretical Chemistry Section (TCS), Bhabha Atomic Research Centre (BARC) who provided me the direction in choosing the topic of research and introduced me to Dr. Niharendu Choudhury as guide. He was the one because of whom I could decide to go ahead with PhD in Chemical Sciences.

My sincere thanks also go to Dr. R. N. Nair, Former Head, Environmental Modeling Section (EMS), Radiation Safety Systems Division (RSSD), BARC who extended his full support to me for undertaking this research. Thanks are also due to Mr. V. D. Puranik, Former Head, Environmental Assessment Division (EAD), BARC and Dr. A. K. Ghosh, Former Director, Health, Safety and Environment Group (HS&EG), BARC for their encouragement to take-up this research work.

I am thankful to Dr. Pradeepkumar K. S., Associate Director, HS&EG and Head, RSSD, Dr. R. B. Oza, Head, EMS, RSSD, BARC and Dr. (Mrs.) Faby Sunny, EMS, RSSD, BARC for their understanding and support during the course of these six years during which I could take some time out of my other professional commitments and get engaged with my PhD research activities.

I would also like to acknowledge my doctoral committee chairman and members including Dr. S. K. Ghosh (Ex-Chairman), Former Head, TCS, BARC, Dr. G. G. Pandit (Chairman), Environmental Monitoring and Assessment Section, BARC, Dr. C. N. Patra

(Member), TCS, BARC and Dr. K. R. S. Chandrakumar (Member), TCS, BARC for their intermittent reviews, valuable suggestions and help throughout the study period.

Family is the ultimate source of inspiration for any human being. I am extremely grateful to my parents, Mr. Devinder Kumar Chopra (Father) and Mrs. Neelam Chopra (Mother) who have always been the pillars of each and every success I had since the day I came down from heavens. It is all because of their sacrifices that I have made all the progress in life. I am thankful to my brother, Mr. Ashish Chopra as growing up along with him helped me to experience and learn the lessons of life which made me the person I am today. I would take this occasion to acknowledge the important role my sister, Ruhi had in shaping up my life since the day she has become a part of it. It is because of her blessings and prayers that I have been able to accomplish not only this PhD thesis but many other goals in my life. I would also like to thank my beloved wife, Priya Chopra for all the lovely experiences we had since we are together as a couple. Her major contribution in this thesis is to help me keep my senses calm and composed to concentrate positively on my work. Nothing related to me can be complete without the mention about our beautiful replica, my adorable son Aarav Chopra. He has brought all the good luck and lucky charm for us to achieve more and more in life.

I would also take this opportunity to acknowledge the contributions of my extended family members, all my teachers/mentors and all the best friends with whom I have shared the course of my life.

Manish Chopra





# **CONTENTS**

	<b>Page No.</b>
<b>SYNOPSIS</b>	i
<b>LIST OF FIGURES</b>	xv
<b>LIST OF TABLES</b>	xxvi
<b>Chapter 1 Introduction and Computational Methodology</b>	1
1.1 Introduction	3
1.2 Classical Molecular Dynamics	9
1.3 Statistical Mechanical Ensembles and Averages	14
1.3.1. Time Averaging (Method of Boltzmann)	15
1.3.2. Ensemble Average	15
1.4 Equilibrium Particle Density Distribution Functions	16
1.5 Time Correlation Functions and Transport Coefficients	17
1.6 Nature and Scope of the Present Work	19
References	23
<b>Chapter 2 Structure and Dynamics of Bulk Water and Aqueous Uranyl Solution</b>	33
2.1 Introduction	35
2.2 Models and Simulation Details	37
2.3 Results and Discussion	39
2.3.1 Radial Distribution of Water Molecules around Uranyl Ions in Aqueous Solutions	39
2.3.2 Orientational Distribution of Water Molecules in the Vicinity of Uranyl Ions	41

2.3.3	Translational Dynamics of Different Species in the Aqueous Uranyl Solution	45
2.3.4	Orientational Dynamics of Water Molecules in the Aqueous Uranyl Solution	46
2.4	Conclusions	48
	References	49
<b>Chapter 3 Effect of Uranyl Ion Concentration and Temperature on Structure and Dynamics of Aqueous Uranyl Solution</b>		53
3.1	Introduction	55
3.2	Models and Simulation Details	57
3.3	Results and Discussion	59
3.3.1	Effect of Uranyl Ion Concentration on the Structural and Dynamics Characteristics of Aqueous Uranyl Solutions	60
3.3.1.1	Radial Distribution of Water Molecules around Uranyl Ions in Aqueous Solutions	61
3.3.1.2	Radial Distribution of Counter Ions (Nitrate Ions) with Respect to Uranyl Ions	63
3.3.1.3	Orientational Distribution of Water Molecules in the Vicinity of Uranyl Ions	65
3.3.1.4	Translational Dynamics of Different Species in the Aqueous Uranyl Solution	65
3.3.1.5	Orientational Dynamics of Water Molecules in the Aqueous Uranyl Solution	71
3.3.2	Effect of Temperature on the Structural and Dynamics	77



Characteristics of Aqueous Uranyl Solutions	
3.3.2.1 Effect of Temperature on the Radial Distribution of Water Molecules around Uranyl Ions	77
3.3.2.2 Effect of Temperature on the Orientational Distribution of Water Molecules in the Vicinity of Uranyl Ions	78
3.3.2.3 Effect of Temperature on the Orientational Dynamics of Water Molecules	79
3.3.2.4 Effect of Temperature on the Translational Dynamics	80
3.4 Conclusions	85
References	87
<b>Chapter 4 Aqueous Solutions of Uranyl Ions in Supercritical Water: Dissecting the Effect of Uranyl Ion Concentration from Solvent Density</b>	91
4.1 Introduction	93
4.2 Models and Simulation Details	96
4.3 Results and Discussion	99
<b>Part A: Structure and Dynamics of Infinitely Diluted Aqueous     Solution of Uranyl Ions</b>	99
4.3.1 Radial Distribution Functions of the Aqueous Uranyl Solution	99
4.3.2 Orientational Distribution of Water Molecules within the First Coordination/hydration Shell of Uranyl Ion or Central Water Molecule	103

<b>4.3.3</b>	Translational Dynamics of Water Molecules and Uranyl Ions in Aqueous Uranyl Solution	106
<b>4.3.4</b>	Orientational Dynamics of the Water Molecules in the Aqueous Uranyl Solution	111
<b>Part B:</b>	Effect of Uranyl Ion Concentration on the Characteristics of the Aqueous Solutions of Uranyl Ions	113
<b>4.3.5</b>	Structural Features of the Aqueous Uranyl Solution	113
<b>4.3.6</b>	Translational Dynamics of Water Molecules and Uranyl Ions in Aqueous Uranyl Solutions	119
<b>4.3.7</b>	Orientational Behaviour of the Water Molecules in the Aqueous Uranyl Solutions	122
<b>4.4</b>	Conclusions	125
	References	127
 <b>Chapter- 5 Structure and Dynamics of Water through Carbon Nanotubes in Comparison to that of a Non- polar Fluid</b>		131
<b>5.1</b>	Introduction	133
<b>5.2</b>	Models and Simulation Details	136
<b>5.3</b>	Results and Discussion	138
<b>5.3.1</b>	Comparison of Structural and Dynamical Features of Water and Methane in the Presence of CNT(6,6)	138
<b>5.3.2</b>	Effect of Nanotube Diameter on the Various Characteristics of CNT-water Systems	151
<b>5.4</b>	Conclusions	156
	References	158

<b>Chapter- 6 Adsorption of Uranyl Ions from Aqueous Solution to the Functionalized Carbon Nanotube</b>	161
6.1 Introduction	163
6.2 Models and Simulation Details	166
6.3 Results and Discussion	170
6.3.1 Radial Density Distribution Functions of Uranyl Ions	171
6.3.2 Adsorption of Uranyl Ions on the Functionalized CNT	173
6.3.3 Diffusion characteristics of various species in the solution	179
6.4 Conclusions	181
References	182
<b>Chapter- 7 Summary and Future Directions</b>	187
7.1 Summary and Conclusions	189
7.2 Future Scope	194



## **SYNOPSIS**

With more and more expansion of nuclear power as a source of energy, the importance of radiotoxic actinyl ions is increasing. As use of these ions in nuclear reactions gives rise to the generation of radioactive waste, the attempts are being made first, to minimize the waste by extracting the reusable material from it and then, to safely dispose the radioactive waste. Uranium makes the fuel of the majority of the nuclear reactors operating all over the world due to fissile/fertile nature of its isotopes. Understanding the behavior of radiotoxic actinyl ions in aqueous solutions is of fundamental as well as technological importance due to its direct relevance to the nuclear fuel cycle. Knowledge of hydration and transport properties of these actinyl ions is essential for designing advanced separation processes for recycling of the radiotoxic material in the waste. Also, the storage of radioactive waste temporarily or the permanent waste disposal involves geological matrices involving the groundwater system. Studying their behavior in aqueous solutions will help in understanding the migration characteristics of these radionuclides in hydro-geological conditions. As high level of radiotoxicity associated with these ions makes it difficult to study the properties of these ions experimentally, computational investigation based on molecular dynamics (MD) simulation has been proved to be a vital alternative for understanding the structural, dynamic and thermodynamic behavior of these ions in different systems.

The present thesis describes MD simulation studies on the behavior of water and aqueous solutions of uranyl ions in bulk at two different conditions, namely at ambient and supercritical conditions and on the manifestation of water transport and uranyl adsorption capabilities of carbon nanotubes (CNTs). The thesis consists of seven chapters where the relevant introduction, conclusion and future prospects of related work are included in the respective chapters. In Chapter 1, general introduction to MD simulations, various

mathematical equations involved and methods adopted to solve these equations are given. This chapter presents a thorough introduction and literature survey related to the topic of research and the simulation tool used i.e. molecular dynamics (MD) simulation. It also includes some introduction to the aqueous solutions of uranyl ions along with their importance in nuclear fuel cycle and also explains the motivation for the work carried out during the course of the Ph. D.

Before proceeding with the simulations of aqueous solutions of uranyl ions under different conditions, bulk water system is simulated first to get acquainted with the MD simulation technique. Various properties and results related to bulk water reported in the literature are reproduced as a learning exercise. Some important results related to bulk water system are included in Chapter 2 of the thesis. Moving further towards studying the behavior of uranyl ions in aqueous solutions, the pioneering work of Guilbaud and Wipff<sup>1-3</sup> on molecular dynamics simulation studies of aqueous solution of uranyl ions helps us to understand various aspects of uranyl hydration. On one hand, they have studied the complexation and hydration behavior of uranyl ions<sup>1,2</sup> and on the other hand they have generated force field parameters for uranyl ions from free energy calculations.<sup>3</sup> In a series of investigations, Maginn and coworkers<sup>4,5</sup> have also developed newer force fields for the different actinyl ions in their aqueous solutions by taking into account the many-body solvation effects. Using this force field, Rai et al.<sup>4</sup> presented a detailed study on the radial and three-dimensional arrangements of water molecules in the solvation shell of the uranyl ions. Very recently, Maginn and coworkers<sup>6</sup> have studied translational dynamics and residence time of water in the solvation shell of different actinyl ions. However, orientational aspects of water and uranyl ions are not touched upon in these studies. In these studies, issues related to solvation structure and dynamics of the counter ions in the solution have not been addressed. Hence, we have carried out MD simulations for aqueous solutions of uranyl ions to analyze

more thoroughly the structural and transport characteristics of various species in the aqueous solutions as discussed in Chapter 2 of the thesis. Structural aspects of the solution are investigated by calculating radial distribution functions (RDF) of water around different sites of uranyl and nitrate ions. In order to calculate diffusivities of different species in solution, mean squared displacements (MSD) of the respective species have been computed from the simulation trajectories. Comparison of diffusivities as obtained from the slopes of the MSDs of different species present in the aqueous solution suggests the sequence of diffusivities ( $D$ ) to be in the order  $D$  (oxygen of water)  $>$   $D$  (nitrogen of nitrate)  $>$   $D$  (uranium of uranyl).<sup>7</sup> Orientational dynamics of water molecules about different molecular axes of water in the vicinity of uranyl ions have also been investigated.<sup>7</sup> The calculated results on orientational dynamics showed a little anisotropy among different molecular vectors of water. Also, to understand the orientation of different water vectors with respect to uranyl ions, the distributions of various angles made by the water vectors with respect to line joining uranium atom of uranyl ion with oxygen atom of water are analyzed. From the distributions of various angles between vectors of water and uranyl ions, it is concluded that the dipole moment vector of water points in the same direction as the vector joining the uranium atom of uranyl ion with oxygen atom of water. Also, water molecule stays in a plane perpendicular to the  $O_U$ -U- $O_U$  line ( $O_U$  being the uranyl oxygen) of the almost linear  $UO_2$  molecule passing through the uranium atom of  $UO_2$ .<sup>8</sup>

In the studies mentioned above and most of the other simulation studies, only one uranyl ion in a box of water (infinite dilution) is considered. Presence of the multiple ions on the solution may modify the properties of the aqueous uranyl solution. Water being a hydrogen-bonded network with tetrahedral structure, it is expected that presence of a large number of uranyl ions in solution will perturb the tetrahedral structure and thereby modify the structure and dynamics of different species in the aqueous uranyl solution. Apart from that,

many of the properties of the aqueous solution are susceptible to change with the change in temperature. Therefore, the effect of concentration of uranyl ions as well as of the temperature of the system on the structural and dynamical characteristics of water as well as uranyl and other co-ions is investigated by simulating three different solutions with uranyl nitrate concentrations of 0.1 M (U1), 0.5 M (U5) and 1.0 M (U10) using atomistic molecular dynamics (MD) simulations. The results related to these systems are presented in Chapter 3. The concentration dependence of the RDFs is shown to be negligibly small. It is also observed that with the increase in uranyl ion concentration, the coordination number of uranyl ion with respect to water molecules reduces slightly. A slight lowering of the peak of the radial distribution function of water molecules around uranyl ions is observed as the temperature of the system is increased, the area under the curves remaining the same. Further, the distribution of nitrate ions (negative ions present in the aqueous solution of uranyl nitrate) with respect to uranyl ions in aqueous solutions are studied by simulating each of the systems for 30 ns. It is shown that the oxygen of nitrate ion ( $O_{NO_3}$ ) occupies positions closer to oxygen atom ( $O_U$ ) of uranyl ion as compared to positively charged nitrogen ( $N_{NO_3}$ ). This is attributed to the overall positive environment around uranyl ions. These simulations led to an interesting result that the location of the first peak of  $g(r)$  of  $O_{NO_3}$  and  $O_W$  (water oxygen) is almost at the same distance from the central uranyl ion. It is concluded that both oxygen atoms are in the solvation shell of the uranyl ion. It is confirmed by calculating the coordinated numbers (CNs), defined as the number of these atoms in the first solvation shell of uranyl ion, of U (first solvation shell radius 3.0 Å) and  $O_U$  (first solvation shell radius 4.0 Å) sites of the uranyl ions with respect to  $O_W$  and  $O_{NO_3}$  atoms in U5 and U10 systems. It is observed that as the concentration of uranyl ion is increased (U5 to U10), the CN with respect to  $O_W$  is reduced whereas that with respect to  $O_{NO_3}$  is increased. In other words, the oxygen atom of water and that of nitrate ion compete with each other to occupy the first coordination



shell of the uranyl ion.<sup>8</sup> For low concentration, the diffusivity of water molecules does not deviate much from that of the bulk water. In systems with higher uranyl ion concentrations however, diffusivity of the water molecules decreases considerably as compared to that of bulk water. Two different models of water (viz. TIP3P and SPC/E) are used to check any dependence of the results on water models. It was concluded that although the absolute values of diffusivities of uranyl ions are quite different for the two water models used, the diffusivity values normalized with respect to corresponding water diffusivities compare fairly well with each other and with experimental as well as other theoretical/simulation results. To understand the variation in diffusivity values with increase in uranyl ion concentration, we have further analyzed the diffusivities of water molecules within the solvation shell of uranyl ion. After studying the diffusivities of water molecules within and outside the first coordination shell of uranyl ions, it is concluded that although it may appear that the reduction in overall diffusivity of water in the uranyl solution is due to highly retarded solvation water, but as the fraction of solvation water is considerably small, contribution of the retarded solvation water to the overall diffusivity is negligibly small. Thus, the reduction in overall water diffusivity is a consequence of the long range effect of the uranyl ions on the water beyond solvation shells.<sup>7</sup> Then effect of temperature was studied separately on the translational movement of water molecules, both for all the water molecules in the solution as well as for solvation shell water molecules only and also for the uranyl ions. It was showed that the diffusion constant becomes higher and higher as the temperature of the system is increased in all the three cases, however the diffusivities are lower in case of solvation shell water molecules.<sup>8</sup> The distributions of various angles between vectors of water and uranyl ions were observed to be independent of uranyl ion concentration in the aqueous solutions. There is slight reduction in the peak intensity values with increase in temperature, however the angles, corresponding to different peaks in the distributions remain the same.<sup>8</sup>

Orientational mobility of water molecules about different molecular axes of water in the vicinity of uranyl ions was observed to be decreasing with increase in uranyl ion concentration. It is concluded that the orientational dynamics remains more or less the same whether all the water molecules in the aqueous solution or only the solvation shell water molecules are considered.<sup>8</sup> In case of orientational dynamics of the water molecules, it was seen that with increase in temperature, the times of relaxation of these functions reduce i.e. the relaxation becomes faster. In other words, the relaxation times of these functions reduce with reduction in concentration of uranyl ions or with increase in temperature of the systems.<sup>8</sup>

Although the properties of aqueous solution of uranyl ions at ambient pressure for different temperatures have been described in the present thesis as well as in different other investigations, investigations on how these actinyl ions behave in supercritical conditions are rather scarce. However, due to many of their interesting properties, supercritical fluids (SCF) have found immense applications in chemistry, physics and chemical engineering due to its high dissolving power, extraction efficiency and enhanced mass transport. Supercritical water is also of huge importance due to its applications in extraction processes and nuclear industry. Nuclear power generation involves the use of actinide species in chain reactions. Various methods of separation of these actinyl ions from the nuclear waste involving supercritical fluids have been proposed.<sup>9</sup> Moreover, supercritical water is proposed to be an efficient coolant for Generation IV nuclear reactors.<sup>10</sup> Thus, knowledge of hydration and transport properties of these actinyl ions in supercritical water generates a lot of interest. Moreover, it will be interesting to investigate fundamental aspects of the behavior of these ions under extreme conditions of temperature and densities. There has been a number of molecular dynamics simulation studies related to various characteristics of supercritical water as well as aqueous solutions of ions under supercritical conditions. As far as uranyl ions are considered, a number of studies related to aqueous solutions of uranyl ions are available under ambient

condition<sup>1-8</sup> where structural and dynamical characteristics of various species in the solutions are analyzed. However, there were no studies related to structural and dynamical aspects of uranyl ions in supercritical water reported in the literature. Hence, we have simulated different systems of aqueous solutions of uranyl ions in supercritical water to first analyze various characteristics of such systems and then to dissect the effect of variation in solvent density from that of uranyl ion concentration on these properties. Findings from this work form the basis of the Chapter 4 of the thesis. The Results and Discussion section of Chapter 4 is divided into two parts: Part A and Part B. In Part A, the behavior of aqueous solution of uranyl ions at infinite dilution in supercritical conditions is studied using molecular dynamics simulations and the results are compared with those of bulk supercritical water. Systems of three different water densities were studied to analyze the hydration structure and dynamical properties of different species present in bulk water as well as in aqueous solution of uranyl ions. Some of the structural and dynamic properties of the aqueous solutions of uranyl ions obtained under supercritical conditions are compared with those reported under normal conditions.<sup>7,8</sup> It was interesting to observe that the radial distribution function is more ordered at low density than at higher densities. However, the coordination/hydration number of uranyl ions (or central water molecule in case of bulk water) increases with increase in the density of water. Moreover, an increase in the coordination/hydration number of water is observed as we go from normal conditions to supercritical conditions.<sup>11</sup> The angular distributions of water within the first coordination/hydration shell of uranium atoms have been found to be similar to what is observed under ambient conditions<sup>8</sup>, however, the spread is more and intensity of the peaks is observed to be lower in case of supercritical water. It is observed that in general, the diffusion coefficients of uranyl ions and water molecules get reduced with the increase in density of water. The diffusion coefficient values estimated for water molecules in bulk supercritical water of different densities compare fairly well with those reported in literature

from theoretical as well as experimental studies. The orientational relaxation of water molecules is found to be slower as the density of water is increased. Comparison of the dynamical (both translational and rotational) properties of the supercritical water or aqueous solution of uranyl ions with those of ambient water (or aqueous solution)<sup>7,8</sup> at water density  $0.98 \text{ g cm}^{-3}$  reveals that the translational and rotational dynamics of the species becomes much faster under supercritical conditions.

Since at ambient condition, the dynamical properties of the aqueous solution of the uranyl ions get modified significantly with the increase in concentrations of the uranyl ions, this idea led us to investigate the effect of increasing concentration of the uranyl ions on the structure and dynamics of aqueous solution of the uranyl ions at supercritical conditions. Moreover, as the change in solvent density or uranyl ion concentration leads to similar effects on the characteristics of the solution, all atom molecular dynamics (MD) simulations of uranyl ions in supercritical water are carried out to dissect the effects of concentration of uranyl ions and density of water on various structural and dynamic properties of the solutions. This forms Part B of the Results and Discussion section of Chapter 4. It is observed that the peak value of the distributions and the coordination number of uranyl ions reduces with increase in uranyl ion concentration whereas the location of the peaks remains more or less the same. The diffusion transport of water molecules as well as uranyl ions becomes slower as there is any increase in the uranyl ion concentration although the percentage reduction is less for more dense solutions.<sup>12</sup> It shows that the trend of diffusion coefficients under supercritical conditions with uranyl ion concentrations is same as was reported under normal conditions of temperature and pressure.<sup>7,8</sup> The angular distribution and dynamics of different orientational vectors of water molecules is also quantified with varying concentrations of uranyl ions. The angular distributions of water within the first coordination shell of uranium atoms are shown to be independent of uranyl ion concentration. It is

observed that for the same water density, the increase in concentration of uranyl ions has negligible impact on the angular dynamics of the water molecules. This observation is a mismatch to the significant variation in angular dynamics of water molecules with uranyl ion concentration observed under normal conditions of temperature and pressure.<sup>7,8</sup>

There is an upsurge in interests now-a-days in using carbon nanotube (CNT) based membranes in desalination of the sea water. This type of nanoporous membrane can also be used in the separation of actinyl ions from their aqueous solutions. Efficiency of such a separation technique will depend on the behavior of water at the CNT-water interface. After analyzing the bulk behavior of water and aqueous solutions of uranyl ions in details in the preceding chapters, we therefore, proceed to investigate the behaviour of water at the CNT-water interface. While studying the literature related to molecular dynamics studies of water in different systems, we came across the flow characteristics of water through CNTs. Transport of water through nanotubes is of fundamental as well as technological importance due to its relevance in nano-fluidics and separation sciences. The behavior of water confined in a narrow pore such as carbon nanotube differs considerably from that in bulk, as the characteristic dimensions of the confining medium are reduced to the nanometer scale.<sup>13-15</sup> The interplay between confinement and hydrophobicity induces modifications in both structural and dynamical properties of water. The engineered water channels based on carbon nanotubes (CNTs) have attracted great attention since Hummer et al.<sup>13</sup> reported water transmission through a nonpolar (6,6) CNT. Interest in this nanochannel has been further rejuvenated by the landmark experimental findings of extraordinarily enhanced transport of water through carbon nanotube membranes by Holt et al.<sup>14</sup> and Majumder et al.<sup>15</sup> In spite of a large number of investigations on the behavior of water in and around carbon nanotubes, many pertinent questions remain unanswered. Even various aspects of the pioneering work<sup>13,16</sup> of Hummer et al., who used MD simulations to show many characteristic features of

the CNT-water systems such as pulse-like transmission of water through the nanotube, empty-filled transitions inside the nanotube etc. have not been fully explored. Although it has been posited<sup>13</sup> that the observed transmission bursts are due to the tight hydrogen bonding network of water inside the nanotube, which provides shield against natural energetic fluctuations in bulk water, it still remains a question whether this conduction burst is associated only with a hydrogen-bonded fluid like water. It is also not clear whether the empty-filled transitions observed in the CNT-water system are specific to water or these can be observed in case of nonpolar fluids as well. This curiosity led us to check whether structural and dynamic properties of a non-polar fluid resemble those of a polar, hydrogen-bonded fluid like water. Hence, molecular dynamic simulations are carried out to check whether pulse-like transmission, empty-filled transition and rapid diffusion can be observed even in case of non-hydrogen bonded fluid when transported through the single-file CNT and the results are presented in Chapter 5. The structure and dynamics of a polar, hydrogen bonded fluid such as water is compared with those of a non-polar (non-hydrogen bonded) fluid like methane in and around the hydrophobic CNT with chirality (6,6) as obtained from extensive MD simulations. It was observed that the methane molecules form a linear chain at the centre of the CNT whereas water molecules were arranged in a zig-zag manner around the nanotube centre. With change in energy interaction parameter, the transitions between filled and empty states were observed in case of water but not in case of methane. The steeper slope of linear portion of Mean Squared Displacement (MSD) curve for methane indicated higher diffusivity in case of non-polar fluid (methane) than in case of polar fluid (water) for the same CNT diameter. Higher probability of translocation for methane, lower residence time inside CNT, lower activation energy for diffusion through the nanotube and lower value of force imposed by the nanotube atoms on methane molecules as compared to those of water molecules further supported the observation that methane molecules are transported faster

through the nanotube as compared to water molecules.<sup>17</sup> This conclusion supported the experimental results of previous studies which reported faster transport of non-polar, non-hydrogen bonded fluid (decane) than that of water through nano-pipes. Interestingly, the pulse-like transmission (so called conduction burst) was observed in case of methane also. Hence, it was concluded that the pulse-like conduction of fluid molecules does not have any relation with the polarity or hydrogen bond forming ability of the fluid molecules.<sup>17</sup> The effect of nanotube diameter on the various features of water-CNT system is also demonstrated by simulating water molecules in the presence of nanotubes of varying diameter. The distribution of water molecules inside the CNT is observed to depend upon the size characteristics of the CNT i.e. the space available for water molecules within the CNT. Moreover, considerable changes in the short timescale behaviors of VCFs in case of different water-CNT systems were observed, indicating interesting changes in the collective vibrations of water in various environments. The power spectra as obtained from VCFs indicates that the behavior of water molecules within CNT(6,6) deviate significantly from bulk behavior, with trend converging to bulk behavior for higher diameter CNTs. The translational movement of water molecules along the axis of the nanotube is observed to become faster and faster as the diameter of the nanotube is increased.

As is clear from Chapter 5 that there occur some interesting changes in the properties of water in the presence of interfaces, this led us to study the behavior of aqueous solutions of uranyl ions in the presence of CNT. Although pristine CNTs can be effectively used for nano-fluidics, its use in separation processes is expected to be limited. Instead of the pristine one, CNT functionalized with suitable organic functional groups will be more useful in capturing various ions from its aqueous solution. The functional groups present on the CNT can induce specific binding of the ions with the CNT. Therefore, behavior of aqueous solution of ions, especially actinyl ions, in presence of the functionalized CNT is an interesting and

contemporary issue to deal with. Hence, Chapter 6 deals with this topic where aqueous solutions of varying concentrations of uranyl ions are simulated in the presence of CNTs functionalized with different functional groups such as  $\text{COO}^-$  and  $\text{OH}$ . Extensive MD simulation studies and consequent analyses of the long trajectories reveal that the functionalization of CNT with carboxylate ion (functional group) has resulted in more structured arrangement of uranyl ions around the nanotube. Moreover, the adsorption capacity of CNT was found to increase with the introduction of carboxylate ion functional group due to the linkage between the negatively charged oxygen atom of the carboxylate ion functional group and positively charged uranyl ion. The adsorption capacity of bare and hydroxyl group functionalized CNT was more or less the same and much lesser than that of the carboxylate ion functionalized CNT due to absence of any such linkage with the uranyl ions. The mobility of uranyl ions in the solution was also observed to decrease with increasing concentration of the uranyl ions or in the presence of  $\text{COO}^-$  functional groups on CNT, resulting into an increase in the magnitude of uranyl ion adsorption. Moreover, with increase in the number of carboxylate ion functional groups on the CNT, the uranyl ion structural arrangement becomes increasingly ordered, leading to higher and higher adsorption.

Finally, Chapter 7 highlights the conclusions and important findings of the work followed by the future scope in the related field of research.

## References

1. P. Guilbaud and G. Wipff, *J. Phys. Chem.*, **1993**, 97, 5685.
2. P. Guilbaud and G., *J. Incl. Phenom. Mol. Chem.*, **1993**, 16, 169.
3. P. Guilbaud and G. Wipff, *J. Phys. Chem.*, **1996**, 366, 55.



4. N. Rai, S. P. Tiwari, E. J. Maginn, M. P. Brown and K. Austin, *J. Phys. Chem. B*, **2012**, *116*, 10885.
5. V. Pomogaev, S. P. Tiwari, N. Rai, G. S. Goff, W. Runde, W. F. Schneider and E. J. Maginn, *Phys. Chem. Chem. Phys.*, **2013**, *15*, 15954.
6. S. P. Tiwari, N. Rai and E. J. Maginn, *Phys. Chem. Chem. Phys.*, **2014**, *16*, 8060.
7. M. Chopra and N. Choudhury, *J. Phys. Chem. B*, **2014**, *118*, 14373.
8. M. Chopra and N. Choudhury, *Phys. Chem. Chem. Phys.*, **2015**, *17*, 27840. Correction: *Phys. Chem. Chem. Phys.*, **2016**, *18*, 1344.
9. L. Zhu, W. Duan, J. Xu and Y. Zhu, *J. Hazard Mater.*, **2012**, *241-242*, 456.
10. G. S. Was, P. Ampornrat, G. Gupta, S. Teyseyre, E. A. West, T. R. Allen, K. Sridharan, L. Tan, Y. Chen, X. Ren and C. Pister, *J. Nucl. Mater.*, **2007**, *371*, 176.
11. M. Chopra and N. Choudhury, *J. Mol. Liq.*, **2016**, *224*, 599.
12. M. Chopra and N. Choudhury, *Chem. Phys.*, **2017**, *495*, 48.
13. G. Hummer, J. C. Rasaiah and J. P. Noworyta, *Nature (London)*, **2001**, *414*, 188.
14. J. K. Holt, H. P. Park, Y. Waang, M. Stadermann, A. B. Artyukhin, C. P. Grigopoulos, A. Noy and O. Bakajin, *Science*, **2006**, *312*, 1034.
15. M. Majumder, N. Chopra, R. Andrews and B. J. Hinds, *Nature*, **2005**, *438*, 44.
16. A. Berezhkovskii and G. Hummer, *Phys. Rev. Lett.*, **2002**, *89*, 064503.
17. M. Chopra and N. Choudhury, *J. Phys. Chem. C*, **2013**, *117*, 18398.



## LIST OF FIGURES

	<b>Page No.</b>
<b>Figure 2.1</b>	Radial distribution functions for (a) $O_w$ around uranium, (b) $H_w$ around uranium (c) $O_w$ around uranyl-oxygen ( $O_U$ ) and (d) $H_w$ around $O_U$ in the aqueous uranyl solution
<b>Figure 2.2</b>	Radial distribution functions for (a) oxygen, $O_w$ and (b) hydrogen, $H_w$ around the oxygen atom of the central water molecule in bulk water
<b>Figure 2.3</b>	Schematic representation of various angles considered for orientational distribution of the water molecules around uranyl ions
<b>Figure 2.4</b>	Distributions of various angles between $U-O_w$ vector and different molecular orientational vectors of a water molecule in the (a) first and (b) second coordination shells of a uranyl ion
<b>Figure 2.5</b>	Pictorial representation of water molecules in the first coordination shell of a linear $UO_2$ molecule
<b>Figure 2.6</b>	Distributions of angles between $O_w-O_w$ vector and different molecular orientational vectors of a water molecule in the (a) first and (b) second coordination shells of a central water molecule in bulk water. The angles are defined in the same way as in Figure 2.3 except that the $UO_2$ ion is replaced by a water molecule
<b>Figure 2.7</b>	MSD for oxygen of water (blue line), uranium of uranyl (red line) and nitrogen of nitrate (green line) in the aqueous

	solution of uranyl ion	
<b>Figure 2.8</b>	(a) First order and (b) second order angular dynamics of water molecules with respect to water dipole moment vector ( $\mu$ ; blue solid line), water H-H vector (HH; red dashed line) and water cross vector (CR; green dotted line) in the aqueous solution of uranyl ion	46
<b>Figure 2.9</b>	(a) First order and (b) second order angular dynamics of water molecules with respect to water dipole moment vector ( $\mu$ ; blue solid line), water H-H vector (HH; red dashed line) and water cross vector (CR; green dotted line) in bulk water	47
<b>Figure 3.1</b>	Radial distribution functions for (a) $O_w$ around uranium, (b) $H_w$ around uranium (c) $O_w$ around uranyl-oxygen ( $O_U$ ) and (d) $H_w$ around $O_U$ for different concentrations of uranyl ions. In the insets of Figures 3.1(a) and (b) first peak of the respective RDF is magnified	61
<b>Figure 3.2</b>	Running coordination number around U as a function of radial distance of water from uranyl ion	62
<b>Figure 3.3</b>	Radial distribution functions of oxygen ( $O_w$ ) atoms of water molecules, nitrogen ( $N_{NO_3}$ ) and oxygen ( $O_{NO_3}$ ) atoms of nitrate ions with respect to (a) uranium (U) and (b) oxygen ( $O_U$ ) atoms of uranyl ions for the U10 system	64
<b>Figure 3.4</b>	MSD profiles for water molecules in bulk water (blue line), U1 system (cyan line), U5 system (red line), and U10 system (green line). The dashed lines represent MSD of only those	66

	water molecules that are outside the first coordination shell (FCS) of uranium in U1, U5 and U10 systems	
<b>Figure 3.5</b>	MSD profiles for uranium atom in U1 (blue line), U5 (red line) and U10 (green line) systems	67
<b>Figure 3.6</b>	MSD profiles for water molecules within the first coordination shell of uranium atom of uranyl ion for U1 (blue line), U5 (red line) and U10 (green line) systems	71
<b>Figure 3.7</b>	First order orientational correlation functions of water molecules with respect to (a) dipole moment vector ( $\mu$ ), (b) H-H vector (HH) and (c) a vector (CR) perpendicular to the plane of the water molecule for different systems of varying uranyl concentrations	72
<b>Figure 3.8</b>	Second order orientational correlation functions of water molecules with respect to (a) water dipole moment vector ( $\mu$ ), (b) water H-H vector (HH) and (c) water cross vector (CR) for different systems of varying uranyl concentrations	73
<b>Figure 3.9</b>	First order orientational correlation functions of solvation shell (black dashed line) and overall water molecules (red solid line) with respect to (a) water dipole moment vector ( $\mu$ ), (b) water H-H vector (HH) and (c) water cross vector (CR) for U1 system	75
<b>Figure 3.10</b>	Second order orientational correlation functions of solvation shell (black dashed line) and overall water molecules (red solid line) with respect to (a) water dipole moment vector ( $\mu$ ), (b) water H-H vector (HH) and (c) water cross vector (CR) for U1	75

system

<b>Figure 3.11</b>	First order orientational correlation functions of solvation shell water molecules with respect to water dipole moment vector ( $\mu$ ) for different trajectories (solid lines). Red color dashed line shows the average first order orientational correlation function of overall water molecules in the solution (a) U1, (b) U5, and (c) U10 systems	76
<b>Figure 3.12</b>	The radial distribution functions of (a) oxygen and (b) hydrogen atoms of water molecules with respect to uranium atom at different temperatures	78
<b>Figure 3.13</b>	Distributions of angles between U-O <sub>w</sub> vector and different molecular orientational vectors of a water molecule in the first coordination shell of a uranium atom of the uranyl ion at different temperatures	79
<b>Figure 3.14</b>	First order orientational correlation functions of water molecules with respect to (a) dipole moment vector ( $\mu$ ), (b) H-H vector (HH) and (c) a vector (CR) perpendicular to the plane of the water molecule for U1 system at different temperatures	80
<b>Figure 3.15</b>	MSD profiles of overall water molecules for U1, U5 and U10 systems at different temperatures	81
<b>Figure 3.16</b>	MSD profiles of water molecules within the first coordination shell of uranyl ions for U1, U5 and U10 systems at different temperatures	82
<b>Figure 3.17</b>	MSD profiles of the uranium atom of uranyl ions for U1, U5	83

and U10 systems at different temperatures

- Figure 4.1** Radial distribution functions for (a)  $O_w$  and (b)  $H_w$  of water molecules around the oxygen of central water molecule for bulk supercritical water at water densities of  $0.38 \text{ g cm}^{-3}$ ,  $0.56 \text{ g cm}^{-3}$  and  $0.98 \text{ g cm}^{-3}$  at 683 K 100
- Figure 4.2** Radial distribution functions for (a)  $O_w$  around uranium, (b)  $H_w$  around uranium (c)  $O_w$  around uranyl-oxygen ( $O_U$ ) and (d)  $H_w$  around  $O_U$  at water densities of  $0.38 \text{ g cm}^{-3}$  (blue solid line),  $0.56 \text{ g cm}^{-3}$  (red dashed line) and  $0.98 \text{ g cm}^{-3}$  (green dotted line) at 683 K 101
- Figure 4.3** Schematic representation of various angles considered for orientational distribution of the water molecules around uranyl ions in the aqueous uranyl nitrate solution, DM vector means Dipole Moment vector 103
- Figure 4.4** Distributions of various angles between  $U-O_w/U-O_U$  vector and different molecular orientational vectors of a water molecule in the first coordination shell of a uranyl ion in the aqueous uranyl nitrate solution (a) at a density of  $0.98 \text{ g cm}^{-3}$  at 298 K and 683 K, (b) at densities of  $0.38 \text{ g cm}^{-3}$  and  $0.98 \text{ g cm}^{-3}$  at 683 K 104
- Figure 4.5** Distributions of various angles between  $O_w-O_w$  vector and different molecular orientational vectors of a water molecule in the first coordination shell of a central water molecule in bulk water (a) at a density of  $0.98 \text{ g cm}^{-3}$  at 298 K and 683 K, (b) at densities of  $0.38 \text{ g cm}^{-3}$  and  $0.98 \text{ g cm}^{-3}$  at 683 K 105

<b>Figure 4.6</b>	Mean squared displacement (MSD) as a function of time for water molecules in the aqueous uranyl solution and in bulk water at densities of 0.38, 0.56 and 0.98 g cm <sup>-3</sup> at 683 K	106
<b>Figure 4.7</b>	Mean squared displacement (MSD) as a function of time for uranium atom of uranyl ions in the aqueous uranyl solution at densities of 0.38, 0.56 and 0.98 g cm <sup>-3</sup> at 683 K	107
<b>Figure 4.8</b>	Power spectra of water molecules for aqueous solutions of uranyl ions at different densities at 683 K	110
<b>Figure 4.9</b>	First order orientational correlation functions of water molecules with respect to (a) water dipole moment vector, (b) water H-H vector and (c) water cross vector at densities of 0.38 (blue solid line), 0.56 (red dashed line) and 0.98 g cm <sup>-3</sup> (green dotted line) of supercritical water at 683 K	111
<b>Figure 4.10</b>	Second order orientational correlation functions of water molecules with respect to (a) water dipole moment vector, (b) water H-H vector and (c) water cross vector at densities of 0.38 (blue solid line), 0.56 (red dashed line) and 0.98 g cm <sup>-3</sup> (green dotted line) of supercritical water at 683 K	112
<b>Figure 4.11</b>	First order orientational correlation functions of water molecules under normal conditions (blue solid line) and under supercritical (SCW) conditions (red dashed line) with respect to (a) water dipole moment vector, (b) water H-H vector and (c) water cross vector at a density of 0.98 g cm <sup>-3</sup>	112
<b>Figure 4.12</b>	Radial distribution functions for (a) O <sub>w</sub> around uranium, (b) H <sub>w</sub> around uranium (c) O <sub>w</sub> around uranyl-oxygen (O <sub>U</sub> ) and (d)	114



	$H_w$ around $O_U$ for solutions in ambient (blue solid line) and supercritical water (red dashed line)	
<b>Figure 4.13</b>	Peak values of radial distribution functions for $O_w$ around uranium, $H_w$ around uranium, $O_w$ around uranyl-oxygen ( $O_U$ ) and $H_w$ around $O_U$ as a function of (a) concentration of uranyl ions at approximate water density of $0.57 \text{ g cm}^{-3}$ and (b) density of water at uranyl concentration of $0.07 \text{ M}$	115
<b>Figure 4.14</b>	Variation in number of water molecules in first solvation shell (FCS) of uranium atom of uranyl ion with change in (a) concentration and (b) water density	116
<b>Figure 4.15</b>	Variation in the number of water molecules in the first coordination shell (FCS) of oxygen atom ( $O_U$ ) of uranyl ion with change in (a) concentration and (b) water density	117
<b>Figure 4.16</b>	Variation of diffusion coefficients of water molecules with change in (a) uranyl ion concentration and (b) water density	120
<b>Figure 4.17</b>	Variation of diffusion coefficients of uranium atom of uranyl ions with change in (a) uranyl ion concentration and (b) water density	120
<b>Figure 4.18</b>	Power spectra of (a) water molecules and (b) uranyl ions for different concentrations of uranyl ions in the aqueous solutions at an approximate water density of $0.57 \text{ g cm}^{-3}$ at $683 \text{ K}$ , insets: Magnified curves around zero wave number	122
<b>Figure 4.19</b>	Angular distributions for different angles between $U-O_w$ or $U-O_U$ vector and water molecular vectors for different uranyl concentrations at a water density of around $0.57 \text{ g cm}^{-3}$ at $683$	123

<b>Figure 4.20</b>	First order and (b) second order orientational autocorrelation functions of different molecular vectors of water i.e. dipole moment vector ( $\mu$ ; blue solid line), H-H vector (HH; red dashed line), cross vector (CR; green dotted line) and of uranyl ions with respect to U-O <sub>U</sub> vector of uranyl ion (dark yellow solid line) for Set 4 system	124
<b>Figure 5.1</b>	Snapshots of the carbon nanotube immersed in the box of water molecules	137
<b>Figure 5.2</b>	(a) Normalized density profile, $\rho(r)/\rho_0$ , of fluids as a function of radial distance, $r$ measured from the center of the nanotube. There is a break in the y-axis of the CNT-methane curve so that both density profiles (CNT-water and CNT-methane) are visible. Normalized density profiles, $\rho(r)/\rho_0$ for (b) water and (c) methane within the nanotube ( $-R \leq r \leq R$ , $R$ being the CNT radius). (d) Snapshots of straight chain arrangement of methane (upper panel) and zig-zag orientation of water (lower panel) inside CNT	139
<b>Figure 5.3</b>	Number of fluid molecules inside the nanotube as a function of time for different carbon-fluid interactions for (a) CNT-water and (b) CNT-methane systems	141
<b>Figure 5.4</b>	Average number of fluid molecules inside the CNT (6, 6) at different temperatures	141
<b>Figure 5.5</b>	Pair correlation functions for water and methane molecules inside the CNT (6, 6)	142

<b>Figure 5.6</b>	Power spectra for CNT (6, 6)-water and CNT (6, 6)-methane systems	143
<b>Figure 5.7</b>	Residence time correlation function and MSD for water (blue curves) and methane (red curves) molecules inside the nanotube along the CNT axis (Residence time - dotted line, MSD - full line). The scale of MSD is on the right axis	144
<b>Figure 5.8</b>	Number of translocation events of fluid molecules per nanosecond through the CNT. Conduction bursts <sup>11,17</sup> as shown by the peaks have been observed in both the CNT-methane and the CNT-water systems	146
<b>Figure 5.9</b>	Mean Square Displacements (MSDs) along the CNT axis for CNT-water and CNT-methane systems at different temperatures	148
<b>Figure 5.10</b>	Arrhenius plots for diffusivities of water and methane molecules along the nanotube axis at different temperatures. Dotted lines are the linear fits to the data (symbols) obtained from MD simulations	148
<b>Figure 5.11</b>	Normalized density profile, $\rho(r)/\rho_0$ , of argon as a function of radial distance, $r$ measured from the center of the nanotube	149
<b>Figure 5.12</b>	MSD profiles for methane (red curve) and argon (green curve) molecules inside the nanotube along the axial direction	150
<b>Figure 5.13</b>	Number of translocation events of fluid molecules per nanosecond through the CNT. Conduction bursts as shown by the peaks have been observed in both the CNT-methane and the CNT-argon systems	150

<b>Figure 5.14</b>	Normalized density profile, $\rho(r)/\rho_0$ , of water as a function of radial distance, $r$ measured from the center of the nanotube for various water-CNT systems	152
<b>Figure 5.15</b>	Axial density distribution functions for various water-CNT systems	152
<b>Figure 5.16</b>	Number of water molecules inside CNTs of different diameters during the period of simulation	153
<b>Figure 5.17</b>	Velocity correlation functions (VCFs) for various water-CNT systems	154
<b>Figure 5.18</b>	Power spectra for bulk water and various water-CNT systems	155
<b>Figure 5.19</b>	Mean Square Displacement (MSD) for various water-CNT systems	155
<b>Figure 6.1</b>	Normalized density profile, $\rho(r)/\rho_0$ , of uranyl ions as a function of radial distance, $r$ measured from the axis of the nanotube functionalized at two carbon atoms at a concentration (a) 0.36 M, (b) 0.55 M and (c) 0.73 M of uranyl ions	172
<b>Figure 6.2</b>	Normalized density profile, $\rho(r)/\rho_0$ , of uranyl ions as a function of radial distance, $r$ measured from the axis of the nanotube functionalized with carboxylate ions at two (blue solid line), four (red dashed line) and six (green dotted line) carbon atoms at a concentration (a) 0.36 M, (b) 0.55 M and (c) 0.73 M of uranyl ions	173
<b>Figure 6.3</b>	Adsorption of uranyl ions per unit CNT mass for bare as well as functionalized CNTs as a function of uranyl ion concentration	174

<b>Figure 6.4</b>	Number of uranyl ions adsorbed to nanotube functionalized at different number of carbon atoms with (a) carboxylate ion and (b) hydroxyl group as a function of uranyl ion concentration	174
<b>Figure 6.5</b>	Snapshot of bonding of uranyl ions to the carboxylate oxygen atom, here blue ball = uranium of uranyl ion, red ball = oxygen, green ball = carbon of carboxylate ion	175
<b>Figure 6.6</b>	Number of uranyl ions adsorbed on $\text{COO}^-$ functionalized CNT as a function of simulation time for uranyl ion concentration of (a) 0.36 M, (b) 0.55 M and (c) 0.73 M	176
<b>Figure 6.7</b>	The minimum distance between uranyl ions and $-\text{COO}^-$ functionalized CNT-sidewall as a function of simulation time for uranyl ion concentration of (a) 0.36 M, (b) 0.55 M and (c) 0.73 M	177
<b>Figure 6.8</b>	The minimum distance between uranyl ions and $-\text{OH}$ functionalized CNT-sidewall as a function of simulation time for three uranyl ions in a solution with uranyl ion concentration of 0.73 M	178
<b>Figure 6.9</b>	Diffusion constants of uranium atom of uranyl ions as a function of concentration of uranyl ions in presence of bare and functionalized CNTs	179
<b>Figure 6.10</b>	Diffusion constants of oxygen atom of water molecules as a function of concentration of uranyl ions in presence of bare and functionalized CNTs	180
<b>Figure 6.11</b>	Diffusion constants of nitrogen atom of nitrate ions as a function of concentration of uranyl ions in presence of bare	181

and functionalized CNTs

## **LIST OF TABLES**

	<b>Page No.</b>
<b>Table 2.1</b> Force Field Parameters	38
<b>Table 3.1</b> Force Field Parameters	58
<b>Table 3.2</b> Average number of water molecules in the first coordination shell	62
<b>Table 3.3</b> Coordination numbers (CN) of uranium and oxygen atoms of uranyl ions with respect to oxygen atoms of water and nitrate for different uranyl ion concentrations	64
<b>Table 3.4</b> Diffusion coefficient values for different systems (BW: bulk water)	68
<b>Table 3.5</b> Comparison of normalised diffusion coefficient values for uranyl ions in U1 system with experimental and theoretical results available in literature	69
<b>Table 3.6</b> Diffusion coefficient values for water molecules within the first coordination shell of uranium atom of uranyl ions for different systems	71
<b>Table 3.7</b> Values of time constants (in picoseconds) of longer and shorter time scales of the relaxation of $S(t)$ ( $\tau_1$ and $\tau_2$ ) and $A$ for different systems	73
<b>Table 3.8</b> Diffusion coefficient values of overall water molecules at different temperatures for U1, U5 and U10 systems	81

<b>Table 3.9</b>	Diffusion coefficient values of water molecules within first coordination shell of uranyl ions at different temperatures for U1, U5 and U10 systems	82
<b>Table 3.10</b>	Diffusion coefficient values for uranium atom of uranyl ions at different temperatures for U1, U5 and U10 systems	83
<b>Table 3.11</b>	Diffusion coefficient values of water molecules and uranyl ions corrected for system size at different temperatures for U1, U5 and U10 systems	84
<b>Table 4.1</b>	Density and box lengths of the systems simulated using Molecular Dynamics Simulation at 683 K	97
<b>Table 4.2</b>	Various sets of systems with different uranyl concentrations and different supercritical water densities considered in present study.	98
<b>Table 4.3</b>	Coordination/Hydration numbers of oxygen atoms of central water molecules in bulk water and uranium and oxygen atoms of uranyl ions in aqueous uranyl solution with respect to oxygen atoms of surrounding water molecules at different densities	102
<b>Table 4.4</b>	Diffusion coefficient values for aqueous solutions of uranyl ions and bulk supercritical water <sup>b</sup> for different water densities	108
<b>Table 4.5</b>	Comparison of corrected diffusion coefficient values for water molecules under supercritical conditions with experimental and theoretical results available in literature	109
<b>Table 4.6</b>	Number of oxygen atoms of nitrate ion within first solvation shell of uranyl ions and uranium-uranium coordination number for different uranyl ion concentrations	118

<b>Table 4.7</b>	Comparison of size corrected diffusion coefficients for supercritical water in very dilute solutions (Set Nos. 1, 4 and 7) with those recorded in earlier experimental and simulation studies	121
<b>Table 6.1</b>	Details of the systems considered in present study	167
<b>Table 6.2</b>	Force Field Parameters	169



# *Chapter 1*

## **Introduction and Computational Methodology**



## 1.1 Introduction

Understanding the structural and thermodynamic properties of salts in aqueous solutions is the first step in optimizing many important industrial processes. This is the case for separation processes based on liquid-liquid extraction, which are widely used in the reprocessing of spent nuclear fuels in nuclear industry. For these procedures, a detailed knowledge of the actinoid ( $An^{3+}$ ) and lanthanoid ( $Ln^{3+}$ ) properties in solution is required. However, their radioactivity and the difficulty of performing controlled experiments at high concentrations make experimental determination of these properties very difficult and time-consuming. Therefore, a theoretical approach, coupled with existing experimental observations, is well suited to describe these systems.<sup>1</sup> The studies on actinides and lanthanides,<sup>2-6</sup> combining both theory and experiments, have succeeded in clearly explaining the structural properties and the nature of the ion-solvent and ion-ion interactions in these solutions, in good agreement with previous experimental<sup>7-18</sup> and theoretical works.<sup>13,19-32</sup> A fundamental understanding of interfacial transport phenomena is essential in developing high fidelity process models for solvent extraction processes.<sup>33</sup>

The well-known PUREX process<sup>34-36</sup> is used for the remediation of contaminated water resulting from spent nuclear fuel. Uranium exists in aqueous solution as the linear uranyl ion  $UO_2^{2+}$ . This ion possesses very stable uranium-oxygen double bonds, leaving the oxygens largely unreactive.<sup>37</sup> Thus, understanding the behavior of uranyl ions in solution is crucial for the development of efficient nuclear waste management tools.<sup>38</sup> Experimental results and molecular-level theories for the chemical speciation, the stability of the resulting molecular complexes, the structure and binding modes of active ligands, and the driving forces for partitioning at interfaces will aid the advancement of extraction technologies.

The radioactive actinide element uranium has always been of great interest to public and science alike due to its key role in civil as well as military nuclear technology. There is a

wide range of uranium containing species soluble in aqueous solution that can pollute rivers and ground water, and detailed knowledge regarding these compounds is crucial to nuclear waste management and the development of new methods to counteract the spread of pollution resulting from accidents.<sup>39</sup> During processes such as uranium mining, production of metallic uranium, military usage of depleted uranium, production and manipulation of nuclear reactor fuels, and manufacture of nuclear weapons, some contaminants are generated<sup>40–42</sup> and mixed with water; not just because water is used as a moderator and coolant in nuclear plants, but because of uranium solvation waste.<sup>43</sup> All these highlight the importance of proper waste disposal. The main chemical form in which uranium is present in water is the  $\text{UO}_2^{2+}$  ion,<sup>44–47</sup> therefore, dissolution of uranium depends on the uranyl ion and its complexes. That is why it is important to understand uranyl chemical behavior and properties such as transport, reactivity, speciation, solvation, among others; uranium oxide particles dissolved in water can be absorbed by plants when they percolate from the surface to groundwater.<sup>41</sup> The understanding of uranyl chemical behavior in water is paramount for the development of nuclear sensors.<sup>48</sup>

Dense fluids at temperatures slightly above the vapour liquid critical temperature (supercritical (SC) fluids) have attracted industrial interest<sup>49–53</sup> as solvents for separation processes and as reaction media, and dilute SC solutions have received considerable recent research attention.<sup>54</sup> Supercritical fluids have played an important role in a wide variety of applications over the past decade due to their high dissolving power combined with enhanced mass transport.<sup>55–59</sup> It is well-known that the density of a SCF in the near critical region can be varied continuously from gas-like to liquid-like values even with a small change in pressure or temperature, causing corresponding changes in solute solvation and dynamics. This feature makes SCFs attractive alternatives to liquid solvents for several uses.<sup>60</sup>

Aqueous fluids under high-pressure, high-temperature conditions near and above the critical point of water ( $P = 22.1$  MPa and  $T = 647$  K) are especially important in a variety of geochemical processes. Due to the large compressibility of supercritical fluid, small changes in pressure can produce very substantial changes in density, which, in turn, affect diffusivity, viscosity, dielectric, and solvation properties, thus dramatically influencing the kinetics and mechanisms of chemical reactions in water.<sup>61</sup> Models of hydrothermal convection suggest that the near-critical conditions provide an optimal convective behaviour due to unique combination of thermodynamic and transport properties in this region of the phase diagram of water.<sup>62,63</sup> Directly measured temperatures of seafloor hydrothermal vents reach near-critical values of 630-680 K, which greatly affects the speciation in these complex chemical systems.<sup>64,65</sup> From an engineering viewpoint, supercritical water has also attracted growing attention in recent years as a promising chemical medium with a wide range of different environment friendly technological applications.<sup>66-68</sup> From either geochemical or technological perspective, a fundamental understanding of the complex properties of supercritical aqueous systems and the ability to reliably predict them using physically meaningful models is of primary importance.

Many techniques have been developed to treat radioactive wastes from facilities of power reactors and reprocessing plants of spent nuclear fuels.<sup>69-72</sup> However, the treatment methods for wastes containing uranium (so-called uranium wastes) have not been developed sufficiently, despite a large amount of their wastes generated throughout the nuclear fuel cycle. It is well known that metal oxides can be synthesized by treating metal salts in sub- and supercritical water.<sup>73-75</sup> Smith et al. have studied the application of such a property of sub and supercritical water to the separation of fission products from the high level liquid wastes.<sup>76,77</sup> The application of supercritical media to radioactive waste treatment is very

attractive, because additional reagents for the separation are unnecessary and this leads to the reduction in amounts of wastes.

Water at interfaces have markedly different properties and local structural arrangements as compared to those of bulk water.<sup>78,79</sup> In case of interfacial water, manifestation of different properties of water changes according to the length scale of the interfaces.<sup>80,81</sup> When confined in small spaces, fluid molecules can act differently compared to under macroscopic conditions, due to the emergence of molecular discrete nature. A special but realistic example is water confined in carbon nanotubes (CNTs). The unique geometrical characteristics endow the CNTs with various interesting properties that can be used for engineering applications.<sup>82</sup> The mechanical, electrical, and thermal properties of CNTs have been extensively investigated so far, and interactions between other molecules have started to attract attention.<sup>83</sup> Carbon nanotubes (CNTs) have gained recognition as prominent building blocks of nanomaterials; they are used in a variety of nanotechnology applications due to their exceptional mechanical and electrical properties.<sup>84,85</sup> The transport of molecules in these nanoporous media could also exhibit interesting characteristics, different from the ones of transport in ordinary bulk media, since the interactions between the pore wall and the molecules become rather strong when the dimensions of the pore approach the size of the transported molecule.<sup>86</sup> The hydrophobic interior of CNTs is also considered as a model for fundamental studies aimed at exploring the structural and phase behavior of water molecules within one-dimensional (1-D) nanochannels,<sup>87-91</sup> which has long been recognized as the key for both theory and practice with various applications, such as gas storage,<sup>92,93</sup> nanoelectronics,<sup>94</sup> molecular detection,<sup>95,96</sup> drug delivery,<sup>97,98</sup> and membrane separation.<sup>99,100</sup> Many recent experimental and theoretical studies have focused specifically on the structural and thermodynamic properties in the vicinity or interior of CNTs.<sup>101-106</sup> For example, despite the hydrophobic nature of CNTs, Hummer et al.<sup>101</sup> have reported that water molecules can

spontaneously and continuously fill into a nonpolar carbon nanotube with a rather strong hydrophobic character and a one-dimensionally ordered chain of water molecules will be shaped inside the CNT. Studies of water transport through the simple idealized pores of CNTs<sup>101</sup> may help us to understand various aspects of molecular scale hydrodynamics and serve as models for transport in biological transmembrane channels. While some experimental work continues to focus on the structure and hydrogen-bond dynamics of bulk water via <sup>1</sup>H NMR<sup>5</sup> or X-ray diffraction,<sup>107</sup> other work has explored the modified properties of water in nanoscopic domains.

Peter and Hummer<sup>108</sup> have studied computationally the Na<sup>+</sup> ion transport through narrow hydrophobic pores in model membranes formed of hexagonally packed armchair type CNTs of chirality (10, 10), evidencing the fact that sub-nanometer pores pose a huge free-energy barrier to ions. As promising candidates for water desalination by reverse osmosis, CNT membranes have been simulated under hydrostatic pressure and equilibrium conditions by Corry.<sup>109</sup> While ions are not able to pass through narrow pores ((5, 5) and (6, 6)), due to the formation of stable hydrogen bonds, water faces no such impediment. The considered membranes thus allow under a hydrostatic pressure difference for high degrees of desalination to be achieved. Beu studied the flow of aqueous NaCl and NaI solutions through carbon nanotubes by extensive molecular dynamics simulations. The dependence of diverse transport features on the solute specificity, the nanotube geometry, and the various atomic models employed, including polarizability, is addressed in detail.<sup>110</sup> Ion separation is an essential process in chemical and biological analysis systems, which is conventionally performed by capillary electrophoresis<sup>111</sup> or by nanofiltration membranes.<sup>112</sup> The nanoscale dimensions of CNTs produce a relatively large surface area-to-volume ratio, making their use attractive in ion separation devices as well as for their desirable chemical stability and electrical conductivity. The presence of electrical partial charges on CNTs has a significant

effect on conduction and acceptance of charged molecules.<sup>113,114</sup> Majumder et al.<sup>114</sup> placed negatively charged functional groups at the CNT tips and found that this significantly increases the flux of positive ions; although, this effect is reduced at higher ionic concentrations. Similarly, Joseph et al.<sup>113</sup> showed that placing partial charges on the rim atoms of a CNT significantly increases ion occupancy.

Due to enormous advancement in the development of supercomputing machines, the theoretical modelling and simulation are proved to be extremely useful and essential to interpret the experimental results and to get information at the atomistic level.<sup>115</sup> In fact, theoretical modeling as well as simulation has emerged as a very powerful tool for investigating structure and dynamics of bulk and interfacial water or aqueous solutions. Theoretical modeling and simulation can yield information at the atomistic level and provide detailed insight, which is sometimes beyond the scope of even modern, state-of-the-art experimental techniques. Among the different available simulation techniques, molecular dynamics (MD) simulation has the advantage of not only predicting the structure of the fluid at the atomistic scale resolution, but providing information about the dynamical time history and hence dynamics of the system as well.<sup>116</sup> In fact, MD simulations not only validate theoretical models and help explaining experimental results but direct new research by raising many new questions as well. The present thesis is aimed at understanding the structure and dynamics of water and aqueous solutions of uranyl ions in bulk and at interfaces such as carbon nanotubes by using extensive atomistic molecular dynamics simulations. Moreover, the characteristics of water and aqueous solutions of uranyl ions in bulk are analyzed under ambient as well as under supercritical conditions to demonstrate the impact of different physical conditions on the behavior of various species present. Also, an attempt has been made to analyze the effect of change of uranyl ion concentration on the different properties related to the structural and dynamical aspects of various species present in the aqueous



solutions of uranyl ions. The nature and scope of the present thesis are discussed in details at the end of this Chapter (see Section 1.6). For all the analysis, the tool of molecular dynamics simulations is used which is described briefly in the following subsection. The MD simulation provides us the detailed microscopic picture in terms of the trajectory (positions and velocities of all the constituent particles) of the system. Statistical mechanics relations are utilized to obtain average thermo-physical and dynamic properties of the system. Hence, a brief description of the statistical mechanics theory pertaining to liquid structure and dynamics is also presented in the following subsection.

## 1.2 Classical Molecular Dynamics

The technique of molecular dynamics (MD) simulation was introduced in 1957 by B. J. Alder and T. E. Wainright where they used it to study phase transition of a system consisting of hard spheres.<sup>117,118</sup> Later in 1964, A. Rahman first used this powerful technique to understand local structure and dynamics of a condensed phase system of argon atoms interacting with each other with an effective interaction potential.<sup>119</sup> This work proved to be a milestone as they introduced equilibrium auto correlation functions to estimate the transport properties of a system of interacting particles. The introduction of high performance supercomputing machines has helped in the prospects of using MD simulation technique in a variety of fields such as Physics, Chemistry, Biology, Chemical Engineering, Material Science, Mechanical Engineering etc. Classical MD simulation is a deterministic method which follows the laws of classical mechanics to depict the time evolution of the phase space of a set of interacting atoms or molecules. For example, by integrating Newton's equations of motion, this method generates a set of coordinates and momenta (velocities) of constituent particles of the system as a function of time. For a simple atomic system, the force ( $\mathbf{F}$ ) experienced by the system as per Newton's second law of motion can be written as

$$\mathbf{F} = m \frac{d^2 \mathbf{r}}{dt^2} \quad (1.1)$$

where  $m$  is the mass of the atom and  $\mathbf{r}$  is the positional coordinate. By integrating the above equation of motion, from a set of positions and velocities at a particular time step, the consecutive positions and velocities of the next time frames separated by a small time interval  $dt$  can be calculated. Various approximate solutions have been used to integrate the above equation of motion. Among these methods, Verlet algorithm, velocity Verlet algorithm, leap-frog algorithm to name a few. According to the velocity Verlet algorithm, the position  $\mathbf{r}(t+dt)$  and velocity  $\mathbf{v}(t+dt)$  of each particle constituting the system at time  $(t+dt)$  can be obtained from position  $\mathbf{r}(t)$ , velocity  $\mathbf{v}(t)$  and force ( $\mathbf{F}(t)$ ) of the same at time  $t$  such that

$$\mathbf{r}(t + dt) = \mathbf{r}(t) + \mathbf{v}(t)dt + \frac{\mathbf{F}(t)}{2m} dt^2 \quad (1.2)$$

$$\mathbf{v}(t + dt) = \mathbf{v}(t) + \frac{\mathbf{F}(t + dt) + \mathbf{F}(t)}{2m} dt \quad (1.3)$$

The force acting on each constituent particle in the system can be calculated from the negative gradient of the total potential energy of the system i.e.

$$\mathbf{F} = -\nabla V(\mathbf{r}^N) \quad (1.4)$$

Hereby,  $V(\mathbf{r}^N)$  is the potential energy of the system which can be calculated from the position of atoms by using an empirical force field corresponding to the simulation system defined by the user. Thus, once empirical force field is defined, above set of equations can be solved successively to obtain positions and velocities as a function of time, commonly known as trajectory of the system.

In a classical MD simulation, the system characteristics are hidden in its potential energy function, commonly known as force field. Depending on the bonding nature in a molecule such a site-site interaction potential function consists of two distinct types of interactions namely, (a) non-bonded interactions and (b) bonded interactions. By suitably

choosing the potential functions for these two types of interactions, total potential energy of the system can be calculated by considering various intra- and inter-molecular interactions among different sites in the system. One of the functional forms for calculating energy of the N-atom molecular system can be expressed as

$$V(\mathbf{r}^N) = \sum_{i=1}^N \sum_{j=i+1}^N \left( 4\epsilon_{ij} \left[ \left( \frac{\sigma_{ij}}{r_{ij}} \right)^{12} - \left( \frac{\sigma_{ij}}{r_{ij}} \right)^6 \right] + \frac{q_i q_j}{4\pi\epsilon_0 r_{ij}} \right) + \sum_{\text{bonds}} 0.5K_b (b - b_0)^2 \\ + \sum_{\text{angles}} 0.5K_\theta (\theta - \theta_0)^2 + \sum_{\text{dihedrals}} \sum_{n=1}^N K_\phi^{(n)} [1 + \cos(n\phi - \delta)] + \sum_{\text{impropers}} K_\omega (\omega - \omega_0)^2 \quad (1.5)$$

Hereby, the total potential  $V(\mathbf{r}^N)$  is the function of coordinates of the N sites of the systems. The first two terms of the right hand sides of the equation correspond to non-bonded interactions and the rest of the terms are bonded parameters. For all nonbonding interactions, a cut-off distance of 12.0 Å in real space is used. The very first term of the equation captures the van der Waals (VDW) interaction between two atoms i and j with interatomic distance  $r_{ij}$ . The parameter  $\epsilon_{ij}$  represents the depth of the potential well and  $\sigma_{ij}$  represents the collision diameter or the inter-atomic distance at which potential energy becomes zero. The second term in the above equation is the non-bonded electrostatics interaction as given by the Coulomb's law due to point charges on different interaction sites of the system. The interacting atoms are separated by distance  $r_{ij}$  and pose partial charge  $q_i$  and  $q_j$  respectively. The third term of the equation is the potential energy for bond vibration or the bond energy and is modeled by using harmonic potential;  $b$  represents the bond length at any instant of time and  $b_0$  is the equilibrium bond length and  $K_b$  is the force constant of the bond. In a similar fashion, the 4<sup>th</sup> term in the equation representing energy change during bending motion of molecule is also modeled by using harmonic potential. Hereby,  $K_\theta$  represents the force constant, and  $\theta$  and  $\theta_0$  are the angles formed by three consecutive atoms and its equilibrium value, respectively. The 5<sup>th</sup> term provides the potential energy change due to

dihedral or torsional motion (dihedral term). Actually, four consecutive atoms in a molecule form a dihedral angle. The angle  $\varphi$  represents torsion angle,  $K_\varphi$  represents height of rotational energy barrier,  $n$  is the multiplicity which illustrates the number of minimum points in the function during a  $360^\circ$  rotation of a bond. The phase factor  $\delta$  decides where the torsion angle goes through the minimum values. The cosine function in this term stands for the periodicity of this function. The 6<sup>th</sup> term in the equation demonstrates improper dihedral potential involving improper torsion/dihedral angle  $\omega$ , its equilibrium value  $\omega_0$  and force constant  $K_\omega$ . The 5<sup>th</sup> and 6<sup>th</sup> terms are absent if the number of atoms in the molecule is less than four which is the case in systems considered in the present work and hence these two terms are considered zero.

The parameters of a force field are mainly obtained from experimental or quantum mechanical studies. In last 30 years, different types of force field have been developed which are extensively used in simulations for many different systems of interests. In our work, we have mostly adopted AMBER<sup>120</sup> and OPLS<sup>121</sup> force-field for solutes and SPC/E and TIP series of models for water.<sup>122-127</sup> The primary requirement of any MD simulation is the modeling of the system by choosing appropriate length scale and force-field or model potentials and subsequent creation of initial configuration for the same. Initial velocities of each atom can be provided by using Maxwell-Boltzmann equation by taking care of the average temperature of the system. Before starting the simulation, a suitable boundary condition to mimic the system of interest should be employed. Periodic boundary condition is one such condition which apart from maintaining the number of atoms/particles fixed in the simulation box, creates bulk environment by removing the surface effects. In our simulations, periodic boundary conditions and minimum image conventions are applied in all three directions. Because of the long-ranged nature of the Coulomb potential, particle mesh Ewald (PME) summation method is used to evaluate the charge-charge interaction correctly.<sup>128-131</sup>

The equation of motion is generally integrated by applying finite difference methods. The basic criteria of a reliable integrator are: it should be (a) accurate (follow the true trajectory) (b) stable (energetically conserved) and (c) robust (allow larger time in propagation of system in phase space). There are several algorithms proposed for the integrators in MD simulations. Throughout this work, we have used velocity Verlet<sup>132</sup> algorithm for our simulation purposes. One usual way of avoiding larger computational requirement is to avoid simulating very fast motions like the one due to bond or angle vibration by constraining these bonds or angles to its equilibrium value during the simulation. Here we have used SHAKE<sup>133</sup> for constraining OH bond lengths and the HH distance of the water molecules.

In general, a trajectory obtained by solving the Newtonian equations of motion corresponds to micro canonical or NVE ensemble. Special thermostating methods are to be employed to simulate systems in any other ensemble. Different types of thermostats such as Berendsen temperature coupling<sup>134</sup>, Velocity rescaling<sup>135</sup>, Nose-Hoover<sup>136</sup> temperature coupling are used to maintain the temperature of the system and different barostats such as Berendsen pressure coupling<sup>134</sup>, Parrinello-Rahman<sup>137</sup> method etc. are used to control the pressure of the system. Some of the well-known ensembles used in this thesis work are canonical or NVT ensemble in which the total number of particles, temperature and volume of the system are fixed and isothermal-isobaric (NPT) ensemble in which the total number of particles, temperature and pressure of the system are fixed.<sup>138</sup> There are some mathematical relations relating a particular statistical ensemble and various thermodynamic properties of the system. As outputs of the MD simulation we obtain phase-space trajectory of the system which contains entire time history of the evolution of the system in terms of macroscopic quantities. The extraction of the macroscopic properties of the system from this microscopic description involves application of statistical mechanics.<sup>139</sup> In the following sections, we shall

describe various aspects of statistical mechanics associated with the static and dynamical properties of a many-particle finite-temperature system.

### 1.3 Statistical Mechanical Ensembles and Averages

The aim of the equilibrium statistical mechanics is to calculate observable properties of a many particle system from its microscopic description. Thermodynamic properties of a system, with some exceptions, are expressible as average of certain functions of the coordinates and/or momenta of the constituent particles of the system. In a state of thermodynamic equilibrium, the average must be independent of time. Let us assume a system consisting of  $N$  identical spherical particles and also assume the system is isolated from its surroundings, in which case we know the Hamiltonian  $H$  is a constant of motion. Given the initial positions and momenta, positions at any later time can in principle be obtained from the solution of Newtonian equation of motion

$$m\ddot{\mathbf{r}}_i = -\nabla U_N(\mathbf{r}^N) \quad (1.6)$$

The above equation is a combination of Eqs. (1.1) and (1.4).

In a conventional MD simulation, we generally deal with positions and momenta of all the  $N$  particles of the system. These positions and momenta of the system are continuously changing with the passage of time and these position and momenta can be thought of as coordinates in a multidimensional space, called “phase space”. Let us use the abbreviation  $\Gamma$  for a particular point in phase space and  $\Gamma$  corresponds to  $N$  coordinates and  $N$ -momenta. Let us assume an instantaneous function  $A(\Gamma)$ , which corresponds to some macroscopic property  $A$  of the system. As the system evolves  $\Gamma$  changes and thus instantaneous value of the property  $A(\Gamma)$  changes, and thus any observable  $A$  can be obtained as average of all the  $A(\Gamma)$  i.e.

$$A = \langle \mathcal{A}(\vec{r}^N, \vec{p}^N) \rangle \quad (1.7)$$

where the angular brackets denote average value.

### 1.3.1 Time Averaging (Method of Boltzmann)

In a MD simulation, as we solve Newtonian equation of motion, we generate phase space point  $\Gamma$  as a function of time. It is therefore reasonable to assume that the experimentally measured value of the property,  $A$  is actually the time average of  $A(\Gamma)$  taken over a long time interval such that

$$\langle \mathcal{A} \rangle_t = \lim_{\tau_{\text{obs}} \rightarrow \infty} \frac{1}{\tau} \int_0^{\tau_{\text{obs}}} \mathcal{A}[\vec{r}^N(t), \vec{p}^N(t)] dt \quad (1.8)$$

The above concept of time averaging is due to Boltzmann. As in practice, we cannot extend the integration up to infinity and we represent a discrete time in MD, it is therefore convenient to express the above averaging procedure as a sum of  $N_t$  number of time steps of discrete step length  $= \tau_{\text{obs}} / N_t$ , viz.

$$A = \langle \mathcal{A} \rangle_t = \frac{1}{N_t} \sum_{\tau=1}^{N_t} \mathcal{A}(\Gamma(\tau)) \quad (1.9)$$

where  $\Gamma(\tau)$  is the phase-space point corresponding to a particular set of  $N$  positions and  $N$  momenta (where  $N$  is number of particles in the system).

### 1.3.2 Ensemble Average

The same averaging of equation (1.8) can be carried out by averaging over ensemble of systems, each of which is a replica of the original system of interest. This is known as the method of Gibbs. An ensemble is an arbitrary large collection of imaginary systems, all of which are replicas of the system of interest in so far as they are characterized by same macroscopic parameter like  $N$ ,  $V$ ,  $T$ ,  $P$ ,  $\mu$  etc. The systems of ensemble differ from each other

in the assignment of coordinates and momenta of the particles of the system. Ensemble is thus represented by a cloud of phase points distributed in space according to some probability density distribution. In Gibbs' formulation of statistical mechanics the distribution of phase points of the ensemble is described by a phase-space probability density  $f^{(N)}(\vec{r}^N, \vec{p}^N, t)$ ; The quantity  $f^{(N)}d\vec{r}^N, d\vec{p}^N$  is the probability that at time  $t$ , the actual physical system is in a microscopic state represented by a phase point lying in the infinitesimal phase space element  $d\vec{r}^N, d\vec{p}^N$ . Given a complete knowledge of the probability density, it would be possible to calculate average values of any functions of the coordinate and momenta. The equilibrium ensemble average of a phase function  $\mathcal{A}(\vec{r}^N, \vec{p}^N)$  is given by

$$\langle \mathcal{A} \rangle_e = \iint \mathcal{A}(\vec{r}^N, \vec{p}^N) f_0^{(N)}(\vec{r}^N, \vec{p}^N) d\vec{r}^N, d\vec{p}^N \quad (1.10)$$

Where  $f_0^{(N)}$  is normalized such that

$$\iint f_0^{(N)}(\vec{r}^N, \vec{p}^N) d\vec{r}^N, d\vec{p}^N = 1 \quad (1.11)$$

The definition of time averaging i.e. Eq. (1.9) is correct when the system is “ergodic” which means that after a suitable time of observation the phase trajectory of the system will have passed equal number of times through every point in phase- space.

## 1.4 Equilibrium Particle Density Distribution Functions

For a system at equilibrium, the radial density distribution function,  $g(r)$  is very useful quantity to understand the structure and thermodynamics of the liquid system, defined as:

$$g(r) = \frac{\rho(r)}{\rho_0} \quad (1.12)$$

where  $\rho_0$  is the average density of the system and  $\rho(r)$  is the density of the spherical shell at a radial distance  $r$  from the central molecule given as:



$$\rho_0 = \frac{N}{V} \quad \text{and} \quad \rho(r) = \frac{N(r)}{V_{\text{shell}}(r)} = \frac{N(r)}{\frac{4}{3}\pi[(r+dr)^3 - r^3]} \quad (1.13)$$

The distribution function measures the extent to which the structure of the fluid deviates from complete randomness. The above equation is the simple formulation of  $g(r)$  in terms of the position of the particles. This structural quantity is experimentally measurable (radiation scattering experiment) and is often used to deduce various physical properties of fluids. The definition of  $g(r)$  implies that on an average the number of particles lying within the range  $r$  to  $(r + dr)$  from a reference particle is  $4\pi r^2 \rho_0 g(r) dr$  and the peaks in  $g(r)$  represent “shells” of neighbors around the reference particle. Integration of  $4\pi r^2 \rho_0 g(r)$  up to the position of the first minimum in the  $g(r)$  therefore provides an estimate of the number of first nearest-neighbours, commonly known as “coordination number” i.e.  $[N(r)]$

$$N(r) = 4\pi \rho_0 \int_0^{r_c} r^2 g(r) dr \quad (1.14)$$

Here,  $r_c$  is the cutoff distance.

## 1.5 Time Correlation Functions and Transport Coefficients

Similar to structural properties, statistical mechanics also provides relation between the time correlation function and dynamical properties.<sup>140</sup> Generally, the time correlation function of a quantity  $A(t)$  normalized with respect to the time origins is described as

$$C_{AA}^{\text{nom}}(t) = \left\langle \frac{A(t) \cdot A(0)}{A(0) \cdot A(0)} \right\rangle_0 \quad (1.15)$$

Here, the quantity  $A(t)$  is a component of positions and velocities of the particles. This relation can be used to calculate time dependency of a function if the desired property is being evaluated at two different time steps. The time integral of time correlation function is often related with macroscopic transport properties.

Transport coefficients are defined in terms of the response of a system to a perturbation. In case of diffusion coefficient, it is related in between particle flux and concentration gradient. Any transport coefficient is in general infinite time integral of an equilibrium time correlation function of the form

$$\gamma = \int_0^{\infty} dt \langle \dot{A}(t) \dot{A}(0) \rangle \quad (1.16)$$

Hereby,  $\gamma$  is the transport coefficient and  $\dot{A}$  is the time derivative of  $A$ , the variable term present in perturbation of the Hamiltonian. The above relation is known as Green-Kubo relation. Similarly, one can integrate the right hand side of the above relation to obtain another relation, known as Einstein relation which relates transport coefficient  $\gamma$  with the quantity  $A$  such that

$$2t\gamma = \langle (A(t) - A(0))^2 \rangle \quad (1.17)$$

For example, the diffusion coefficient ( $D$ ) of  $d$  dimensional fluid can be expressed by using these equations i.e.

$$D = \frac{1}{d} \int_0^{\infty} dt \langle v_i(t) v_i(0) \rangle \quad (1.18)$$

Where  $v_i(t)$  is the centre of mass velocity of a single molecule. The corresponding Einstein relation, valid at long times is

$$D = \frac{1}{2d} \lim_{t \rightarrow \infty} \frac{\langle \Delta r^2 \rangle}{\Delta t} = \frac{1}{2d} \lim_{t \rightarrow \infty} \frac{\langle |\mathbf{r}_i(t) - \mathbf{r}_i(0)|^2 \rangle}{\Delta t} \quad (1.19)$$

$\mathbf{r}_i(t)$  is the position vector of the molecule at time  $t$ .

The diffusion coefficient values obtained from MD simulations with periodic boundary conditions ( $D_{PBC}$ ) have been reported to be system size dependent.<sup>141,142</sup> The system size dependence of the calculated diffusivity ( $D_{PBC}$ ) can however be corrected by using the

method adopted by Kerisit et al.<sup>141</sup> and Yeh et al.<sup>142</sup> The corrected system size independent diffusivity ( $D_0$ ) is obtained using the equation

$$D_o = D_{PBC} + \frac{2.837297 K_B T}{6\pi\eta L} \quad (1.20)$$

where  $\eta$  and  $L$  are shear viscosity of water and simulation box length respectively.

The orientational dynamics of the water molecules are analyzed by calculating time correlation function of various molecular vectors of water. Here, three different unit vectors ( $u_\alpha$ ) along three different molecular axes of water are considered, namely, (i) dipole moment vector ( $u_\alpha = \mu$ ) (ii) H-H vector ( $u_\alpha = HH$ ) (iii) a cross vector ( $u_\alpha = CR$ ) i.e. a vector perpendicular to plane of water molecule. The time evolution of these three orientational vectors,  $u_\alpha$ , can be defined in terms of autocorrelation functions of the form

$$\Gamma_n^\alpha(t) = \langle P_n(u_\alpha(t) \cdot u_\alpha(0)) \rangle \quad (1.21)$$

where  $P_n$  is the Legendre polynomial of order  $n$ . The angular brackets in the above equation represent average over time origins as well as the number of molecules.<sup>143</sup>

## 1.6 Nature and Scope of the Present Work

In the present thesis, molecular dynamics (MD) simulation results on structure and dynamics of water and aqueous solutions of uranyl ions in bulk, and at molecular and nanoscopic interfaces are presented. The thesis consists of seven chapters where the relevant introduction, conclusion and future prospects of related work are included in the respective chapters. As discussed in the Introduction section, due to the importance of uranyl ions in the nuclear fuel cycle and its radioactive nature, studying the characteristics of solutions of uranyl ions using computational techniques may contribute significantly with respect to better management of nuclear waste. **In Chapter 1**, the importance of studying the characteristics of aqueous solutions of various ions is touched upon and the contribution of such studies in

the development of various solvent extraction processes is highlighted. The significance of actinyl ions specific to the nuclear fuel cycle is elaborated. The mention of the small amount of literature available on the behaviour of actinyl ions in different systems is worth noticing. Molecular dynamics simulations provide the time evolution of the phase-space in terms of trajectories i.e. sets of positions and momenta of all the particles of the system. The various structural, thermodynamic and dynamic properties of the system can be obtained from these microscopic variables by the application of classical statistical mechanics. Finally, in the last part of the **Chapter 1**, the nature and scope of the present thesis is discussed. In general, **Chapter 1** gives the general introduction to MD simulations, various mathematical equations involved and methods adopted to solve these equations. It also explains the motivation for the work carried out during the course of the thesis.

Before proceeding with the simulations of aqueous solutions of uranyl ions under different conditions, bulk water system is simulated first to get acquainted with the tool of MD simulations. Various properties and results related to bulk water reported in literature are reproduced as a learning exercise. Some important results related to bulk water system are included in **Chapter 2** of the thesis. Moving further towards studying the behaviour of uranyl ions in aqueous solutions, the pioneering work of Guilbaud and Wipff<sup>144-146</sup> on molecular dynamics simulation studies of aqueous solution of uranyl ions helps us to understand various aspects of uranyl hydration. In a series of investigations, Maginn and co-workers<sup>147-149</sup> have developed and utilized the force fields for the different actinyl ions in their aqueous solutions by taking into account the many-body solvation effects. We carried out MD simulations for aqueous solutions of uranyl ions to analyze the structural and transport characteristics of various species in the aqueous solutions as discussed in **Chapter 2** of the thesis. The structural quantities such as radial distribution functions and distributions of angles formed

by various water and uranyl vectors, and translational diffusion and dynamics of various water vectors are analyzed.

In the studies mentioned above and most of the other simulation studies, only one uranyl ion in a box of water is considered. Presence of the multiple ions on the solution may perturb the tetrahedral structure and thereby modify the structure and dynamics of the aqueous uranyl solution. Therefore, the effect of concentration of uranyl ions as well as that of the temperature of the system on its structural and dynamical characteristics is investigated by simulating three different solutions with uranyl nitrate concentrations of 0.1 M (U1), 0.5 M (U5) and 1.0 M (U10) using atomistic molecular dynamics (MD) simulations and the results are presented in **Chapter 3** of the thesis.

Further, supercritical fluids are also of huge importance due to its applications in extraction processes and nuclear industry. Various methods of separation of the actinyl ions from the nuclear waste involving supercritical fluids have been proposed.<sup>150</sup> Moreover, supercritical water is proposed to be an efficient coolant for Generation IV nuclear reactors.<sup>151</sup> Thus, knowledge of hydration and transport properties of these actinyl ions in supercritical water generates a lot of interest. Hence, the behaviour of aqueous solution of uranyl ions under supercritical conditions for systems of varying water densities and uranyl ion concentrations is reported in **Chapter 4** along with the comparison with that of bulk supercritical water.

Carbon nanotube (CNT) based membranes have shown great potential for desalination of the sea water. These nanoporous membrane can also be used in the separation of actinyl ions from their aqueous solutions. Hence, after analysing the bulk behaviour of water and aqueous solutions of uranyl ions, the effect of presence of CNT in a box of water is investigated. While studying the literature related to molecular dynamics studies of water in different systems, we came across the flow characteristics of water through CNTs. The

behaviour of water confined in a narrow pore such as carbon nanotube differs considerably from that in bulk, as the characteristic dimensions of the confining medium are reduced to the nanometer scale.<sup>152-154</sup> The engineered water channels based on carbon nanotubes (CNTs) have attracted great attention since Hummer et al.<sup>155</sup> reported water transmission through a nonpolar (6,6) CNT. In spite of a large number of investigations on the behaviour of water in and around carbon nanotubes, many pertinent questions remain unanswered. Hence in **Chapter 5**, we analyzed whether the structural and dynamic properties of a non-polar fluid resemble those of a polar, hydrogen-bonded fluid like water. Hence, molecular dynamic simulations are carried out to check whether characteristics such as pulse-like transmission, empty-filled transition and rapid diffusion can be observed even in case of non-hydrogen bonded fluid when transported through the single-file CNT. The effect of nanotube diameter on the various features of water-CNT system is also demonstrated by simulating water molecules in the presence of nanotubes of varying diameter.

The variation in the characteristics of the fluids at interfaces as discussed above led us to study the behavior of aqueous solutions of uranyl ions in the presence of CNT. Moreover, CNTs can be functionalized with specific functional groups for specific purposes. Hence, **Chapter 6** deals with this topic where aqueous solutions of varying concentrations of uranyl ions are simulated in the presence of CNTs functionalized with different functional groups such as  $\text{-COO}^-$  and  $\text{-OH}$ . The modification in the adsorption capacity of bare and functionalized CNT with respect to uranyl ions due to variation in type and number of functional group, and uranyl ion concentration in the solution is analyzed.

These chapters are followed by **Chapter 7** which highlights the conclusions and important findings of the work. A brief summary of the work described so far has been presented in this chapter. This chapter also describes how the present work can be extended in the related field of research in near future.

## References

1. T. Nguyen, M. Duvail, A. Villard, J. J. Molina, P. Guilbaud and J. Dufrêche, *J. Chem. Phys.*, **2015**, *142*, 024501.
2. P. D'Angelo, A. Zitolo, V. Migliorati, G. Chillemi, M. Duvail, P. Vitorge, S. Abadie and R. Spezia, *Inorg. Chem.*, **2011**, *50*, 4572.
3. C. Marie, M. Miguiriditchian, D. Guillaumont, A. Tosseng, C. Berthon, P. Guilbaud, M. Duvail, J. Bisson, D. Guillaneux, M. Pipelier and D. Dubreuil, *Inorg. Chem.*, **2011**, *50*, 6557.
4. M. Duvail, A. Ruas, L. Venault, P. Moisy and P. Guilbaud, *Inorg. Chem.*, **2010**, *49*, 519.
5. R. Spezia, M. Duvail, P. Vitorge and P. D'Angelo, *J. Phys.: Conf. Ser.*, **2009**, *190*, 012056.
6. R. Spezia, C. Beuchat, R. Vuilleumier, P. Dangelo and L. Gagliardi, *J. Phys. Chem. B*, **2012**, *116*, 6465.
7. J. Jiang, J. C. Renshaw, M. J. Sarsfield, F. R. Livens, D. Collison, J. M. Charnock and H. Eccles, *Inorg. Chem.*, **2003**, *42*, 1233.
8. A. Ruas, P. Guilbaud, C. den Auwer, C. Moulin, J.-P. Simonin, P. Turq and P. Moisy, *J. Phys. Chem. A*, **2006**, *110*, 11770.
9. A. Ruas, O. Bernard, B. Caniffi, J.-P. Simonin, P. Turq, L. Blum and P. Moisy, *J. Phys. Chem. B*, **2006**, *110*, 3435.
10. P. G. Allen, J. J. Bucher, D. K. Shuh, N. M. Edelstein and T. Reich, *Inorg. Chem.*, **1997**, *36*, 4676.
11. A. Ikeda-Ohno, C. Hennig, S. Tsushima, A. C. Scheinost, G. Bernhard and T. Yaita, *Inorg. Chem.*, **2009**, *48*, 7201.
12. S. Cotton, *Lanthanide and Actinide Chemistry, IC: A Textbook Series*, Wiley, 2007.

13. V. Vallet, U. Wahlgren, B. Schimmelpfennig, H. Moll, Z. Szab and I. Grenthe, *Inorg. Chem.*, **2001**, *40*, 3516.
14. C. Hennig, J. Tutschku, A. Rossberg, G. Bernhard and A. C. Scheinost, *Inorg. Chem.*, **2005**, *44*, 6655.
15. L. Soderholm, S. Skanthakumar and R. E. Wilson, *J. Phys. Chem. A*, **2011**, *115*, 4959.
16. M. Aaberg, D. Ferri, J. Glaser and I. Grenthe, *Inorg. Chem.*, **1983**, *22*, 3986.
17. J. Neuefeind, L. Soderholm and S. Skanthakumar, *J. Phys. Chem. A*, **2004**, *108*, 2733.
18. L. Soderholm, S. Skanthakumar and J. Neuefeind, *Anal. Bioanal. Chem.*, **2005**, *383*, 48.
19. Y. Tianxiao and B. E. Bursten, *Inorg. Chem.*, **2006**, *45*, 5291.
20. D. Hagberg, E. Bednarz, N. M. Edelstein and L. Gagliardi, *J. Am. Chem. Soc.*, **2007**, *129*, 14136.
21. M. Duvailm and P. Guilbaud, *Phys. Chem. Chem. Phys.*, **2011**, *13*, 5840.
22. A. Ruas, P. Moisy, J.-P. Simonin, O. Bernard, J.-F. Dufreche and P. Turq, *J. Phys. Chem. B*, **2005**, *109*, 5243.
23. S. O. Odoh and G. Schreckenbach, *J. Phys. Chem. A*, **2011**, *115*, 14110.
24. M. Duvail, F. Martelli, P. Vitorge and R. Spezia, *J. Chem. Phys.*, **2011**, *135*, 044503.
25. M. Hirata, P. Guilbaud, M. Dobler and S. Tachimori, *Phys. Chem. Chem. Phys.*, **2003**, *5*, 691.
26. S. Spencer, L. Gagliardi, N. C. Handy, A. G. Ioannou, C.-K. Skylaris, A. Willetts and M. A. Simper, *J. Phys. Chem. A*, **1999**, *103*, 1831.
27. P. J. Hay, R. L. Martin and G. Schreckenbach, *J. Phys. Chem. A*, **2000**, *104*, 6259.
28. L. Hemmingsen, P. Amara, E. Ansoborlo and M. J. Field, *J. Phys. Chem. A*, **2000**, *104*, 4095.
29. S. Tsushima, T. Yang and A. Suzuki, *Chem. Phys. Lett.*, **2011**, *334*, 365.



30. C. Clavagura-Sarrio, V. Brenner, S. Hoyau, C. J. Marsden, P. Milli and J.-P. Dognon, *J. Phys. Chem. B*, **2003**, *107*, 3051.
31. D. Hagberg, G. Karlström, B. O. Roos and L. Gagliardi, *J. Am. Chem. Soc.*, **2005**, *127*, 14250.
32. C. Beuchat, D. Hagberg, R. Spezia and L. Gagliardi, *J. Phys. Chem. B*, **2010**, *114*, 15590.
33. X. Ye, S. Cui, V. de Almeida and Bamin Khomami, *J. Phys. Chem. B*, **2009**, *113*, 9852.
34. G. R. Choppin and M. K. Khankhasayev, *Chemical Separation Technologies and Related Methods of Nuclear Waste Management: Applications, Problems, and Research Needs*, 1st ed., Springer, New York, 1999, p 320.
35. G. R. Choppin and M. K. Khankhasayev, and H. S. Plendl, *Chemical Separations in Nuclear Waste Management: The State of the Art and a Look to the Future*, Battelle Press, Columbus, OH, 2002, p 96.
36. A. L. Mills and W. R. Logan, *Solvent Extraction Chemistry*, North- Holland, Amsterdam, Netherlands, 1967, p 322.
37. M. Jayasinghe and T. L. Beck, *J. Phys. Chem. B*, **2009**, *113*, 11662.
38. *Department of Energy Five Year Plan FY 2007-FY 2011*, Vol. 2, 2006.  
[http://www.em.doe.gov/PDFs/170016EM\\_FYP\\_Final\\_3-6-06.pdf](http://www.em.doe.gov/PDFs/170016EM_FYP_Final_3-6-06.pdf).
39. R. J. Frick, T. S. Hofer, A. B. Pribil, B. R. Randolph and B. M. Rode, *Phys. Chem. Chem. Phys.*, **2010**, *12*, 11736.
40. V-. A. Glezakou and W. A. deJong, *J. Phys. Chem. A*, **2011**, *115*, 1257.
41. I. Anicin, R. Banjanac, A. Dragic, D. Jokovic and V. Udovicic, *Phys. Scripta*, **2005**, *T118*, 39.
42. J. A. Greathouse, R. J. O'Brien, G. Bemis and R. T. Pabalan, *J. Phys. Chem. B*, **2002**, *106*, 1646.

43. S. P. Pasilis and A. Blumenfeld, *Inorg. Chem.*, **2011**, 50, 8302.
44. Z. S. A. Yu and K. J. Stetzenbach, *Geochemical modeling of solubility and speciation of uranium, neptunium, and plutonium*. Paper 66. University of Nevada, Las Vegas, 2007.
45. U. Wahlgren, H. Moll, I. Grenthe, B. Schimmelpfennig, L. Maron, V. Vallet and O. Groppen, *J. Phys. Chem. A*, **1999**, 103, 8257.
46. D. Hagberg, G. Karlstrom, B. O. Roos and L. Gagliardi, *J. Am. Chem. Soc.*, **2005**, 127, 14250.
47. J. Roques, E. Veilly and E. Simoni, *Int. J. Mol. Sci.*, **2009**, 10, 2633.
48. J. H. Lee, Z. Wang, J. Liu and Y. Lu, *J. Am. Chem. Soc.*, **2008**, 130, 14217.
49. G. M. Schneider, E. Stahl and G. Wilke. *Extraction with Supercritical Gases*, Verlag Chemie, Weinheim, 1980.
50. M. E. Paulaitis, J. M. L. Penninger, R.D. Gray and P. Davidson, *Chemical Engineering at Supercritical Fluid Conditions*, Ann Arbor Science, Ann Arbor, Mich., 1983.
51. J. M. L. Penninger, M. Radosz, M. A. McHugh and V. J. Krukoni, *Supercritical Fluid Techniques*, Elsevier, New York, 1985.
52. M. Perrut, *Proceedings of the International Symposium on Supercritical Fluids*, Societe Francaise de Chemie, Vandoeuvre, 1988.
53. K. P. Johnston and J. M. L. Penninger, *Supercritical Fluid Science and Technology*, American Chemical Society, Washington, D. C., 1989.
54. H. D. Cochran, L. L. Lee and D. M. Pfund, in *Fluctuation Theory of Mixtures*, edited by E. Matteoli and G. A. Mansoori, Taylor & Francis, New York, 1990, p. 69.
55. E. Kiran and J. M. H. Levelt Sengers, Eds. *Supercritical Fluids Fundamentals and Applications*, NATO ASI Series 271, Kluwer Academic Publishers: Dordrecht, The Netherlands, 1994.

56. J. M. H. Levelt Sengers, *Thermodynamics of Solutions Near the Solvent's Critical Temperature*. In *Supercritical Fluid Technology: ReViews in Modern Theory and Applications*; Bruno, T. J., Ely, J. F., Eds., CRC Press, Boston, 1991.
57. R. Fernandez-Prini and M. L. Japas, *Chem. Soc. ReV.*, **1994**, 23, 155.
58. C. A. Eckert; B. L. Knuston and P. G. Debenedetti, *Nature*, **1996**, 383, 313.
59. S. C. Tucker and M. W. Maddox, *J. Phys. Chem. B*, **1998**, 102, 2437.
60. C. A. Eckert, B. L. Knutson and P. G. Debenedetti, *Nature*, **1996**, 383, 313.
61. A. G. Kalinichev. *Molecular Simulations of Liquid and Supercritical Water: Thermodynamics, Structure, and Hydrogen Bonding. From: "Molecular Modeling Theory: Applications in the Geosciences"*, R. T. Cygan and J. D. Kubicki., Editors. *Reviews in Mineralogy and Geochemistry*, v.42, Mineralogical Society of America, Washington, D.C., 2001, pp. 83-130.
62. D. L. Norton, *Annu. Rev. Earth. Planet. Sci.*, **1984**, 12, 155.
63. T. Jupp and A. Schultz, *Nature*, **2000**, 403, 880.
64. M. K. Tivey, L. O. Olson, V. W. Miller and R. D. Light, *Nature*, **1990**, 346, 51.
65. K. L. Von Damm, *Annu. Rev. Earth Planet Sci.*, **1990**, 18, 173.
66. J. M. H. Levelt-Sengers, *Int. J. Thermophys.*, **1990**, 11, 399.
67. R. W. Shaw, T. B. Brill, A. A. Clifford, C. A. Eckert and E. U. Franck, *Chem & Eng News*, **1991**, 69, 26.
68. J. W. Tester, H. R. Holgate, F. J. Armellini, P. A. Webley, W. R. Killiea, G. T. Hong and H. E. Barner, *Supercritical water oxidation technology. In: Emerging Technologies in Hazardous Waste Management III*, ACS Symp. Series, 1993, 518, p 35-76.
69. IAEA, *Advanced Technologies for the Treatment of Low and Intermediate Level Radioactive Liquid Wastes*, International Atomic Energy Agency, Vienna, 1993.

70. M. Shibuya, T. Sasaki and S. Mihara, *Application of alkali activated slag cement for solidification of radioactive wastes in reprocessing plant*, Proc. 5th Int. Nuclear Conf. on Recycling, Conditioning and Disposal, Vol. 1, p. 285, 1998.
71. M. Asou, S. Tamura, T. Kobayashi, M. Toyohara, S. Miyamoto, T. Kikuchi, Y. Ikeda and M. Noguchi, *Oxide formation and vitrification of molten salt wastes from pyrochemical reprocessing*, Proc. 5th Int. Nuclear Conf. on Recycling, Conditioning and Disposal, Nice, France, Oct. 25–28, 1998, Vol. 1, p. 465.
72. A. D. Turner and R. M. Dell, *Atom*, **1984**, 327, 14.
73. T. Adschiri and K. Kanazawa, et al., *J. Am. Ceram. Soc.*, **1992**, 75, 2615.
74. W. S. Sheldrick and M. Wachhold, *Chem. Int. Ed. Engl.*, **1997**, 36, 206.
75. J. A. Darr and M. A. Poliakoff, *Chem. Rev.*, **1999**, 99, 195.
76. R. L. Smith, Jr., P. Atmaji, Y. Hakuta, T. Adschiri and K. Arai, *Separation of Metals from Simulated Mixed Waste Streams through Hydrothermal Crystallization in Supercritical Water*, Ph. Rudolph Von Rohr and Ch. Trepp (Eds.), High Pressure Chemical Engineering, Elsevier, Netherlands, 1996, 315.
77. R. L. Smith, Jr., P. Atmaji, Y. Hakuta, M. Kawaguchi, T. Adschji and K Arai, *J. Supercrit. Fluids*, **1997**, 11, 103.
78. E. A. Vogler, *Adv. Colloid Interface Sci.*, **1998**, 74, 69.
79. K. Ataka, T. Yotsuyanagi and M. Osawa, *J. Phys. Chem.*, **1996**, 100, 10664.
80. N. Choudhury, *J. Phys. Chem. B*, **2008**, 112, 6296.
81. N. Choudhury and B. M. Pettitt, *J. Am. Chem. Soc.*, **2005**, 127, 3556.
82. Y. Saito and S. Bandow *Introduction to Carbon Nanotubes*, Corona Publishing, Tokyo, 1998.
83. I. Hanasaki, A. Nakamura, T. Yonebayashi and S. Kawano. *J. Phys. Condens. Matter*, **2008**, 20, 015213.

84. M. J. O'Connell, *Carbon Nanotubes: Properties and Applications*, CRC Press, Boca Raton, FL, 2006.
85. S. Iijima, *Nature*, **1991**, 354, 56.
86. T. Nanok, N. Artrith, P. Pantu, P. A. Bopp and J. Limtrakul. *J. Phys. Chem. A*, **2009**, 113, 2103.
87. M. S. P. Sansom and P. C. Biggin, *Nature*, **2001**, 414, 156.
88. K. Koga, G. T. Gao, H. TanaKa and X. C. Zeng, *Nature*, **2001**, 412, 802.
89. H. Tanaka and K. Koga, *J. Chem. Phys.*, **2005**, 123, 094706.
90. P. K. Thallapally, G. O. Lloyd, J. L. Atwood and L. J. Barbour, *Angew. Chem., Int. Ed.*, **2005**, 44, 3848.
91. I. Kolesnikov, J. M. Zanotti, C. K. Loong, P. Thiyagarajan, A. P. Moravsky, R. O. Loutfy and C. J. Burnham, *Phys. Rev. Lett.*, **2004**, 93, 035503.
92. D. P. Cao, X. R. Zhang, J. F. Chen, W. C. Wang and J. Yun, *J. Phys. Chem. B*, **2003**, 107, 13286.
93. C. Liu, Y. Fan, H. T. Cong, H. M. Cheng and M. S. Dresselhaus, *Science*, **1999**, 286, 1127.
94. V. Sazonova, Y. Yaish, H. Ustunel, D. Roundy, T. A. Arias and P. L. McEuen, *Nature*, **2004**, 431, 284.
95. E. S. Snow, F. K. Perkins, E. J. Houser, S. C. Badescu and T. L. Reinecke, *Science*, **2005**, 307, 1942.
96. J. Kong, N. R. Franklin, C. W. Zhou, M. G. Chapline, S. Peng, K. J. Cho and H. J. Dai, *Science*, **2000**, 287, 5453.
97. N. G. Portney and M. Ozkan, *Anal. Bioanal. Chem.*, **2006**, 384, 620.
98. R. Singh, D. Pantarotto, L. Lacerda, G. Pastorin, C. Klumpp, M. Prato, A. Bianco and K. Kostarelos, *Proc. Natl. Acad. Sci. U.S.A.*, **2006**, 103, 3357.

99. B. J. Hinds, N. Chopra, T. Rantell, R. Andrews, V. Gavalas and L. G. Bachas, *Science*, **2004**, *303*, 5654.
100. A. Kalra, S. Garde and G. Hummer, *Proc. Natl. Acad. Sci. U.S.A.*, **2003**, *100*, 10175.
101. G. Hummer, J. C. Rasaiah and J. P. Noworyta, *Nature (London)*, **2001**, *414*, 188.
102. Y. Gogotsi, J. A. Libera, A. Guvenc-Yazicioglu and C. M. Megaridis, *Appl. Phys. Lett.*, **2001**, *79*, 1021.
103. K. Koga, G. T. Gao, H. Tanaka and X. C. Zeng, *Nature (London)*, **2001**, *412*, 802.
104. M. C. Gordillo and J. Marti, *Chem. Phys. Lett.*, **2000**, 329, 341.
105. O. Beckstein, P. C. Biggin and M. S. P. Sansom, *J. Phys. Chem. B*, **2001**, *105*, 12902.
106. R. Allen, S. Melchionna and J.-P. Hansen, *Phys. Rev. Lett.*, **2002**, *89*, 175502.
107. P. Wernet, D. Nordlund, U. Bergmann, M. Cavalleri, M. Odelius, H. Ogasawara, L. Naäslund, T. Hirsch, L. Ojamaäe, P. Glatzel, L. Pettersson and A. Nilsson, *Science*, **2004**, *304*, 995.
108. C. Peter and G. Hummer, *J. Biophys.*, **2005**, *89*, 2222.
109. B. Corry, *J. Phys. Chem. B*, **2008**, *112*, 1427.
110. T. A. Beu. *Comput. Phys. Commun.*, **2011**, *182*, 2004.
111. C. A. Monnig and R.T. Kennedy, *Capillary Electrophoresis*, Analytical Chemistry 66, 280–314, 1994.
112. A. M. Hollman and D. Bhattacharyya, *Langmuir*, **2004**, *20*, 5418.
113. S. Joseph, R. J. Mashl, E. Jakobsson and N. R. Aluru, *Nano Lett.*, **2003**, *3*, 1399.
114. M. Majumder, N. Chopra and B.J. Hinds, *J. Am. Chem. Soc.*, **2005**, *127*, 9062.
115. E. Winsberg, *Philosophy of Science*, **2003**, *70*, 105.
116. D. Frenkel and B. Smit, *Understanding Molecular Simulation*, Academic Press, 1996.
117. B. J. Alder and T. E. Wainwright, *J. Chem. Phys.*, **1957**, *27*, 1208.
118. B. J. Alder and T. E. Wainwright, *J. Chem. Phys.*, **1959**, *31*, 459.

119. A. Rahman, *Phys. Rev.*, **1964**, 136, A405.
120. W. D. Cornell, P. Cieplak, C. I. Bayly, I. R. Gould, K. M. Merz, D. M. Ferguson, D. C. Spellmeyer, T. Fox, J. W. Caldwell and P. A. Kollman, *J. Am. Chem. Soc.*, **1995**, 117, 5179.
121. W. L. Jorgensen, D. S. Maxwell and J. Tiradorives, *J. Am. Chem. Soc.*, **1996**, 118, 11225.
122. W. L. Jorgensen, J. Chandrasekhar, J. D. Madura, R. W Impey, and M. L. Klein, *J. Chem. Phys.*, **1983**, 79, 926.
123. E. Neria, S. Fischer and M. Karplus, *J. Chem. Phys.*, **1996**, 105, 1902.
124. P. Vanderploeg and H.J.C. Berendsen, *J. Chem. Phys.*, **1982**, 76, 3271.
125. H. J. C. Berendsen, J. R. Grigera and T. P. Straatsma, *J. Phys. Chem.*, **1987**, 91, 6269.
126. J. L. F. Abascal and C. A. Vega, *J. Chem. Phys.*, **2005**, 123, 234505.
127. M. W. Mahoney and W. L. Jorgensen, *J. Chem. Phys.*, **2000**, 112, 8910.
128. E. L. Pollock and B. J. Alder, *Physica*, **1980**, 102, 1.
129. P. Ewald, *Ann. Phys.*, **1921**, 369, 253.
130. P. Ewald, *Ann. Phys.*, **1921**, 64, 253.
131. T. Darden, D. York and L. Pedersen, *J. Chem. Phys.*, **1993**, 98, 10089.
132. L. Verlet, *Phys. Rev.*, **1967**, 159, 98.
133. T. R. Forester and W. Smith, *J. Comp. Chem.*, **1998**, 19, 102.
134. H. J. C. Berendsen, J. P. M. Postma, W. F. van Gunsteren, A. DiNola and J. R. Haak, *J. Chem. Phys.*, **1984**, 81, 3684.
135. G. Bussi, D. Donadio and M. Parrinello, *J. Chem. Phys.*, **2007**, 126, 014101.
136. S. Nose, *Molec. Phys.*, **1984**, 52, 255.
137. M. Parrinello and A. Rahman, *J. Appl. Phys.*, **1981**, 52, 7182.
138. D. A. McQuarrie, *Statistical Mechanics*, University Science book, 1975.

139. J. P. Hansen and I. R. McDonald, *Theory of Simple Liquids*, 2nd ed., Academic, London, 1986.
140. W. E. van Gunsteren and H. J. C. Berendsen, *Angew. chem. Int. Ed. Engl*, **1990**, 29, 992.
141. S. Kerisit, C. Liu, *Geochim. Cosmochim. Acta*, **2010**, 74, 4937.
142. I. Yeh and G. Hummer, *J. Phys. Chem. B*, **2004**, 108, 15873.
143. N. Choudhury, *J. Chem. Phys.*, **2010**, 133, 154515.
144. P. Guilbaud and G. Wipff, *J. Phys. Chem.*, **1993**, 97, 5685.
145. P. Guilbaud and G. Wipff, *J. Incl. Phenom. Mol. Chem.*, **1993**, 16, 169.
146. P. Guilbaud and G. Wipff, *J. Phys. Chem.*, **1996**, 366, 55.
147. N. Rai, S. P. Tiwari, E. J. Maginn, M. P. Brown and K. Austin, *J. Phys. Chem. B*, **2012**, 116, 10885.
148. V. Pomogaev, S. P. Tiwari, N. Rai, G. S. Goff, W. Runde, W. F. Schneider and E. J. Maginn, *Phys. Chem. Chem. Phys.*, **2013**, 15, 15954.
149. S. P. Tiwari, N. Rai and E. J. Maginn, *Phys. Chem. Chem. Phys.*, **2014**, 16, 8060.
150. L. Zhu, W. Duan, J. Xu, and Y. Zhu, *J. Hazard Mater.*, **2012**, 241-242, 456.
151. G. S. Was, P. Ampornrat, G. Gupta, S. Teyseyre, E. A. West, T. R. Allen, K. Sridharan, L. Tan, Y. Chen, X. Ren and C. Pister, *J. Nucl. Mater.*, **2007**, 371, 176.
152. G. Hummer, J. C. Rasaiah, and J. P. Noworyta, *Nature (London)*, **2001**, 414, 188.
153. J. K. Holt, H. P. Park, Y. Waang, M. Stadermann, A. B. Artyukhin, C. P. Grigopoulos, A. Noy and O. Bakajin, *Science*, **2006**, 312, 1034.
154. M. Majumder, N. Chopra, R. Andrews and B. J. Hinds, *Nature*, **2005**, 438, 44.
155. A. Berezhkovskii and G. Hummer, *Phys. Rev. Lett.*, **2002**, 89, 064503.



# *Chapter 2*

## **Structure and Dynamics of Bulk Water and Aqueous Uranyl Solution**



## 2.1 Introduction

With more and more expansion of nuclear power as a source of energy, the importance of radiotoxic actinyl ions is increasing. Understanding the behavior of radiotoxic actinyl ions in aqueous solutions is of fundamental as well as technological importance due to its direct relevance to the nuclear fuel cycle. As use of these ions in nuclear reactions gives rise to the generation of radioactive waste, the attempts are being made first, to minimize the waste by extracting the reusable material from it and then, to safely dispose the radioactive waste. Knowledge of hydration and transport properties of these actinyl ions is essential for designing advanced separation processes for recycling of the radiotoxic material in the waste. Also, the storage of radioactive waste temporarily or the permanent waste disposal involves geological matrices involving the groundwater system. Studying their behavior in aqueous solutions will help in understanding the migration characteristics of these radionuclides in hydrogeological conditions in geological structures. As the experimental investigations involving actinyl ions are quite difficult to execute because of their highly radiotoxic nature, molecular dynamics and other computational investigations have been shown to be a useful alternative for understanding the structural, dynamic and thermodynamic behavior of these ions.<sup>1-28</sup>

Theoretical studies involving actinyl ions in aqueous and other environments can be classified into two broad categories. In one hand, one can use computationally expensive quantum mechanical calculations and ab-initio molecular dynamics simulations<sup>14,16,25-27</sup> to understand the characteristics of uranyl ions in water clusters and bulk aqueous solutions. Garcia-Hernandez et al<sup>25</sup> and Buhl et al<sup>26,27</sup> have not only investigated the effect of counter ions on the stability of uranyl(VI) complexes but also predicted the free energy profile of the dynamic solvent exchange between the bulk and the solvation shell. On the other hand, force-field based classical molecular dynamics simulations, which provide a computationally

inexpensive but accurate enough method to understand structure as well as dynamics of these ions in different condensed phase environments, are extensively used now-a-days.<sup>1-4,6-9,12-13,19-</sup>

<sup>24</sup> In a classic review, Buhl and Wipff<sup>28</sup> have discussed the abilities of ab-initio MD simulations in the framework of Car-Parrinello approach as well as force-field based classical MD simulations to describe various aspects of coordination and solvation shell structures and energetics of different actinyl ions in presence of different counter-ions.

Although many literature reports deal with the structural arrangement of water molecules around the uranyl ions and the translational dynamics of various species in aqueous solutions of uranyl ions, studies on the orientational distribution and dynamics of water molecules in bulk water as well as in aqueous solutions of uranyl ions are rather few. For instance, Clavaguera-Sarrio<sup>17</sup> has carried out modeling of uranyl cation-water system and from the analysis of cation-water and water-water interactions it is shown that water molecules are strongly oriented around the uranyl cation. Frick et al.<sup>17</sup> have estimated the distribution of the first shell water molecules around the uranyl ion in terms of tilt angle (i.e. the angle between the plane defined by the three atoms of a water molecule and the straight line that connects uranium and the oxygen atom of the respective water) and the  $\Theta$  angle (i.e. the angle between the same straight line and the water dipole vector). The tilt and  $\Theta$  angles show peaks at around  $0^\circ$  and  $180^\circ$  respectively. Later, they extended the same approach to understand the orientational distribution of water molecules around uranyl (V) ( $\text{UO}_2^+$ ) cations.<sup>18</sup> The angular distribution of  $\text{O}_\text{U}-\text{U}-\text{O}_\text{U}$  angle showed a peak at around  $180^\circ$  which corresponds to a perfectly linear geometry with a tilt of not more than about  $10^\circ$ . The  $\text{O}_\text{W}-\text{U}-\text{O}_\text{W}$  angle showed two main peaks, one at around  $90^\circ$  and the other one close to  $180^\circ$  which corresponds to a square planar configuration.

In this Chapter, we will present the analysis of the structural and dynamical aspects of aqueous solution of uranyl ions along with its comparison with those of bulk water. The

structural characteristics of bulk water and aqueous solution of uranyl ions are presented in terms of radial distribution functions. The orientational structure of water around a uranyl ion has been thoroughly investigated by calculating different orientational probability distributions corresponding to different molecular axes of water. Translational dynamics of various species are studied in terms of mean squared displacement functions. Orientational dynamics of water about different molecular axes of water have also been analyzed.

## 2.2 Models and Simulation Details

In the present investigation, we have prepared aqueous solutions of divalent uranyl ions,  $\text{UO}_2^{2+}$ , by solvating one uranyl ion in a cubic box containing around 500 water molecules with a bulk water density of around 0.98 g/cc. The electro-neutrality of the system is maintained by introducing required number of negative ions (nitrate) in the system. Simulations are performed in canonical (NVT) ensemble with molecular dynamics extended system approach of Nose.<sup>29</sup> All the simulations are carried out at a target temperature of 298 K using periodic boundary conditions and minimum image convention in all three directions. We have used atomistic model with one uranium and two oxygen sites for the uranyl ion<sup>4</sup> and one nitrogen and three oxygen sites for the nitrate ion.<sup>1</sup> Non-bonded site-site inter-molecular interaction is modeled with Lennard–Jones (LJ) plus Coulomb interactions and intra-molecular interaction for uranyl and nitrate ions consist of bond and angle terms. TIP3P model has been used for water model. The potential energy of the system is given by Eq. 1.5 as given in Chapter 1, neglecting dihedral terms. The parameter sets for both inter- and intra-molecular interactions are given in Table 2.1. The LJ parameters for solvated uranyl ion are taken from the work of Rai et al.<sup>4</sup> whereas for water molecules, those reported by Jorgensen et al.<sup>30</sup> for TIP3P are taken. The parameters related to bonded interactions and the LJ parameters for the nitrate ion are taken from the work of Guilbaud et al.<sup>1</sup> All cross parameters

for the LJ potential were obtained by using Lorentz–Berthelot mixing rule. The equations of motion are integrated with a time step of 1 fs. For all nonbonding interactions, a cut-off distance of 12.0 Å in real space is used. For each system, the production run was for 1 ns after equilibration for 1 ns and the trajectories are saved at every 0.01 ps.

**Table 2.1: Force Field Parameters**

**Non-bonded Parameters**

Atom Type	$\sigma$ (nm)	$\epsilon$ (kJ)	$q/e$
U	0.335	0.1145	+2.500
O <sub>U</sub> (Uranyl oxygen)	0.285	1.8328	-0.250
N	0.312	0.6694	+0.626
O <sub>N</sub> (Nitrate oxygen)	0.294	0.6276	-0.542
O <sub>W</sub> (TIP3P)	0.315	0.6364	-0.834
H <sub>W</sub> (TIP3P)	-	-	+0.417

**Bonded Parameters**

Bond Type	$r_{eq}$ (nm)	$K_r$ (kJ mol <sup>-1</sup> nm <sup>-2</sup> )
U-O <sub>U</sub>	0.180	418400
N-O <sub>N</sub>	0.126	251040

Angle Type	$\theta_{eq}$ (°)	$K_\theta$ (kJ mol <sup>-1</sup> rad <sup>-2</sup> )
O <sub>U</sub> -U-O <sub>U</sub>	180	1255.2
O <sub>N</sub> -N-O <sub>N</sub>	120	1255.2

## 2.3 Results and Discussion

The structure and dynamics of aqueous solution of uranyl ions have been estimated using MD simulations and compared with that of bulk water system. The structural aspects are analyzed by calculating radial distribution functions (RDF) of water around different sites of the uranyl ion in aqueous solutions and water around central water molecule in bulk water system. Translational dynamics of different species including water molecules, uranyl and nitrate ions has been investigated by analyzing mean squared displacement (MSD) of the corresponding species in solution. The orientational dynamics of water is also investigated by calculating orientational correlation functions around different molecular axes of the water molecules. All these results pertaining to the aqueous uranyl solution are presented in the following subsections.

### 2.3.1 Radial Distribution of Water Molecules around Uranyl Ions in Aqueous Solutions

In order to investigate the structural arrangements of water molecules around uranyl ions in the aqueous solution, we have calculated RDFs of two different water sites ( $O_w$  and  $H_w$ ) with respect to two uranyl sites ( $U$  and  $O_U$  of uranyl ion) which are presented in Figure 2.1. First hydration shell of uranium atom of the uranyl ion as indicated by a sharp peak (see Figure 2.1(a)) is observed to be at a distance of 2.44 Å; whereas first peak of  $H_w$  RDF (see Figure 2.1(b)) around  $U$  appears at 3.12 Å. Thus, the  $O_w$  atom of water is closer to the uranium of  $UO_2^{2+}$  as compared to  $H_w$  atom of water. Around the oxygen atom of the uranyl ion,  $O_w$  sites of water are distributed with first peak at around 3.0 Å (see Figure 2.1(c)); whereas RDF for hydrogen ( $H_w$ ) atoms of water shows a broad first peak with two small humps at around 3.2 Å and 3.7 Å (see Figure 2.1(d)). It is surprising to notice that water oxygen ( $O_w$ ) comes closer to  $O_U$  of the uranyl ion than  $H_w$  of water. This is probably because

of the fact that large positive charge (+2.5) on U site overcompensates the negatively charged oxygen atoms leading to an overall positively charged environment around the uranyl ion as a whole. Similar RDFs have been reported in many previous investigations on uranyl ion.<sup>1,2,4,16,17,19,20</sup> The first minimum for distribution of  $O_w$  atoms around uranium and oxygen atoms of uranyl ion comes at around 3.0 Å and 4.1 Å respectively and this value is used as the radius of the first coordination shells around respective atoms of uranyl ion for calculating coordination number and analyzing dynamical behavior of the solvation water (discussed in Chapter 3).

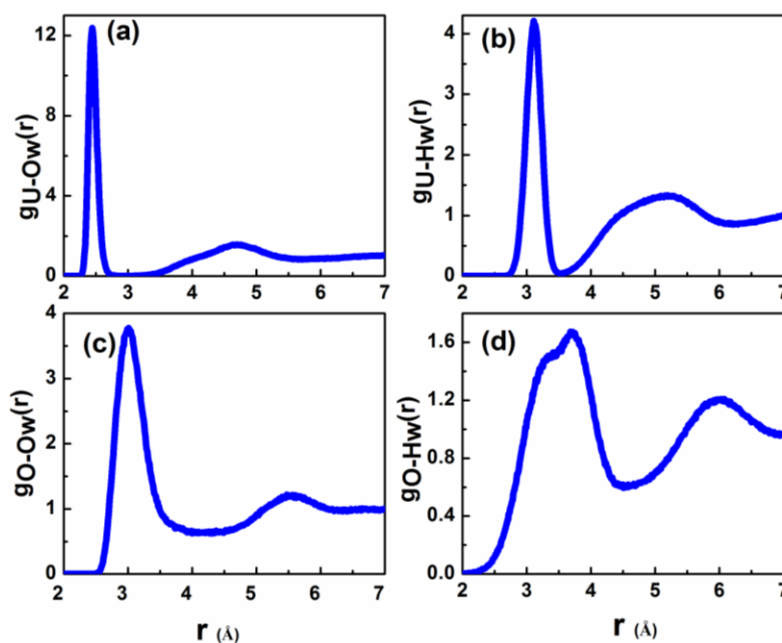


**Figure 2.1: Radial distribution functions for (a)  $O_w$  around uranium, (b)  $H_w$  around uranium (c)  $O_w$  around uranyl-oxygen ( $O_U$ ) and (d)  $H_w$  around  $O_U$  in the aqueous uranyl solution.**

Similarly, the RDFs for bulk water are given in Figure 2.2 where the distribution of oxygen ( $O_w$ ) and hydrogen ( $H_w$ ) atoms of water molecules with respect to the oxygen atom of the central water molecule is demonstrated. In  $O_w$ - $O_w$  RDF, a single peak is observed at a radial distance of around 2.78 Å followed by bulk behavior. However, two peaks (1.82 Å and



3.22 Å) are present in case of  $O_w-H_w$  RDF corresponding to two hydrogen atoms of the water molecule. Similar RDFs have been reported in literature related to structural distribution for TIP3P water.<sup>31,32</sup>

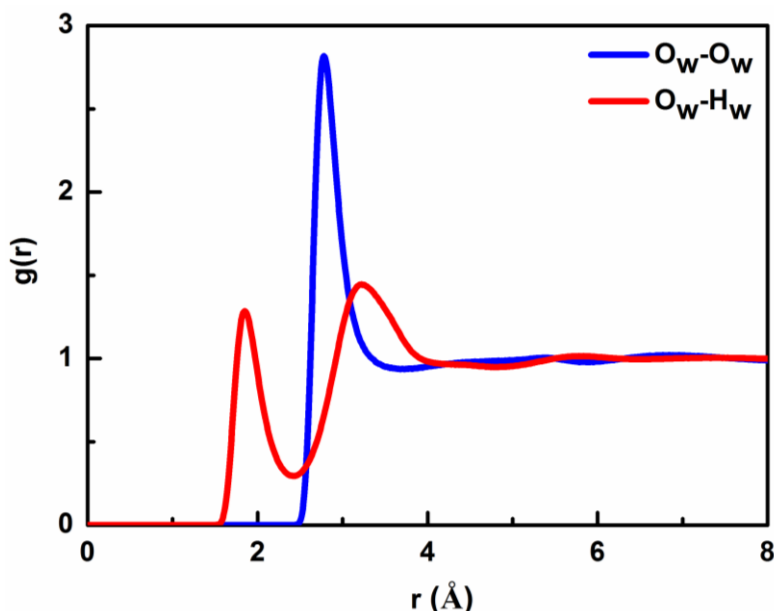


**Figure 2.2: Radial distribution functions for (a) oxygen,  $O_w$  and (b) hydrogen,  $H_w$  around the oxygen atom of the central water molecule in bulk water.**

### 2.3.2 Orientational Distribution of Water Molecules in the Vicinity of Uranyl Ions

We have calculated angular distributions of the water molecules around uranyl ion in its first coordination shell (FCS) and second coordination shell in the aqueous solution of uranyl ions. The first coordination or solvation shell boundary is defined by the position of first minimum (3.0 Å), whereas the lower and upper boundaries of the second coordination or solvation shell are defined by the first minimum and second minimum (5.5 Å) of the respective radial distribution functions,  $g(r)$ . We have considered four different angles (Figure 2.3), namely, angle formed between the line joining uranium atom of the uranyl ion and oxygen atom of the solvation water molecule (i.e. U- $O_w$  distance vector) and (i) water dipole moment vector ( $\theta$ ), (ii) a vector perpendicular to plane of water molecule ( $\psi$ ), (iii) O-H bond

vector ( $\gamma$ ) and (iv) U-O<sub>U</sub> bond vector ( $\chi$ ), O<sub>U</sub> being the oxygen atom of uranyl ion. The distribution of these angles for the water molecules in the first and second coordination shells of uranyl ions are shown in Figure 2.4 (a) and (b) respectively. In Figure 2.4 (a), the distribution of  $\theta$  reveals a peak at around  $0^\circ$  with a spread in the distribution of around  $22^\circ$  indicating that the dipole moment vectors of the FCS water molecules are directed along the U-O<sub>W</sub> vector as demonstrated earlier by Frick et al.<sup>17</sup> Thus  $\theta=0^\circ$  reveals that H atoms of water are away from the U of UO<sub>2</sub>.

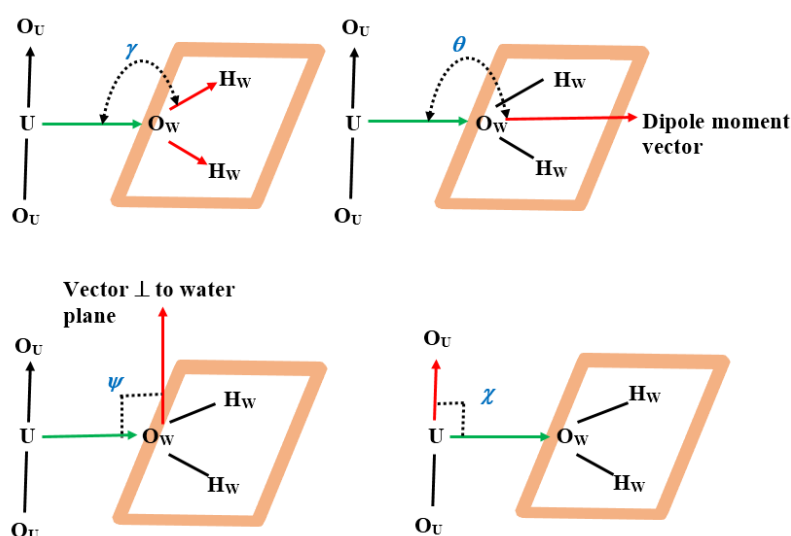


**Figure 2.3: Schematic representation of various angles considered for orientational distribution of the water molecules around uranyl ions.**

As the water dipole moment vector and U-O<sub>W</sub> vectors point in the same direction, it is expected that the plane-perpendicular (CR) vector will be perpendicular to U-O<sub>W</sub> vector and in fact, the distributions for  $\psi$  shows a peak at around  $90^\circ$ . This result is consistent with the tilt angle distribution given by Frick et al.<sup>17</sup> The distribution of  $\gamma$  has a peak at around  $52.4^\circ$ , which is consistent with other orientations (Figure 2.4a); in particular the dipole orientation of  $0^\circ$ . The peak corresponding to  $90^\circ$  for angle  $\chi$  indicates that the U-O<sub>U</sub> bond vector preferably remains perpendicular to U-O<sub>W</sub> vector. All these orientational distributions suggest that the

water molecule stays in a plane perpendicular to  $O_U-U-O_U$  line ( $UO_2$  being almost a linear molecule) passing through the uranium atom of  $UO_2$  (see Figure 2.5). The analysis of Figure 2.4 (b) shows that the water molecules within the second coordination shell of uranium atom do not show such preferred orientations as evident from the comparison of the intensities of different distributions in Figure 2.4(a) with the corresponding distributions in Figure 2.4(b).

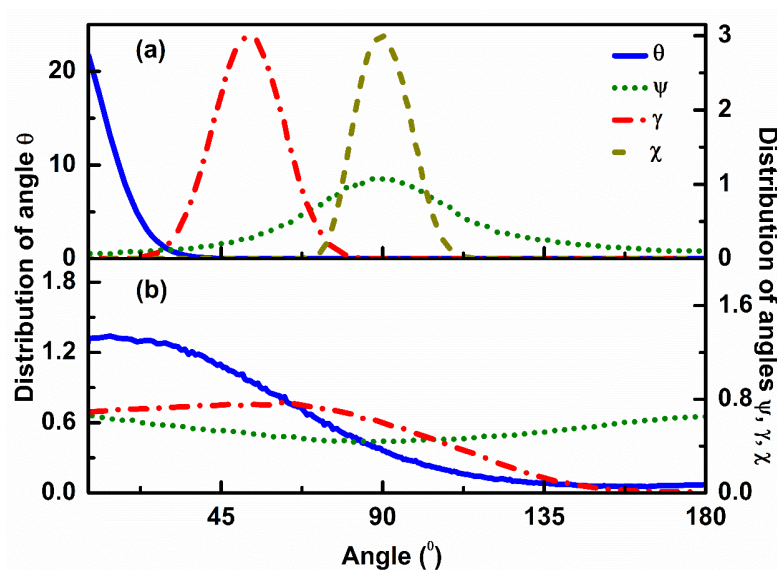


**Figure 2.4: Distributions of various angles between U-O<sub>w</sub> vector and different molecular orientational vectors of a water molecule in the (a) first and (b) second coordination shells of a uranyl ion.**

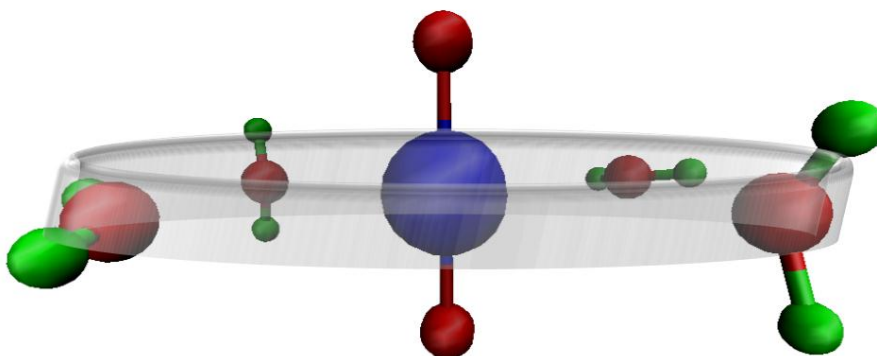


**Figure 2.5: Pictorial representation of water molecules in the first coordination shell of a linear  $UO_2$  molecule.**

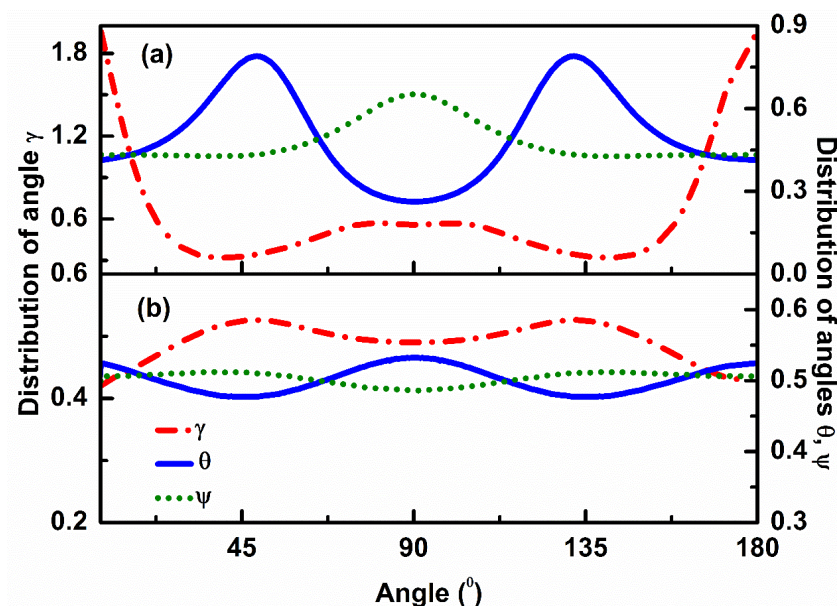


**Figure 2.6: Distributions of angles between Ow-Ow vector and different molecular orientational vectors of a water molecule in the (a) first and (b) second coordination shells of a central water molecule in bulk water. The angles are defined in the same way as in Figure 2.3 except that the  $\text{UO}_2$  ion is replaced by a water molecule.**

For comparison, the angular distributions of water molecules around a central water molecule have also been estimated for bulk water i.e. for a water molecule in the solvation shell of another water molecule. Here, the angles are considered between OW-OW distance vector and three molecular orientational vectors of the water molecules as mentioned above within first and second coordination shells. A water molecule around a central water molecule can act as a hydrogen bond acceptor or donor depending on whether it offers its oxygen or hydrogen atom for the formation of hydrogen bond with the central molecule. Depending on this, the OH bond vector can form two angles with the OW-OW vector; one at 0° and another at 180° and in fact we found (see Figure 2.6(a)) these two peaks in the distribution of angle  $\gamma$ . If a neighbor acts as a hydrogen donor, then the OH bond should point towards the central OW and in that case the dipole moment vector should form an angle with the OW-OW vector of around 126°; whereas for an acceptor, the angle should be around 54° and in fact, two

peaks at  $\theta$  equals to 1260 and 540 are observed in this case. As expected, the angle  $\psi$  shows a peak at 900 as it is a vector perpendicular to the plane of water molecules and hence to the OW-OW vector. As in the case of aqueous solution of uranyl ions, the water molecules in the second coordination shell of a central water molecule in bulk water also do not show much preference to any particular orientation (see Figure 2.6(b)).

### 2.3.3 Translational Dynamics of Different Species in the Aqueous Uranyl Solution

For dynamical aspects, we analyze the dynamic behavior of different species in the aqueous uranyl solution. The translational dynamics is analyzed in terms of MSD of uranium atom of the uranyl, nitrogen atom of the nitrate ions and oxygen atom of water molecules as shown in Figure 2.7. The mean squared displacements for different ions and water molecules reveal considerable difference in diffusivities of these species.

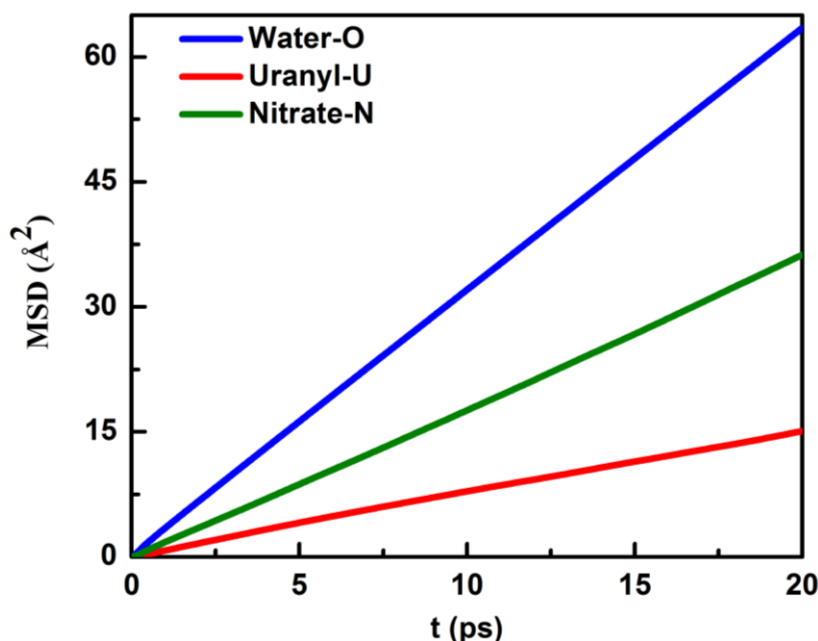


**Figure 2.7: MSD for oxygen of water (blue line), uranium of uranyl (red line) and nitrogen of nitrate (green line) in the aqueous solution of uranyl ion.**

The sequence of decreasing diffusivities as observed from the slopes of the MSD curves is oxygen (water) > nitrogen (nitrate) > uranium (uranyl) (see Figure 2.7). Water is the

most mobile of all the species. It is not surprising that uranium being the heaviest atom in the system has the lowest diffusivity. Nitrogen has diffusivity in between that of uranium and water  $O_w$ . The estimation of diffusivity from the slope of MSD curves is discussed in the following chapter i.e. Chapter 3.

### 2.3.4 Orientational Dynamics of Water Molecules in the Aqueous Uranyl Solution

The orientational dynamics of the water molecules are analyzed by calculating time correlation functions of various molecular vectors of water as explained in Section 1.5, Eq. 1.21 of Chapter 1. The first ( $n=1$ ) and second ( $n=2$ ) order autocorrelation functions for the above mentioned three unit vectors are given in Figure 2.8. As the figure suggests, there is a little anisotropy in case of  $\Gamma_1$ . Similar anisotropy is also found to be present in the rotational correlation function of bulk TIP3P water (Figure 2.9).

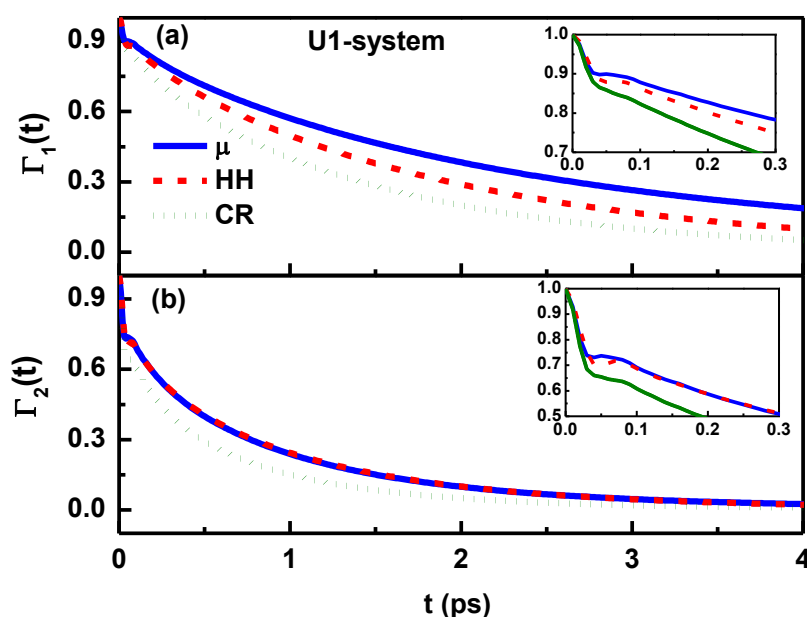


**Figure 2.8:** (a) First order and (b) second order angular dynamics of water molecules with respect to water dipole moment vector ( $\mu$ ; blue solid line), water H-H vector (HH; red dashed line) and water cross vector (CR; green dotted line).

The anisotropy is almost absent in case of  $\Gamma_2$ . The orientational correlation functions for water vectors are found to be more or less the same, both for bulk water as well as aqueous solution of uranyl ion. Similar observations have been reported by Praprotnik and Janezic<sup>33</sup> while applying the new symplectic MD integrators to perform MD simulations of bulk water. The faster relaxation in case of cross vector as obtained in present work as compared to HH and dipole moment vector in this order is consistent with the trend reported by them. This orientational anisotropy of water has also been confirmed by some of the experimental studies.<sup>34-36</sup> Water is a hydrogen bonded network forming liquid and the anisotropy in orientational relaxation may be a consequence of some preferred orientation to maintain the tetrahedral local structure.

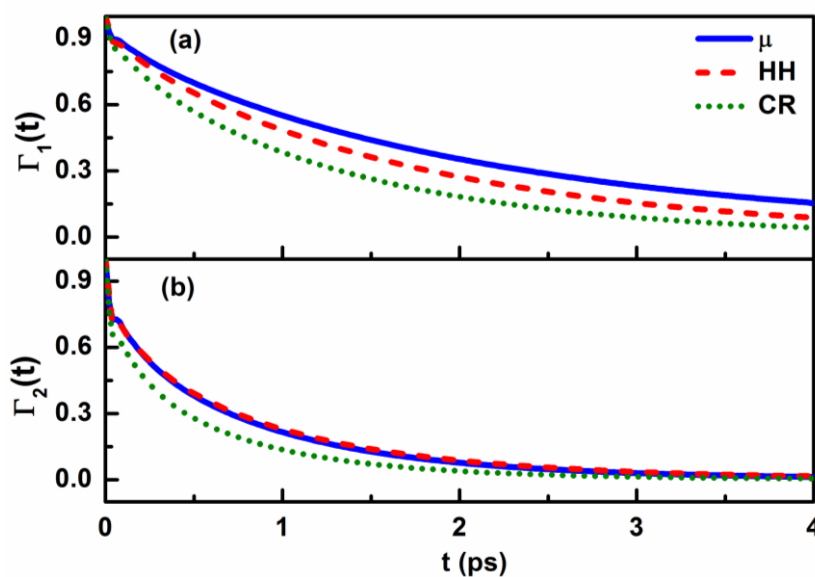


**Figure 2.9: (a) First order and (b) second order angular dynamics of water molecules with respect to water dipole moment vector ( $\mu$ ; blue solid line), water H-H vector (HH; red dashed line) and water cross vector (CR; green dotted line) in bulk water.**

Visual inspection of the plots of the orientational correlation functions as shown in Figure 2.8 insets, indicates that there are two timescales in the relaxation of these functions: a very fast decay initially followed by a long-time relaxation. Therefore, in order to assess the two timescales, we have used a double exponential function  $S(t)$  of the form

$$S(t) = A \exp\left(-\frac{t}{\tau_1}\right) + (1 - A) \exp\left(-\frac{t}{\tau_2}\right), \quad (2.1)$$

to fit the orientational time correlation functions. In the above equation,  $\tau_1$  and  $\tau_2$  represents respectively the time constants of longer and shorter time scales of the relaxation of  $S(t)$ , with  $A$  and  $(1-A)$  respectively being their relative contributions.<sup>37</sup> The fitting of such a curve and estimation of relaxation times is discussed further in Chapter 3.

## 2.4 Conclusions

In summary, behavior of aqueous solutions of uranyl ions is studied by analyzing both structural and dynamical aspects. The arrangement of water molecules around uranyl ion in the aqueous uranyl solution is demonstrated in terms of radial distribution of water around the uranyl ion. A comparison of the diffusivities of uranyl ions, water and nitrate ions indicates uranyl ions diffuse slower than nitrate ions as well as water. It is expected as the uranyl ion is heavier than nitrate ion, which in turn is heavier than water. The angular distributions of water within the first coordination shell of uranium atoms have demonstrated that dipole moment vectors of water molecules are oriented along U-O<sub>w</sub> distance vector and all other orientational vectors show consistent orientations. Moreover, all these orientational distributions suggest that the water molecule stays in a plane perpendicular to O<sub>U</sub>-U-O<sub>U</sub> line passing through the uranium atom of UO<sub>2</sub>. Similarly, the angular distributions of various angles made by the different vectors of the water molecule with respect to the central water molecule in bulk water system are presented. The rotational dynamics of water in terms of orientational time correlation functions have also been estimated. The results showed a little anisotropy among different vectors of water in terms of orientational dynamics. The above results are presented for an aqueous solution containing a single uranyl ion. Water being a hydrogen-bonded liquid with tetrahedral structure, it is very likely that presence of a large



number of ions will modify the hydrogen-bonding and tetrahedral structure of water and therefore it is expected that the dynamics of the solution will also be modified with increasing concentration of the ions. Apart from that, many of the properties of the aqueous solution are susceptible to change with the change in temperature. Hence, the effect of increasing uranyl ion concentration as well as of the temperature of the system on the various structural and dynamical features of aqueous solutions of uranyl ions is studied and analyzed in the next chapter i.e. Chapter 3.

## References

1. P. Guilbaud and G. Wipff, *J. Phys. Chem.*, **1993**, 97, 5685.
2. P. Guilbaud and G. Wipff, *J. Incl. Phenom. Mol. Chem.*, **1993**, 16, 169.
3. P. Guilbaud and G. Wipff, *J. Phys. Chem.*, **1996**, 366, 55.
4. N. Rai, S. P. Tiwari, E. J. Maginn, M. P. Brown and K. Austin, *J. Phys. Chem. B*, **2012**, 116, 10885.
5. F. Hutschka, A. Dedieu, L. Troxler and G. Wipff, *J. Phys. Chem. A*, **1998**, 102, 3773.
6. M. Baaden, F. Berny, C. Madic and G. Wipff, *J. Phys. Chem. A*, **2000**, 104, 7659.
7. A. Chaumont and G. Wipff, *Inorg. Chem.*, **2003**, 42, 5348.
8. A. Chaumont and G. Wipff, *Inorg. Chem.*, **2004**, 43, 5891.
9. R. Schurhammer, and G. Wipff, *J. Phys. Chem. A*, **2005**, 109, 5208.
10. M. Bühl, N. Sieffert, A. Chaumont and G. Wipff, *J. Am. Chem. Soc.*, **2006**, 128, 6357.
11. M. Bühl, N. Sieffert, A. Chaumont and G. Wipff, *Inorg. Chem.*, **2012**, 51, 1943.
12. S. Kerisit and C. Liu, *J. Phys. Chem. A*, **2013**, 117, 6421.
13. S. Kerisit and C. Liu, *Geochim Cosmochim. Acta*, **2010**, 74, 4937.
14. S. Spencer, L. Gagliardi, N. C. Handy, A. G. Ioannou, C. Skylaris, A. Willetts and A. M. Simper, *J. Phys. Chem. A*, **1999**, 103, 1831.

15. C. Clavaguera-Sarrio, V. Brenner, S. Hoyau, C. J. Marsden, P. Millie and J. P. Dognon, *J. Phys. Chem. B*, **2003**, *107*, 3051.
16. D. Hagberg, G. Karlstrom, B. O. Roos and L. Gagliardi, *J. Am. Chem. Soc.*, **2005**, *127*, 14250.
17. R. J. Frick, T. S. Hofer, A. B. Pribil, B. R. Randolph and B. M. Rode, *J. Phys. Chem. A*, **2009**, *113*, 12496.
18. R. J. Frick, T. S. Hofer, A. B. Pribil, B. R. Randolph and B. M. Rode, *Phys. Chem. Chem. Phys.*, **2010**, *12*, 11736.
19. J. A. Greathouse, R. J. O'Brien, G. Bemis and R. T. Pabalan, *J. Phys. Chem. B*, **2002**, *106*, 1646.
20. T. Patsahan and M. Holovko, *Condens. Matter Phys.*, **2007**, *10*, 143.
21. M. Jayasinghe and T. L. Beck, *J. Phys. Chem. B*, **2009**, *113*, 11662.
22. X. Ye, R. B. Smith, S. Cui, V. de Almeida and B. Khomami, *Solvent Extr. Ion Exc.*, **2010**, *28*, 1.
23. V. Pomogaev, S. P. Tiwari, N. Rai, G. S. Goff, W. Runde, W. F. Schneider and E. J. Maginn, *Phys. Chem. Chem. Phys.*, **2013**, *15*, 15954.
24. S. P. Tiwari, N. Rai and E. J. Maginn, *Phys. Chem. Chem. Phys.*, **2014**, *16*, 8060.
25. M. Garcia-Hernandez, C. Willnauer, S. Kruger, L. V. Moskaleva and N. Rosch, *Inorg. Chem.*, **2006**, *45*, 1356.
26. M. Buhl and H. Kabrede, *Inorg. Chem.*, **2006**, *45*, 3834.
27. M. Buhl, G. Schreckenbach, N. Sieffert and G. Wipff, *Inorg. Chem.*, **2009**, *48*, 9977.
28. M. Buhl and G. Wipff, *Chem. Phys. Chem.*, **2011**, *12*, 3095.
29. M. P. Allen and D. J. Tildesley, *Computer Simulation of Liquids*; Oxford University, New York, 2004.

30. W. L. Jorgensen, J. Chandrashekhara, J. D. Madura, R. W. Impey and M. L. Klein, *J. Chem. Phys.*, **1983**, 79, 926.
31. P. Mark and L. Nilsson, *J. Phys. Chem. A*, **2001**, 105, 9954.
32. V. S. Indrajith and N. Baskaran, *AIP Conf. Proc.*, **2015**, 1665, 040002.
33. M. Praprotnik and D. Janezic, *J. Chem. Phys.*, **2005**, 122, 174103.
34. B. Halle and H. Wennerstrom, *J. Chem. Phys.*, **1981**, 75, 1928.
35. A. Wallqvist and B. J. Berne, *J. Chem. Phys.*, **1993**, 97, 13841.
36. J. Jonas, T. DeFries and D. J. Wilbur, *J. Chem. Phys.*, **1976**, 65, 582.
37. N. Choudhury, *J. Chem. Phys.*, **2010**, 133, 154515.



# *Chapter 3*

## **Effect of Uranyl Ion Concentration and Temperature on Structure and Dynamics of Aqueous Uranyl Solution**



### 3.1 Introduction

The pioneering work of Guilbaud and Wipff<sup>1-3</sup> on molecular dynamics simulation studies of aqueous solution of uranyl ions helps us to understand various aspects of uranyl hydration. On one hand, they have studied the complexation and hydration behavior of uranyl ions<sup>1-2,4-9</sup> and on the other hand they have generated force field parameters for uranyl ions from free energy calculations.<sup>3</sup> Wipff and coworkers<sup>10</sup> have carried forward their work on the behavior of uranyl and lanthanide ions in different solvation media. A detailed study on structure and free energy of uranyl hydration has also been presented recently by Rai et al.<sup>11</sup> and Kerisit et al.<sup>12</sup> Based on the free energy calculation, they have proposed modified force-fields for the uranyl-water system. These groups have also studied the bulk diffusion of uranyl ions at infinite dilution.<sup>13-15</sup> Kerisit et al.<sup>12,13</sup> have also generated a modified force-field of uranyl-water system based on free energy calculations to study in detail the structure, diffusion and free energy of uranyl hydration.

In a series of investigations, Maginn and coworkers<sup>11,14</sup> have developed force fields for the different actinyl ions in their aqueous solution by taking into account the many-body solvation effects. Using this force field, Rai et al.<sup>11</sup> presented a detailed study on the radial and three-dimensional arrangements of water molecules in the solvation shell of the uranyl ions. In most of these studies structural arrangement of water molecules around the uranyl ions and free energy aspect of uranyl hydration have been investigated. Very recently, Maginn and coworkers<sup>15</sup> have studied translational dynamics and residence time of water in the solvation shell of different actinyl ions. There have been other researchers who have studied the characteristics of uranyl ion using first principle calculations or molecular dynamics simulations. For instance, Spencer et al.<sup>16</sup> have studied the hydration of the actinyl cations, uranyl ( $\text{UO}_2^{2+}$ ) and plutonyl ( $\text{PuO}_2^{2+}$ ), by performing Kohn-Sham Density Functional Theory calculations. They have provided preliminary evidence that there will be no

qualitative and very little quantitative difference between the uranium and plutonium species. Various other groups have also used quantum mechanical methods to understand uranyl-water interaction<sup>17</sup> and coordination environments.<sup>18</sup> Frick et al.<sup>19,20</sup> employed quantum mechanical charge field molecular dynamics (QMCF-MD) framework for simulating the behavior of uranyl (VI) ( $\text{UO}_2^{2+}$ ) and uranyl (V) ( $\text{UO}_2^+$ ) ions in aqueous solution. Apart from these investigations, several other investigations on structure and dynamics of the uranyl ion and its different complexes at various solid-liquid and liquid-liquid interfaces have been reported.<sup>21-24</sup>

Most of the existing molecular dynamics based investigations involving aqueous solution of uranyl ion have dealt with single uranyl ion in an aqueous solution. Presence of the multiple ions in the solution may modify the properties of the aqueous uranyl solution. In a recent study, it is shown that a neutral solute like urea does not really break the H-bonding structure of water, but many of the tetrahedral oxygen sites of water get replaced by nitrogen or oxygen site of urea.<sup>25</sup> Uranyl ion being a doubly positive molecular ion, it has a greater chance of modifying the structure and dynamics of its aqueous solution at high concentrations. As far as we are aware of, the effect of concentration of the uranyl ions on liquid structure and dynamics of different species in the solution has not been investigated in detail. Not only that, not enough literature reports are available on the effect of temperature on the structure and dynamics of the uranyl solution. Therefore, in the present study we intend to investigate the effect of concentration of uranyl ions as well as the temperature of the system on structural and dynamic characteristics of water as well as uranyl and other co-ions present in the aqueous solution using atomistic molecular dynamics (MD) simulations.<sup>26</sup> Proper understanding of the structure and dynamics of the ionic solution can be achieved from the knowledge of the behavior of water molecules in the solvation shells of ions. Therefore, we use MD simulation here to understand the effect of concentration of the uranyl



salt on the dynamics of solvation shell water too. The present study can be divided into two parts. In the first part, we intend to analyze the effect of uranyl ion concentration on the various characteristics of the aqueous solution using molecular dynamics (MD) simulations and in part two, we have presented the results on the effect of temperature on the structural and dynamical properties of these systems too. In order to get an idea about the effect of concentration of uranyl ions on local structural arrangements of water molecules around the uranyl ion, radial distribution functions of water molecules around the uranyl ion are analyzed for aqueous uranyl solutions of various concentrations. The concentration effect on translational dynamics has also been analyzed by calculating diffusion coefficients of various species in solution from their respective mean squared displacements. Orientational dynamics of water about different molecular axes of water have also been analyzed. All atom molecular dynamics simulations have been employed to study orientational structure and dynamics of aqueous solutions of uranyl ions of varying concentrations. The effect of temperature on the translational and orientational characteristics of the aqueous uranyl solutions has also been studied in detail.

### 3.2 Models and Simulation Details

In the present investigation, we have prepared aqueous solutions of divalent uranyl ions,  $\text{UO}_2^{2+}$ , of different concentrations by solvating appropriate number of uranyl ions in a cubic box containing around 500 water molecules with a bulk water density of around 0.98 g/cc. The electrical neutrality of the system is maintained by introducing required number of negative ions (nitrate) in the system. Three different systems are considered: (i) one uranyl ion (hereinafter we call it system U1), (ii) five uranyl ions (hereinafter we call it system U5) and (iii) ten uranyl ions (hereinafter we call it system U10). Total number of molecules i.e. water plus uranyl nitrate in the system are kept fixed at 513 molecules. The corresponding

concentrations of the aqueous solutions of uranyl ions are 0.106 M for U1, 0.53 M for U5 and 1.06 M for U10 systems. The concentration range used here is relevant to the back end of the nuclear fuel cycle during the reprocessing of the spent fuel from uranium based reactors.<sup>27-28</sup> It is also of academic interest to investigate the effect of concentration and temperature on the structural and dynamical aspects of the uranyl solution. Simulations are performed in canonical (NVT) ensemble with molecular dynamics extended system approach of Nose.<sup>26</sup>

**Table 3.1: Force Field Parameters**

**Non-bonded Parameters**

Atom Type	$\sigma$ (nm)	$\epsilon$ (kJ/mol)	$q/e$
U	0.295	0.5299	+2.500
O <sub>U</sub> (Uranyl oxygen)	0.383	0.0567	-0.250
O <sub>W</sub> (SPC/E)	0.317	0.6502	-0.8476
H <sub>W</sub> (SPC/E)	-	-	+0.4238

**Bonded Parameters**

Bond Type	$r_{eq}$ (nm)	$K_r$ (kJ mol <sup>-1</sup> nm <sup>-2</sup> )
U-O <sub>U</sub>	0.176	622300

Angle Type	$\theta_{eq}$ (°)	$K_\theta$ (kJ mol <sup>-1</sup> rad <sup>-2</sup> )
O <sub>U</sub> -U-O <sub>U</sub>	180	198

All the simulations are carried out at a target temperature of 298 K using periodic boundary conditions and minimum image convention in all three directions. We have used atomistic model with one uranium and two oxygen sites for the uranyl ion<sup>4</sup> and one nitrogen and three oxygen sites for the nitrate ion.<sup>1</sup> Non-bonded site-site inter-molecular interaction is

modeled with Lennard–Jones plus Coulomb interactions and intra-molecular interaction for uranyl and nitrate ions consist of bond and angle terms. Although TIP3P model has been used in most of the calculation presented here, for comparison we have also used SPC/E water model and corresponding force field parameters are taken from a recently published work<sup>14</sup> and are given in Table 3.1. The LJ parameters and the bonded parameters for solvated uranyl ion has been taken from the work of Pomogaev et al.<sup>14</sup> The parameters related to bonded interactions and the LJ parameters for the nitrate ion have been taken from the work of Guilbaud et al.<sup>1</sup> The potential energy of the system is given by Eq. 1.5 as given in Chapter 1. The parameter sets for both inter- and intra-molecular interactions for the atoms of water and uranyl ion for TIP3P model are given in Table 2.1 of Chapter 2.<sup>1,4,29</sup> All cross parameters for the LJ potential are obtained by using Lorentz–Berthelot mixing rule.

A time step of 1 fs is used for integrating the equations of motion. For each system, the production run is for 8 ns after equilibration for 1 ns and the trajectories were saved at every 0.01 ps. For uncertainty in the calculated quantities, usual standard deviations are obtained from block averaging of eight independent simulations of 1 ns each. All the results on radial distribution functions and coordination numbers related to nitrate ions are obtained from averaging over a 30 ns simulation trajectory. Most of the simulations are carried out at a target temperature of 298 K. To study the effect of temperature, additional simulations are carried out at temperatures of 240 K, 270 K, 330 K and 360 K. In these simulations, after an equilibration period of 1 ns, trajectories are saved at every 0.01 ps during the next 1 ns production run for post analyses.

### 3.3 Results and Discussion

The structure and dynamics of aqueous solution of uranyl ions have been estimated using MD simulations. Our aim is to investigate the effect of uranyl ion concentration and

temperature of the system on the structure and dynamics of water and different ions present in the solution. The structural aspects are analyzed by calculating radial distribution functions (RDF) of water around different sites of the uranyl ion. Translational dynamics of different species including water has been investigated by analyzing mean squared displacement (MSD) of the corresponding species in solution. Orientational dynamics of water in the vicinity of uranyl ions is also investigated by calculating orientational time correlation functions involving different molecular axes of the water molecules. The orientational dynamics of the water molecules within the first coordination shell of uranyl ions is then compared with those obtained for all the water molecules (hereafter we call these as overall water molecules) in the aqueous solution. In order to investigate the effect of uranyl ion concentration on various properties, we have compared results obtained from U1, U5 and U10 systems. In order to get further insight, we have also analyzed the effect of uranyl concentration on the dynamics of water in the solvation shells of uranyl ions. The effect of uranyl ion concentration and that of temperature on the various characteristics is discussed in Sections 3.1 and 3.2 respectively.

### **3.3.1 Effect of Uranyl Ion Concentration on the Structural and Dynamic Characteristics of Aqueous Uranyl Solutions**

In this section, we will be elaborating on the implications of the change in uranyl ion concentration on the behavior of various species present in the aqueous uranyl solution. The various structural and angular distributions are presented along with the translational and rotational transport properties of the constituents of the solution in the following subsections.

### 3.3.1.1 Radial Distribution of Water Molecules around Uranyl Ions in Aqueous Solutions

In order to investigate the effect of increasing uranyl salt concentration on the structural aspects of the solution, we have calculated RDFs of two different water sites ( $O_w$  and  $H_w$ ) with respect to two uranyl sites ( $U$  and  $O_U$  of uranyl ion) and are presented in Figure 3.1. The first minimum for distribution of  $O_w$  atoms around uranium atom of uranyl ion comes at around 3.0 and this value is used as the radius of the first coordination shells around respective atoms of uranyl ion for calculating coordination number and analyzing dynamical

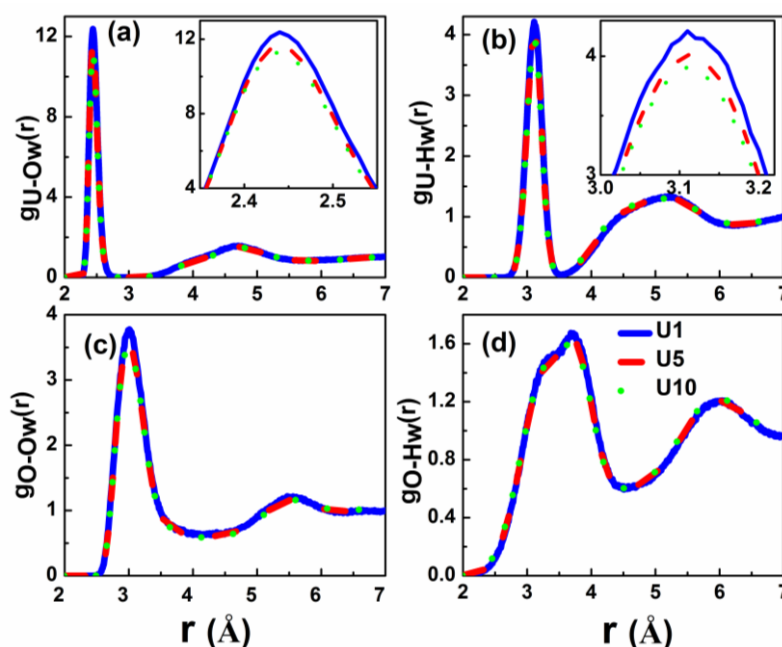


**Figure 3.1: Radial distribution functions for (a)  $O_w$  around uranium, (b)  $H_w$  around uranium (c)  $O_w$  around uranyl-oxygen ( $O_U$ ) and (d)  $H_w$  around  $O_U$  for different concentrations of uranyl ions. In the insets of Figures 3.1(a) and (b) first peak of the respective RDF is magnified.**

behavior of the solvation water. It is interesting to note that with the change in uranyl concentration, overall RDF and hence liquid structure does not change much, although there is slight reduction in the peak of the RDF as we go from U1 to U10 system (see the insets of Figure 3.1(a) and (b)). We have also calculated the coordination number as defined by the

number of water molecules in the first solvation shell (defined by the position of the first minimum in the RDF) around different species in the solution and tabulated in Table 3.2.

**Table 3.2: Average number of water molecules in the first coordination shell.**

System	Central atom	Coordination number as defined by number of water molecules in the first shell
Bulk-water (TIP3P)	Water-oxygen	5.4
Bulk-water (SPC/E)	Water-oxygen	4.4
U1 (TIP3P)	Uranium	5.0
U5 (TIP3P)	Uranium	4.7
U10 (TIP3P)	Uranium	4.6

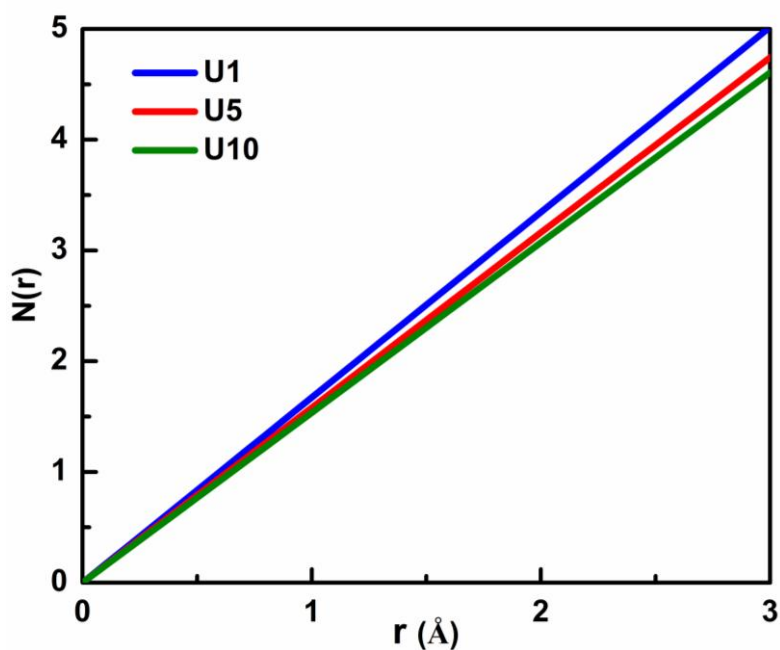


**Figure 3.2: Running coordination number around U as a function of radial distance of water from uranyl ion.**

The coordination number of water on an average was observed to be around 5.4 for bulk TIP3P water whereas it is around 4.4 for bulk SPC/E water. In case of aqueous solution of uranyl ions, the coordination number of uranium with respect to water molecules comes out to be around 5 and is consistent with the reported value.<sup>1,3,4,10,14,16-19,22,23</sup> There is a slight reduction in the coordination number values as we move from U1 to U5 to U10, and this slight reduction is due to decrease in the peak height of RDF as shown in insets of Figure 3.1. The running coordination number  $N(r)$  defined by Eq. 1.14 is also calculated as a function of radial distance from uranyl ions, and shown in Figure 3.2. It is obvious that running coordination number  $N(r)$  decreases from U1 to U5 to U10 systems.

### 3.3.1.2 Radial Distribution of Counter Ions (Nitrate Ions) with Respect to Uranyl Ions

As already mentioned, we have studied the distribution of counter ions (nitrate ions) with respect to uranyl ions in U1, U5 and U10 systems by simulating each of the systems for 30 ns. The radial distribution functions of oxygen atoms of water molecules (solid blue line), nitrogen atoms of nitrate ions (dashed red line) and oxygen atoms of nitrate ions (dotted green line) with respect to uranium and oxygen atoms of the uranyl ion are given for U10 system in Figures 3.3 a and b respectively. Figure 3 shows that the oxygen of nitrate ion ( $O_{NO_3}$ ) occupies positions closer to  $O_U$  of uranyl ion as compared to positively charged nitrogen ( $N_{NO_3}$ ). However, positively charged U gets closer to negatively charged oxygen atoms ( $O_W$  or  $O_{NO_3}$ ) as compared to negatively charged  $O_U$ . It is interesting to observe that the location of the first peak of  $g(r)$ s of  $O_{NO_3}$  and  $O_W$  being almost at the same distance from the central uranyl ion, one can conclude that both are in the solvation shell of the uranyl ion. We have also calculated the coordinated numbers (CNs), defined as the number of these atoms in the first solvation shell of uranyl ion, of  $O_W$  and  $O_{NO_3}$  around the U (first solvation shell radius 3.0 Å) and  $O_U$  (first solvation shell radius 4.0 Å) sites of the uranyl ions in U5

and U10 systems (Table 3.3). For U1 system, the first peak of  $g(r)$  for  $O_{NO_3}$  around uranyl ion is not observed most of the time during the 30 ns trajectory analyzed here. It can be seen (see Table 3.3) that as the concentration of uranyl ion is increased (U5 to U10), the CN of  $O_W$  is reduced whereas that of  $O_{NO_3}$  is increased. It is interesting to note that the oxygen atom of water and that of nitrate ion compete with each other to occupy the first coordination shell of the uranyl ion (blue solid and dotted green lines in Figure 3.3).

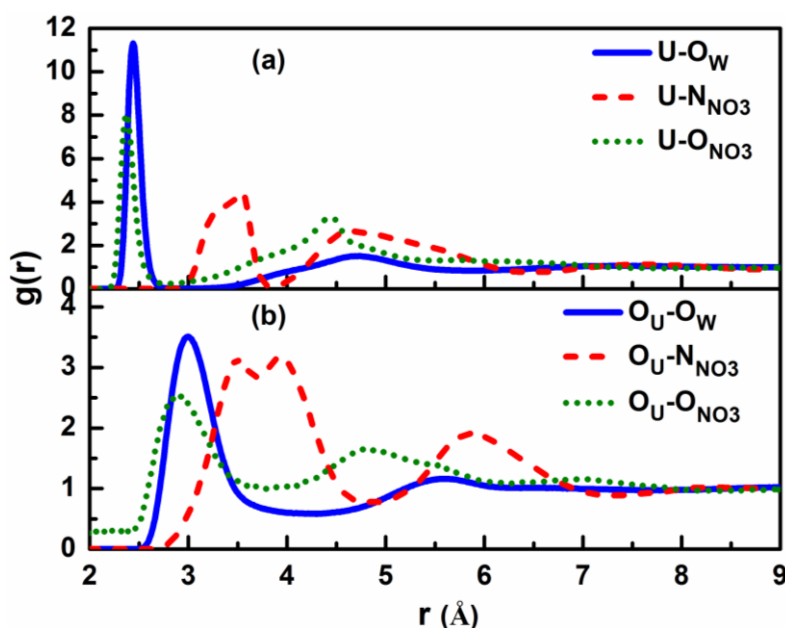


**Figure 3.3: Radial distribution functions of oxygen ( $O_W$ ) atoms of water molecules, nitrogen ( $N_{NO_3}$ ) and oxygen ( $O_{NO_3}$ ) atoms of nitrate ions with respect to (a) uranium (U) and (b) oxygen ( $O_U$ ) atoms of uranyl ions for the U10 system.**

**Table 3.3: Coordination numbers (CN) of uranium and oxygen atoms of uranyl ions with respect to oxygen atoms of water and nitrate for different uranyl ion concentrations**

System	CN: $O_W$ around		CN: $O_{NO_3}$ around	
	U	$O_U$	U	$O_U$
<b>U5</b>	4.70	9.50	0.32	0.84
<b>U10</b>	4.61	9.34	0.43	1.32



### 3.3.1.3 Orientational Distribution of Water Molecules in the Vicinity of Uranyl Ions

We have calculated angular distributions of the water molecules around uranyl ion in its coordination shell for U1, U5 and U10 systems in the same way as explained in subsection (ii) of Section 2.3 of Chapter 2. The angular distribution remains more or less the same with change in concentration of uranyl ions in the solution as given in Figure 2.4 of Chapter 2.

### 3.3.1.4 Translational Dynamics of Different Species in the Aqueous Uranyl Solution

The translational dynamics of various species in the solution is analyzed in terms of their mean squared displacements (MSDs). The effect of increasing concentration of uranyl ion on the dynamics of water i.e. both for all water molecules and solvation shell water molecules, and uranyl ion is investigated in following subsections.

#### 3.3.1.4.1 Translational Dynamics of Overall Water Molecules in the Aqueous Solution

Let us first analyze translational dynamics of all the water molecules present in the aqueous uranyl solutions of different concentrations. The MSD profiles for water oxygen in bulk water and in the aqueous solution of uranyl ions of different concentrations are compared in Figure 3.4. In case of U1 system, diffusivity of water molecules does not deviate much from that of the bulk water. In systems with higher uranyl concentrations i.e. in U5 and U10 systems, there is a prominent variation of the MSD line from that of the bulk water, indicating a considerable change in the dynamics of water. From the slopes of these MSD lines it is evident that average diffusivity of the water molecules in the concentrated uranyl solution decreases as compared to bulk water. It may be due to the fact that water molecules in the solvation shells of uranyl ions are probably diffusing slowly along with the slower moving uranyl ions. We shall try to get further insight into this aspect by analyzing the dynamics of solvation water in the next subsection.

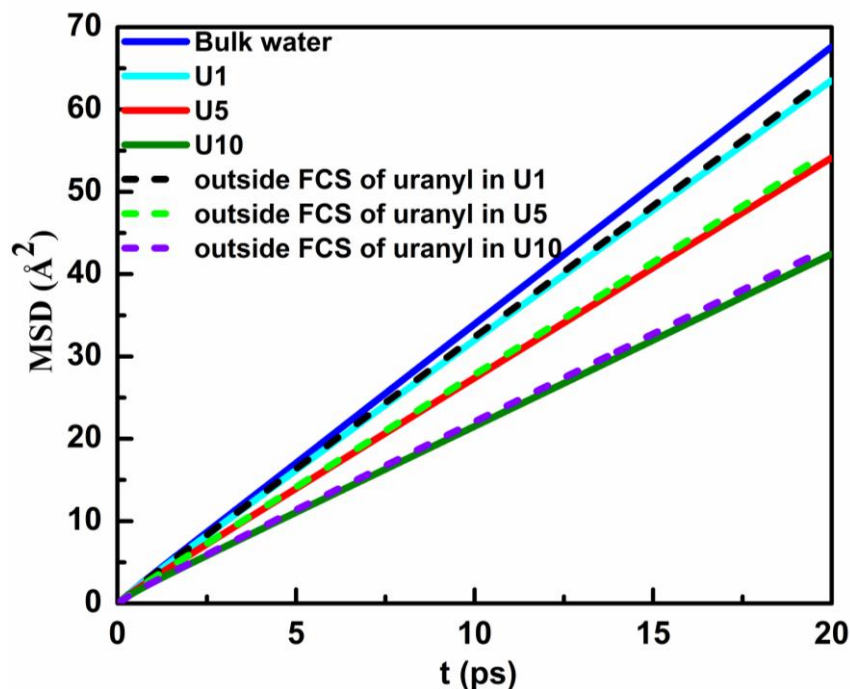


**Figure 3.4:** MSD profiles for water molecules in bulk water (blue line), U1 system (cyan line), U5 system (red line), and U10 system (green line). The dashed lines represent MSD of only those water molecules that are outside the first coordination shell (FCS) of uranium in U1, U5 and U10 systems.

Also, to confirm whether there is any long range effect of the uranyl ions on the water dynamics, the MSD of water molecules outside the first coordination shell (FCS) of uranyl ions is estimated for U1, U5 and U10 systems (dashed lines in Figure 3.4). Since there is not much difference in the MSD of these water molecules (dashed lines) as compared to that calculated by taking all the water molecules in the system (solid lines) for all the three systems, it can be concluded that one of the reasons for the slowing down of the overall translational mobility of water is the long range effects of the uranyl ions on the mobility of water outside the solvation shell.

### 3.3.1.4.2 Translational Dynamics of Uranyl Ions in the Aqueous Solution

Now, we turn our attention to the effect of increasing concentration on the diffusivity of uranyl ion. In Figure 3.5, we have shown the MSD of U atom of the uranyl ion in three different systems with different uranyl ion concentrations. In this case also, the diffusivity of the uranyl ion is found to be reducing with increasing concentration of uranyl ions in aqueous solution (see Figure 3.5).

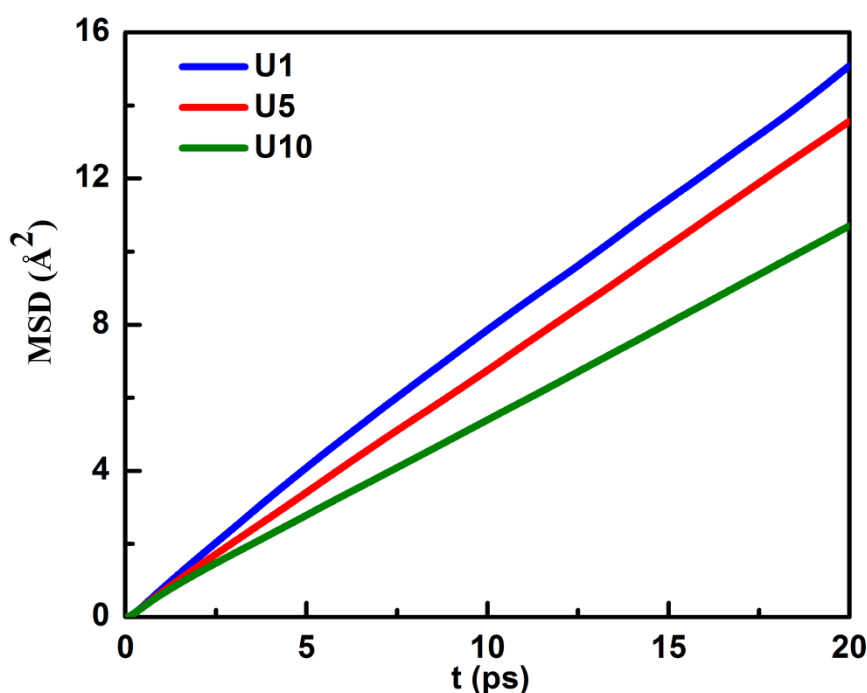


**Figure 3.5: MSD profiles for uranium atom in U1 (blue line), U5 (red line) and U10 (green line) systems.**

The diffusion coefficients of various species in the solution are estimated from the slope of respective MSD curves by using the Eq. 1.19 given in section 1.5 of Chapter 1. The diffusivity values along with the associated uncertainty (standard deviation) as estimated from the slopes of the MSD lines obtained from different simulation runs are given in Table 3.4. The diffusivity values tabulated in Table 3.4 suggest that there is concentration dependence of the diffusivity for all the three species namely, uranyl ions, nitrate ions and water molecules. The value of diffusion coefficients for bulk water, water in U1 system and

**Table 3.4: Diffusion coefficient values for different systems (BW: bulk water)**

S. No.	Atom/Group	System	$D_{\text{PBC}} (10^{-5} \text{cm}^2 \text{s}^{-1})$	$D_0 (10^{-5} \text{cm}^2 \text{s}^{-1})$
1	U of $\text{UO}_2$ (TIP3P water)	U1	$1.37 \pm 0.11$	$2.16 \pm 0.11$
2	U of $\text{UO}_2$ (TIP3P water)	U5	$1.09 \pm 0.05$	$1.88 \pm 0.05$
3	U of $\text{UO}_2$ (TIP3P water)	U10	$0.87 \pm 0.02$	$1.66 \pm 0.02$
4	U of $\text{UO}_2$ (SPC/E water)	U1	$0.60 \pm 0.04$	$0.94 \pm 0.04$
5	U of $\text{UO}_2$ (SPC/E water)	U5	$0.56 \pm 0.02$	$0.90 \pm 0.02$
6	U of $\text{UO}_2$ (SPC/E water)	U10	$0.46 \pm 0.01$	$0.80 \pm 0.01$
7	N of nitrate (TIP3P water)	U1	$2.88 \pm 0.16$	$3.67 \pm 0.16$
8	N of nitrate (TIP3P water)	U5	$2.33 \pm 0.13$	$3.12 \pm 0.13$
9	N of nitrate (TIP3P water)	U10	$1.82 \pm 0.06$	$2.61 \pm 0.06$
10	$\text{O}_w$ (TIP3P water)	BW	$5.60 \pm 0.12$	$6.39 \pm 0.12$
11	$\text{O}_w$ (TIP3P water)	U1	$5.28 \pm 0.02$	$6.07 \pm 0.02$
12	$\text{O}_w$ (TIP3P water)	U5	$4.50 \pm 0.02$	$5.29 \pm 0.02$
13	$\text{O}_w$ (TIP3P water)	U10	$3.58 \pm 0.02$	$4.37 \pm 0.02$
14	$\text{O}_w$ (SPC/E water)	BW	$2.76 \pm 0.08$	$3.1 \pm 0.08$
15	$\text{O}_w$ (SPC/E water)	U1	$2.52 \pm 0.01$	$2.86 \pm 0.01$
16	$\text{O}_w$ (SPC/E water)	U5	$2.20 \pm 0.02$	$2.54 \pm 0.02$
17	$\text{O}_w$ (SPC/E water)	U10	$1.80 \pm 0.02$	$2.14 \pm 0.02$

uranium atom of uranyl ion in U1 system are similar to those given by Tiwari et al. for TIP3P model of water.<sup>15</sup> The self-diffusion coefficients for uranyl ion were observed to be lower for SPC/E water as compared to those for TIP3P water. The diffusivity values obtained for water molecules and uranyl ions in aqueous uranyl solution with SPC/E water model are in good

agreement with those obtained earlier using molecular dynamic simulations.<sup>15</sup> Using the shear viscosity values for TIP3P<sup>30</sup> and SPC/E<sup>13</sup> water models, the diffusion coefficient values have been corrected for system size dependence (according to Eq. 1.20 as given in section 1.5 of Chapter 1) and are given in Table 3.4.

**Table 3.5: Comparison of normalised diffusion coefficient values for uranyl ions in U1 system with experimental and theoretical results available in literature**

S. No.	Source	$D_{\text{UO}_2}/D^{\text{aH}_2\text{O}}$
1.	<sup>e</sup> Awakura et al., 1987 <sup>31</sup>	0.204
2.	<sup>e</sup> Kern and Orlemann, 1949 <sup>32</sup>	0.296
3.	<sup>e</sup> Brown et al., 1954 <sup>33</sup>	0.295
4.	<sup>e</sup> Marx and Bischoff, 1976 <sup>34</sup>	0.330
5.	<sup>t</sup> Kerisit and Liu, 2010 <sup>13</sup>	0.333
6.	Present study (TIP3P water), U1 system	$0.338 \pm 0.018$
7.	Present study (SPC/E water), U1 system	$0.303 \pm 0.015$

a = pure water, e = experimental value, t = theoretical value

The un-normalized diffusivity of the uranyl ions for the concentration range of 0.1-0.5 M is in the range of  $(2.16\text{-}1.88) \times 10^{-5} \text{ cm}^2 \text{ s}^{-1}$  for TIP3P water, whereas for SPC/E water it is in the range of  $(0.94\text{-}0.90) \times 10^{-5} \text{ cm}^2 \text{ s}^{-1}$ . Higher diffusivity of the uranyl ions in TIP3P water can be attributed to higher bulk water diffusivity ( $6.39 \times 10^{-5} \text{ cm}^2 \text{ s}^{-1}$ ) in this case. The experimental values of un-normalized diffusivities as given by Awakura et al.<sup>31</sup> are in the range of  $(0.47\text{-}0.39) \times 10^{-5} \text{ cm}^2 \text{ s}^{-1}$  for similar concentration range (0.1 to 0.5 M). It is to note that the experimental diffusivity value in 0.1 M uranyl solution as given by Awakura et al.<sup>31</sup> normalised with respect to water diffusivity<sup>13</sup> ( $2.3 \times 10^{-5} \text{ cm}^2 \text{ s}^{-1}$ ) is considerably lower as compared to the same obtained from other experimental and simulation studies (see Table 3.5). The corrected, normalized diffusivity values of uranyl ions with respect to the respective

bulk water diffusivities in U1 system are observed to be in overall good agreement with the diffusivity ratios obtained experimentally<sup>32-34</sup> or theoretically<sup>13</sup> (except the one given by Awakura et al.<sup>31</sup>) as shown in Table 3.5.

#### 3.3.1.4.3 Translational Dynamics of Water in the Solvation Shell of Uranyl Ions

In the earlier subsection, we have shown that the translational dynamics of water (considering all the water molecules in the system) becomes slower with the increase in uranyl concentration. The reduced diffusivity of water in the concentrated solution may be due to solvation water. It is, therefore, important to look into the dynamics of those water molecules residing in the first solvation shell of the uranium atom of the uranyl ion. In Figure 3.6, the MSD profiles of the water molecules in the solvation shell of the uranium atom in three different systems namely U1, U5 and U10 systems are shown. The comparison of the MSDs of the coordination shell (of uranyl ion) water molecules in the system with that of bulk water as well as all water molecules in solution (see Figure 3.4) indicates a considerable decrease in diffusivity of solvation shell water as compared to the bulk water. Probably, the strong electrostatic interaction between the uranyl ion and water molecules in the solvation shell is responsible for the lower diffusivity of solvation water as compared to that of bulk water. The diffusivity values as estimated using MSD along with the size independent diffusivities and their standard deviations for solvation water are given in Table 3.6. It may appear at this point that the reduction (see Figure 3.4 and Table 3.4) in overall diffusivity of water in the uranyl solution is due to these retarded solvation water. But, as the fraction of solvation water (around 1 % in U1 system and around 9% in U10 system) is considerably small, contribution of the retarded solvation water to the overall diffusivity is negligibly small (see Figure 3.4). Thus, the reduction in overall water diffusivity is a consequence of the long range effect (as shown in Figure 3.4) of the uranyl ions on the water beyond solvation shells.

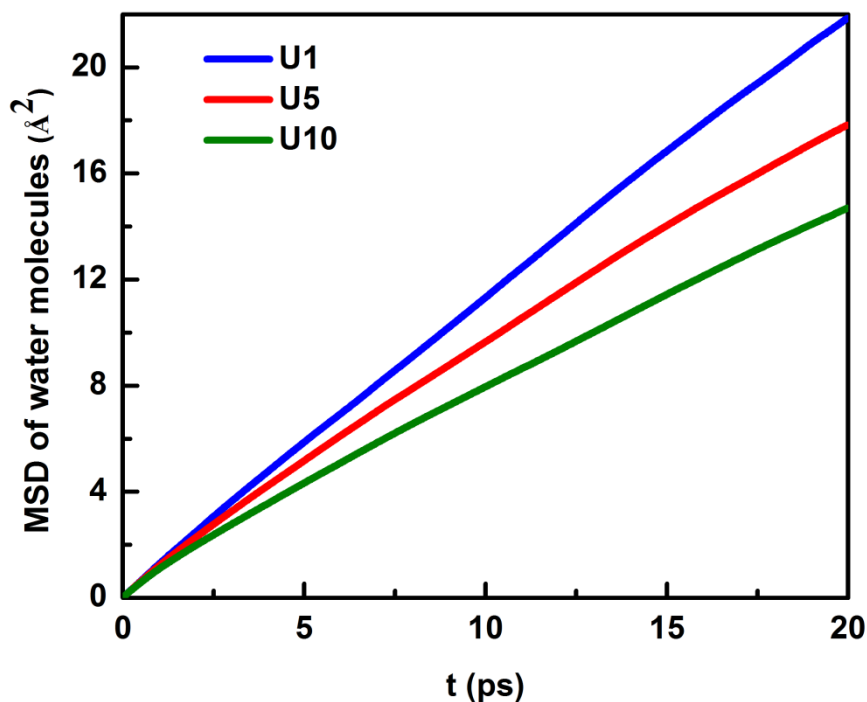


Figure 3.6: MSD profiles for water molecules within the first coordination shell of uranium atom of uranyl ion for U1 (blue line), U5 (red line) and U10 (green line) systems.

Table 3.6: Diffusion coefficient values for water molecules within the first coordination shell of uranium atom of uranyl ions for different systems

S. No.	System	$D_{\text{PBC}} (10^{-5} \text{ cm}^2 \text{ s}^{-1})$	$D_0 (10^{-5} \text{ cm}^2 \text{ s}^{-1})$
1	U1	$1.86 \pm 0.11$	$2.65 \pm 0.11$
2	U5	$1.35 \pm 0.01$	$2.26 \pm 0.01$
3	U10	$1.20 \pm 0.02$	$1.99 \pm 0.02$

### 3.3.1.5 Orientational Dynamics of Water Molecules in the Aqueous Uranyl Solution

The orientational dynamics of the water molecules are analyzed by calculating time correlation function of various molecular vectors of water as explained in Section 1.5, Eq.

1.21 of Chapter 1. Effect of concentration of the uranyl ions on the rotational dynamics of water (all water molecules in solution) can be understood from plots in Figures 3.7 and 3.8.

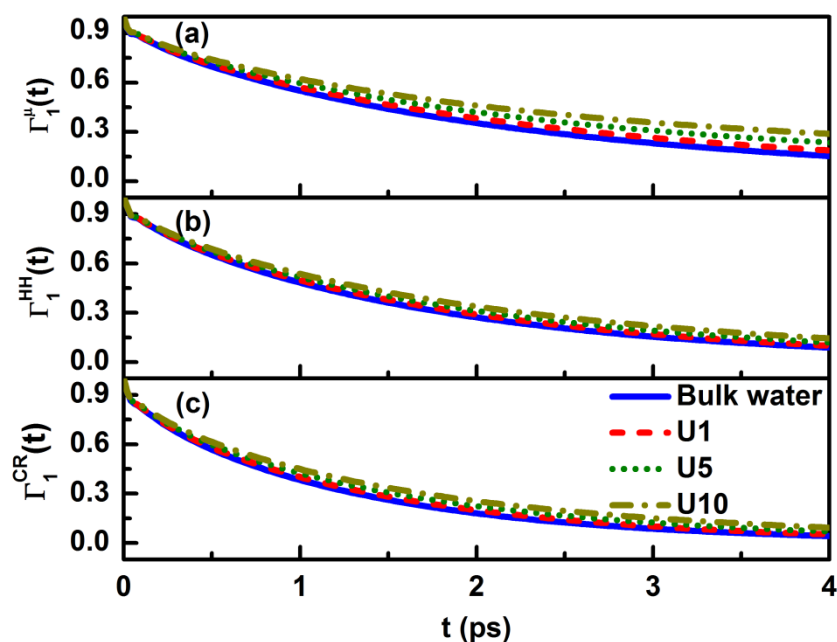


**Figure 3.7: First order orientational correlation functions of water molecules with respect to (a) dipole moment vector ( $\mu$ ), (b) H-H vector (HH) and (c) a vector (CR) perpendicular to the plane of the water molecule for different systems of varying uranyl concentrations.**

It is observed that for all the three different orientational correlation functions, the effect of increase in concentration of uranyl ions in aqueous solutions leads to a slight retardation of the rotational motion of water and this effect is more for the rotational motion of dipole moment vector as compared to other orientational vectors of water. The values of fitting parameters as discussed in subsection (iv) of Section 2.3 of Chapter 2 i.e.  $A$ ,  $\tau_1$  and  $\tau_2$  for different systems as obtained from the fitting are given in Table 3.7. From the discussion on translational dynamics, it is clear that the translational mobilities of solvation shell water molecules get reduced significantly as compared to those of water molecules not residing in the solvation shell. Therefore, it will be interesting to investigate whether similar slowdown is observed in case of angular dynamics of the solvation water molecules.



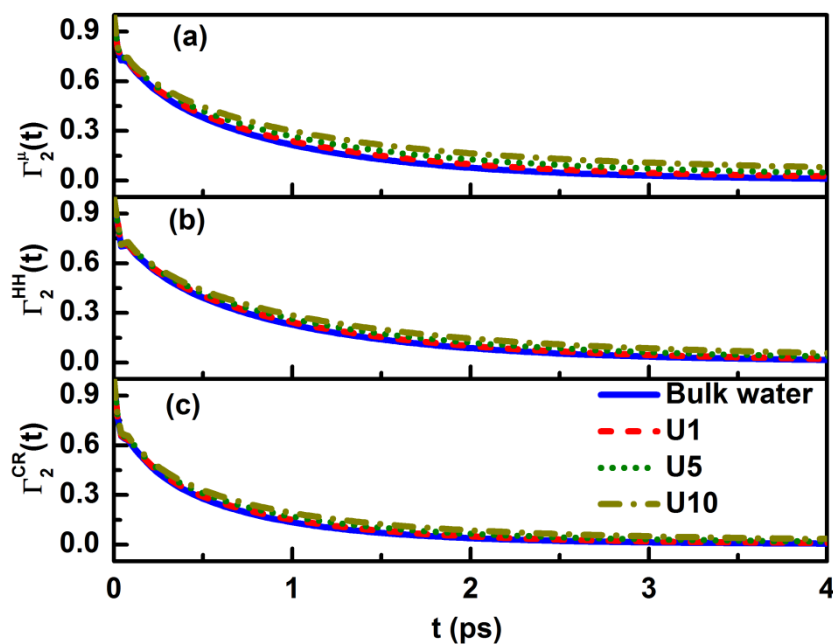


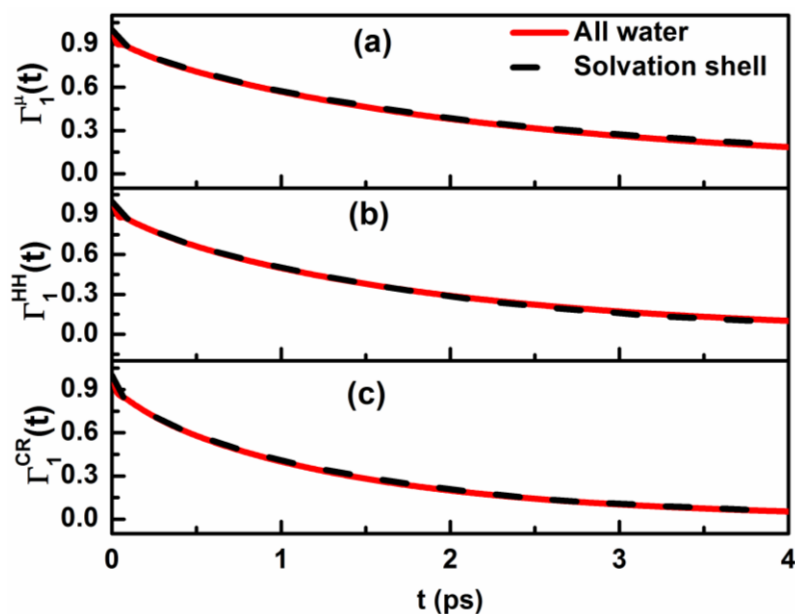
Figure 3.8: Second order orientational correlation functions of water molecules with respect to (a) water dipole moment vector ( $\mu$ ), (b) water H-H vector (HH) and (c) water cross vector (CR) for different systems of varying uranyl concentrations.

Table 3.7: Values of time constants (in picoseconds) of longer and shorter time scales of the relaxation of  $S(t)$  ( $\tau_1$  and  $\tau_2$ ) and  $A$  for different systems.

Correlation Function	Bulk water	U1	U5	U10
$\Gamma_1^\mu$				
$A$	$0.83 \pm 0.004$	$0.75 \pm 0.01$	$0.57 \pm 0.008$	$0.54 \pm 0.004$
$\tau_1$	$2.37 \pm 0.01$	$2.93 \pm 0.08$	$4.55 \pm 0.09$	$6.32 \pm 0.17$
$\tau_2$	$0.20 \pm 0.01$	$0.4 \pm 0.04$	$0.82 \pm 0.02$	$0.91 \pm 0.006$
$\Gamma_1^{HH}$				
$A$	$0.86 \pm 0.02$	$0.861 \pm 0.003$	$0.85 \pm 0.004$	$0.83 \pm 0.006$
$\tau_1$	$1.75 \pm 0.02$	$1.85 \pm 0.02$	$2.02 \pm 0.02$	$2.28 \pm 0.03$

$\tau_2$	$0.07 \pm 0.004$	$0.092 \pm 0.004$	$0.13 \pm 0.01$	$0.18 \pm 0.01$
$\Gamma_1^{CR}$				
<b>A</b>	$0.835 \pm 0.001$	$0.82 \pm 0.004$	$0.8 \pm 0.007$	$0.76 \pm 0.008$
$\tau_1$	$1.31 \pm 0.004$	$1.42 \pm 0.01$	$1.61 \pm 0.02$	$1.88 \pm 0.04$
$\tau_2$	$0.07 \pm 0.004$	$0.09 \pm 0.004$	$0.13 \pm 0.006$	$0.19 \pm 0.01$
$\Gamma_2^{\mu}$				
<b>A</b>	$0.703 \pm 0.001$	$0.67 \pm 0.005$	$0.50 \pm 0.01$	$0.33 \pm 0.004$
$\tau_1$	$0.869 \pm 0.008$	$1.0 \pm 0.009$	$1.57 \pm 0.05$	$3.14 \pm 0.09$
$\tau_2$	$0.036 \pm 0.008$	$0.057 \pm 0.002$	$0.17 \pm 0.01$	$0.32 \pm 0.004$
$\Gamma_2^{HH}$				
<b>A</b>	$0.697 \pm 0.02$	$0.68 \pm 0.006$	$0.62 \pm 0.006$	$0.52 \pm 0.008$
$\tau_1$	$1.02 \pm 0.03$	$1.03 \pm 0.004$	$1.25 \pm 0.02$	$1.73 \pm 0.04$
$\tau_2$	$0.037 \pm 0.003$	$0.045 \pm 0.001$	$0.08 \pm 0.006$	$0.15 \pm 0.006$
$\Gamma_2^{CR}$				
<b>A</b>	$0.638 \pm 0.005$	$0.621 \pm 0.002$	$0.56 \pm 0.007$	$0.46 \pm 0.007$
$\tau_1$	$0.651 \pm 0.01$	$0.72 \pm 0.005$	$0.88 \pm 0.01$	$1.28 \pm 0.03$
$\tau_2$	$0.03 \pm 0.001$	$0.034 \pm 0.0005$	$0.058 \pm 0.001$	$0.11 \pm 0.006$

The first ( $n=1$ ) and second ( $n=2$ ) order autocorrelation functions for the above mentioned three unit vectors as obtained by considering all the water molecules in the system, and water molecules in the first coordination shell are given in Figures 3.9 and 3.10 respectively for U1 system. Similar curves are obtained for U5 and U10 systems too. For all the three different orientational correlation functions, a slight slowing down of the rotational motion of water is observed with increase in concentration of uranyl ions, this effect being



**Figure 3.9:** First order orientational correlation functions of solvation shell (black dashed line) and overall water molecules (red solid line) with respect to (a) water dipole moment vector ( $\mu$ ), (b) water H-H vector (HH) and (c) water cross vector (CR) for U1 system.

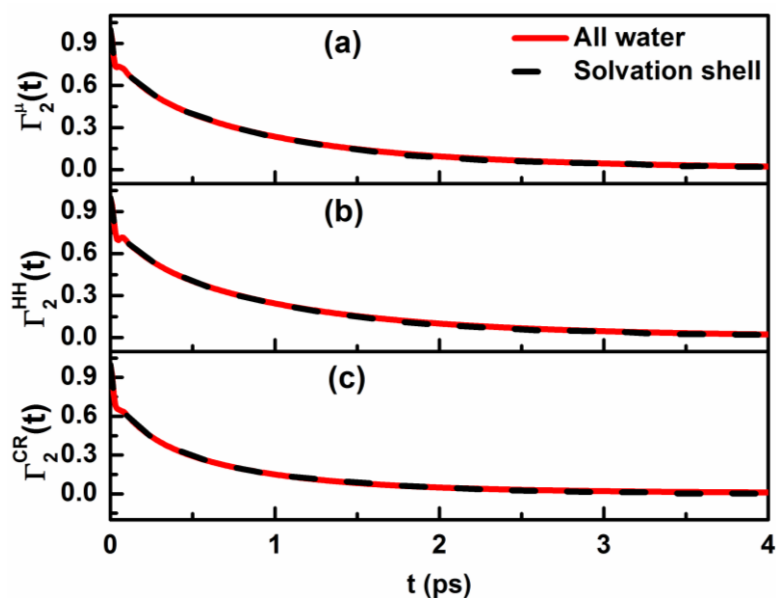


**Figure 3.10:** Second order orientational correlation functions of solvation shell (black dashed line) and overall water molecules (red solid line) with respect to (a) water dipole moment vector ( $\mu$ ), (b) water H-H vector (HH) and (c) water cross vector (CR) for U1 system.

more prominent for the dipole moment vector. Figures 3.9 and 3.10 suggest that there is not much difference between the autocorrelation functions calculated by considering all water molecules (red solid lines) and only the coordination shell water molecules (black dashed lines).

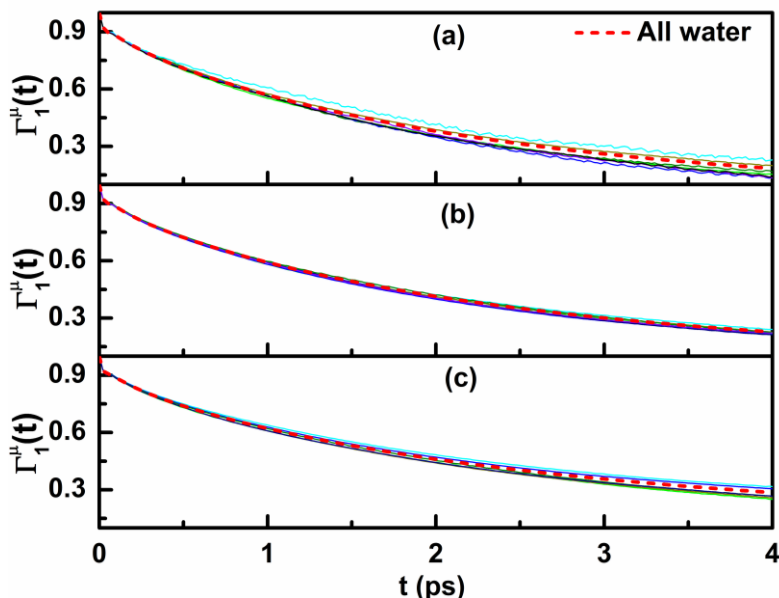


**Figure 3.11: First order orientational correlation functions of solvation shell water molecules with respect to water dipole moment vector ( $\mu$ ) for different trajectories (solid lines). Red color dashed line shows the average first order orientational correlation function of overall water molecules in the solution (a) U1, (b) U5, and (c) U10 systems.**

To confirm this, more simulations i.e. six simulations of 1 ns each were carried out and it was observed that the variation in the orientational correlation functions as we go from all water molecules to only solvation shell water molecules, is within the statistical uncertainties for different trajectories. For instance, Figure 3.11 shows the first order dipole moment orientational correlation functions of solvation shell water molecules (black dashed lines) for different trajectories for all the three systems U1, U5 and U10 overlapped by the corresponding orientational correlation function (red solid lines) for overall water molecules.

It is clear from the Figure 3.11 that orientational dynamics of water molecules remains the same whether they are inside or outside the solvation shell of uranyl ions. Thus, both the orientational structure and dynamics of solvation water remain the same as that obtained for all the water molecules in the system.

### **3.3.2 Effect of Temperature on the Structural and Dynamic Characteristics of Aqueous Uranyl Solutions**

To study the effect of temperature on the structural, translational and orientational properties of overall water molecules as well as those within the solvation shell around uranyl ions, the U1, U5 and U10 systems are simulated at different temperatures around 298 K i.e. 240 K, 270 K, 330 K and 360 K. As observed in the simulations discussed above, translational dynamics show a considerable difference for overall water molecules and those within the coordination shell of uranyl ions. Hence, the effect of temperature on the translational dynamics will be discussed separately for overall water molecules and for those in the vicinity of the uranyl ions. The effect of temperature on diffusivities of water and uranyl ions, radial and orientational distribution, and orientational dynamics of the water molecules are analyzed and the results are presented in the following sub-sections.

#### **3.3.2.1 Effect of Temperature on the Radial Distribution of Water Molecules around Uranyl Ions**

The radial distribution functions for the oxygen and hydrogen atoms of the water molecules around the uranium atom of the uranyl ion are plotted at various temperatures (Figure 3.12). It can be seen that there is slight lowering of the peak as the temperature of the system is increased; however the area under the curve appears to remain the same.

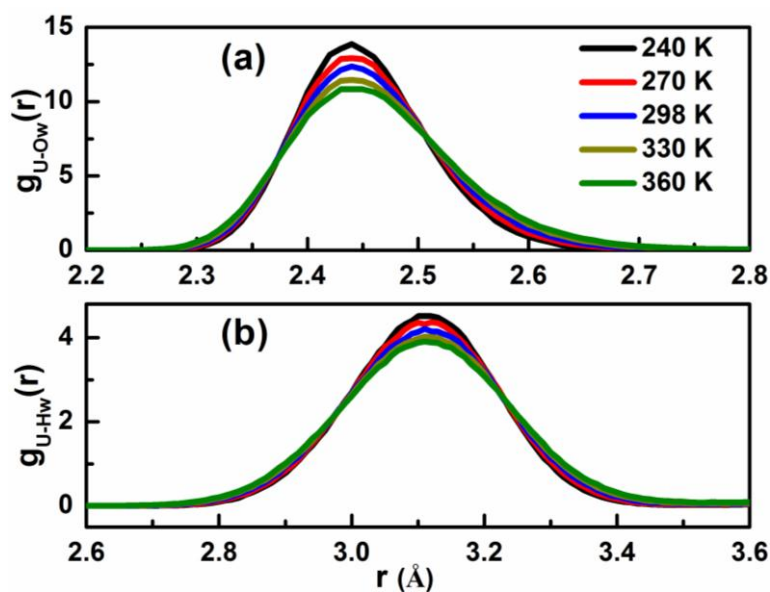


**Figure 3.12: The radial distribution functions of (a) oxygen and (b) hydrogen atoms of water molecules with respect to uranium atom at different temperatures.**

### 3.3.2.2 Effect of Temperature on the Orientational Distribution of Water Molecules in the Vicinity of Uranyl Ions

The distributions of four angles discussed above i.e.  $\theta$ ,  $\psi$ ,  $\gamma$  and  $\chi$  between different vectors of water molecules and uranyl ions are estimated at different temperatures and are shown in Figure 3.13. In Figure 3.13, only peaks are shown rather than showing the whole range of angles from  $0^\circ$  to  $180^\circ$  for better visual representation. It is observed that there is slight reduction in the peak values with increase in temperature. However the angles, corresponding to which the peaks in the distributions occur remain the same.

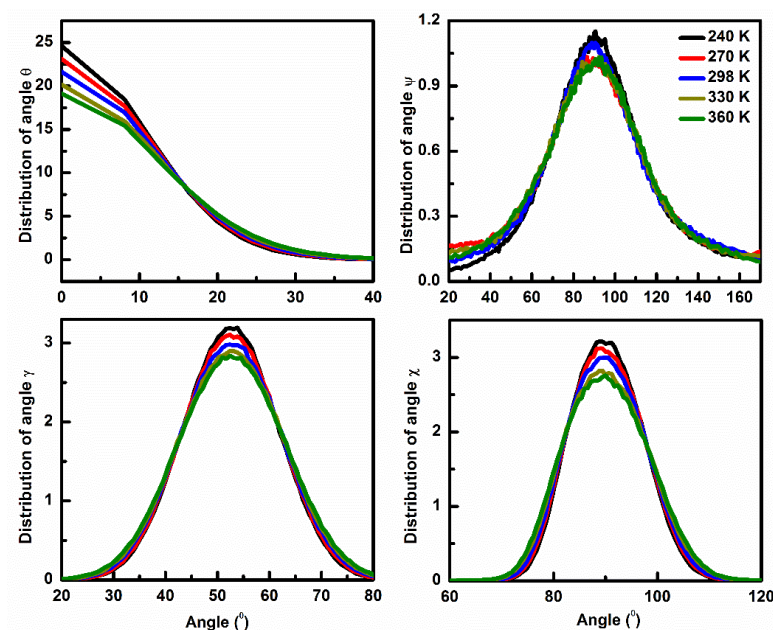


**Figure 3.13: Distributions of angles between U-O<sub>w</sub> vector and different molecular orientational vectors of a water molecule in the first coordination shell of a uranium atom of the uranyl ion at different temperatures.**

### 3.3.2.3 Effect of Temperature on the Orientational Dynamics of Water Molecules

The orientational dynamics of water molecules with respect to three vectors (i) dipole moment vector ( $u_{\alpha}=\mu$ ) (ii) H-H vector ( $u_{\alpha}=\text{HH}$ ) (iii) a cross vector ( $u_{\alpha}=\text{CR}$ ) i.e. a vector perpendicular to plane of water molecule are analyzed at different temperatures and results are given in Figure 3.14. The Figure 3.14 shows the orientational correlation functions of water molecules at different temperatures for these three vectors in case of U1 system. It can be seen that with increase in temperature, the times of relaxation of these functions reduce i.e. the relaxation becomes faster. In other words, the relaxation times of these functions reduce with reduction in concentration of uranyl ions or with increase in temperature of the systems.

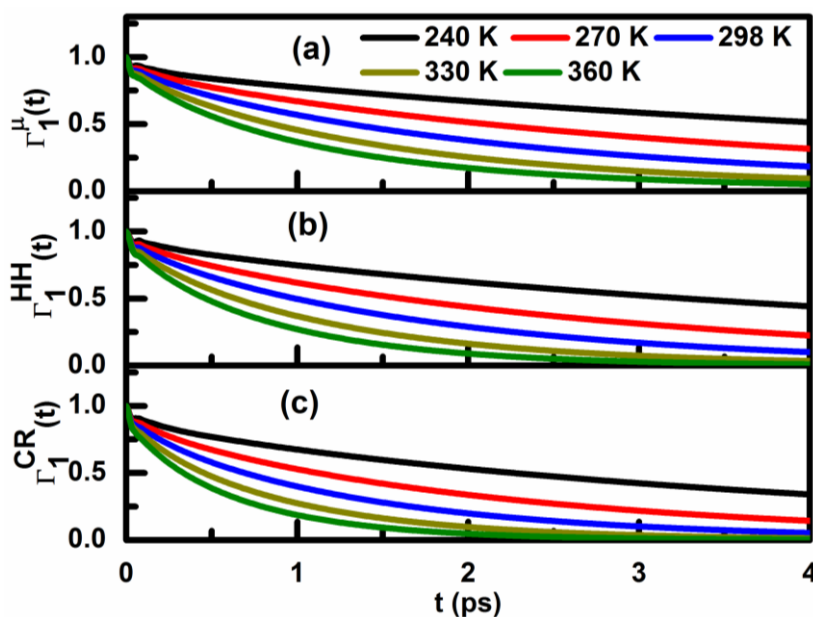


**Figure 3.14: First order orientational correlation functions of water molecules with respect to (a) dipole moment vector ( $\mu$ ), (b) H-H vector (HH) and (c) a vector (CR) perpendicular to the plane of the water molecule for U1 system at different temperatures.**

### 3.3.2.4 Effect of Temperature on the Translational Dynamics

The mean squared displacements (MSDs) obtained by considering overall water molecules in the solution as well as for water molecules within the coordination shell of uranyl ions and of uranyl ions for U1, U5 and U10 systems are analyzed at different temperatures. Hence, the variation in diffusion coefficients with temperature is studied.

#### 3.3.2.4.1 Overall water molecules in the solution

The variation of mean squared displacements (MSDs) of overall water molecules with temperature for the U1, U5 and U10 systems are given in Figure 3.15. The slopes of the MSD curve becomes higher and higher as the temperature of the system is increased. In other



words, diffusivity of water molecules increases with increase in temperature. The diffusion coefficients of overall water molecules at various temperatures are given in Table 3.8.

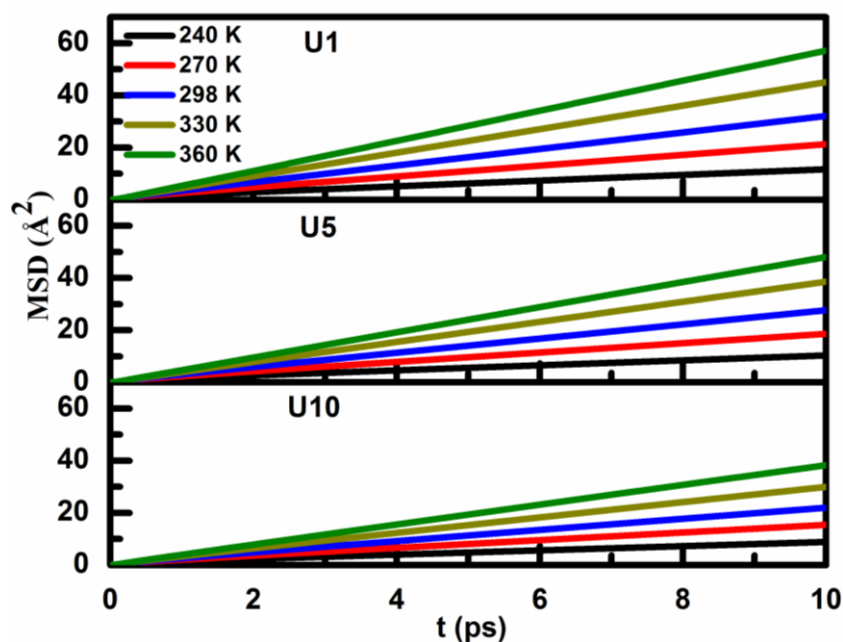


Figure 3.15: MSD profiles of overall water molecules for U1, U5 and U10 systems at different temperatures.

Table 3.8: Diffusion coefficient values of overall water molecules at different temperatures for U1, U5 and U10 systems

Diffusion coefficients, $D_{PBC}$ ( $10^{-5} \text{ cm}^2 \text{ s}^{-1}$ ) of overall water molecules					
	240 K	270 K	298 K	330 K	360 K
<b>U1</b>	1.82	3.43	5.28	7.51	9.60
<b>U5</b>	1.59	2.98	4.50	6.42	8.01
<b>U10</b>	1.36	2.45	3.58	4.88	6.27

#### 3.3.2.4.2 Water molecules within the first coordination shell of uranyl ions

The water molecules within the first coordination shell of uranyl ions also show an enhanced diffusivity with increase in temperature from 240 K to 360 K, although the

diffusivity values are lower for these as compared to those for the overall water molecules. The MSD curves are shown in Figure 3.16 for U1, U5 and U10 systems and the diffusivity values are given in Table 3.9.

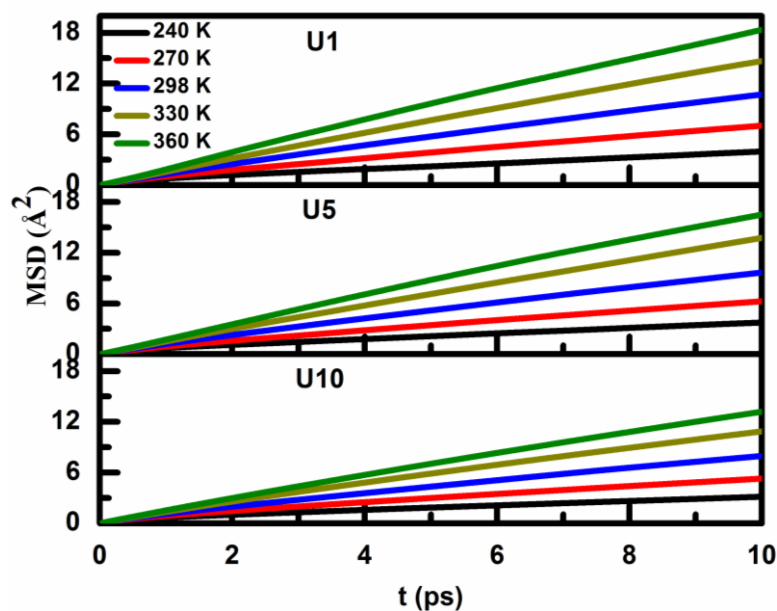


Figure 3.16: MSD profiles of water molecules within the first coordination shell of uranyl ions for U1, U5 and U10 systems at different temperatures.

Table 3.9: Diffusion coefficient values of water molecules within first coordination shell of uranyl ions at different temperatures for U1, U5 and U10 systems

Diffusion coefficients, $D_{PBC}$ ( $10^{-5} \text{ cm}^2 \text{ s}^{-1}$ ) of coordination shell water molecules					
	240 K	270 K	298 K	330 K	360 K
<b>U1</b>	0.56	0.93	1.86	2.19	2.94
<b>U5</b>	0.54	0.86	1.35	2.09	2.44
<b>U10</b>	0.43	0.75	1.20	1.61	1.94

### 3.3.2.4.3 Uranyl ions

The diffusivity values of uranyl ions show an increasing trend with the increase in temperature from 240 K to 360 K, although the diffusivity values are smaller as compared to those of water as uranyl ion is heavier than water. The MSD curves for uranyl ions are shown in the Figure 3.17 for U1, U5 and U10 systems and the diffusivity values are given in Table 3.10.

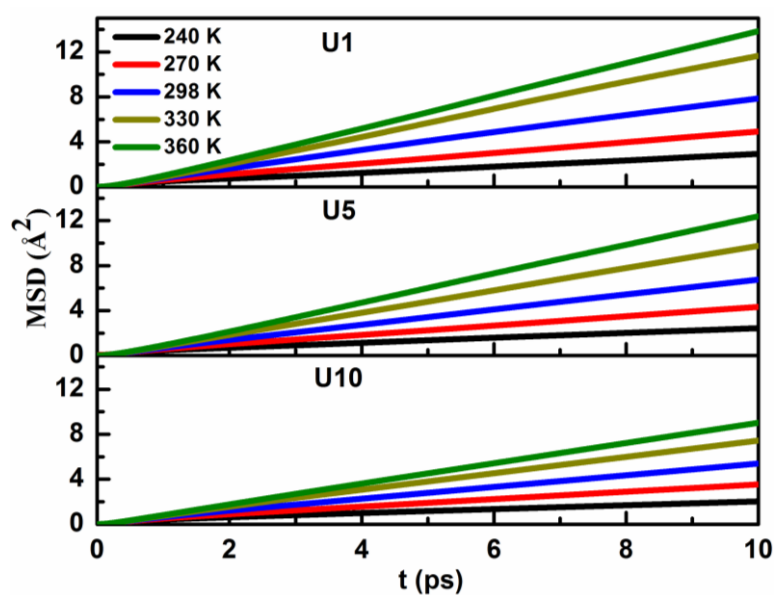


Figure 3.17: MSD profiles of the uranium atom of uranyl ions for U1, U5 and U10 systems at different temperatures.

Table 3.10: Diffusion coefficient values for uranium atom of uranyl ions at different temperatures for U1, U5 and U10 systems

Diffusion coefficients, $D_{PBC}$ ( $10^{-5} \text{ cm}^2 \text{ s}^{-1}$ ) for uranium atom of uranyl ion					
	240 K	270 K	298 K	330 K	360 K
<b>U1</b>	0.46	0.76	1.37	1.89	2.43
<b>U5</b>	0.36	0.70	1.09	1.63	2.12
<b>U10</b>	0.29	0.55	0.87	1.19	1.46

The values of diffusion coefficients for overall water molecules in U1 system and uranium atom of uranyl ion in U1 system are similar to those given by Tiwari et al. for TIP3P model of water.<sup>15</sup> Using the shear viscosity values for TIP3P water<sup>35</sup> at different temperatures, the diffusion coefficient values are corrected for system size dependence and are given in Table 3.11. As the shear viscosity values are not available at low temperatures (240 K and 270 K), an exponential function  $[A \cdot \exp(-xT)]$  is fitted to the shear viscosity data given for temperature range 283 K to 363 K.<sup>35</sup> From the fitted function, the shear viscosity of water is generated at 240 K and 270 K which is used to estimate the corrected diffusion coefficients (Table 3.11).

**Table 3.11: Diffusion coefficient values of water molecules and uranyl ions corrected for system size at different temperatures for U1, U5 and U10 systems**

<b>Corrected diffusion coefficients, <math>D_o</math> (<math>\text{cm}^2 \text{s}^{-1}</math>) of overall water molecules</b>					
	<b>240 K</b>	<b>270 K</b>	<b>298 K</b>	<b>330 K</b>	<b>360 K</b>
<b>U1</b>	2.25	4.01	6.07	8.59	10.98
<b>U5</b>	2.02	3.56	5.29	7.50	9.39
<b>U10</b>	1.79	3.03	4.37	5.96	7.65
<b>Corrected diffusion coefficients, <math>D_o</math> (<math>\text{cm}^2 \text{s}^{-1}</math>) of coordination shell water molecules</b>					
<b>U1</b>	0.99	1.51	2.65	3.27	4.32
<b>U5</b>	0.97	1.44	2.26	3.17	3.82
<b>U10</b>	0.86	1.33	1.99	2.69	3.32
<b>Corrected diffusion coefficients, <math>D_o</math> (<math>\text{cm}^2 \text{s}^{-1}</math>) of uranium atom of uranyl ions</b>					
<b>U1</b>	0.89	1.34	2.16	2.97	3.81
<b>U5</b>	0.79	1.28	1.88	2.71	3.50
<b>U10</b>	0.72	1.13	1.66	2.27	2.84

### 3.4 Conclusions

In summary, behavior of aqueous solutions of uranyl ions is studied by analyzing both structural and dynamical aspects. In particular, we are interested in the effect of concentration of the uranyl nitrate on the structural and dynamical properties of the system. The radial distribution of water around the uranyl ion does not change appreciably with the concentration of the salt. At very low concentrations, the presence of uranyl ions does not affect much the diffusion characteristics of different species in solution. However, significant changes in diffusivities of ions as well as water are observed at higher concentrations of uranyl ions. The diffusivity of the uranyl ion in the solution decreases considerably (by about 23% in TIP3P water and around 15% in SPC/E water) with the increase in uranyl ion concentration from 0.106 M to 1.06 M. The observed decrease in water diffusivity in presence of uranyl ion/s may originate from (i) retardation of the solvation water and/or (ii) long range effect of uranyl ion on the diffusion of water beyond FCS. We have therefore examined in detail translational dynamics of water in the solvation shell as well as outside the first coordination shell of the uranyl ion. The analyses of the MSDs for water molecules within the first coordination shell of uranyl ions reveal that the motion of the water molecules in the hydration shell of uranyl ion is considerably retarded. The analyses of the MSD of the water molecules outside the FCS suggest (see Figure 3.4) that long range effect of the uranyl ions on these water molecules also reduces water diffusivity. But, as the fraction of solvation water (around 1 % in U1 system and around 9% in U10 system) is considerably small, contribution of the retarded solvation water to the overall diffusivity is negligibly small. Therefore, decrease in overall diffusivity of water in presence of uranyl ion is a consequence of long range effect. The effect of finite concentration of the actinyl ions on the tetrahedral structure<sup>36</sup> of water is an interesting aspect to investigate and the work in this direction is in progress. Orientational behavior of aqueous solutions of uranyl ions is studied with respect to

the water molecules within first coordination of the uranyl ions. Also the effect of concentration of uranyl ions on the orientational structure and dynamics of water molecules is investigated. The angular distribution remains more or less the same with change in concentration of uranyl ions in aqueous solution. From the positions of the first peaks of the radial distribution functions of oxygen atom of the water and that of the nitrate ions with respect to uranyl ion it transpires that the oxygen atoms of water and nitrate both are in the first solvation shell of uranyl ions. From the coordinated numbers of water oxygen and oxygen atom of the nitrate ion as a function of uranyl nitrate concentration it is evident that a competition exists between the nitrate ion and the water molecules for occupying the first solvation shell of the uranyl ion. The rotational dynamics of water in terms of orientational time correlation functions have also been estimated and the results demonstrate that there is only slight retardation of the orientational motion of water at high concentration of uranyl ions in solution. We also investigated the orientational correlation functions of water molecules within the solvation shell of uranyl ions. It is observed that the orientational dynamics of the water molecules remains the same whether they are inside or outside the solvation shell of uranyl ions. The effect of temperature is studied on the various structural, translational and orientational features of the systems with varying uranyl ion concentrations. As expected, the effect of increasing temperature enhances the translational and orientational mobilities of water molecules. This chapter presents the analysis of the various properties of aqueous solution of uranyl ions at ambient pressure for different temperatures, however, it will be interesting to investigate on how these actinyl ions behave in supercritical conditions. Moreover, Supercritical water is of huge importance due to its applications in extraction processes and nuclear industry. Hence, it will be interesting to investigate fundamental aspects of the behavior of these ions under extreme conditions of temperature and densities. The results of present Chapter show interesting modifications in the structural and transport

characteristics of aqueous solutions of uranyl ions as a response to changes in the concentration of uranyl ions in the solutions. Hence, It will also be interesting to check whether similar variations are observed under extreme conditions of temperature and pressures i.e. when the solvent water is in supercritical state. We will be discussing such systems in the following chapter i.e. Chapter 4.

## References

1. P. Guilbaud and G. Wipff, *J. Phys. Chem.*, **1993**, 97, 5685.
2. P. Guilbaud and G. Wipff, *J. Incl. Phenom. Mol. Chem.*, **1993**, 16, 169.
3. P. Guilbaud and G. Wipff, *J. Phys. Chem.*, **1996**, 366, 55.
4. F. Hutschka, A. Dedieu, L. Troxler and G. Wipff, *J. Phys. Chem. A*, **1998**, 102, 3773.
5. A. Chaumont and G. Wipff, *Inorg. Chem.*, **2003**, 42, 5348.
6. A. Chaumont and G. Wipff, *Inorg. Chem.*, **2004**, 43, 5891.
7. R. Schurhammer, and G. Wipff, *J. Phys. Chem. A*, **2005**, 109, 5208.
8. M. Bühl, N. Sieffert, A. Chaumont and G. Wipff, *J. Am. Chem. Soc.*, **2006**, 128, 6357.
9. M. Bühl, N. Sieffert, A. Chaumont and G. Wipff, *Inorg. Chem.*, **2012**, 51, 1943.
10. M. Baaden, F. Berny, C. Madic and G. Wipff, *J. Phys. Chem. A*, **2000**, 104, 7659.
11. N. Rai, S. P. Tiwari, E. J. Maginn, M. P. Brown and K. Austin, *J. Phys. Chem. B*, **2012**, 116, 10885.
12. S. Kerisit and C. Liu, *J. Phys. Chem. A*, **2013**, 117, 6421.
13. S. Kerisit and C. Liu, *Geochim Cosmochim. Acta*, **2010**, 74, 4937.
14. V. Pomogaev, S. P. Tiwari, N. Rai, G. S. Goff, W. Runde, W. F. Schneider and E. J. Maginn, *Phys. Chem. Chem. Phys.*, **2013**, 15, 15954.
15. S. P. Tiwari, N. Rai and E. J. Maginn, *Phys. Chem. Chem. Phys.*, **2014**, 16, 8060.

16. S. Spencer, L. Gagliardi, N. C. Handy, A. G. Ioannou, C. Skylaris, A. Willetts and A. M. Simper, *J. Phys. Chem. A*, **1999**, *103*, 1831.
17. C. Clavaguera-Sarrio, V. Brenner, S. Hoyau, C. J. Marsden, P. Millie and J. P. Dognon, *J. Phys. Chem. B*, **2003**, *107*, 3051.
18. D. Hagberg, G. Karlstrom, B. O. Roos and L. Gagliardi, *J. Am. Chem. Soc.*, **2005**, *127*, 14250.
19. R. J. Frick, T. S. Hofer, A. B. Pribil, B. R. Randolph and B. M. Rode, *J. Phys. Chem. A*, **2009**, *113*, 12496.
20. R. J. Frick, T. S. Hofer, A. B. Pribil, B. R. Randolph and B. M. Rode, *Phys. Chem. Chem. Phys.*, **2010**, *12*, 11736.
21. J. A. Greathouse, R. J. O'Brien, G. Bemis and R. T. Pabalan, *J. Phys. Chem. B*, **2002**, *106*, 1646.
22. T. Patsahan and M. Holovko, *Condens. Matter Phys.*, **2007**, *10*, 143.
23. M. Jayasinghe and T. L. Beck, *J. Phys. Chem. B*, **2009**, *113*, 11662.
24. X. Ye, R. B. Smith, S. Cui, V. de Almeida and B. Khomami, *Solvent Extr. Ion Exc.*, **2010**, *28*, 1.
25. D. Bandyopadhyay, S. Mohan, S. K. Ghosh and N. Choudhury, *J. Phys. Chem. B*, **2014**, *118*, 11757.
26. M. P. Allen and D. J. Tildesley, *Computer Simulation of Liquids*; Oxford University, New York, 2004.
27. A. P. Karande, G. K. Mallik, J. P. Panakkal, H. S. Kamath, V. K. Bhargava and J. N. Mathur, *J. Radioanal. Nucl. Chem.*, **2003**, *256*, 185.
28. NEA. Spent Nuclear Fuel Reprocessing Flowsheet, Nuclear Science, NEA/NSC/WPFC/DOC, Nuclear Energy Agency, Organization for Economic Co-operation and Development, Paris, 2012.



29. W. L. Jorgensen, J. Chandrashekar, J. D. Madura, R. W. Impey and M. L. Klein, *J. Chem. Phys.*, **1983**, 79, 926.
30. I. Yeh and G. Hummer, *J. Phys. Chem. B*, **2004**, 108, 15873.
31. Y. Awakura, K. Sato, H. Majima, S. Hirono, *Metall. Trans. B*, **1987**, 18, 19.
32. D. M. H. Kern, E. F. Orlemann, *J. Am. Chem. Soc.*, **1949**, 71, 2102.
33. R. D. Brown, W. B. Bunger, W. L. Marshall, C. H. Secoy, *J. Am. Chem. Soc.*, **1954**, 76, 1532.
34. G. Marx, H. Bischoff, *J. Radioanal. Chem.*, **1976**, 30, 567.
35. Y. Mao, Y. Zhang, *J. Nanotechnol. Eng. Med.*, **2012**, 3, 030110.
36. D. Bandyopadhyay, S. Mohan, S. K. Ghosh and Choudhury, N. *J. Phys. Chem. B* **2013**, 117, 8831.



# *Chapter 4*

## **Aqueous Solutions of Uranyl Ions in Supercritical Water: Dissecting the Effect of Uranyl Ion Concentration from Solvent Density**



## 4.1 Introduction

Supercritical fluids (SCF) are of immense importance due to their wide applications in chemistry, physics and chemical engineering. The wide applicability of the SCF is due to its high dissolving power, extraction efficiency and enhanced mass transport.<sup>1-4</sup> High compressibility and inherent density inhomogeneity leading to voids and clusters of the supercritical fluid may have direct consequence on the manifestation of different properties of the SCF. One of the most important aspects of the SCF is that the density can be fine-tuned through small changes in the temperature or pressure. Another important aspect of the SCF is the availability of a wide range of densities without changing the phase of the system. In order to understand detailed microscopic origin of different properties of the supercritical solutions and neat solvents, fundamental understanding of the solvation structure and dynamics, taking both atomic correlations and density fluctuations into account, is essential.

Water is one of the most important fluids due to its unique properties<sup>5-7</sup> and universal use as solvents in chemical and industrial processes. Supercritical water is also of huge importance due to its applications in extraction processes and nuclear industry. Nuclear power generation involves the use of actinide species in chain reactions. The actinides are present both as the fuel as well as the waste during the course of nuclear reactions. Radiotoxic actinyl ions find their importance in the nuclear fuel cycle, mostly because of their fissile nature and long half-lives. The methods are being developed worldwide to recycle these actinides by reprocessing of the spent fuel or by extraction of these from other species in the radioactive waste. This practice has an additional advantage of reducing the quantity of waste which needs to be disposed of safely. Various methods of separation of these actinyl ions from the nuclear waste involving supercritical fluids have been proposed.<sup>4,8-11</sup> Moreover, supercritical water is proposed to be an efficient coolant for Generation IV nuclear reactors.<sup>12</sup> Supercritical water is observed to have an important role in hydrothermal reactions involving actinyl

ions.<sup>13</sup> Thus, knowledge of hydration and transport properties of these actinyl ions becomes essential for designing advanced separation processes for recycling of the radiotoxic material in the waste. Moreover, it will be interesting to analyze how these ions behave under extreme conditions of temperature and densities. The radiotoxic nature leads to the practical difficulties in performing experiments involving actinyl ions. The computational investigation based on molecular dynamics simulation has become a useful and creditable tool for analyzing the behavior of these ions in various systems.

There has been a number of molecular dynamics simulation studies related to various characteristics of supercritical water<sup>14-21</sup> as well as aqueous solutions<sup>21-26</sup> of ions under supercritical conditions. For instance, Cummings et al.<sup>21</sup> and Balbuena et al.<sup>22</sup> studied the structural features of bulk water and the aqueous solutions of various positive and negative ions under supercritical conditions whereas Lee<sup>26</sup> demonstrated the structural and dynamical characteristics of hydroxide ion in supercritical water. Rasaiah and coworkers reported<sup>23,24</sup> the structure and dynamics of the aqueous solutions of a number of positive and negative ions, and neutral solutes at infinite dilution under supercritical conditions. Yui et al.<sup>25</sup> estimated and compared the thermodynamic properties of the aqueous solution of NaCl under normal and supercritical conditions. As far as uranyl ions are considered, a number of studies related to aqueous solutions of uranyl ions are available under ambient condition<sup>27-32</sup> where structural and dynamical characteristics of various species in the solutions are analyzed. Moreover, Chapter 3 of the present thesis also deals with the aqueous uranyl solution under normal conditions of temperature and pressure where effect of uranyl ion concentration and temperature on the various characteristics of the solution is analyzed. To the best of our knowledge, studies on aqueous solutions of uranyl ions under supercritical conditions had not been reported.

The Results and Discussion section of this Chapter consists of two parts: Part A and B. In Part A, we intend to study the behavior of aqueous solution of uranyl ions at infinite dilution under supercritical conditions using molecular dynamics simulations. Moreover, we aim to investigate the effect of density of water on hydration structure and dynamical properties of different species present in bulk water as well as in aqueous solution of uranyl ions. From Chapter 3 related to aqueous uranyl solution at ambient condition, it is observed that the dynamical properties of the aqueous solution of the uranyl ions get modified significantly with the change in uranyl ions concentrations. This led to our curiosity to investigate the effect of increasing concentration of the uranyl ions on the dynamics of aqueous solution of the uranyl ions at supercritical conditions and compare it with the effect of changing the density of the solvent in Part B of the Results and Discussion section. All atom molecular dynamics (MD) simulations of uranyl ions in supercritical water are used to dissect the effects of concentration of uranyl ions and density of water on various structural and dynamic properties of the solutions. The combined effect of water density and uranyl concentration in the solution on the behavior of various species is also analyzed by simulating systems of different densities. The hydration structure of ions and water molecules are analyzed by calculating radial distribution functions and orientational probability distribution functions. Orientational structures are obtained by calculating the distributions of different molecular orientation vectors of water in the first solvation shells around a central water molecule or an ionic species. Translational diffusivities of water and ionic species have also been calculated from the slope of the mean squared displacements and the power spectra of the collective vibrations of water molecules is used to corroborate the sequence of diffusion coefficients for various densities and concentrations. Orientational mobility of water molecules in pure water and in the uranyl solution has also been assessed by calculating the time correlation functions of different molecular vectors of water. Some of the structural and

dynamic properties of the aqueous solutions of uranyl ions obtained under supercritical conditions are compared with those reported under normal conditions (Chapters 2 and 3).

## 4.2 Models and Simulation Details

In the present work, we considered both bulk water and aqueous solutions of uranyl ion in supercritical states. A box of around 2400 water molecules with appropriate bulk density is prepared using PACKMOL program.<sup>33</sup> In case of aqueous solutions of uranyl ion, one uranyl ion is solvated in a cubic box of 2400 water molecules of appropriate density. We considered here three different water densities viz., 0.38, 0.56 and 0.98 g cm<sup>-3</sup> with equilibrium box lengths and pressures as given in Table 4.1. In order to investigate the effect of varying uranyl ion concentration in Part B, different systems of aqueous solutions of uranyl ions are prepared using PACKMOL by solvating different number of uranyl ions in specified number of water molecules within a cubical box with approximate dimensions 5.0 nm x 5.0 nm x 5.0 nm. Nine different sets of aqueous solutions of uranyl ions in supercritical water are simulated for different water densities and uranyl ion concentrations as given in Table 4.2 along with their equilibrium box lengths and pressures. The Set No. 4 is same as S. No. 2 in Table 4.1. The range of concentrations studied in this work are of the order of concentrations encountered generally in the back end of the nuclear fuel cycle, especially during reprocessing of uranium based spent fuel.<sup>34,35</sup> The nitrate (negative) ions are introduced in the solution as counter-ions to maintain the electrical neutrality of the aqueous uranyl system. Molecular dynamics simulations are performed in isothermal-isobaric (NPT) ensemble, in which temperature and pressure of the system are maintained by using extended system approach of Nose, Andersen, Parrinello, and Rahman.<sup>36-40</sup> The pressures for densities around 0.38 and 0.56 g cm<sup>-3</sup> are in good agreement with those reported in experimental<sup>41</sup> and theoretical



studies.<sup>42</sup> The uncertainties in densities are estimated from the uncertainty in box lengths during the NPT simulation.

**Table 4.1: Density and box lengths of the systems simulated using Molecular Dynamics**

**Simulation at 683 K for Part A**

S. No.	Density (g cm <sup>-3</sup> )	Pressure (atm)	Equilibrium Box Length (nm)
1.	0.38 ± 0.008	315	5.715
2.	0.56 ± 0.006	640	5.028
3.	0.98 ± 0.003	7100	4.183

Atomistic models are used for uranyl ion with one uranium and two oxygen sites, and for the nitrate ion with one nitrogen and three oxygen sites<sup>32,43</sup> whereas SPC/E model<sup>44</sup> for water was used in all simulations. Lennard–Jones and Coulomb (for charged sites) potentials are considered for non-bonded site-site interactions and usual harmonic terms are used for bonds and angles in the intra-molecular potential terms for uranyl and nitrate ions. The potential energy of such a system is described by Eq. 1.5 given in Chapter 1 of this thesis. The values of the potential parameters for both inter- and intra-molecular interactions for water and uranyl ion with SPC/E water model are given in Table 2.1 of Chapter 2 and Table 3.1 of Chapter 3.<sup>32,43,44</sup> The cross parameters for the LJ potential are estimated by using Lorentz–Berthelot mixing rule.

For supercritical states, all the simulations were carried out at 683 K, a temperature greater than the critical temperature of water (experimental value of 647 K and 638.6 K for SPC/E water<sup>45</sup>). A simulation of aqueous uranyl solution is also performed at 298 K and 1 atm pressure to generate some of the results for comparison wherever specified in the text.

The equations of motion are integrated with a time step of 1 fs. The simulation for equilibration is carried out for a period of 2 ns. The trajectories are saved at every 0.01 ps during the next 2 ns production run, thereby ensuring the convergence of results.

**Table 4.2: Various sets of systems with different uranyl concentrations and different supercritical water densities considered in present study for Part B**

<b>Set No.</b>	<b>Density (g cm<sup>-3</sup>)</b>	<b>Number of water molecules in the system</b>	<b>Number of uranyl ions in the system</b>	<b>Concentration (M)</b>	<b>Box Length at equilibrium (nm)</b>
1	0.38 ± 0.01	1600	1	0.013 ± 0.0003	4.999
2	0.40 ± 0.01	1596	5	0.070 ± 0.0017	4.924
3	0.41 ± 0.01	1591	10	0.144 ± 0.0036	4.843
4	0.56 ± 0.006	2400	1	0.013 ± 0.0002	5.028
5	0.57 ± 0.006	2400	5	0.066 ± 0.0007	5.016
6	0.57 ± 0.006	2400	10	0.132 ± 0.0015	5.002
7	0.98 ± 0.003	3920	1	0.014 ± 0.00004	4.922
8	0.98 ± 0.003	3916	5	0.069 ± 0.0002	4.928
9	0.97 ± 0.003	3911	10	0.138 ± 0.0004	4.934

\*Set 4 is same as serial No. 2 in Table 4.1

## 4.3 Results and Discussion

### Part A

#### **Structure and Dynamics of Infinitely Dilute Aqueous Solution of Uranyl Ions**

The structure and dynamics of infinitely dilute aqueous solution of uranyl ions in supercritical water have been estimated using MD simulations. The motive is to understand radial and orientational structure as well as translational and rotational dynamics of the various species present in the solution and the effect of the water density on these properties. Also, the aim is to check how the results under supercritical conditions compare with those reported for normal conditions of temperature and pressure. The radial structure of water and other species in the solution is studied by estimating the radial distribution functions (RDFs). The angular distribution of water molecules around uranyl ions is studied in terms of the distributions of various angles. These angular distributions of solvation shell water molecules are compared with those obtained for water around a central water molecule in bulk supercritical water. The mean squared displacement (MSD) of the different species including water is analyzed to understand the translational dynamics of these species in the solution. The results obtained for different densities i.e. 0.38, 0.56 and 0.98 g cm<sup>-3</sup> are compared to quantify the impact of density on various properties. Structural characteristics of the water molecules in the simulated systems of aqueous uranyl solutions are presented in Subsections 4.3.1 and 4.3.2. The translational and angular dynamics of the different species in the systems are discussed in Subsections 4.3.3 and 4.3.4 respectively.

##### **4.3.1 Radial Distribution Functions of the Aqueous Uranyl Solution**

The structural distribution of water molecules is studied by estimating the radial distribution functions of water molecules around uranyl ions or around central water

molecule. For bulk supercritical water, distributions of oxygen ( $O_w$ ) and hydrogen ( $H_w$ ) atoms of water molecules around the central water molecule ( $O_w$ ) i.e.  $O_w$ - $O_w$  and  $O_w$ - $H_w$  RDFs are given in Figure 4.1. Figure 4.1(a) has shown a peak of distribution of oxygen atoms of water molecules around the oxygen atom of the central water molecule at around 2.8 Å with first minimum occurring at around 4.3 Å. The distribution of hydrogen atoms of water molecules show two small humps at around 1.9 Å and 3.4 Å radial distance from the central water molecule (Figure 4.1b). Similar experimental as well as simulated radial distribution functions have been reported in literature for bulk water under supercritical conditions.<sup>16,19,21</sup> As expected, positively charged hydrogen atoms appear closer to negatively charged oxygen atoms.

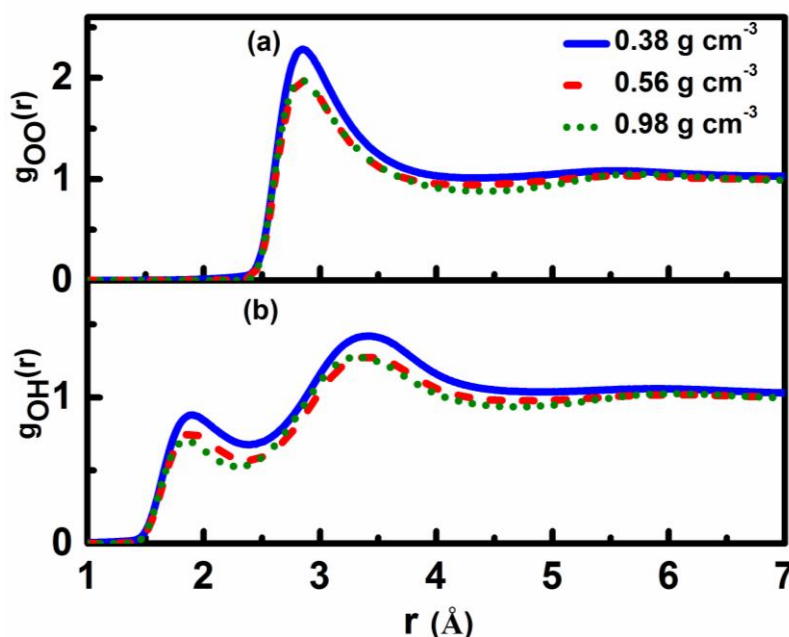


**Figure 4.1: Radial distribution functions for (a)  $O_w$  and (b)  $H_w$  of water molecules around the oxygen of central water molecule for bulk supercritical water at water densities of 0.38 g cm<sup>-3</sup>, 0.56 g cm<sup>-3</sup> and 0.98 g cm<sup>-3</sup> at 683 K.**

The distributions of oxygen ( $O_w$ ) and hydrogen ( $H_w$ ) atoms of water molecules around uranium (U) and oxygen ( $O_U$ ) atoms of the uranyl ions for aqueous uranyl solution at different densities are plotted in Figure 4.2. It is worth mentioning here that the RDFs are cut

at a radial distance of 7.0 Å for better clarity of peaks, otherwise all RDFs converge to 1.0 at long distances i.e. bulk behavior. The first peak of the distribution of oxygen atoms of water around uranium atom appears at around 2.46 Å (Figure 4.2a) whereas for oxygen atom of uranyl ion appears at around 2.96 Å (Figure 4.2c) indicating that positively charged uranium is closer to negatively charged oxygen atoms of water molecules as compared to negatively charged oxygen atom of uranyl ions. The positively charged hydrogen atoms are directed away from the overall positively charged uranyl ions as compared to negatively charged oxygen atoms of the water molecules. It can be seen that the peak value of the radial distribution increases with decrease in the density of the system, both for bulk water and aqueous solution of uranyl ions.

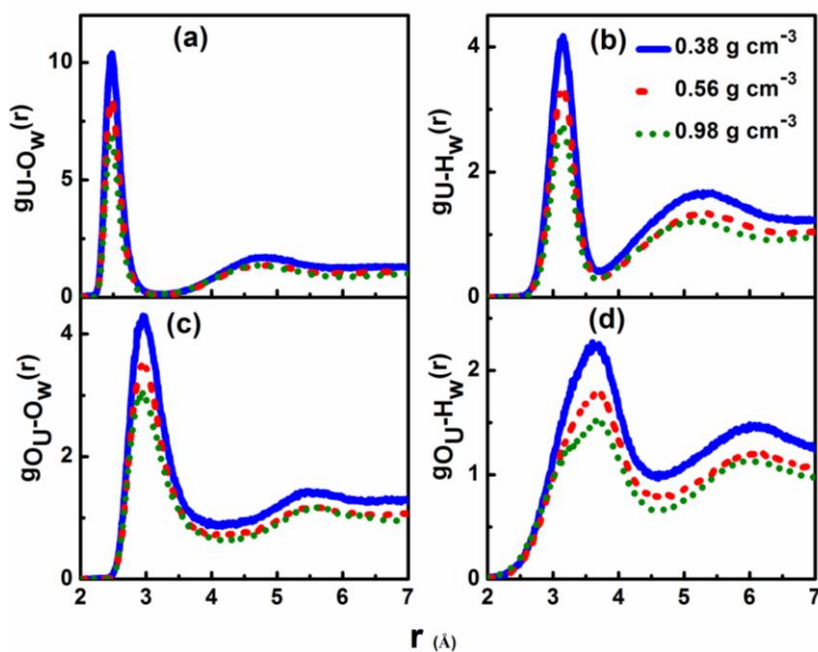


**Figure 4.2: Radial distribution functions for (a) O<sub>w</sub> around uranium, (b) H<sub>w</sub> around uranium (c) O<sub>w</sub> around uranyl-oxygen (O<sub>U</sub>) and (d) H<sub>w</sub> around O<sub>U</sub> at water densities of 0.38 g cm<sup>-3</sup> (blue solid line), 0.56 g cm<sup>-3</sup> (red dashed line) and 0.98 g cm<sup>-3</sup> (green dotted line) at 683 K.**

To quantify this variation, coordination or hydration numbers of central water molecule and, uranium and oxygen atoms of uranyl are estimated for densities varying from

0.38 to 0.98 g cm<sup>-3</sup> (Table 4.3). It should be noted that the coordination numbers for uranium and oxygen atoms of uranyl ion are calculated independently. Hence, there may be overlapping of their coordination shells leading to some water molecules which will be common to both. Here, coordination/hydration number of a central species is computed using Eq. 1.14 as given in Chapter 1. The cutoff distance is chosen as the distance at which the first trough appears in the corresponding RDF and these are 4.3 Å, 3.3 Å and 4.1 Å for the central species oxygen of water, uranium and oxygen atoms of the uranyl ion respectively. It is important to note that although the height of the RDF peak reduces with increase in density, the multiplication by bulk density ( $\rho_0$ ) leads to an increase in the coordination/hydration number as reported earlier for alkali metal and halide ions by Rasaiah et al.<sup>23,24</sup> The coordination number of water at different densities are found to be in good agreement with those reported earlier.<sup>19,21,22</sup> The coordination number of water is observed to be higher at supercritical conditions than under ambient conditions whereas that of uranium is observed to be almost same (Chapter 3).

**Table 4.3: Coordination/Hydration numbers of oxygen atoms of central water molecules in bulk water and uranium and oxygen atoms of uranyl ions in aqueous uranyl solution.**

Density (g cm <sup>-3</sup> )	Coordination/Hydration number		
	Bulk water	Aqueous uranyl solution	
	O <sub>w</sub>	U	O <sub>U</sub>
0.38	4.50 ± 0.01	3.02 ± 0.26	5.11 ± 0.38
0.56	5.97 ± 0.003	3.73 ± 0.40	6.38 ± 0.50
0.98	10.33 ± 0.001	5.06 ± 0.17	9.89 ± 0.20

### 4.3.2 Orientational Distribution of Water Molecules within the First Coordination/hydration Shell of Uranyl Ion or Central Water Molecule

Angular distributions of the water molecules around uranium atom of uranyl ion in its first coordination/hydration shell (FCS) are estimated for different water densities varying from 0.38 to 0.98 g cm<sup>-3</sup>. The first minimum (3.3 Å) of the respective  $g(r)$  is defined as the first coordination/hydration shell boundary. Three different angles were considered, namely, angle formed between the line joining uranium atom of the uranyl ion and oxygen atom of the solvation water molecule (i.e. U-O<sub>w</sub> distance vector) and (i) water dipole moment vector ( $\theta$ ), (ii) a vector perpendicular to plane of water molecule ( $\psi$ ), and angle between U-O<sub>U</sub> bond vector and water dipole moment vector or U-O<sub>w</sub> vector ( $\chi$ ) (Figure 4.3).

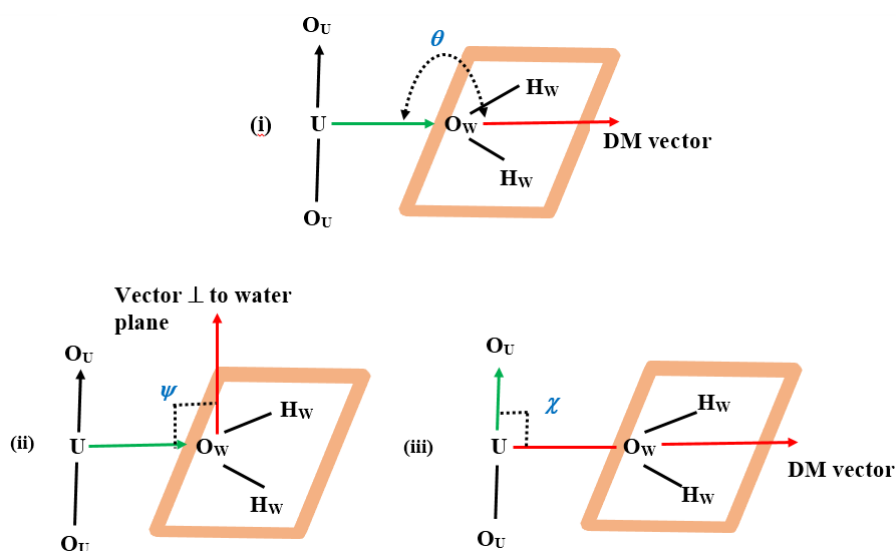


**Figure 4.3: Schematic representation of various angles considered for orientational distribution of the water molecules around uranyl ions in the aqueous uranyl nitrate solution, DM vector means Dipole Moment vector.**

The distributions of these angles for the water molecules in the first coordination shell of uranium atom of uranyl ions for density of 0.98 g cm<sup>-3</sup> at ambient (Chapter 2) and supercritical conditions are shown in Figure 4.4a. The distribution of angle  $\chi$  is generated by carrying out a simulation at 298 K. In Figure 4.4a, a peak in the distribution of  $\theta$  is observed

at around  $0^\circ$  which implies that the dipole moment vectors of the FCS water molecules are directed along the U-O<sub>w</sub> vector. Moreover, peak at  $\theta=0^\circ$  indicates that the H atoms of water are directed away from the U of UO<sub>2</sub>. The similar results have been reported for uranyl solution in water at normal temperature and pressure<sup>46</sup> (Chapter 2).

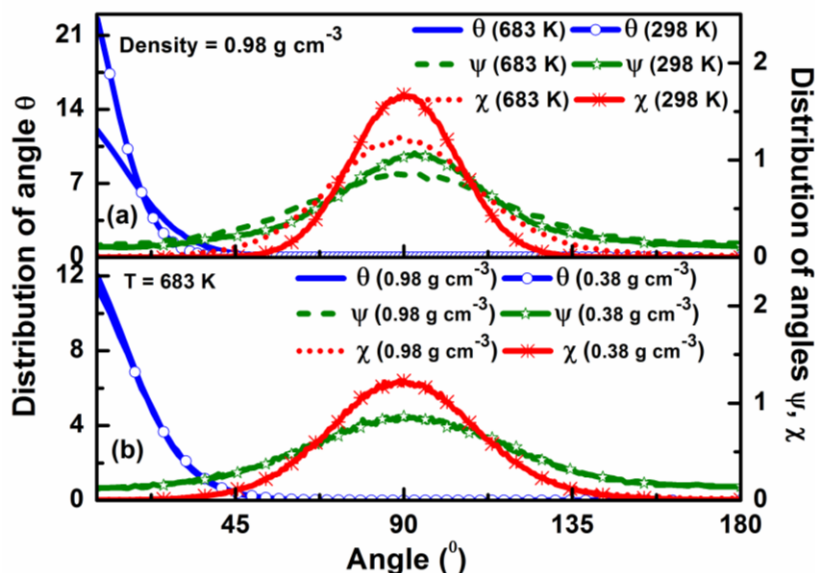


**Figure 4.4: Distributions of various angles between U-O<sub>w</sub>/U-O<sub>u</sub> vector and different molecular orientational vectors of a water molecule in the first coordination shell of a uranyl ion in the aqueous uranyl nitrate solution (a) at a density of 0.98 g cm<sup>-3</sup> at 298 K and 683 K, (b) at densities of 0.38 g cm<sup>-3</sup> and 0.98 g cm<sup>-3</sup> at 683 K.**

As the water dipole moment vector and U-O<sub>w</sub> vectors point in the same direction, accordingly the distributions of angle for orientation of plane perpendicular vector ( $\psi$ ) showed a peak at around  $90^\circ$  as expected. This result is consistent with the corresponding results for aqueous uranyl solution under normal conditions<sup>46</sup> (Chapter 2). The preferred distribution of U-O<sub>u</sub> vector is observed to be at right angle to the water dipole moment vector as indicated by the peak at around  $\chi=90^\circ$ . All these angular distributions reveal that the orientations of different water vectors with respect to uranyl ions remain the same whether water is under normal or supercritical conditions (Chapter 2) however, the spread is observed to be more and intensity of the peak is lower in case of supercritical water. Moreover, the



angular distribution remains more or less the same with change in the density of the supercritical water in the solution (Figure 4.3b).

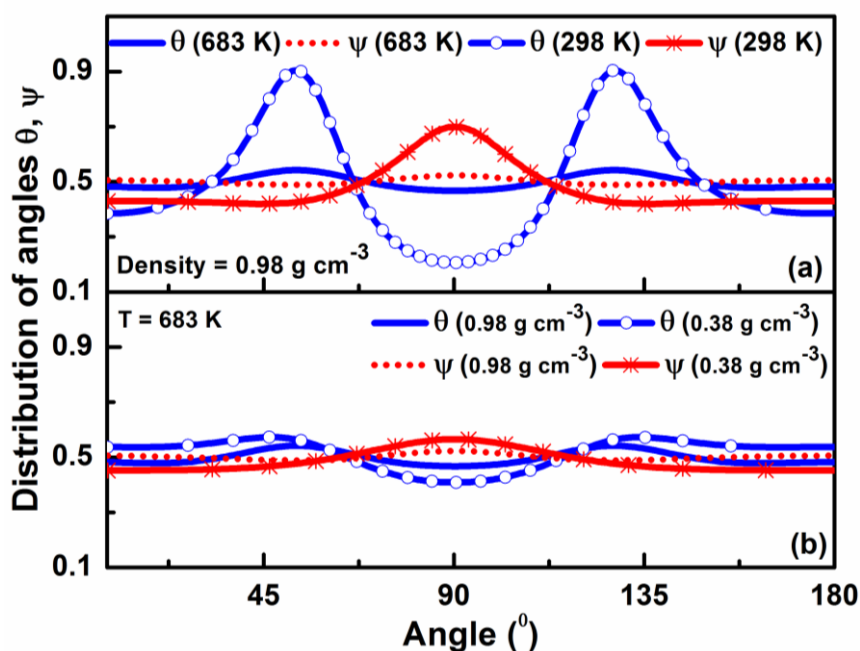


**Figure 4.5:** Distributions of various angles between Ow-Ow vector and different molecular orientational vectors of a water molecule in the first coordination shell of a central water molecule in bulk water (a) at a density of  $0.98 \text{ g cm}^{-3}$  at 298 K and 683 K, (b) at densities of  $0.38 \text{ g cm}^{-3}$  and  $0.98 \text{ g cm}^{-3}$  at 683 K.

For comparison, the angular distributions of water molecules around a central water molecule have also been estimated for bulk supercritical water of same density ( $0.98 \text{ g cm}^{-3}$ ). Two angles are considered similar to angles (i) and (ii) in Figure 4.4 with U-Ow vector replaced with Ow-Ow distance vector. In this case, the first minimum of the  $g(r)$  is at radius of  $4.3 \text{ \AA}$ . The angular distributions of the bulk water in supercritical state as shown in Figure 4.5 are observed to be similar as those for bulk water under normal conditions (Chapter 2), the only difference being the lower intensities of the peaks of angular distribution in case of supercritical water (Figure 4.5a). As observed in case of aqueous uranyl solution, the angular distribution remains the same with change in the density of water (Figure 4.5b).

### 4.3.3 Translational Dynamics of Water Molecules and Uranyl Ions in Aqueous Uranyl Solution

Translational diffusion of water molecules and uranyl ions is analyzed in terms of mean squared displacement functions (MSD) as it is related to the self-diffusion coefficient ( $D$ ) of the fluid through the well-known Einstein relation as given by Eq. 1.19 in Chapter 1. The MSD curves are obtained for solutions of different water densities ( $0.38, 0.56$  and  $0.98 \text{ g cm}^{-3}$ ) to analyze the effect of solvent density on the translational motion of water molecules and uranyl ions. The MSD curves of water molecules and uranyl ions in aqueous uranyl solution are plotted for water densities varying from  $0.38$  to  $0.98 \text{ g cm}^{-3}$  in Figures 4.6 and 4.7 respectively.

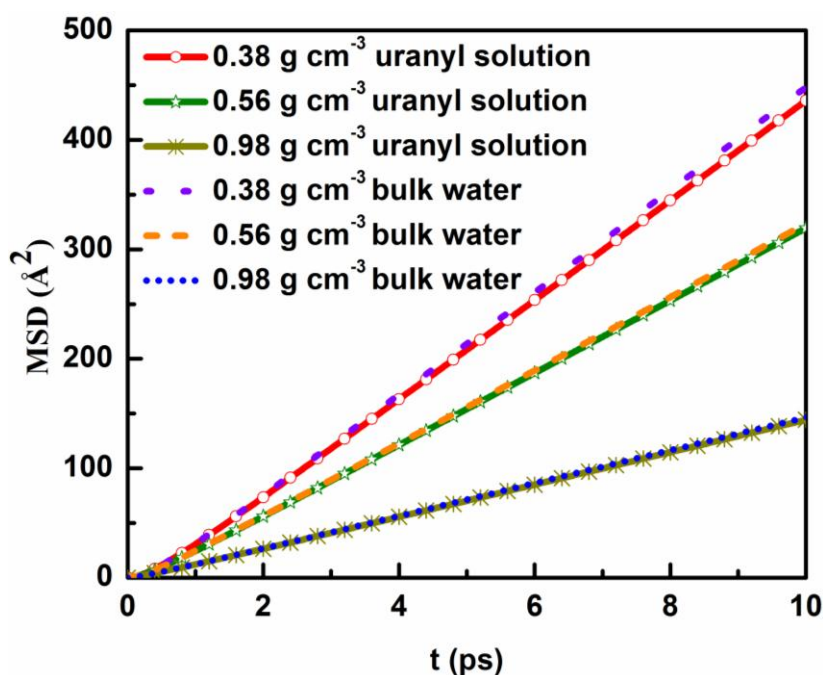


**Figure 4.6:** Mean squared displacement (MSD) as a function of time for water molecules in the aqueous uranyl solution and in bulk water at densities of  $0.38, 0.56$  and  $0.98 \text{ g cm}^{-3}$  at  $683 \text{ K}$ .

These figures show that the translational movement of these species slows down as there is an increase in the water density. The MSD curves of water molecules for bulk water as well as for aqueous uranyl solution of infinite dilution almost overlap, however there is

slight slowing down of the movement in aqueous uranyl solution. Similar results were obtained for bulk water and very dilute aqueous solution of uranyl ion under normal conditions of temperature and pressure (Chapter 3). The diffusion coefficient as estimated from the slopes of the straight line fittings to the MSD profiles for aqueous uranyl solutions and bulk water with different water densities along with the corresponding uncertainties are given in Table 4.4. It is observed that the water molecules diffuse slower and slower as the solution becomes denser and denser, both in bulk water and in aqueous solutions of uranyl ions (Figure 4.6). However for uranyl ion, the effect of density on diffusion coefficient is negligible from 0.38 to 0.56 g cm<sup>-3</sup> as the diffusion coefficients are almost same considering their uncertainty. However, for large density difference such as between 0.38 and 0.98 g cm<sup>-3</sup>, there is significant slowing down in translational transport of uranyl ions (Figure 4.7).

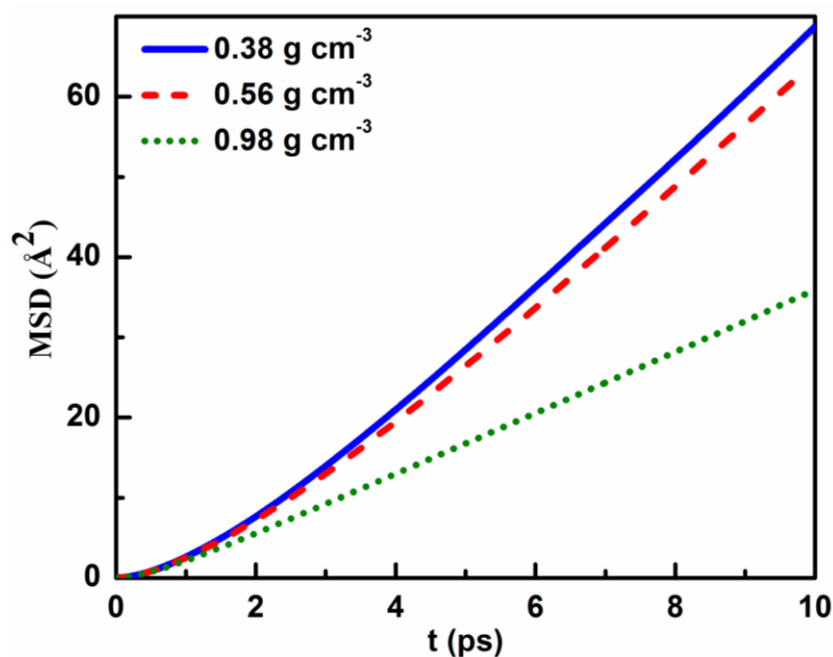


**Figure 4.7** Mean squared displacement (MSD) as a function of time for uranium atom of uranyl ions in the aqueous uranyl solution at densities of 0.38, 0.56 and 0.98 g cm<sup>-3</sup> at 683 K.

The diffusion coefficient values have been corrected for system size dependence as per Eq. 1.20 given in Chapter 1 and are also given in Table 4.4. The shear viscosity values for

water under supercritical conditions at different densities are estimated by fitting an exponential curve of the form  $\eta = a \times \exp(b\rho) + \eta_0$  to the viscosity data given by Lamb et al.<sup>41</sup>,  $\rho$  being the density of the system,  $a$  and  $b$  are the fitting parameters. We have compared the water diffusion coefficient values with the earlier reported values for bulk supercritical water from experiments<sup>41</sup> and simulations<sup>16</sup> at 673 K. The diffusion coefficient values are interpolated or extrapolated in case those are not available in these references for the exactly same densities.

**Table 4.4: Diffusion coefficient values for aqueous solutions of uranyl ions and bulk supercritical water<sup>b</sup> for different water densities.**

S. No.	Atom	$D_{\text{PBC}} (10^{-5} \text{ cm}^2 \text{ s}^{-1})$ for densities ( $\text{g cm}^{-3}$ )			$D_0 (10^{-5} \text{ cm}^2 \text{ s}^{-1})$ for different densities ( $\text{g cm}^{-3}$ )		
		0.38	0.56	0.98	0.38	0.56	0.98
1	U	$12.1 \pm 3.3$	$12.1 \pm 2.0$	$6.6 \pm 1.1$	$17.1 \pm 3.3$	$16.2 \pm 2.0$	$9.0 \pm 1.1$
2	O <sub>w</sub>	$76.0 \pm 0.5$	$55.1 \pm 0.3$	$24.7 \pm 0.2$	$81.0 \pm 0.5$	$59.2 \pm 0.3$	$27.1 \pm 0.2$
3	O <sub>w</sub> <sup>b</sup>	$78.4 \pm 0.5$	$56.1 \pm 0.3$	$24.9 \pm 0.2$	$83.4 \pm 0.5$	$60.2 \pm 0.3$	$27.3 \pm 0.2$

The interpolation is done linearly as used by Marti et al.<sup>16</sup> whereas the extrapolation is carried out by fitting the reported data with a function of the form<sup>41</sup>

$$D_0 T^{-0.763} = \frac{A}{\rho} \quad (4.1)$$

Here,  $T$  is the temperature (K),  $A$  is a constant to be obtained from the fitting and  $\rho$  is the density of the system ( $\text{g cm}^{-3}$ ). For experimental data reported by Lamb et al.<sup>41</sup>, the value of  $A$  is given as  $2.24 \times 10^{-6}$ . We have estimated the water diffusion coefficient for a density of  $0.38 \text{ g cm}^{-3}$  as  $83.4 \times 10^{-5} \text{ cm}^2 \text{ s}^{-1}$  which is comparable to the experimentally obtained value of

$91.9 \times 10^{-5} \text{ cm}^2 \text{ s}^{-1}$  given by Lamb et al.<sup>41</sup> for the same density and close to the value of  $75.5 \times 10^{-5} \text{ cm}^2 \text{ s}^{-1}$  extrapolated (using Eq. 4.1) from the values reported by Marti et al.<sup>16</sup> Similarly, the diffusion coefficient value of  $60.2 \times 10^{-5} \text{ cm}^2 \text{ s}^{-1}$  estimated in present study for a density of  $0.56 \text{ g cm}^{-3}$  is found to be closer to the experimental<sup>41</sup> (interpolated) value of  $62.3 \times 10^{-5} \text{ cm}^2 \text{ s}^{-1}$  than the earlier simulated<sup>16</sup> (interpolated) value of  $55.3 \times 10^{-5}$ . Similar comparison for other densities is given in Table 4.5. It can be observed from Table 4.5 that the diffusion coefficients obtained in present study compare fairly well with those reported in literature from experimental<sup>41</sup> and theoretical studies.<sup>16</sup>

**Table 4.5: Comparison of corrected diffusion coefficient values for bulk water molecules under supercritical conditions with experimental and theoretical results available in literature (superscript \* signifies interpolated value and # signifies extrapolated value using the fitting of the function of the type as given in Eq. 4.1)**

S. No.	Density ( $\text{g cm}^{-3}$ )	Diffusion Coefficient ( $10^{-5} \text{ cm}^2 \text{ s}^{-1}$ )		
		Present Study	Experimental <sup>41</sup>	Theoretical <sup>16</sup>
1.	0.38	$83.4 \pm 0.4$	91.9*	75.5 <sup>#</sup>
2.	0.56	$60.2 \pm 0.3$	62.3*	55.3*
3.	0.98	$27.3 \pm 0.2$	33.2 <sup>#</sup>	30.0 <sup>#</sup>

The diffusion coefficient values obtained for water molecules in aqueous uranyl solutions are slightly lower than the corresponding values obtained for pure supercritical water as was observed under ambient conditions too (Chapter 3). The comparison of the diffusion coefficient of water molecules present in aqueous solution of uranyl ions in supercritical water with those of water molecules in aqueous solution under normal conditions (Chapter 3) of same density i.e.  $0.98 \text{ g cm}^{-3}$  shows that the diffusion coefficient

value for water molecules increases from  $2.86 \times 10^{-5} \text{ cm}^2 \text{ s}^{-1}$  at 298 K (Chapter 3) to  $27.1 \times 10^{-5} \text{ cm}^2 \text{ s}^{-1}$  at 683 K. Similarly for uranyl ions, the diffusion coefficient increases from  $0.94 \times 10^{-5} \text{ cm}^2 \text{ s}^{-1}$  at 298 K (Chapter 3) to  $9.0 \times 10^{-5} \text{ cm}^2 \text{ s}^{-1}$  at 683 K. In other words, the translational mobility of uranyl ions as well as water molecules at a solvent density of  $0.98 \text{ g cm}^{-3}$ , at 683 K becomes about 10 times faster as compared to the same under ambient condition.

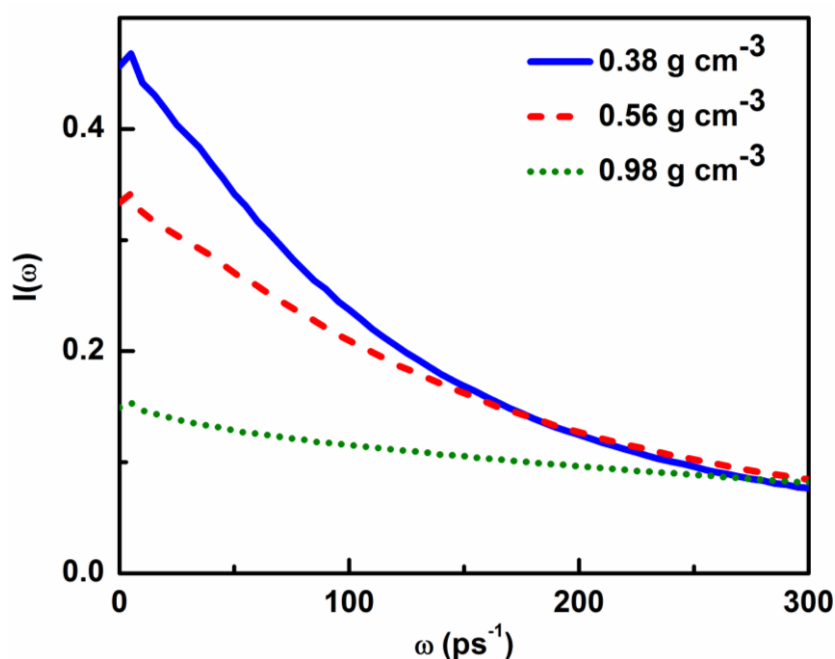


**Figure 4.8: Power spectra of water molecules for aqueous solutions of uranyl ions at different densities at 683 K.**

Further, the power spectrum is obtained for water molecules in the aqueous uranyl solution for various densities by applying Fourier Transform<sup>40</sup> on their velocity autocorrelation functions (VCFs) and is given in Figure 4.8. The zero frequency limit of the power spectrum is thus related to diffusion coefficient by the Green-Kube relation (Eq. 1.16 in Chapter 1).<sup>40</sup> In the present case, the intensity at zero frequency is observed to reduce with increase in the density of water and thus corroborates our previous observation that the diffusion coefficient reduces as the density of the solution is increased.

#### 4.3.4 Orientational Dynamics of the Water Molecules in the Aqueous Uranyl Solution

The orientational dynamics of the water molecules are analyzed by calculating time correlation function of various molecular vectors of water as explained in Section 1.5, Eq. 1.21 of Chapter 1.

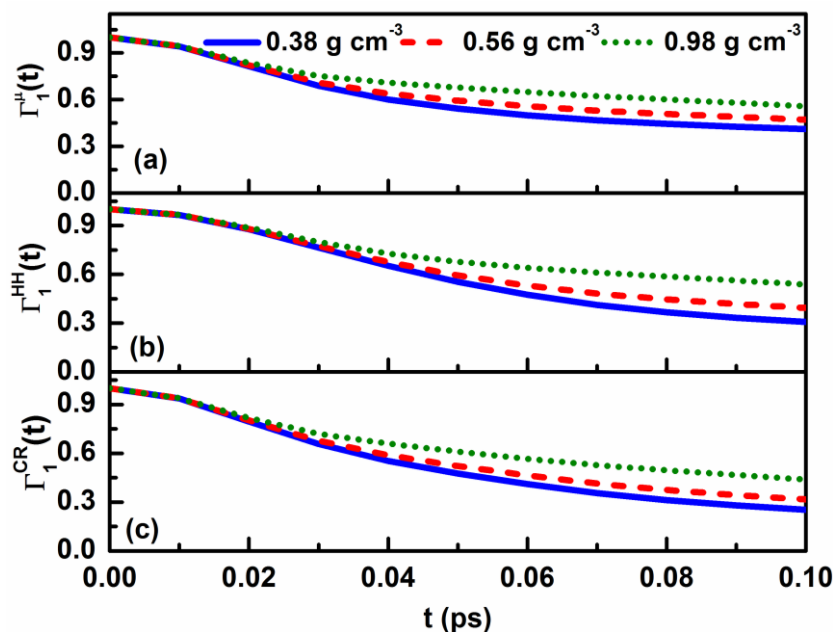


**Figure 4.9:** First order orientational correlation functions of water molecules with respect to (a) water dipole moment vector, (b) water H-H vector and (c) water cross vector at densities of 0.38, 0.56 and 0.98 g cm<sup>-3</sup> of supercritical water at 683 K.

The effect of water density on the orientational dynamics is analyzed by generating first and second order autocorrelation functions for aqueous solution at water densities varying between 0.38 to 0.98 g cm<sup>-3</sup> (Figures 4.9 and 4.10 respectively). From these Figures, it can be concluded that the orientational dynamics of water molecules gets slightly restricted as the water becomes more and more dense, effect being more dominant in case of first order correlation function (Figure 4.9) as compared to second order correlation function (Figure 4.10). From the comparison of orientational relaxations of water at a density of 0.98 g cm<sup>-3</sup> in supercritical and ambient states (Chapters 2 and 3) (see Figure 4.11), it is evident that the orientational relaxation in supercritical state is much faster than that in ambient condition.

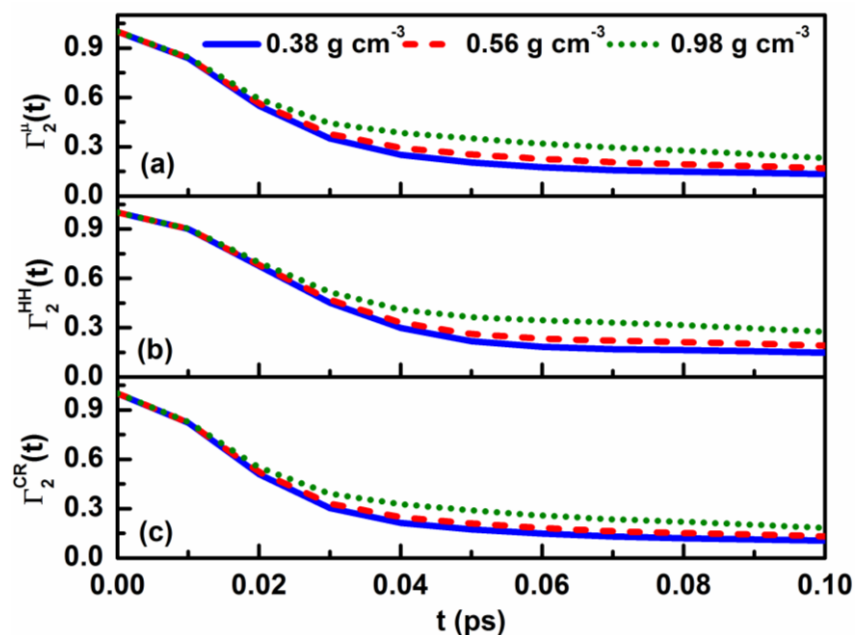


Figure 4.10: Second order orientational correlation functions of water molecules with respect to (a) water dipole moment vector, (b) water H-H vector and (c) water cross vector at densities of 0.38, 0.56 and 0.98 g cm<sup>-3</sup> of supercritical water at 683 K.

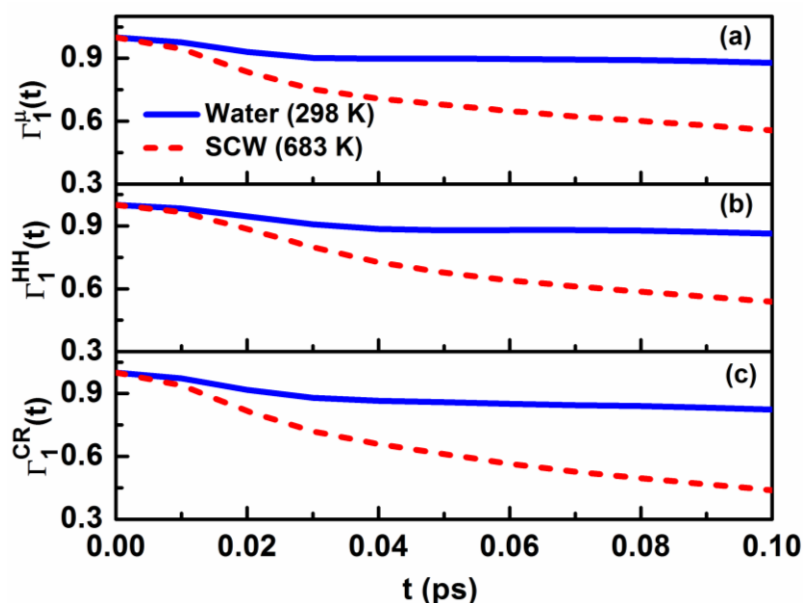


Figure 4.11: First order orientational correlation functions of water molecules under normal conditions and under supercritical (SCW) conditions with respect to (a) water dipole moment vector, (b) water H-H vector and (c) water cross vector at a density of 0.98 g cm<sup>-3</sup>.



## **Part B**

### **Dissecting the Effect of Uranyl Ion Concentration from that of Solvent Density on the Characteristics of the Aqueous Solutions of Uranyl Ions**

The combined effect of variation in uranyl concentration and solvent density on the distribution and transport behavior of aqueous solution of uranyl ions under supercritical conditions have been studied using MD simulations. We tried to understand the effect of uranyl ion concentration and/or that of the density of the system on the structure and transport behavior of the different species present in the solutions. The results obtained for different uranyl ion concentrations at different (solvent) densities varying from 0.38 to 0.98 g cm<sup>-3</sup> are compared to quantify the impact of uranyl ion concentration and density (of the solvent) on various properties. The distribution of water molecules radially outwards from uranyl ions under different conditions of uranyl concentration and water density is discussed in Subsection 4.3.5. The translational movement or in other words, the diffusion characteristics of water molecules are explained in Subsection 4.3.6. Further, we have analyzed the orientational characteristics of water molecules in aqueous solutions of different densities and uranyl ion concentrations in Subsection 4.3.7.

#### **4.3.5 Structural Features of the Aqueous Uranyl Solution**

The radial distribution functions provide information about the local arrangement of water molecules around the uranyl ions. Figure 4.12 provides the RDFs for water atoms (O<sub>w</sub> and H<sub>w</sub>) with respect to uranium (U) and oxygen (O<sub>U</sub>) atoms of the uranyl ions for aqueous solutions in ambient and supercritical water with uranyl concentration of around 0.1 M at water density of 0.98 g cm<sup>-3</sup>. It can be seen that the peak heights are lower for solutions in supercritical water (red dashed line) as compared to those in ambient water (blue solid line). In order to quantify the change in radial structure of water molecules around the uranyl ion

with variation in uranyl ion concentration, we have chosen set Nos. 4, 5 and 6 in each of which water density is approximately  $0.57 \text{ g cm}^{-3}$  but uranyl concentrations are different (varying in the range 0.013 to 0.132 M).

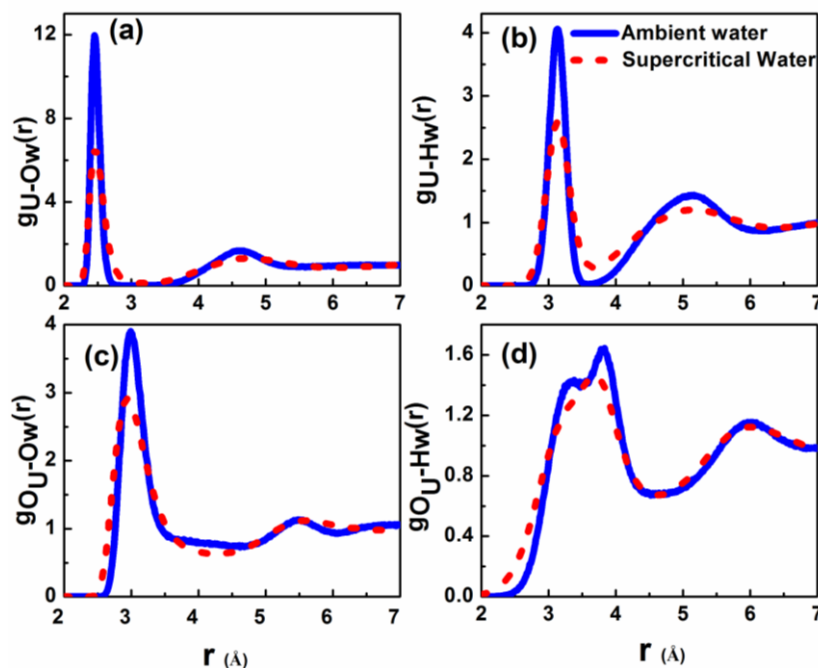


**Figure 4.12: Radial distribution functions for (a)  $O_w$  around uranium, (b)  $H_w$  around uranium (c)  $O_w$  around uranyl-oxygen ( $O_U$ ) and (d)  $H_w$  around  $O_U$  for solutions in ambient (blue solid line) and supercritical water (red dashed line).**

The peak intensity values of the RDFs of oxygen and hydrogen atoms of water with respect to uranium (U) and oxygen ( $O_U$ ) atoms of the uranyl ions for aqueous solutions corresponding to set Nos. 4-6 are given in Figure 4.13a. It is observed from this figure that the peak intensity value reduces slightly with the increase in uranyl ion concentration; however, the positions of the peaks remain more or less the same. The effect of density on the RDF of water molecules is demonstrated by plotting the peak intensities of the RDF for a uranyl concentration of 0.07 M at different densities (Set No. 2, 5 and 8) in Figure 4.13b. Here also, the peak intensity is reduced when the solution becomes denser. The reduction is more in case of density than that observed in case of concentration variation.

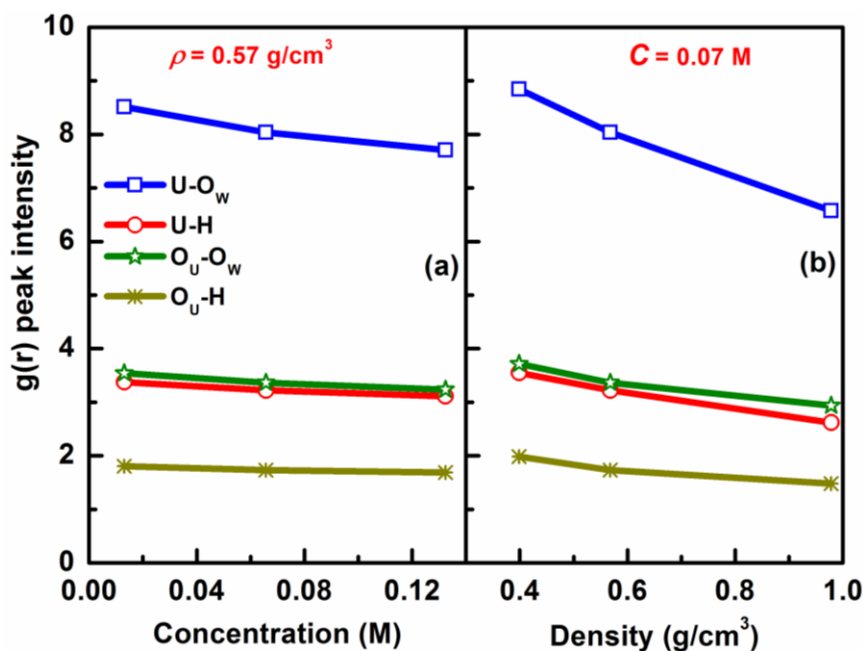


**Figure 4.13: Peak values of radial distribution functions for  $\text{O}_w$  around uranium,  $\text{H}_w$  around uranium,  $\text{O}_w$  around uranyl-oxygen ( $\text{O}_U$ ) and  $\text{H}_w$  around  $\text{O}_U$  as a function of (a) concentration of uranyl ions at approximate water density of  $0.57 \text{ g cm}^{-3}$  and (b) density of water at uranyl concentration of  $0.07 \text{ M}$ .**

This variation in the radial distributions is quantified in terms of the water coordination numbers (CNs) of different atoms (U and  $\text{O}_U$ ) of uranyl ions and the estimated values of CNs are given in Figures 4.14 and 4.15 respectively. Here, CN means the number of water molecules within the first coordination shell (FCS) of uranium ( $3.3 \text{ \AA}$ ) and oxygen ( $4.1 \text{ \AA}$ ) atoms of uranyl ions. It can be seen that although the peak values show same downward trend with increase in uranyl concentration (Figure 4.13a) and with increase in density (Figure 4.13b), but the CNs show an opposite trend (Figures 4.14 and 4.15). In other words, the CN reduces if there is an increase in the uranyl ion concentration (Figures 4.14a and 4.15a) but it increases when the solution is made denser (Figures 4.14b and 4.15b). The reduction in peak height and coordination number with increase in uranyl ion concentration is consistent with similar results reported under normal temperature and pressure (Chapter 3). The slight deviation from this trend in case of density of  $0.4 \text{ g cm}^{-3}$  is observed for number of water

molecules around  $O_U$  when uranyl concentration is increased from 0.07 M to 0.144 M. This may be due to greater uncertainty (see error bars corresponding to these points in Figure 4.15a) with respect to the absolute value in this case.

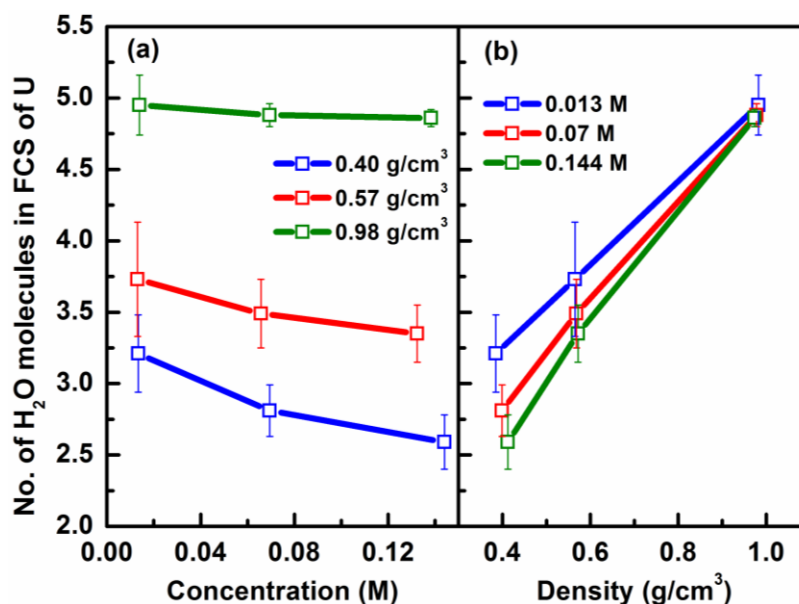


**Figure 4.14: Variation in number of water molecules in first solvation shell (FCS) of uranium atom of uranyl ion with change in (a) concentration and (b) water density.**

From Figures 4.14 and 4.15, it is observed that with increase in water density from 0.38 to 0.98 g cm<sup>-3</sup>, the percentage reduction in coordination number with increase in uranyl concentration reduces. Also, for water density of 0.98 g cm<sup>-3</sup> (Sets 7 to 9) where the concentration increases from 0.01 to 0.1 M, the percentage reduction in coordination number with increase in concentration is less as compared to that in case of similar systems at normal temperature and pressure (Chapter 3). However, it is to be noted that the range of concentration as reported in Chapter 3 is from 0.1 to 1.0 M. Also for the same uranyl concentration of about 0.1 M and solvent density of 0.98 g cm<sup>-3</sup>, the coordination number of the uranyl ion with respect to water molecules is slightly lower under supercritical conditions (U atom 4.8,  $O_U$  atom 9.6) as compared to that under ambient conditions (U atom 5.0,  $O_U$  atom 9.9) (Chapter 3).

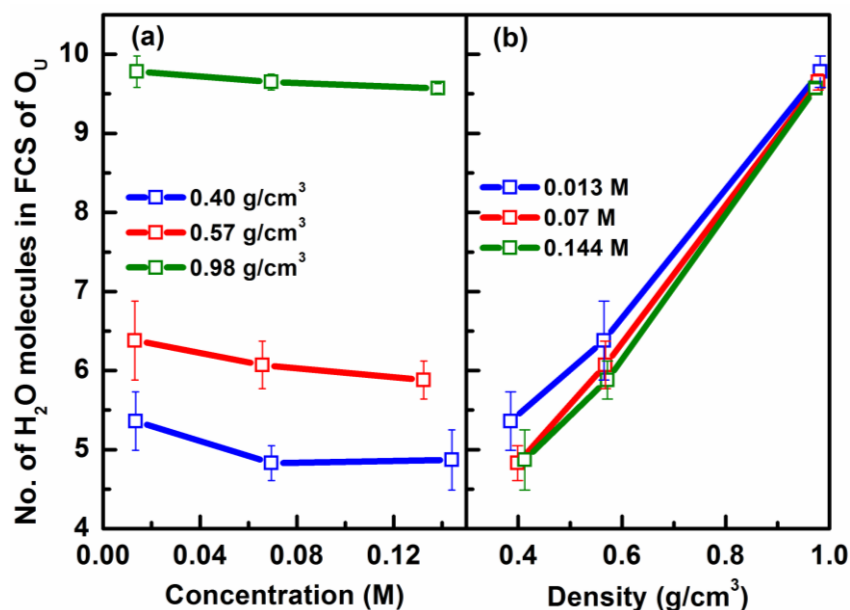


**Figure 4.15: Variation in the number of water molecules in the first solvation shell (FCS) of oxygen atom ( $O_U$ ) of uranyl ion with change in (a) concentration and (b) water density.**

The reduction in coordination number with increase in uranyl ion concentration is because of the replacement of some of the water molecules in the solvation shell of uranyl ions by nitrate ions (Chapter 3). In Chapter 3, it is reported that the oxygen atoms of water as well as of nitrate ions compete for the space within the solvation shell of uranyl ions as shown by peaks at same radial distances from the uranyl ions in the corresponding RDFs. The number of nitrate oxygens within the first solvation shell of uranium (3.1 Å) and oxygen (3.8 Å) atoms of the uranyl ions are shown in Table 4.6. It is observed that the number of nitrate oxygens in the solvation shell of uranyl ions keeps on increasing as the concentration of uranyl ions is increased, confirming the reason for the reduction of number of water molecules with increase in uranyl concentration. Moreover, as expected the number of nitrate oxygen atoms within the solvation shell of uranyl ions reduces as the water density of the system is increased.

**Table 4.6: Number of oxygen atoms of nitrate ion within first solvation shell of uranyl ions and uranium-uranium coordination number for different uranyl ion concentrations.**

Set	Number of O <sub>NO3</sub> atoms in the solvation shell of uranyl ion		Uranium-uranium coordination number
	U	O <sub>U</sub>	
<b>1</b>	2.13	2.61	---
<b>2</b>	2.57	3.21	2.29
<b>3</b>	2.58	3.24	2.55
<b>4</b>	1.46	1.82	---
<b>5</b>	1.65	2.10	1.82
<b>6</b>	1.76	2.24	2.03
<b>7</b>	0.29	0.41	---
<b>8</b>	0.32	0.48	1.61
<b>9</b>	0.38	0.60	1.81

We have also estimated the U-U coordination number (first solvation shell till 7.4 Å) for systems where more than one uranyl ion is present (see Table 4.6). The U-U coordination number is observed to increase with increase in uranyl ion concentration in the solution. More the water density, more ordered is the hydration shell of the uranyl ion and therefore, lesser is the probability of association of uranyl ions in the solution. The same is indicated by the reducing U-U coordination number with increase in solvent density (cf. Table 4.6).

### 4.3.6 Translational Dynamics of Water Molecules and Uranyl Ions in Aqueous Uranyl Solutions

The MSD functions are estimated for various systems with different water densities and different uranyl ion concentrations to analyze their effect on the translational transport of water molecules and uranyl ions. The MSD curves are fitted with straight lines and the slopes of the lines are translated into the diffusion coefficients for systems with different water densities and uranyl ion concentrations. The diffusion coefficient values have been corrected for system size dependence (Eq. 1.20 of Chapter 1). The variation of diffusion coefficients of water and uranyl ions with change in uranyl ion concentration and water density are plotted in Figures 4.16 and 4.17 respectively. It is important to point out that the error bars are not visible in Figure 4.16 as the uncertainty in diffusion coefficients values of water is much less in comparison to the absolute values. Figures 4.16a and 4.17a demonstrate the effect of variation in uranyl ion concentration on the translational transport of water molecules and uranyl ions at a specified water density. It is observed that both the water molecules and uranyl ions, in general diffuse slower as the uranyl ion concentration in the solution is increased. This behavior in case of supercritical water is similar to what has been observed in the case of water under normal conditions (Chapter 3). The effect of water density on the movement of water and uranyl ions is demonstrated in Figures 4.16b and 4.17b respectively. In general, the diffusion coefficients show a reducing trend as the concentration of uranyl ions or the solvent density is increased. However, due to higher uncertainty in the diffusion coefficient values of uranyl ions, the trend may not be observed all the time (For instance in case when uranyl ion concentration is increased from 0.014 M to 0.069 M at water density of  $0.98 \text{ g cm}^{-3}$ ). Moreover, it is concluded that the percentage change in diffusion coefficient of any species with change in uranyl ion concentration shows a reducing trend as the density of the solution becomes more and more.

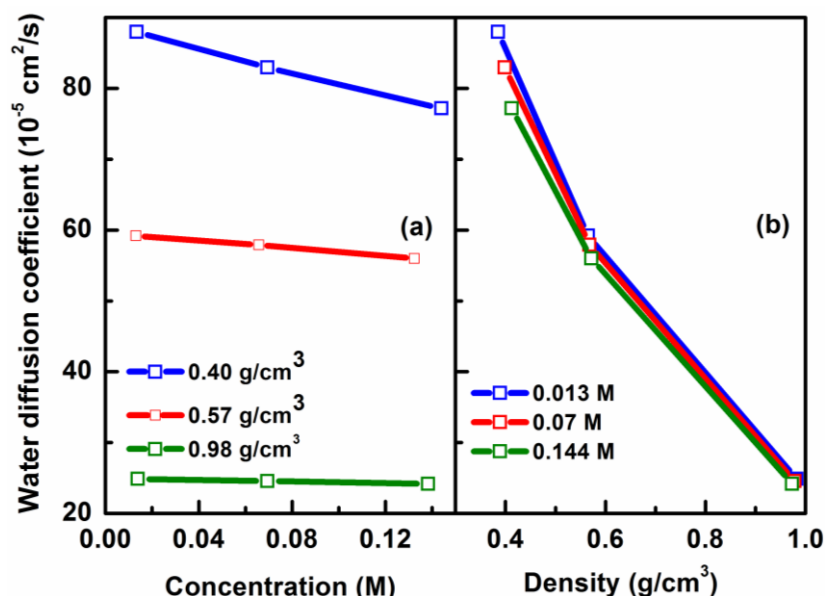


**Figure 4.16:** Variation of diffusion coefficients of water molecules with change in (a) uranyl ion concentration and (b) water density.

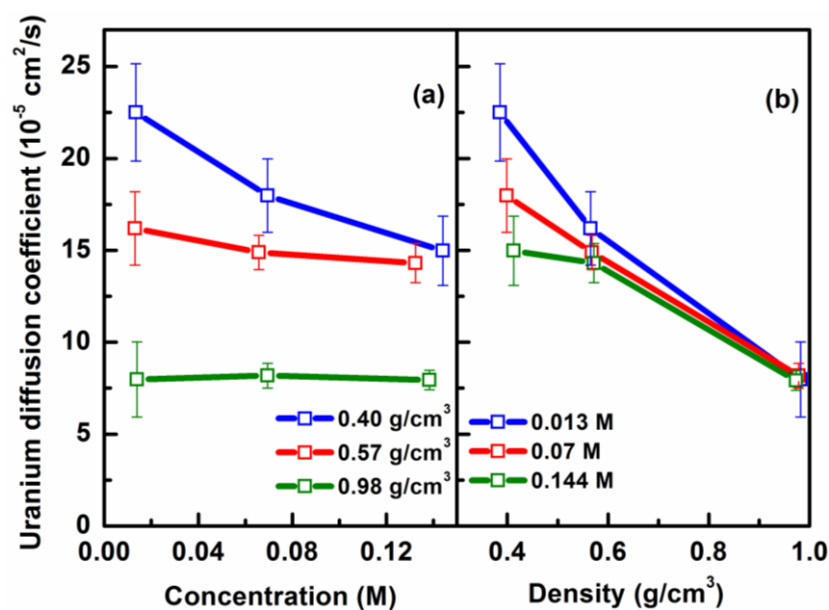


**Figure 4.17:** Variation of diffusion coefficients of uranium atom of uranyl ions with change in (a) uranyl ion concentration and (b) water density.

To validate our results, the diffusion coefficients of water molecules in very dilute solutions of different densities are compared with those reported for bulk supercritical water by various experimental<sup>41</sup> and simulation<sup>16</sup> studies at 673 K. The diffusion coefficients of water molecules in very dilute solutions obtained here (Set Nos. 1, 4 and 7) are also compared



with those given in Table 4.4 above for same densities but different number of water molecules and box size as given in Table 4.7. Table 4.7 shows that the estimated diffusion coefficient values match fairly well with those reported using experimental<sup>41</sup> and theoretical studies.<sup>16</sup> Moreover, for a density of  $0.98 \text{ g cm}^{-3}$  (Set 9) the diffusion coefficient of water increases from  $2.86 \times 10^{-5} \text{ cm}^2 \text{ s}^{-1}$  at 298 K (Chapter 3) to  $24.17 \times 10^{-5} \text{ cm}^2 \text{ s}^{-1}$  at 683 K for a uranyl concentration of the order of 0.1 M. Also, the diffusion coefficient of uranyl ions increases from  $0.94 \times 10^{-5} \text{ cm}^2 \text{ s}^{-1}$  at 298 K (Chapter 3) to  $7.95 \times 10^{-5} \text{ cm}^2 \text{ s}^{-1}$  at 683 K. Also, it is worth noticing that the percentage reduction in diffusion coefficient values with increase in concentration (Sets 7 to 9) at supercritical conditions is much less as compared to that in case of similar systems at normal temperature and pressure (Chapter 3), however the concentrations involved in present case are lower (0.01 to 0.1 M in present case as compared to 0.1 to 1.0 M in Chapter 3). This may be due to higher values of diffusion coefficients at supercritical conditions which suppress the percentage impact of uranyl concentration on the transport of various species in the aqueous solutions.

**Table 4.7: Comparison of size corrected diffusion coefficients for supercritical water in very dilute solutions (Set Nos. 1, 4 and 7) with those recorded in earlier experimental and simulation studies**

S. No.	Density ( $\text{g cm}^{-3}$ )	Diffusion Coefficient ( $10^{-5} \text{ cm}^2 \text{ s}^{-1}$ )			
		Present Study	Simulation (Table 4.4)	Simulation <sup>16</sup>	Experimental <sup>41</sup>
1.	$0.38 \pm 0.01$	$87.96 \pm 0.64$	$81.0 \pm 0.5$	75.5 <sup>#</sup>	91.9
2.	$0.56 \pm 0.006$	$59.20 \pm 0.30^{\$}$	$59.2 \pm 0.3^{\$}$	55.3 <sup>*</sup>	62.3 <sup>*</sup>
3.	$0.98 \pm 0.003$	$24.87 \pm 0.11$	$27.1 \pm 0.2$	30.0 <sup>#</sup>	33.2 <sup>#</sup>

<sup>\\$</sup>As both are same systems

The reduction in diffusion coefficients of water molecules as well as uranyl ions with increase in concentration is further confirmed by analyzing the power spectra of these species in solutions of different concentrations (Figure 4.18). From Figures 4.18 (a) and (b) insets, it is observed that the intensity at zero frequency reduces for both the water molecules as well as for uranyl ions as the uranyl ion concentration is increased in the aqueous solution. This again confirms the observation that the diffusion coefficients of these species reduce with increase in uranyl ion concentration.

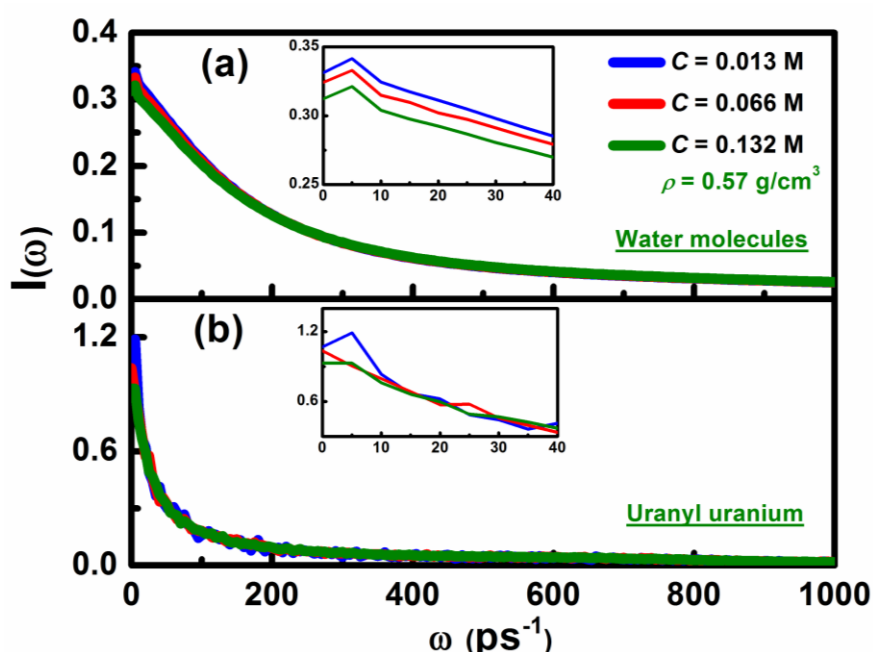


**Figure 4.18: Power spectra of (a) water molecules and (b) uranyl ions for different concentrations of uranyl ions in the aqueous solutions at an approximate water density of 0.57 g cm<sup>-3</sup> at 683 K, insets: Magnified curves around zero wave number.**

#### 4.3.7 Orientational Behaviour of the Water Molecules in the Aqueous Uranyl Solutions

The orientational distribution of various angles and orientational dynamics of various water vectors for the different systems under supercritical conditions as given in Table 4.2 are analyzed. Our aim was to understand the effect of uranyl ion concentration or the density of

the system on the orientational distribution and dynamics of the systems studied in present work. The various angles considered for studying orientational distribution are as given in Figure 4.3. The angular distributions of water molecules within the first hydration shell of uranyl ions in aqueous solutions of different concentrations are observed to be same as given in Figure 4.4. No marked impact of uranyl ion concentration is observed on these angular distributions (Figure 4.19) as was reported for the same under ambient conditions (Chapter 2).

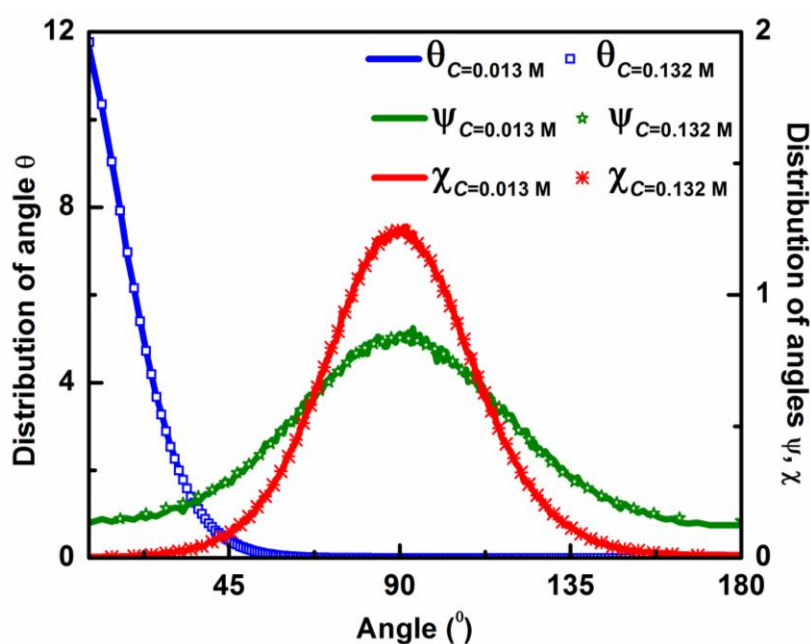


**Figure 4.19: Angular distributions for different angles between U-O<sub>w</sub> or U-O<sub>u</sub> vector and water molecular vectors for different uranyl concentrations at a water density of around 0.57 g cm<sup>-3</sup> at 683 K.**

The orientational dynamics of various molecular vectors of water are studied in terms of three unit vectors ( $u_\alpha$ ) along molecular axes of water as explained in Section 1.5, Eq. 1.21 of Chapter 1. The autocorrelation functions of 1<sup>st</sup> order ( $n=1$ ) and 2<sup>nd</sup> order ( $n=2$ ) for the three unit vectors of water for Set 4 is given in Figure 4.20. It is clear from the figure that there is a little anisotropy in case of  $\Gamma_1$ . The anisotropy is almost absent in case of  $\Gamma_2$ . Similar

observations have been reported by Praprotnik and Janezic<sup>47</sup> while applying the new symplectic MD integrators to perform MD simulations of bulk water.

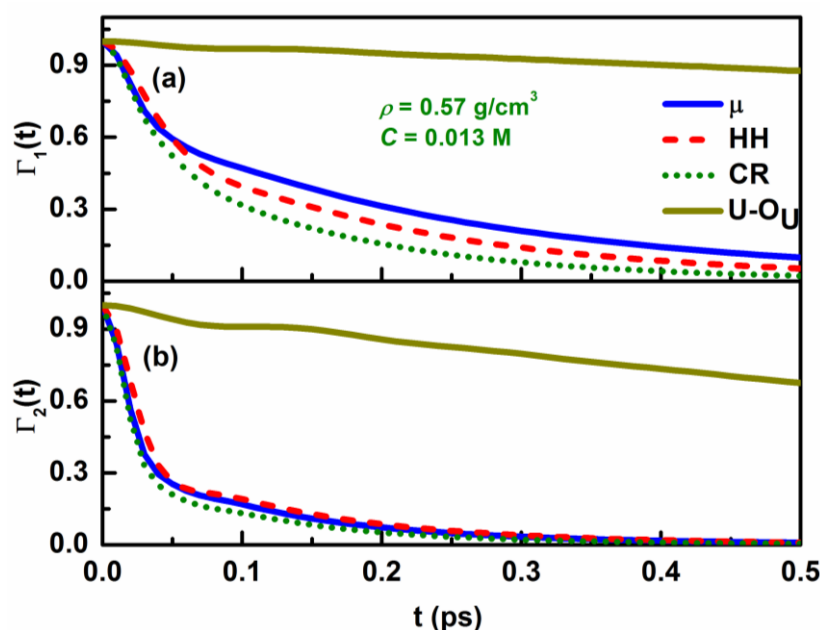


**Figure 4.20: First order and (b) second order orientational autocorrelation functions of different molecular vectors of water i.e. dipole moment vector ( $\mu$ ; blue solid line), H-H vector (HH; red dashed line), cross vector (CR; green dotted line) and of uranyl ions with respect to U-O<sub>U</sub> vector of uranyl ion (dark yellow solid line) for Set 4 system.**

The faster relaxation in case of cross vector as obtained in present work as compared to HH and dipole moment vector in this order is consistent with the trend reported by them. This orientational anisotropy of water has also been confirmed by some of the experimental studies.<sup>48-50</sup> Water is a hydrogen bonded network forming liquid and the anisotropy in orientational relaxation may be a consequence of some preferred orientation to maintain the tetrahedral local structure. Moreover, the orientational relaxation of U-O<sub>U</sub> (dark yellow line) vector is much slower as compared to that of different vectors of water molecule. The effect of uranyl ion concentration on the rotational dynamics of water molecules in aqueous solutions of uranyl ions is studied. It is observed for the entire density range considered in present work that for the same water density, the increase in concentration of uranyl ions has

no impact on the angular dynamics (first as well as second order autocorrelations) of the water molecules. This observation shows a mis-match with the significant variation in angular dynamics of water molecules with uranyl ion concentration observed under ambient conditions (Chapter 3).

## 4.4 Conclusions

In summary, structural and dynamical properties of aqueous solutions of uranyl ions in supercritical water have been thoroughly investigated. In particular, effect of increasing water density and uranyl ion concentration on the properties of different species present in the medium has been studied. It is interesting to observe that the radial distribution function is more ordered at low density than at higher densities. However, the coordination/hydration number of uranyl ions (or central water molecule in case of bulk water) increases with increase in the density of water. Moreover, an increase in the coordination/hydration number of water is observed as we go from normal conditions to supercritical conditions. It is observed that the peak value of the distributions and the coordination number of uranyl ions reduces with increase in uranyl ion concentration whereas the location of the peaks remains more or less the same. The angular distributions of water within the first coordination/hydration shell of uranium atoms have been found to be similar to what is observed under ambient conditions (Chapters 2 and 3), however, the spread is more and intensity of the peaks is observed to be lower in case of supercritical water. Moreover, the orientational structures of water in the first solvation shells around a central water molecule or an ionic species remain almost invariant with increase in water density or uranyl ion concentration. The diffusion coefficient of uranyl ions and water molecules are estimated from the slopes of the mean squared displacements. The diffusion coefficients of water as well as uranyl ions are found to be reducing as either the concentration of uranyl ions in the

solution or the solvent density is increased, although the percentage reduction with the change in uranyl ion concentration becomes lower as the solvent density becomes higher and higher. Moreover, the effect of solvent density change at a particular concentration of the uranyl ion is observed to be much higher as compared to that of change in uranyl ion concentration. The same has been further corroborated by analyzing the zero frequency limits of the power spectra obtained from velocity correlation functions of water at different densities. The diffusion coefficient values estimated for water molecules in bulk supercritical water of different densities compare fairly well with those reported in literature from theoretical<sup>16</sup> as well as experimental studies.<sup>41</sup> Orientational mobility of water molecules in pure water and in the uranyl solution has also been assessed by calculating the time correlation functions of different molecular vectors of water. Although the uranyl ion concentration is shown to have negligible impact on the orientational dynamics of various orientational vectors of water molecules, the effect of density of the solvent on the same is noticeable. Irrespective of the orientational vector, orientational relaxation has been found to decrease with increasing density of water both in pure water and in solutions. Comparison of the dynamical (both translational and rotational) properties of the supercritical water or aqueous solution of uranyl ions with those of ambient water (or aqueous solution) (Chapters 2 and 3) at water density  $0.98 \text{ g cm}^{-3}$  reveals that the translational and rotational dynamics of the species becomes much faster under supercritical conditions. As discussed in the Introduction Chapter 1, the behavior of the fluids show marked changes when we move from the bulk to the interfacial region. Moreover, carbon nanotubes (CNTs) have been reported as a strong potential candidate for use in the purification/decontamination of aqueous solutions. In particular, this type of nanomaterials can be used in the separation of actinyl ions from their aqueous solutions. Efficiency of such a separation technique will depend on the behavior of water at

the CNT-water interface. Hence, in the next chapter i.e. Chapter 5, we will be presenting our investigations on the behaviour of water at the CNT-water interface.

## References

1. C. A. Eckert, B. L. Knuston and P. G. Debenedetti, *Nature*, **1996**, 383, 313.
2. R. Fernandez-Prini and M. L. Japas, *Chem. Soc. Rev.*, **1994**, 23, 155.
3. J. M. H. Levelt Sengers, *Thermodynamics of Solutions Near the Solvent's Critical Temperature*. In *Supercritical Fluid Technology: ReViews in Modern Theory and Applications*; Bruno, T. J., Ely, J. F., Eds., CRC Press, Boston, 1991, pp. 1-56.
4. M. J. Carrott, B. E. Waller, N. G. Smart and C. M. Wai, *Chem. Commun.*, **1998**, 3, 373.
5. D. Bandyopadhyay, S. Mohan, S. K. Ghosh and N. Choudhury, *J. Phys. Chem. B*, **2014**, 118, 11757.
6. D. Bandyopadhyay, S. Mohan, S. K. Ghosh and N. Choudhury, *J. Phys. Chem. B*, **2013**, 117, 8831.
7. D. Bandyopadhyay, K. Bhanja, S. Mohan, S. K. Ghosh and N. Choudhury, *J. Phys. Chem. B*, **2015**, 119, 11262.
8. R. Schurhammer, and G. Wipff, *J. Phys. Chem. A*, **2005**, 109, 5208.
9. C. M. Wai, Y. Liao, W. Liao, G. Tian, R. R. Addleman, D. Quach and S. P. Pasilis, *Dalton Transactions*, **2011**, 40, 5039.
10. L. Zhu, W. Duan, J. Xu and Y. Zhu, *J. Hazard Mater.*, **2012**, 241-242, 456.
11. D. L. Quach, B. J. Mincher and C. M. Wai, *J. Hazard Mater.*, **2014**, 274, 360.
12. G. S. Was, P. Ampornrat, G. Gupta, S. Teyseyre, E. A. West, T. R. Allen, K. Sridharan, L. Tan, Y. Chen, X. Ren and C. Pister, *J. Nucl. Mater.*, **2007**, 371, 176.

13. W. Runde and M. P. Neu, *Hydrothermal synthesis and crystal structures of actinide compounds*, in: L. R. Morss, N. M. Edelstein, J. Fuger (Eds.), *The Chemistry of the Actinide and Transactinide Elements*, Springer, Netherlands, 2011, pp. 4157-4191.
14. G. Kalinichev, *Phys. Chem.*, **1993**, 97, 872.
15. T. I. Mizan, P. E. Savage and R. M. Ziff, *J. Comput. Chem.*, **1996**, 17, 1757.
16. J. Marti, *J. Chem. Phys.*, **1999**, 110, 6876.
17. K. Yoshida, N. Matubayasi and M. Nakahara, *J. Chem. Phys.*, **2006**, 125, 074307.
18. K. Ueda, T. Komai, I. Yu and H. Nakayama, *J. Comput. Chem. Jpn.*, **2002**, 1, 83.
19. Skarmoutsos, D. Dellis and J. Samios, *J. Phys. Chem. B*, **2009**, 113, 2783.
20. S. H. Lee, *Bull. Korean Chem. Soc.*, **2014**, 35, 644.
21. P. T. Cummings, H. D. Cachran, J. M. Simonson, R. E. Mesmer and S. Karaborni, *J. Chem. Phys.*, **1991**, 94, 5606.
22. P. B. Balbuena, K. P. Johnston and P. J. Rossky, *J. Phys. Chem.*, **1996**, 100, 2706.
23. J. C. Rasaiah, J. P. Noworyta and S. Koneshan, *J. Am. Chem. Soc.*, **2000**, 122, 11182.
24. J. P. Noworyta, S. Koneshan and J. C. Rasaiah, *J. Am. Chem. Soc.*, **2000**, 122, 11194.
25. K. Yui, M. Sakuma and T. Funazukuri, *Fluid Phase Equilib.*, **2010**, 297, 227.
26. S. H. Lee, *Bull. Korean Chem. Soc.*, **2013**, 34, 2925.
27. S. Kerisit and C. Liu, *Geochim Cosmochim. Acta*, **2010**, 74, 4937.
28. N. Rai, S. P. Tiwari, E. J. Maginn, M. P. Brown and K. Austin, *J. Phys. Chem. B*, **2012**, 116, 10885.
29. M. Bühl, N. Sieffert, A. Chaumont and G. Wipff, *Inorg. Chem.*, **2012**, 51, 1943.
30. S. Kerisit and C. Liu, *J. Phys. Chem. A*, **2013**, 117, 6421.
31. S. P. Tiwari, N. Rai and E. J. Maginn, *Phys. Chem. Chem. Phys.*, **2014**, 16, 8060.
32. V. Pomogaev, S. P. Tiwari, N. Rai, G. S. Goff, W. Runde, W. F. Schneider and E. J. Maginn, *Phys. Chem. Chem. Phys.*, **2013**, 15, 15954.



33. L. Martínez, R. Andrade, E. G. Birgin and J. M. Martínez, *J. Comput. Chem.*, **2009**, *30*, 2157.
34. A. P. Karande, G. K. Mallik, J. P. Panakkal, H. S. Kamath, V. K. Bhargava and J. N. Mathur, *J. Radioanal. Nucl. Chem.*, **2003**, *256*, 185.
35. NEA. Spent Nuclear Fuel Reprocessing Flowsheet, Nuclear Science, NEA/NSC/WPFC/DOC, Nuclear Energy Agency, Organization for Economic Co-operation and Development, Paris, 2012.
36. S. Nose and M. L. Klein, *Mol. Phys.*, **1983**, *50*, 1055.
37. S. Nose, *Mol. Phys.*, **2002**, *100*, 191.
38. H. C. Andersen, *J. Chem. Phys.*, **1980**, *72*, 2384.
39. M. Parrinello and A. Rahman, *J. Appl. Phys.*, **1981**, *52*, 7182.
40. M. P. Allen, D. J. Tildesley, *Computer Simulation of Liquids*, Oxford University, New York, 2004.
41. W. J. Lamb, G. A. Hoffman and J. Jonas, *J. Chem. Phys.*, **1981**, *74*, 6875.
42. Y. Kubo, *Molecular dynamics and self-diffusion in supercritical water*, M.Sc. thesis, Massachusetts Institute of Technology, Cambridge, MA, 2000.
43. P. Guilbaud and G. Wipff, *J. Phys. Chem.*, **1993**, *97*, 5685.
44. H. J. C. Berendsen, J. R. Grigera and T. P. Straatsma, *J. Phys. Chem.*, **1987**, *91*, 6269.
45. C. Vega and J. L. F. Abascal, *Phys. Chem. Chem. Phys.*, **2011**, *13*, 19663.
46. R. J. Frick, T. S. Hofer, A. B. Pribil, B. R. Randolph and B. M. Rode, *J. Phys. Chem. A*, **2009**, *113*, 12496.
47. M. Praprotnik and D. Janezic, *J. Chem. Phys.*, **2005**, *122*, 174103.
48. B. Halle and H. Wennerstrom, *J. Chem. Phys.*, **1981**, *75*, 1928.
49. A. Wallqvist and B. J. Berne, *J. Chem. Phys.*, **1993**, *97*, 13841.
50. J. Jonas, T. DeFries and D. J. Wilbur, *J. Chem. Phys.*, **1976**, *65*, 582.



# *Chapter 5*

**Structure and Dynamics of  
Water through Carbon  
Nanotubes in Comparison to  
those of a Non-polar Fluid**



## 5.1 Introduction

Transport of water through nanotubes is of fundamental as well as technological importance due to its relevance in chemistry, biology, material science and nanoscience.<sup>1-6</sup> From the fundamental point of view, understanding behavior of water confined in nanoscale channels and cavities is of prime importance as the nanoconfined water presents unusual properties that differ from both the bulk liquid and gas phases. Nanochannel-water systems find wide applications in nanofluidics including electrophoretic, and thermophoretic channels, membranes, sensors, filters, and gating devices. As a molecular transporter, single wall nanotubes can shuttle various cargoes across the cellular membrane, thus opening a new route for drug delivery and giving rise to a novel mechanism for cancer therapy.<sup>7</sup> Central to many of these applications is the capacity to store or convey fluids, and in particular aqueous solutions, at nanoscale precision. In fact, water-filled and water-permeable pores are present in biological cells, membranes, and surface of proteins<sup>8</sup> and in other relevant biological and geological (e.g., zeolites<sup>9</sup>) systems.<sup>10</sup> The interplay between confinement and hydrophobicity induces modifications in both structural and dynamical properties of water. In recent years an extensive effort has been dedicated to understand how the properties of a particular fluid change upon nanoscale confinement and how these changes influence flow of a fluid through a wide range of systems, e.g., biological channels and pores, organic and inorganic porous media such as zeolites and cements, etc.

The engineered water channels based on carbon nanotubes (CNTs) have attracted great attention since Hummer et al.<sup>11</sup> reported water transmission through a nonpolar (6, 6) CNT. Interest in this nanochannel has been further rejuvenated<sup>1,12-18</sup> by the landmark findings of Holt et al.<sup>19</sup> and Majumder et al.,<sup>20</sup> who observed extraordinarily enhanced transport of water through carbon nanotube membranes. The behavior of water confined in a narrow pore such as carbon nanotube differs considerably from that in bulk, as the characteristic

dimensions of the confining medium are reduced to the nanometer scale.<sup>1,11,15,16,19-22</sup> The results of exceptionally fast water transport through CNT as reported by Holt et al.<sup>19</sup> as well as by Majumder et al.<sup>20</sup> however have been contended<sup>13,23</sup> recently. Thomas et al. have shown<sup>23</sup> that the enhancement is much lower than that obtained from the previously reported<sup>19,20</sup> experimental results. It has also been shown<sup>13,23,24</sup> that enhancement in flow decreases with increase in diameter of the nanotube. The TEM measurements of Naguib et al.<sup>25</sup> not only showed the water filled ultrathin CNT channels, but also indicated that the fluid mobility inside the CNT is greatly reduced. Similar conclusions, but for different confining surfaces, are reached by Major et al.<sup>26</sup> who observed a dramatic change in the mechanical properties of water at the nanometer scale. In recent studies carried out by Farimani et al.<sup>27</sup>, the axial and radial diffusion coefficients of water molecules indicated significant enhancement of diffusion rate near the CNT wall. They explained it on the basis of depletion of hydrogen bonds, weak carbon-water interaction and water orientation near the surface. Ohba et al.<sup>28</sup> observed 3-5 times faster transport of water through narrow 1D channels as compared to that through wide 1D channels. They attributed this rapid transportation to the formation of fewer hydrogen bonds between water molecules adsorbed in the narrow 1D channel. Su et al.<sup>29</sup> studied the effect of nanochannel dimensions on the flow characteristics of water. An exponentially decaying relation is observed between water flow and CNT lengths at different pressures. Also for a given CNT length, a power law dependence of CNT diameter on the flow of water has been observed. Rana et al.<sup>30</sup> found that both the solvation characteristics and hydrogen bond distributions can depend rather strongly on the strength of the attractive part of the solute–water interaction potential. The thickness of the nanotube wall, however, is found to have only minor effects on the density profiles, hydrogen bond network and the wetting characteristics.

In spite of a large number of investigations on the behavior of water in and around carbon nanotubes, many pertinent questions remain unanswered. Even various aspects of the

pioneering work<sup>11,17</sup> of Hummer et al., who used molecular dynamics (MD) simulations to show many characteristic features of the CNT-water systems such as pulse-like transmission of water through the nanotube, empty-filled transitions inside the nanotube etc. have not been fully explored. Although it has been posited<sup>11</sup> that the observed transmission bursts are due to the tight hydrogen bonding network of water inside the nanotube, which provides shield against natural energetic fluctuations in bulk water, it still remains a question whether this conduction burst is associated only with a hydrogen-bonded fluid like water. It is also not clear whether the empty-filled transitions observed in the CNT-water system are specific to water or these can be observed in case of nonpolar fluids as well.

The curiosity leading to the present study is to check whether structural and dynamic properties of a non-polar fluid resemble those of a polar, hydrogen-bonded fluid like water. In particular, it is to verify whether pulse-like transmission, empty-filled transition and rapid diffusion can be observed even in case of non-hydrogen bonded fluid when transported through the single-file CNT. To achieve this goal, a comparison of structure and dynamics of a polar, hydrogen bonded fluid such as water with those of a non-polar (non-hydrogen bonded) fluid like methane in and around the hydrophobic CNT with chirality (6, 6) as obtained from extensive MD simulations is presented here. The structural properties in terms of radial distribution functions and transport characteristics in terms of self-diffusion coefficients and translocation events through the CNT are studied. The effect of change of diameter of the CNT is also studied in case of water by taking (n, n) nanotubes of different diameters, n being the chirality parameter. We also determined the probabilities for a particle that newly entered the channel to exit on the same side (termed as returned particle), or to pass through the channel and lead to a conduction event (termed as translocated particle), respectively.<sup>17</sup>

## 5.2 Models and Simulation Details

In the present investigation, CNT-fluid systems with two different fluids, namely water and methane are studied. The  $sp^2$  carbon atoms of the CNT are modeled as uncharged Lennard–Jones particles (Eq. 1.5 given in Chapter 1 of this thesis) with size and energy parameters  $\sigma_{CC} = 3.4 \text{ \AA}$  and  $\varepsilon_{CC} = 0.3598 \text{ kJ mol}^{-1}$  respectively. These values correspond to the AMBER96 force-field parameters.<sup>11</sup> For water, Extended Simple Point Charge (SPC/E)<sup>31</sup> model and TIP3P model are employed and for methane Optimized Potentials for Liquid Simulations-United Atom (OPLS-UA)<sup>32</sup> model is used. The applicability of this simplified model of methane to CNT-fluid system has been tested recently by comparing behavior of united atom and all-atom models of methane inside the CNT and the results from united atom model has been found to compare well with those of its all-atom counterpart.<sup>33</sup> Not only that, even experimental observation of filling-ejecting transition of methane in CNT as obtained from electrical resistance, X-ray diffraction and NMR measurements has also been nicely reproduced by molecular dynamics simulation using united atom model of methane.<sup>34</sup> Recent study on adsorption behavior of methane in CNT<sup>35</sup> has also used united atom model of methane in the molecular dynamics and GCMC simulations. Since in the present work, the intention is to compare the behavior of a nonpolar fluid with that of water, united atom model, which cannot form intermolecular hydrogen bond and has no polarity, can serve as a general model for nonpolar fluids encompassing methane as well as many other monoatomic fluids like argon, krypton etc. In order to check whether the present result for methane is in general true for other nonpolar fluids, an argon-CNT system is also simulated and the primary results of the argon-CNT system have been compared with those obtained from the united atom methane. For the water-CNT systems, the results presented in this Chapter are obtained by using SPC/E model of water. The TIP3P model is used only to estimate and compare the probability of translocation through the CNT with the already reported value<sup>17</sup> obtained using



TIP3P water model. The non-bonded Lennard-Jones (LJ) parameters for SPC/E water model<sup>31</sup> are  $\sigma_{\text{OO}} = 3.17 \text{ \AA}$ ,  $\varepsilon_{\text{OO}} = 0.6502 \text{ kJ mol}^{-1}$  (corresponding fluid-CNT interaction parameters are  $\sigma_{\text{CO}} = 3.285 \text{ \AA}$  and  $\varepsilon_{\text{CO}} = 0.4837 \text{ kJ mol}^{-1}$ ), and those for TIP3P model<sup>11</sup> are  $\sigma_{\text{OO}} = 3.15 \text{ \AA}$ ,  $\varepsilon_{\text{OO}} = 0.6364 \text{ kJ mol}^{-1}$  (with  $\sigma_{\text{CO}} = 3.275 \text{ \AA}$  and  $\varepsilon_{\text{CO}} = 0.4785 \text{ kJ mol}^{-1}$ ). In case of united atom model of methane, the non-bonded Lennard-Jones (LJ) parameters used are  $\sigma_{\text{C4C4}} = 3.817 \text{ \AA}$ ,  $\varepsilon_{\text{C4C4}} = 1.2324 \text{ kJ mol}^{-1}$  (corresponding fluid-CNT interaction parameters are  $\sigma_{\text{CC4}} = 3.6085 \text{ \AA}$  and  $\varepsilon_{\text{CC4}} = 0.6659 \text{ kJ mol}^{-1}$ ). The armchair (6, 6) CNT consisting of 144 carbon atoms corresponding to the tube diameter of  $8.1 \text{ \AA}$  and of length  $13.4 \text{ \AA}$ , is solvated in the center of a periodic box of fluid molecules with the axis of the nanotube coincident with the z-axis of the box. To analyze the effect of CNT diameter on the various characteristics, CNTs of different diameters i.e. CNT(n,n),  $n = 8, 10$  and  $12$  (corresponding to diameters of  $10.8, 13.68$  and  $16.15 \text{ \AA}$  respectively) but same length are also considered. The partial charges on the oxygen and hydrogen atoms respectively are taken as  $-0.8476e$  and  $+0.4238e$  (SPC/E model) and  $-0.8340e$  and  $+0.4170e$  (TIP3P model), where  $e$  is the magnitude of the charge of an electron. Typical configurations for this system are shown in Figure 5.1 below.

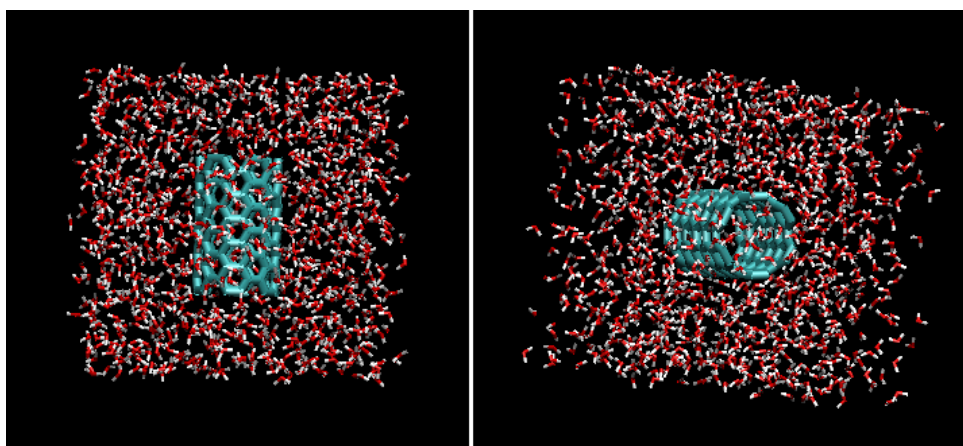


**Figure 5.1** Snapshots of the carbon nanotube immersed in the box of water molecules

The MD simulations are performed at a target temperature of  $298 \text{ K}$  and a target pressure of  $1 \text{ atm}$  for water and at a target temperature of  $136 \text{ K}$  and at a bulk density  $\rho\sigma^3 = 0.72$  (where  $\sigma$  is the Lennard-Jones size parameter of united atom methane and  $\rho$  is the

number density) corresponding to a density of  $0.35 \text{ g cm}^{-3}$  for methane.<sup>36</sup> Periodic boundary conditions are applied in all three directions. For the CNT-water system, number of water molecules inside the box is taken to be 978 and for the CNT-methane systems, number of united atom methane molecules inside the box is taken to be 858. For integrating equations of motion, a time step of 2 fs is used. For each system, the production run is for 50 ns after equilibration for 1 ns.

### 5.3 Results and Discussion

This section is divided into two parts: the subsection 5.3.1 deals with the structural and dynamical characteristics of water-CNT system in comparison to those of the methane-CNT system and the subsection 5.3.2 brings out the effect of change of nanotube diameter on these features.

#### 5.3.1 Comparison of Structural and Dynamical Features of Water and Methane in the Presence of CNT(6,6)

The structure and dynamics of fluid molecules in and around CNT(6,6) have been estimated for different fluid-CNT systems. In Figure 5.2a, the radial density profiles of water and methane molecules in and around (6, 6) nanotube are compared. Figures 5.2b and c show the symmetrical radial density profile around the centre of the nanotube within its diameter. In the (6, 6) nanotube, due to smaller size of a water molecule as compared to the diameter of the CNT, water molecules although cannot overtake but maintain a zig-zag orientation leading to two possible positions inside the CNT so that the chain of water molecules can have maximum number of H-bonds. Thus two small peaks around the center of the CNT appear in the density profile (Figure 5.2b).

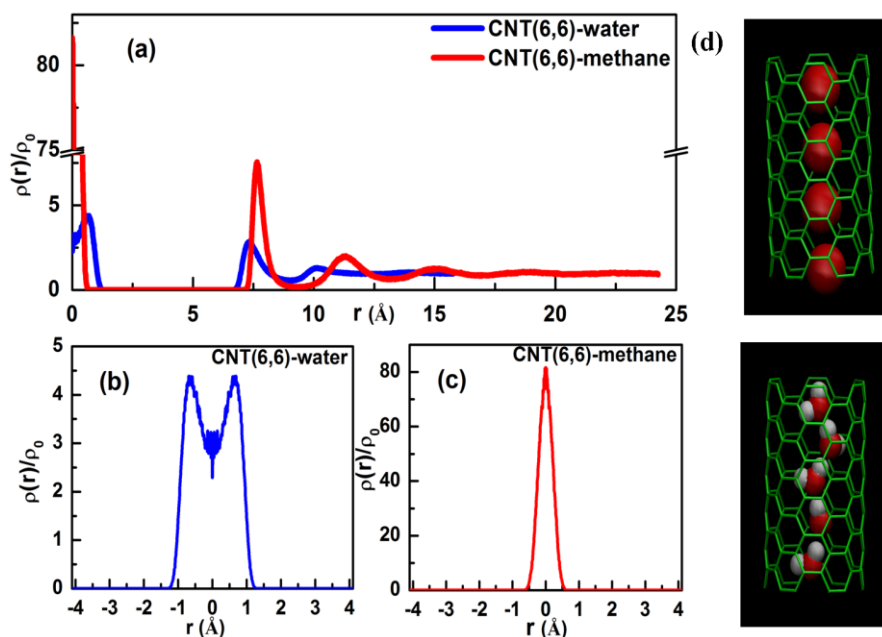


**Figure 5.2:** (a) Normalized density profile,  $\rho(r)/\rho_0$ , of fluids as a function of radial distance,  $r$  measured from the center of the nanotube. There is a break in the y-axis of the CNT-methane curve so that both density profiles (CNT-water and CNT-methane) are visible. Normalized density profiles,  $\rho(r)/\rho_0$  for (b) water and (c) methane within the nanotube ( $-R \leq r \leq R$ ,  $R$  being the CNT radius). (d) Snapshots of straight chain arrangement of methane (upper panel) and zig-zag orientation of water (lower panel) inside CNT.

On the other hand, there is just enough space to accommodate only a single-molecular chain of bigger methane molecules as indicated by one peak at the center as fluid molecules inside the CNT cannot cross each other (Figure 5.2c). It is to note that the density peak in the middle of the nanotube is observed to be much higher for CNT (6, 6)-methane system than that for the CNT (6, 6)-water system. Due to comparable sizes of CNT interior and the methane molecule, which exactly fits into the nanotube, all the methane molecules are preferably occupying center of the nanotube showing a large single density peak in the profile. In fact, the snapshots presented in Figure 5.2d show a straight-chain arrangement of the methane molecules (see upper panel of Figure 5.2d) and a zig-zag orientation of the water

chain (see lower panel) inside the CNT. The fluid structure outside the CNT as obtained from the radial distribution shows two peaks irrespective of the nature of the fluids.

Despite its hydrophobic character, the nanotube channel gets rapidly filled with water. The CNT remains occupied on an average with 5-6 water molecules (see Figure 5.3a, upper panel) during the 20 ns simulation. This persistent presence of water molecules inside the CNT is consistent with the previously reported theoretical<sup>11,38</sup> and experimental<sup>39</sup> results. When CNT-water interaction is reduced, transitions between filled (around 5 molecules) and empty (almost zero molecule) states are observed (see the bottom panel of Figure 5.3a). Like water, OPLS-UA methane also occupies (see Figure 5.3b, upper panel) the CNT and on an average 3-4 methane molecules are present within the CNT throughout the 20 ns simulation time. Interestingly, number fluctuation in this case is much less as compared to that in case of water (compare upper panel of Figure 5.3a with that of Figure 5.3b). Because of the larger size of the methane molecule as compared to water, number of molecules inside the CNT is less for methane than water. When fluid-CNT van der Waals interaction is reduced, no empty-filled like transition (as seen in case of water) is observed, instead, we have found that average number of methane molecules inside the CNT is gradually decreasing with the decrease in fluid-CNT interaction parameter  $\epsilon_{CC4}$  (see three panels of Figure 5.3b). Also, simulations are carried out at different temperatures for water (250 K, 275 K, 298 K, 325 K and 350 K) and methane (120 K, 136 K, 150 K, 165 K and 180 K) to analyze the effect of temperature on the average number of fluid molecules present inside the CNT at any time. It is observed that within the range considered, with change in temperature, there is not much change in the average number of fluid molecules inside the CNT in both the cases (Figure 5.4).

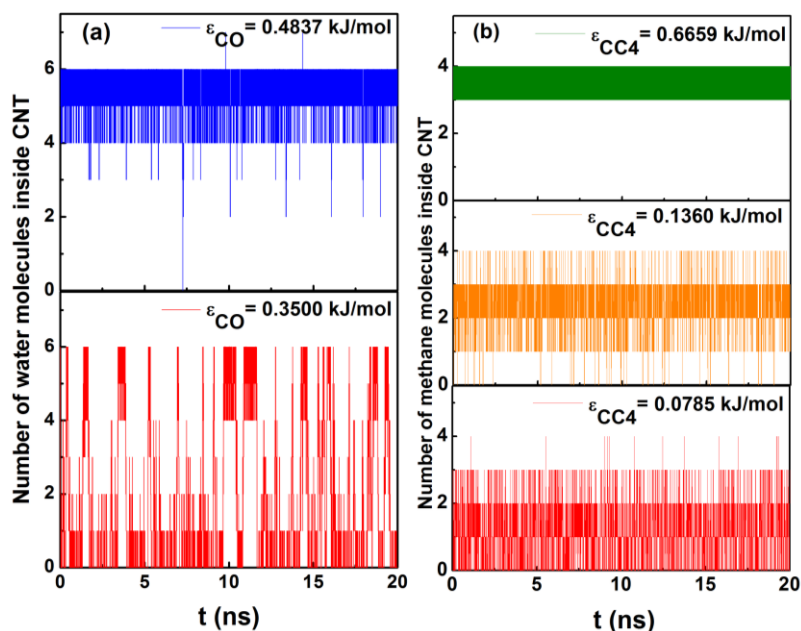


**Figure 5.3:** Number of fluid molecules inside the nanotube as a function of time for different carbon-fluid interactions for (a) CNT-water and (b) CNT-methane systems.

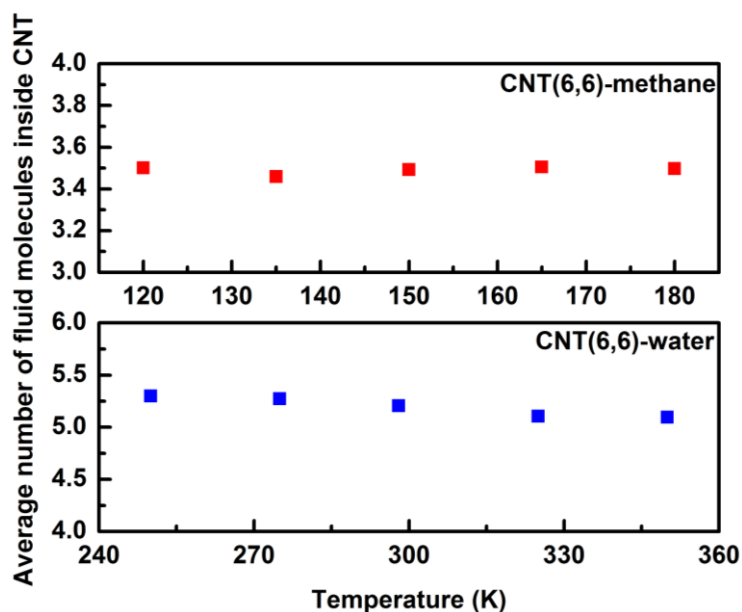


**Figure 5.4:** Average number of fluid molecules inside the CNT (6, 6) at different temperatures.

In order to estimate extent of positional ordering of fluid particles along the axis of the nanotube (z-direction), we have calculated the pair correlation function for the fluid molecules inside the nanotube using the relation<sup>18</sup>

$$g(z) = \frac{1}{N} \sum_{i=1}^N \sum_{j=1, j \neq i}^N \langle \delta(z - z_{ij}) \rangle, \quad (5.1)$$

where  $z_{ij}$  is the axial separation between the  $i^{\text{th}}$  and the  $j^{\text{th}}$  fluid molecules,  $N$  is the number of fluid molecules inside the nanotube, and the angular brackets indicate an average over time. The estimated pair correlation functions for methane and water in the nanotube are shown in Figure 5.5. The distinct, well-separated peaks of  $g(z)$  suggest that there is solid-like ordering<sup>18</sup> of the fluid molecules inside the nanotube in both the cases. A closer look reveals that methane has more solid-like structure as compared to water inside the nanotube. The nearest-neighbor distance between two molecules for water and methane are estimated to be 2.5 Å and 3.8 Å respectively.

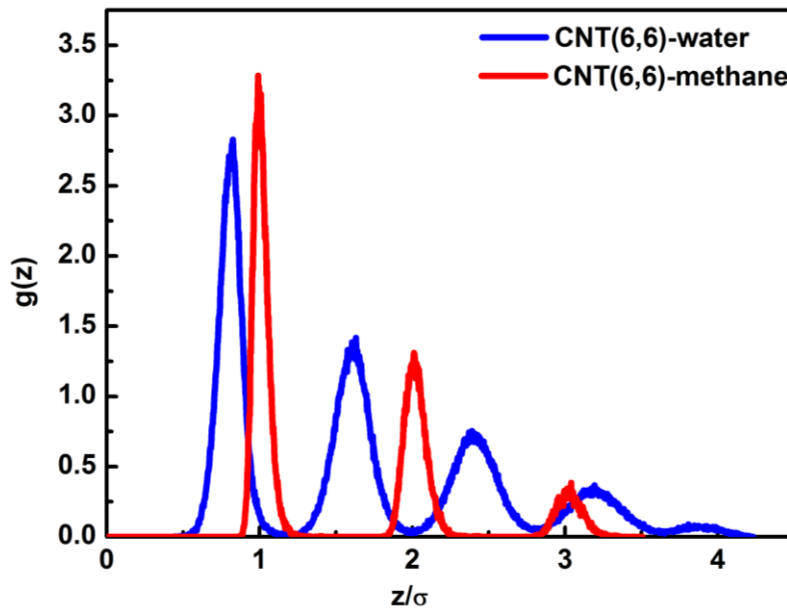


**Figure 5.5: Pair correlation functions for water and methane molecules inside the CNT (6, 6).**

Power spectra as obtained from the Fourier transform of the velocity auto correlation function for collective vibrational motions are shown in Figure 5.6 for both CNT-water and CNT-methane systems. The CNT-fluid systems exhibit prominent vibrations as shown by sharp peaks in the power spectra similar to those obtained by Choudhury and Pettitt.<sup>40</sup> As seen in Figure 5.6, the intensity,  $I(\omega)$  and vibrational frequency,  $\omega$  (around 20 ps<sup>-1</sup>) are higher

in case of methane than in case of water (around  $10 \text{ ps}^{-1}$ ). The frequency distributions in the power spectrum are indicative of the relative population of the density of states of independent oscillators corresponding to a particular frequency, related here to the local motions of fluid molecules. The shift in the peak for methane toward higher frequency can be attributed to a larger forces acting on the molecules imparted by the restrictive environment in this state.

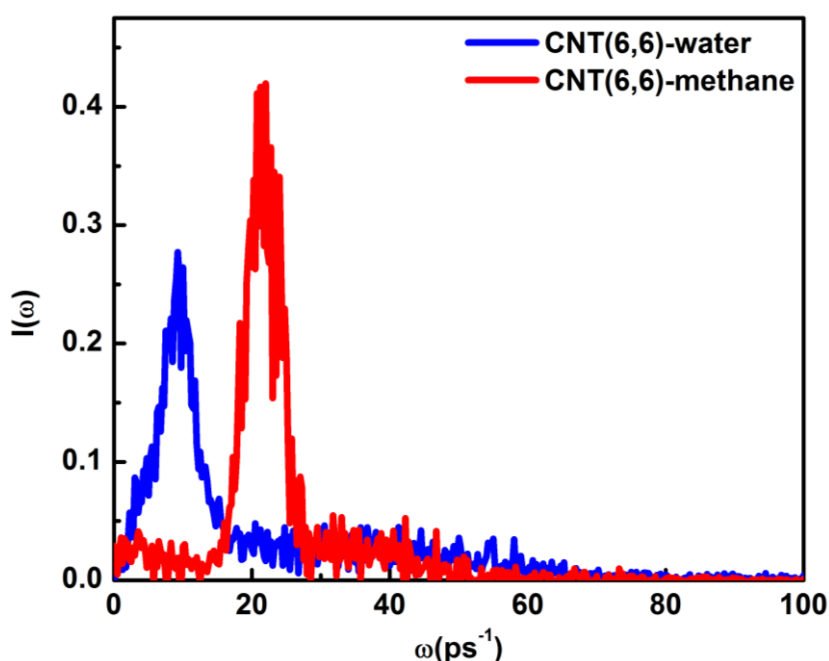


**Figure 5.6: Power spectra for CNT (6, 6)-water and CNT (6, 6)-methane systems.**

For dynamical behavior, we have calculated Mean Square Displacements (MSDs) along the nanotube axis for water as well as methane inside the CNT. The diffusion coefficient is estimated from the slope of the mean squared displacement curves by using Eq. 1.19 given in Chapter 1 of this thesis. The diffusion constant along the axis of the CNT (i.e. dimension,  $d=1$ ) is obtained for each of the two fluids (water and methane) inside the nanotube from the slope of a linear fit of the respective MSD data calculated from simulation trajectory as a function of time. The steeper slope of linear portion of MSD curve for methane indicates higher diffusivity in case of non-polar fluid (methane) than in case of polar fluid (water) for the same CNT diameter (Figure 5.7). The radial MSD profiles for both CNT-water

and CNT-methane systems are obtained to be non-linear and therefore calculation of diffusivity from the radial MSD is not possible.

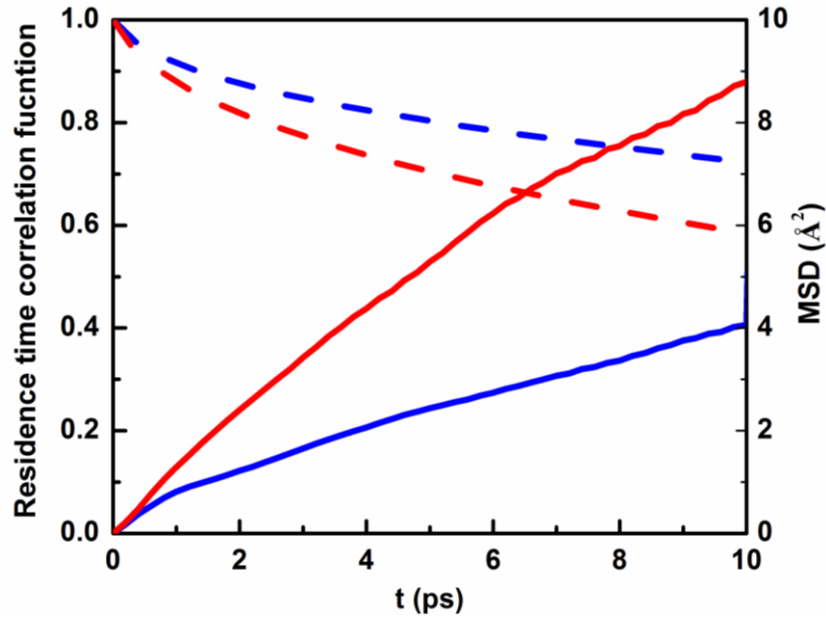


**Figure 5.7: Residence time correlation function and MSD for water (blue curves) and methane (red curves) molecules inside the nanotube along the CNT axis (Residence time - dotted line, MSD - full line). The scale of MSD is on the right axis.**

The residence time correlation functions are estimated for both CNT-water and CNT-methane systems using the relation:<sup>18</sup>

$$R(t) = \frac{1}{N} \sum_{i=1}^N \prod_{t_k=t_0}^{t_0+t} P_i(t_k), \quad (5.2)$$

where the summation is over all the water molecules and the angular brackets denote an average over the time origin  $t_0$ .  $P_i(t)$  in the above equation is equal to 1 if the  $i^{\text{th}}$  molecule is inside the nanotube at time  $t$  and zero otherwise. Also the function  $R(t)$  is normalized to unity at  $t = 0$  by dividing the function value at any time  $t$  by its value at  $t = 0$ . The function  $R(t)$  gives the probability that a fluid molecule remains inside the nanotube for all times between  $t_0$  and  $t_0+t$ , averaged over the initial time  $t_0$ . The residence time plots show the reverse trend, that is, the residence time of a molecule inside nanotube is higher for water than that for a methane molecule and this trend is consistent with that of MSD results (Figure 5.7). The



higher diffusivity of methane as compared to water inside the CNT is somewhat contradictory to the fact that methane is more ordered (see Figure 5.5) inside the CNT as compared to water. Before analyzing the reason behind it, we have examined how these two fluids flow through the CNT with an emphasis on the existence or nonexistence of conduction burst or pulse-like transmission.

Fluid molecules penetrate into the CNT and are also conducted through it (Figure 5.8). During the 50 ns simulation, the number of fluid molecules that entered the CNT from one side and left from the other side (translocation events) are observed to be 342 and 658 respectively for CNT (6,6)-water (SPC/E) and CNT (6,6)-methane (OPLS-UA) which correspond to an average of about 7 (for water) and 13 (for methane) molecules per nanosecond respectively. The total numbers of exiting events are counted to be 3701 and 4048 for water and methane respectively. To overcome the ambiguity in definition of dividing surfaces leading to correlated exit and entry events, especially on short time scales, an exit event is registered if the particle that exits the CNT does not reenter within 5 ps.<sup>41</sup> Also, the events are counted irrespective of the conduction direction and the individual conduction events are smoothed with a 1-ns-wide triangular filter.<sup>11</sup>

Further  $P_r$ , the return probability that a particle that enters into the channel through one end exits from the same end, and  $P_{tr} = 1 - P_r$ , the transmission probability that a particle passes through the entire channel (i.e. enters from one end and exits from the other end) leading to a conduction event are determined.<sup>17</sup> The probabilities for the occurrence of translocation events ( $P_{tr}$ ) are estimated to be 0.092 and 0.162 for SPC/E water and OPLS-UA methane respectively. In order to check accuracy of the results, the probabilities for TIP3P water are also calculated for which results are already reported. The  $P_{tr}$  value of 0.129 obtained for TIP3P-water system is close to the reported<sup>17</sup> value of 0.137. If the gap time required for reentry is increased from 5 to 10 ps,  $P_{tr}$  values are increased to 0.124 and 0.190 respectively for CNT (6,6)-water (SPC/E) and CNT (6,6)-methane (OPLS-UA) systems. The

higher probability of translocation for methane is consistent with the fact that the diffusivity of methane is higher than that of water. In Figure 5.8 we have shown rate of flow of the fluid particles per nanosecond through the nanotube.<sup>42</sup> We found that the conduction of water occurred in pulses through the nanotube as reported earlier.<sup>11,17</sup>

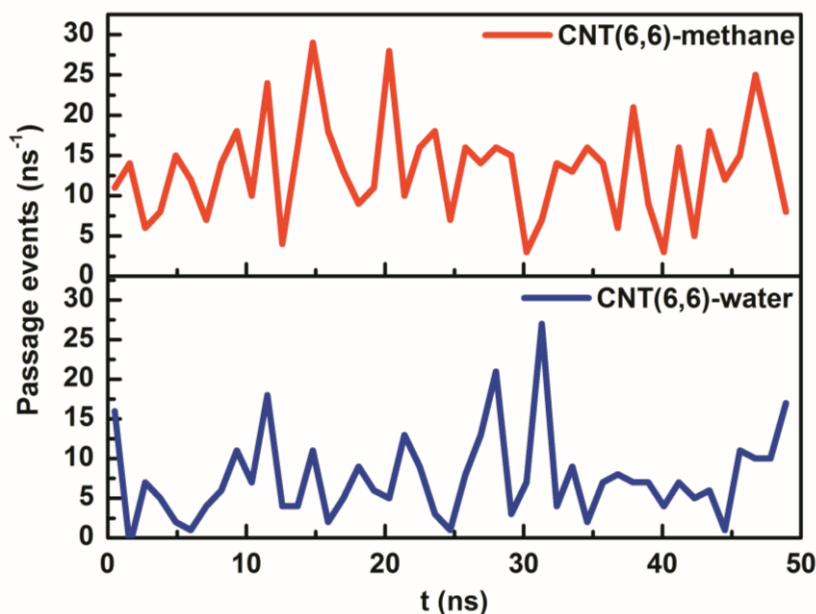


**Figure 5.8: Number of translocation events of fluid molecules per nanosecond through the CNT. Conduction bursts<sup>11,17</sup> as shown by the peaks have been observed in both the CNT-methane and the CNT-water systems.**

The most interesting observation during the present study is that the pulse-like transmission through the CNT or the so called conduction burst (Figure 5.8) is observed in case of methane also. It contradicts the explanation given by Hummer et al.<sup>11</sup> for the observed pulse-like conduction of water molecules through the CNT. They attributed this conduction burst of water to the tight hydrogen-bonding network inside the nanotube. If this is the case, then such a pulsed transmission should not have been observed in case of methane-CNT system. Hence, we conclude that the pulse-like conduction of fluid molecules does not have any relation with the polarity or hydrogen bond forming ability of the fluid molecules. It may be attributed to the single-file nature of the CNT-fluid system. From the results discussed above, it is clear that diffusion as well as transport of methane molecules through CNT (6, 6)

is faster as compared to that of water, though the methane molecules are having more ordered structure inside the nanotube. Similar behavior is observed by Whitby et al.<sup>43</sup> when they carried out experiments to understand the flow of water, ethanol and decane through carbon nanopipes. They observed that the transport of non-polar, non-hydrogen bonded decane is faster than that of water.

In order to get more insight into this behavior, the activation energies of diffusion for both methane and water are calculated by analyzing the Arrhenius plot, in which logarithm of diffusivity  $D$  is plotted as a function of inverse of absolute temperature. The Arrhenius relationship as represented by  $D = D_0 e^{-E_a/k_B T}$  gives an estimate of the activation energy  $E_a$  for diffusion of the fluid particles at a temperature  $T$ , where  $k_B$  is the Boltzmann constant. For this purpose, MD simulations are carried out at different temperatures for 2.0 ns each and the diffusivities in  $\text{cm}^2 \text{s}^{-1}$  are calculated from the MSD plots for both CNT-water and CNT-methane systems at five different temperatures i.e. 250 K, 275 K, 298 K, 325 K and 350 K for water and 120 K, 136 K, 150 K, 165 K and 180 K for methane (Figure 5.9). Arrhenius plots of  $\ln(D)$  as a function of inverse of temperature ( $1/T$ ) are drawn and activation energies for the diffusion are estimated from the slopes of the straight lines<sup>44</sup> (Figure 5.10). The activation energy values are found out to be  $11.066 \text{ KJ mol}^{-1}$  and  $1.668 \text{ KJ mol}^{-1}$  for CNT-water and CNT-methane systems respectively. Lower activation energy for the diffusion of methane as compared to that for water supports faster transport of methane molecules than that of water molecules through the nanotube.

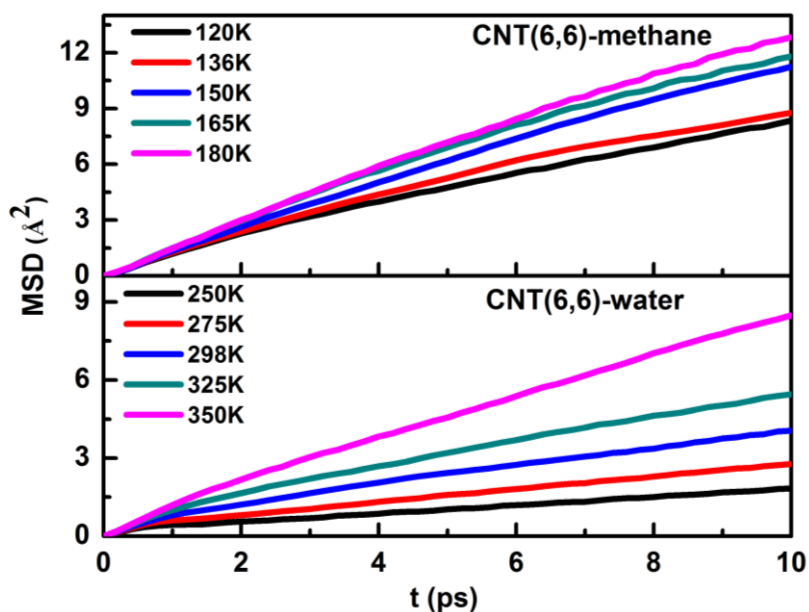


**Figure 5.9:** Mean Square Displacements (MSDs) along the CNT axis for CNT-water and CNT-methane systems at different temperatures.

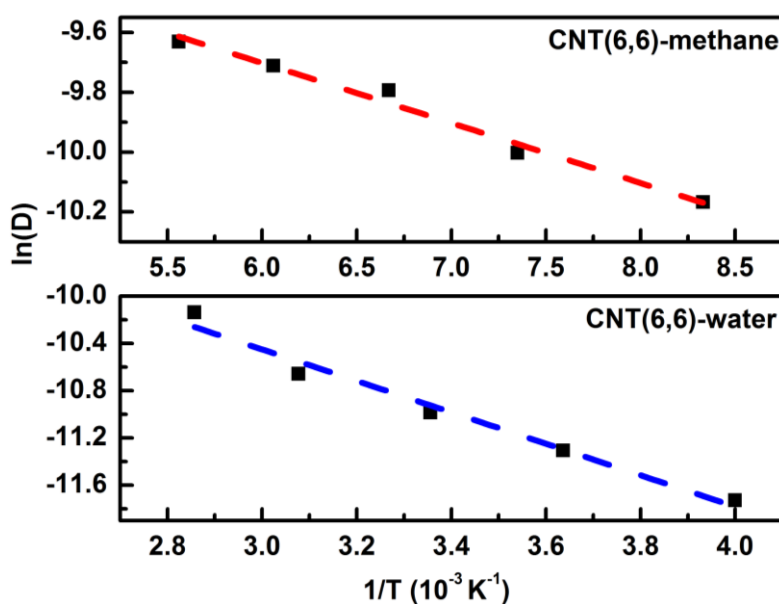


**Figure 5.10:** Arrhenius plots for diffusivities of water and methane molecules along the nanotube axis at different temperatures. Dotted lines are the linear fits to the data (symbols) obtained from MD simulations.

To confirm it, the average force experienced by a fluid particle inside the CNT only due to the CNT atoms has also been calculated.<sup>45</sup> The estimated values for square of magnitude of force are  $1.69 \times 10^{28} \text{ N}^2$  and  $1.19 \times 10^{28} \text{ N}^2$  for CNT-water and CNT-methane

systems respectively. Lower value of force due to CNT cage in case of methane molecules again confirms that due to levitation effect<sup>44,45</sup> the transport of methane molecules through carbon nanotube is faster as compared to that of water molecules.

In order to check whether the results presented here for the nonpolar fluid is specific to methane or it is general to any other nonpolar fluid, we have also investigated various properties of another nonpolar fluid argon in and around the CNT. We have simulated liquid argon in and around a CNT(6,6) with  $\rho\sigma^3 = 0.72$  (same as that of methane),  $\sigma$  and  $\rho$  being the Lennard-Jones size parameter and number density respectively of argon, using  $\sigma_{\text{ArAr}} = 3.4 \text{ \AA}$  and  $\varepsilon_{\text{ArAr}}/k = 120 \text{ K}$  (i.e.  $\varepsilon_{\text{ArAr}} = 0.9972 \text{ kJ mol}^{-1}$ )<sup>46</sup> at a temperature of 155 K (greater than its critical temperature of 150.7 K).<sup>47</sup> The corresponding argon-CNT interaction parameters are  $\sigma_{\text{CAr}} = 3.4 \text{ \AA}$  and  $\varepsilon_{\text{CAr}} = 0.5990 \text{ kJ mol}^{-1}$ . The results for radial density profile, mean squared displacement and flow of argon through the CNT are shown in comparison with those of methane in the Figures 5.11-5.13 below.

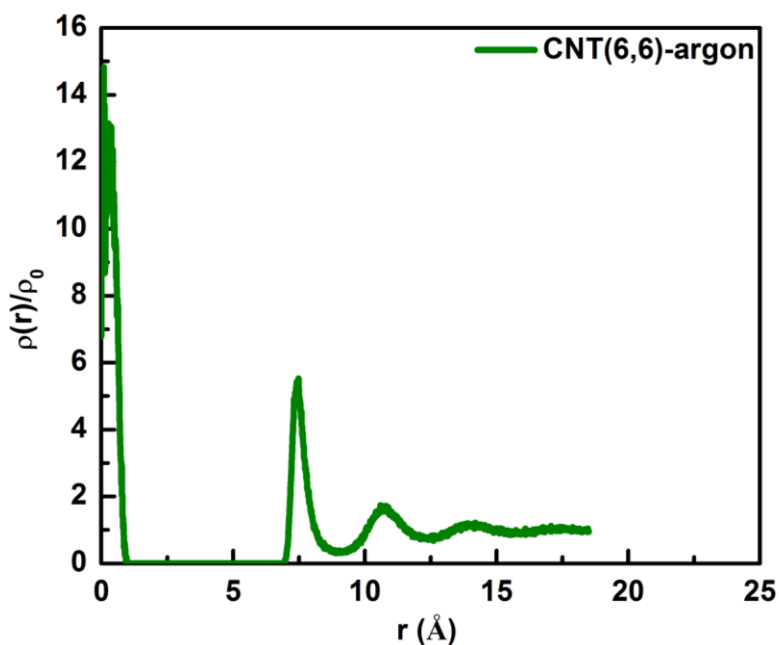


**Figure 5.11:** Normalized density profile,  $\rho(r)/\rho_0$ , of argon as a function of radial distance,  $r$  measured from the center of the nanotube.

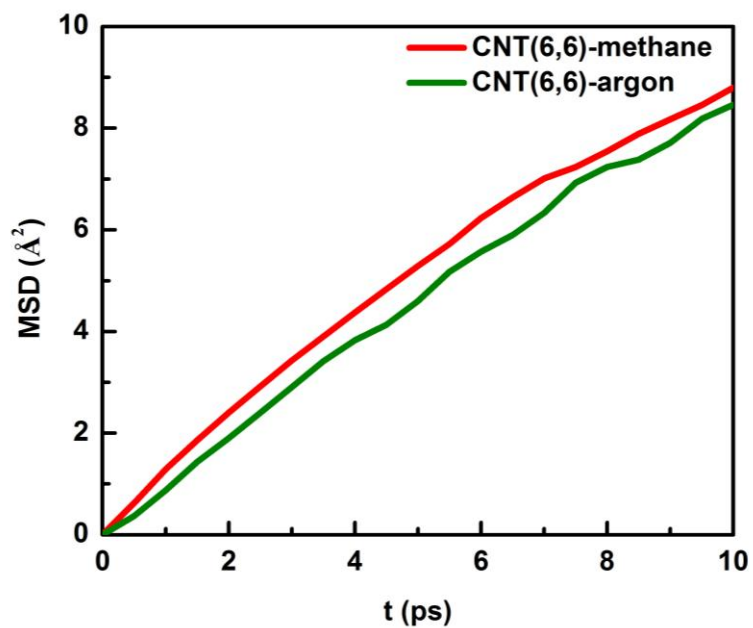


**Figure 5.12:** MSD profiles for methane (red curve) and argon (green curve) molecules inside the nanotube along the axial direction.

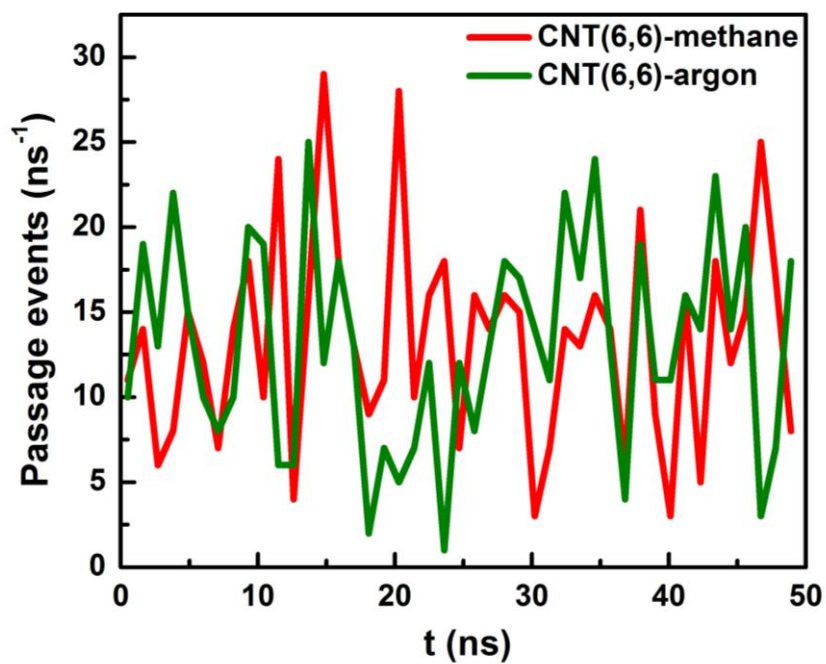


**Figure 5.13:** Number of translocation events of fluid molecules per nanosecond through the CNT. Conduction bursts as shown by the peaks have been observed in both the CNT-methane and the CNT-argon systems.

The behavior of argon in general resembles that of methane. The radial density profile of argon as a function of radial distance from the CNT axis is very much similar to that of methane with one single peak in the middle. Because of the smaller size of the argon as compared to that of methane, the width of the peak in the middle ( $r=0$ ) is broader and height is smaller than the corresponding quantities for methane. The MSD and flow patterns are almost similar for both argon and methane.

### 5.3.2 Effect of Nanotube Diameter on the Various Characteristics of CNT-water Systems

The effect of nanotube diameter on the radial distribution of water molecules is demonstrated in Figure 5.14. In the (6, 6) nanotube, there is just enough space for only a single-molecular chain of fluid molecules (Figure 5.14a). For this reason, only one peak near the centre is observed. The CNT (8,8) does not have any fluid molecules chain in the middle, instead it contains a single cylindrical solvation shell such that all the water/methane molecules have moved towards the walls of the nanotube as shown by a peak at around 2.0 Å (Figure 5.14b). As the diameter increases, it is possible to have a second layer of fluid molecules, which gives rise to a second peak in the radial distribution. For instance, as in the case of CNT(10,10)-water system, another peak appears at the centre in addition to the cylindrical layer at around 3.4 Å (Figure 5.14c). Similar results were obtained by Xiao-Yan et al. for CNT-water systems.<sup>48</sup> In case of CNT (12,12)-water system, it shows a cylindrical shell near the CNT wall along with the water density similar to bulk near the centre of the CNT (Figure 5.14d). The fluid structure outside the CNT is almost the same for all the nanotubes with two peaks followed by a uniform density of one. The observations in Figure 5.14 are corroborated by estimating the distribution of water molecules along the axis of a cylindrical shell around the centre of the box, of length extending up to the box size and of diameter very small as compared to the CNT diameter.

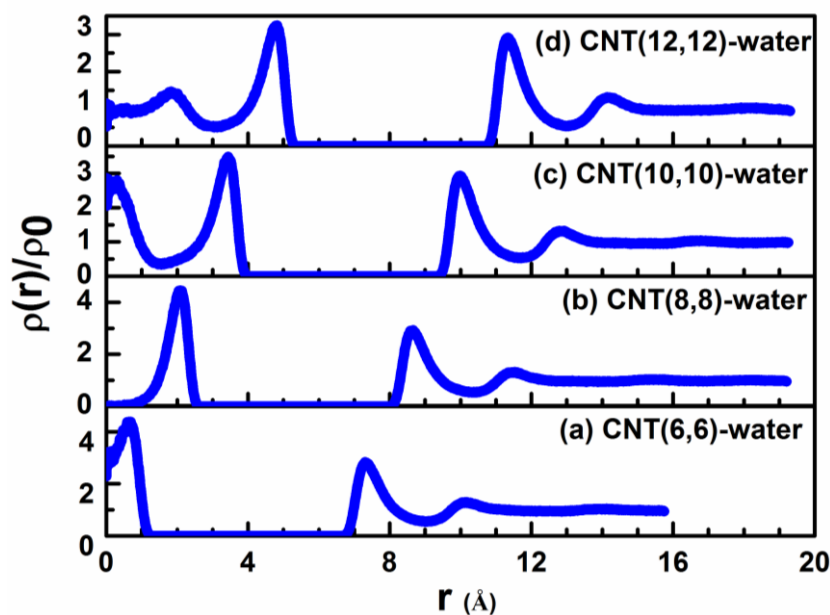


**Figure 5.14:** Normalized density profile,  $\rho(r)/\rho_0$ , of water as a function of radial distance,  $r$  measured from the center of the nanotube for various water-CNT systems.

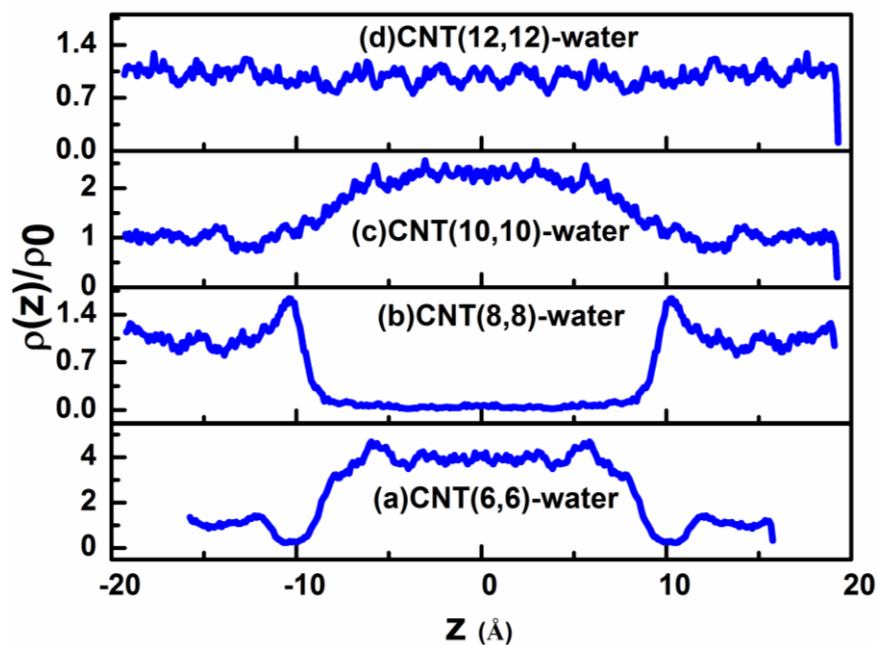


**Figure 5.15:** Axial density distribution functions for various water-CNT systems.

A cylindrical shell of radius  $0.8 \text{ \AA}$  is considered for the same and the axial distribution profiles are given in Figure 5.15 for the various CNT-water systems. It is obvious from the axial profile that there are no water molecules at the middle for CNT(8,8)-water system



whereas these are present in all other cases (Figure 5.15b). Also, Figure 5.15(d) confirmed that the CNT (12,12)-water system shows bulk behavior at the middle.

The average number of water molecules as calculated from the simulation trajectories inside various CNTs during the simulation are given in Figure 5.16. It is observed from Figure 5.16 that in case of CNT (6,6), the number of water molecules inside CNT varies between 4 and 6. In case of CNT (12, 12), the number of water molecules inside CNT varies between 44 and 60. The average number of water molecules inside CNT is around 5, 17, 33 and 51 respectively for CNTs (6, 6), (8, 8), (10, 10) and (12, 12).

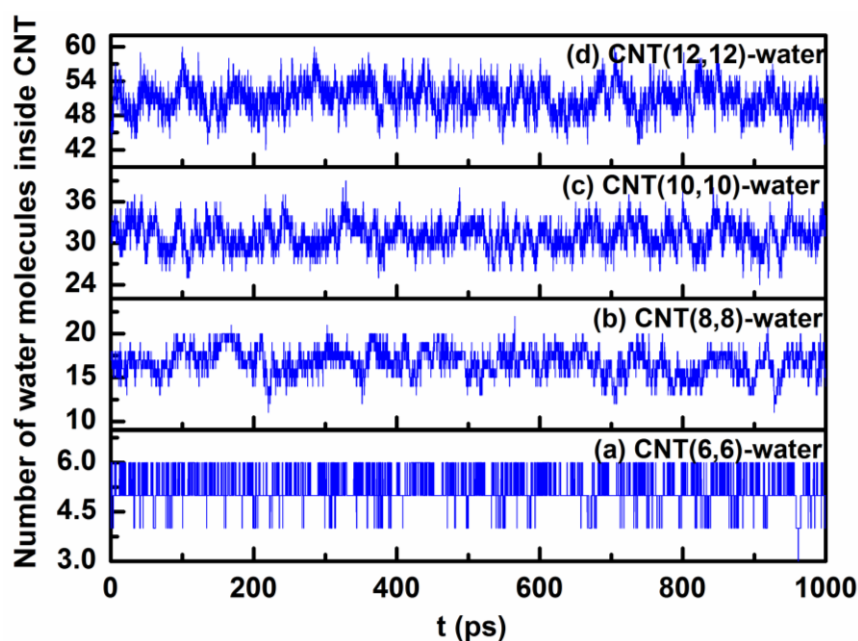


**Figure 5.16: Number of water molecules inside CNTs of different diameters during the period of simulation.**

We have calculated velocity correlation functions (VCFs) for water molecules inside different CNTs which are shown in Figure 5.17. It is observed that the VCFs are different for different CNTs (Figure 5.17). There are considerable changes in the short timescale behaviors of different VCFs, indicating interesting changes in the collective vibrations of water in various environments. Also, the VCFs of water molecules for CNT (6,6) are markedly different from those for other CNTs (Figure 5.17a). In other words, the vibrational behavior

of the water molecules are significantly different in presence of CNT(6,6) than with any other CNT. These results are further analyzed by estimating the power spectra of molecules for different CNTs as explained in the following paragraph.

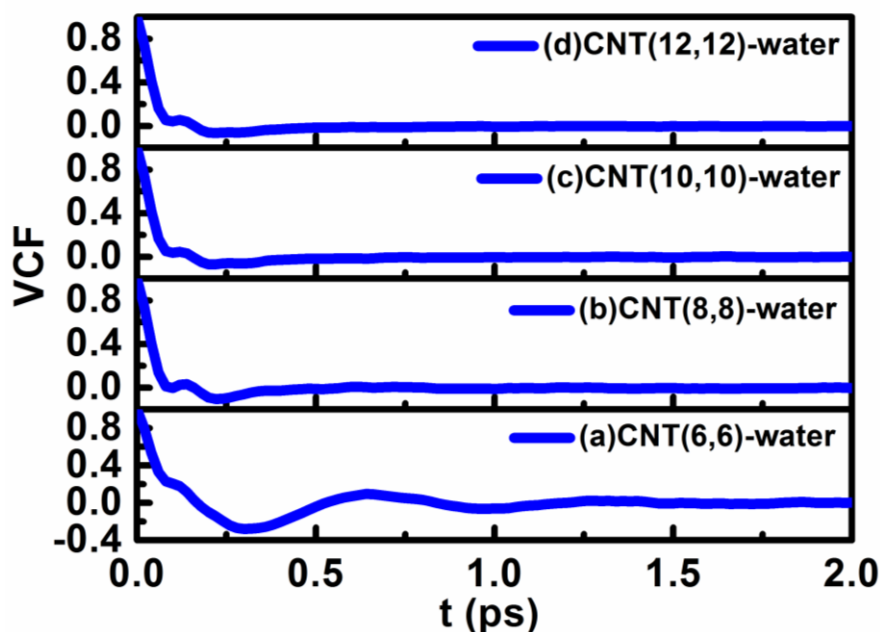


**Figure 5.17: Velocity correlation functions (VCFs) for various water-CNT systems.**

The power spectra obtained from the Fourier transform of the VCFs of water molecules for CNTs of different diameters is given in Figure 5.18. It is observed from this Figure that the frequency spectrum for the bulk water has a major peak around  $9\text{--}10\text{ ps}^{-1}$ , attributed to many-body motions<sup>49</sup> and a broad shoulder-like peak at around  $40\text{--}45\text{ ps}^{-1}$ , attributed to pairwise intermolecular oxygen-oxygen vibrations<sup>50,51</sup> and is in good agreement with a recent study<sup>52</sup> on bulk water as well as that from early computer simulations of water.<sup>50</sup> The CNT (6,6)-water system exhibits prominent vibrations at a frequency of around  $10\text{ ps}^{-1}$ , as shown by a sharp peak in the power spectra whereas the vibrational spectra of bigger CNTs (although shown only for CNT(8,8)) tend towards that of the bulk water.<sup>40</sup> This confirms the observation from VCF that the behavior of water molecules within CNT(6,6) deviate significantly from bulk behavior, with trend converging to bulk behavior for higher CNTs.

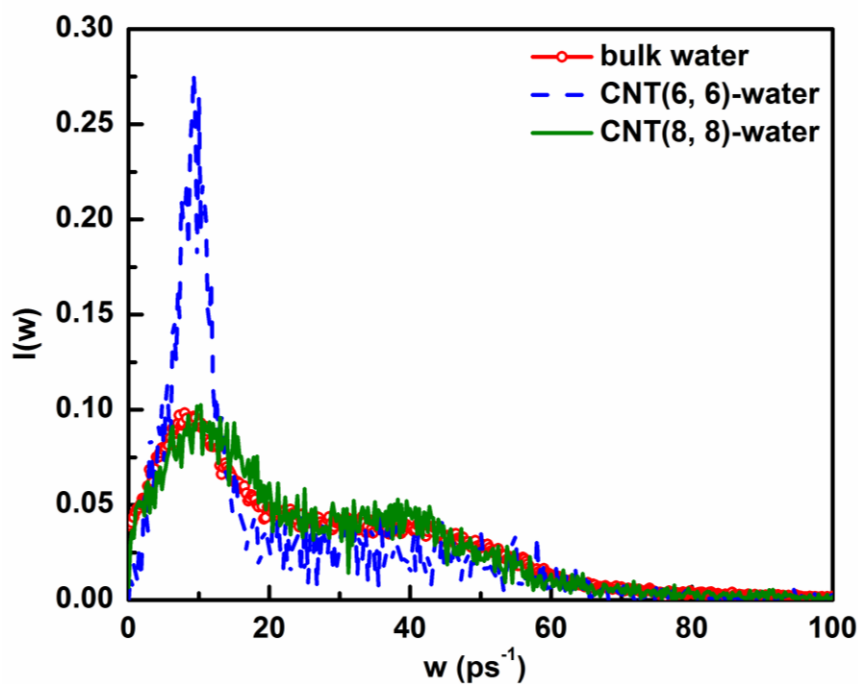


Figure 5.18: Power spectra for bulk water and various water-CNT systems.

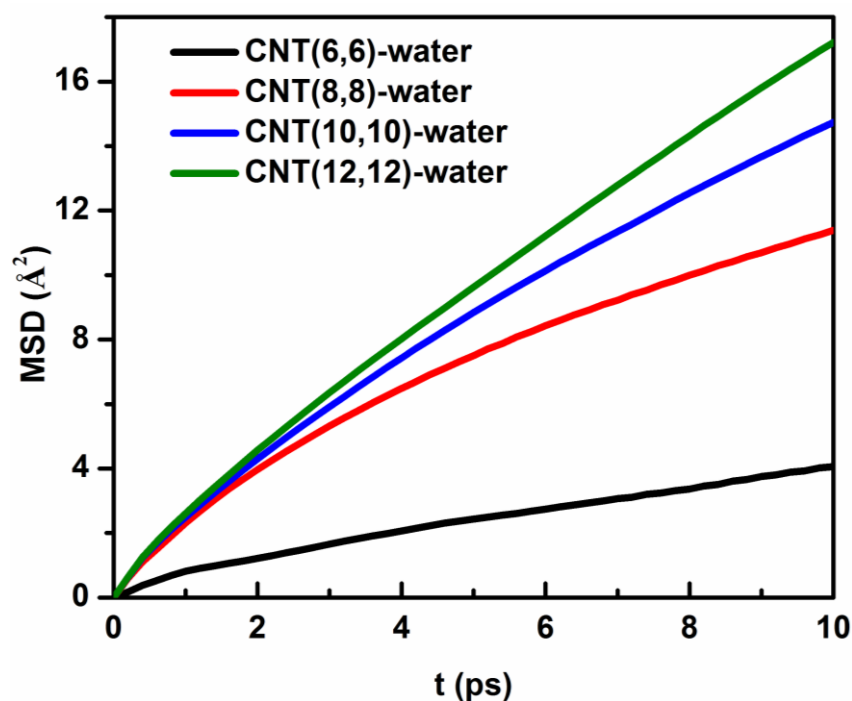


Figure 5.19: Mean Square Displacement (MSD) for various water-CNT systems.

The dynamics of the water molecules under confinement due to the presence of CNTs of various diameters is also studied in terms of mean squared displacement (MSD) functions (Figures 5.19). As all other time correlation functions, MSD also has been calculated by

averaging over only those water molecules that are in the confined region at the initial time (i.e., time origin  $t_0$ ). As the slope of MSD curves after sufficiently long time are related to the self-diffusion of the fluid molecules in the system, it is concluded that the axial diffusivity of water molecules is enhanced with increase in the diameter of the CNT (Figure 5.19).

## 5.4 Conclusions

In summary, the behavior of fluids inside the nanotubes largely depends on the extent of confinements and polarity of the fluid under investigation. The extensive molecular dynamics (MD) simulations are employed to make a comparative analysis of structure and dynamics of polar, hydrogen-bonded water and nonpolar methane molecules inside the carbon nanotube (CNT) with the intention to find out differences if any in structure, diffusion and translocation of a polar and a non-polar fluid. It has been observed that methane is more ordered inside the CNT as compared to water. This is probably because of larger size of a methane molecule, which in the present case almost exactly fits into the inside diameter of the CNT. On the other hand, due to smaller size of a water molecule as compared to the diameter of the CNT, water molecules although cannot overtake but maintain a zig-zag orientation suitable for intermolecular hydrogen bond formation and thus the density profile has two small peaks around the center of the nanotube and the height of the density peak is smaller than that of methane. One interesting difference between water and methane is that, in case of water, empty-filled transitions are observed, whereas in case of methane, no such transitions have been observed. The flow and the diffusion inside the CNT are faster for methane as compared to the same for water. This is in accordance with the experimental result of Whitby et al.<sup>43</sup>, who showed nonpolar decane flows faster than water. The faster diffusion of methane through the CNT has been rationalized by calculating activation energy (for diffusion), which is smaller for methane as compared to water. This is further corroborated by smaller force

acting on the methane molecules as compared to water molecules inside the CNT. It is also shown that pulsed transmission or conduction burst of fluid through the CNT is not the sole characteristic of water like hydrogen bonded fluid. This conduction burst is also observed in case of a nonpolar fluid like methane, which cannot form intermolecular hydrogen bonds. It may be attributed to the single-file arrangement of the fluid molecules inside the CNT. Further it has been demonstrated considering argon as another nonpolar fluid that the results presented here for nonpolar fluid are not specific to methane and in general applicable to any other nonpolar, non-hydrogen bonded fluid. The effect of nanotube diameter on the various features of water-CNT system is also demonstrated by simulating water molecules in the presence of nanotubes of varying diameter. The distribution of water molecules inside the CNT is observed to depend upon the size characteristics of the CNT i.e. the space available for water molecules within the CNT. Moreover, considerable changes in the short timescale behaviors of VCFs in case of different water-CNT systems were observed, indicating interesting changes in the collective vibrations of water in various environments. The power spectra as obtained from VCFs indicates that the behavior of water molecules within CNT(6,6) deviate significantly from bulk behavior, with trend converging to bulk behavior for higher diameter CNTs. The translational movement of water molecules along the axis of the nanotube is observed to become faster and faster as the diameter of the nanotube is increased. Although pristine CNTs can be effectively used for nano-fluidics, their use in separation processes is expected to be limited. The CNT functionalized with suitable organic functional groups will be more useful in capturing various ions such as uranyl ions from their aqueous solution. The functional groups present on the CNT can induce specific binding of the ions with the CNT. With the basic knowledge obtained in this analysis of fluids under nano-confinement, in next chapter i.e. Chapter 6, we will move ahead with the simulation studies of aqueous solutions of uranyl ions in the presence of bare and functionalized CNTs to study the relative capacity of these CNTs in removal of ions from their aqueous solutions.

## References

1. O. Beckstein, P. C. Biggin and M. S. P. Sansom, *J. Phys. Chem. B*, **2001**, *105*, 12902.
2. G. C. Zuo, R. Shen, S. J. Ma and W. L. Guo, *ACS Nano*, **2010**, *4*, 205.
3. J. Kofinger, G. Hummer and C. Dellago, *Proc. Natl. Acad. Sci. U. S. A.*, **2008**, *105*, 13218.
4. A. Alexiadis and S. Kassinos, *Chem. Rev.*, **2008**, *108*, 5014.
5. A. Kalra, S. Garde and G. Hummer, *Proc. Natl. Acad. Sci. U. S. A.*, **2003**, *100*, 10175.
6. S. Ghosh, A. K. Sood and N. Kumar, *Science*, **2003**, *299*, 1042.
7. N. W. S. Kam, M. O'Connell, J. A. Wisdom and H. Dai, *Proc. Natl. Acad. Sci. U.S.A.*, **2005**, *102*, 11600.
8. M. S. P. Sansom and P. C. Biggin, *Nature*, **2001**, *414*, 156.
9. N. Floquet, J. P. Coulomb, N. Dufau and G. Andre, *J. Phys. Chem. B*, **2004**, *108*, 13107.
10. D. Y. Lu, A. Aksimentiev, A. Y. Shih, E. Cruz-Chu, P.L. Freddolino, A. Arkhipov and K. Schulten, *Phys. Biol.*, **2006**, *3*, 40.
11. G. Hummer, J. C. Rasaiah and J. P. Noworyta, *Nature (London)*, **2001**, *414*, 188.
12. K. F. Rinne, S. Gekle, D. J. Bonthuis and R. R. Netz, *Nano Lett.*, **2012**, *12*, 1780.
13. X. Qin, Q. Yuan, Y. Zhao, S. Xie and Z. Liu, *Nano Lett.*, **2011**, *11*, 2173.
14. M. Melillo, F. Zhu, M. A. Snyder and J. Mittal, *J. Phys. Chem. Lett.*, **2011**, *2*, 2978.
15. R. J. Mashl, S. Joseph, N. R. Aluru and E. Jakobsson, *Nano Lett.*, **2003**, *3*, 589.
16. K. Koga, G. T. Gao, H. Tanaka and X. C. Zeng, *Nature*, **2001**, *412*, 802.
17. A. Berezhkovskii and G. Hummer, *Phys. Rev. Lett.*, **2002**, *89*, 064503.
18. B. Mukherjee, P. K. Maiti, C. Dasgupta and A. K. Sood, *J. Chem. Phys.*, **2007**, *126*, 124704.

19. J. K. Holt, H. P. Park, Y. Waang, M. Stadermann, A. B. Artyukhin, C. P. Grigopoupulos, A. Noy and O. Bakajin, *Science*, **2006**, *312*, 1034.
20. M. Majumder, N. Chopra, R. Andrews and B. J. Hinds, *Nature*, **2005**, *438*, 44.
21. L. Maibaum and D. A Chandler, *J. Phys. Chem. B*, **2003**, *107*, 1189.
22. D. Chandler, *Nature*, **2005**, *437*, 640 and references therein.
23. J. A. Thomas and A. J. H. McGaughey, *Nano. Lett.*, **2008**, *8*, 2788.
24. S. Majumder, N. Choudhury and S. K. Ghosh, *J. Chem. Phys.*, **2007**, *127*, 054706.
25. N. Naguib, H. Ye, Y. Gogotsi, A. G. Yazicioglu, C. M. Megaridis and M. Yoshimura, *Nano Lett.*, **2004**, *4*, 2237.
26. R. C. Major, J. E. Houston, M. J. McGrath, J. I. Siepmann and X. Y. Zhu, *Phys. Rev. Lett.*, **2006**, *96*, 177803.
27. A. B. Farimani and N. R. Aluru, *J. Phys. Chem. B*, **2011**, *115*, 12145.
28. T. Ohba, K. Kaneko, M. Endo, K. Hata and H. Kanoh, *Langmuir*, **2013**, *29*, 1077.
29. J. Su and H. Guo, *J. Phys. Chem. B*, **2012**, *116*, 5925.
30. M. Rana and A. Chandra, *J. Chem. Sci.*, **2007**, *119*, 367.
31. H. J. C. Berendsen, J. R. Grigera and T. P. Straatsma, *J. Phys. Chem.*, **1987**, *91*, 6269.
32. H. J. C. Jorgensen, J. D. Madura and C. J. Swenson, *J. Am. Chem. Soc.*, **1984**, *106*, 6638.
33. K. Bartus and A. Brodka, *Mol. Phys.*, **2011**, *109*, 1691.
34. Y. Maniwa, K. Matsuda, H. Kyakuno, S. Ogasawara, T. Hibi, H. Kadowaki, S. Suzuki, Y. Achiba and H. Kataura, *Nat. Mat.*, **2007**, *6*, 135.
35. D. Cao and J. Wu, *Langmuir*, **2004**, *20*, 3759.
36. D. Y. Kuan, P. K. Kilpatrick, M. Sahimi, L. E. Scriven and H. T. Davis, *SPE Res. Engg.*, **1986**, 61.

37. M. P. Allen and D. J. Tildesley, *Computer Simulation of Liquids*; Oxford University, New York, 2004.
38. M. Wilson and P. A. Madden, *J. Am. Chem. Soc.*, **2001**, *123*, 2101.
39. A. Zahab, L. Spina, P. Poncharal and C. Marliee, *Phy. Rev. B*, **2000**, *62*, 10000.
40. N. Choudhury and B. M. Pettitt, *J. Phys. Chem. B*, **2005**, *109*, 6422.
41. Impey, R. W.; Madden, P. A.; McDonald, I. R. Hydration and mobility of ions in solution. *J. Phy. Chem.* **1983**, *87*, 5071-5083.
42. M. Chopra, R. Phatak and N. Choudhury, *AIP Conf. Proc.*, **2013**, *1512*, 562.
43. M. Whitby, L. Cagnon, M. Thanou and N. Quirke, *Nano Lett.*, **2008**, *8*, 2632.
44. B. J. Borah, H. Jobic and S. Yashonath, *J. Chem. Phys.*, **2010**, *132*, 144507.
45. P. K. Ghorai, S. Yashonath, P. Demontis and G. B. Suffritti, *J. Am. Chem. Soc.*, **2003**, *125*, 7116.
46. S. H. Lee, D. K. Park and D. B. Kang, *Bull. Kor. Chem. Soc.*, **2003**, *24*, 178.
47. P. S. Vogt, R. Liapine, B. Kirchner, A. J. Dyson, H. Huber, G. Marcelli and R. J. Sadus, *Phys. Chem. Chem. Phys.*, **2001**, *3*, 1297.
48. Z. Xiao-Yan and L. Hang-Jun, *Chinese Phys.*, **2007**, *16*, 335.
49. D. A. Zichi and P. J. Rossky, *J. Chem. Phys.*, **1986**, *84*, 2814.
50. A. Rahman and F. H. Stillinger, *J. Chem. Phys.*, **1971**, *55*, 3336.
51. D. Eisenberg and W. Kauzmann, *The Structure and Properties of Water*; Oxford University, New York, 1969.
52. U. Balucani, J. P. Brodholt and R. Vallauri, *J. Phys. Condens. Matter*, **1996**, *8*, 6139.



# *Chapter 6*

## **Adsorption of Uranyl Ions from Aqueous Solution to the Functionalized Carbon Nanotube**



## 6.1 Introduction

Water is known to exhibit significantly different characteristics and local structural arrangements at interfaces as compared to those in the bulk.<sup>1-9</sup> It is well-known that the manifestation of different properties of water depends on the length scales of the interfaces.<sup>3,4</sup> This has generated a lot of scientific interests to analyze and understand behavior of various solvents and aqueous solutions at interfaces. Among various interfacial systems, water-carbon nanotube (CNT) (Chapter 5) and water-fullerene<sup>10,11</sup> interfaces are of recent interests due to their unique physical and chemical properties. The unique geometrical characteristics and exceptional mechanical and electrical properties of the CNTs have made them immensely useful in a variety of bio-medical, nanotechnology and engineering applications.<sup>12-14</sup> Recent years have witnessed upsurge in interests in these carbonaceous nanomaterials owing to possibilities of wide applications of such systems in various fields of science and technology.<sup>15-20</sup> Among numerous applications, CNT based systems have found utmost applications in the field of water purification and decontamination.<sup>21-24</sup> Das et al.<sup>21</sup> have given an overview of the molecular modeling and experimental aspects of CNT-membrane fabrication and functionalization for desalination of saline water. Goh et al.<sup>22</sup> described the desalination applications of CNTs along with the hurdles and challenges in this field. Kar et al.<sup>23</sup> not only highlighted the opportunities provided by the CNT membrane systems in the field of water purification but also pointed out the challenges presented by the alignment of the CNTs. Nasrabadi et al.<sup>24</sup> demonstrated the strength of charged CNTs in separating ions from their aqueous solutions. The transport of fluids through CNTs have been studied with reference to many biological, geological and medical applications.<sup>25-30</sup> The nanoscale dimensions of the CNTs and a relatively large surface area-to-volume ratio modify significantly the structural and dynamical aspects of fluids and ions surrounding these nanomaterials. The higher adsorption capacity of CNTs with respect to various contaminants

has given them an edge over the traditional activated carbon based removal systems. Yang et al. have reported that plasma modified CNTs have salt adsorption capacity of two orders of magnitude higher than state-of-the-art activated carbon-based water treatment systems.<sup>31</sup> Functionalization of CNT is often done for specific purposes to get better outcomes.<sup>32</sup> The presence of functional groups on the surface of the CNT has been found to improve the performance of CNT based membranes for various types of liquid purification applications.<sup>33</sup> Mishra et al.<sup>34</sup> have proposed functionalized graphene sheets as a much better option for adsorbing inorganic species containing arsenic as well as sodium. The above discussion suggests that the adsorption and transport capacity of CNTs has made them a useful system in separation and purification processes and in nanofluidics.

Separation processes based on the liquid-liquid extraction have been utilized for many years in the nuclear industry, especially for the reprocessing of the spent fuel.<sup>35-38</sup> The actinyl ions such as uranyl ions have direct relevance to the nuclear fuel cycle as uranium is utilized as fuel in many types of nuclear reactors. Studying the characteristics of uranyl ions in different systems may open new gateways of procedures for better management of the radioactive waste generated in the nuclear fuel cycle.<sup>39-41</sup> Nanomembrane based separation may be one such option which can be thought of while analyzing the behavior of uranyl ions in the presence of CNTs. A fundamental understanding of interfacial structure and transport phenomena is essential in developing high fidelity process models for solvent extraction processes.<sup>35</sup> The radioactive nature of uranyl ions and difficulty in performing controlled experiments made the experimental determination of their properties very difficult and time-consuming. Hence, a computational approach such as molecular dynamic (MD) simulations coupled with existing experimental observations provide a useful alternative for understanding the structural, dynamic and thermodynamic behavior of these ions.<sup>42</sup>

There has been a lot of modeling and simulation work related to understanding the characteristics of aqueous solutions of uranyl ions in the recent times.<sup>43,44</sup> Many interesting results are also reported in Chapters 2 to 4 in this thesis. These studies not only provide the much needed potential parameters for the uranyl ions<sup>43,45</sup> but also give important prior knowledge of the features and molecular level understanding of such systems. Many researchers have reported the behavioral changes in the fluid molecules/ions when the carbon nanotubes are modified by substitution with functional groups or varying the charge. For instance, Huang et al.<sup>46</sup> studied the temperature and helicity effects on the static properties of water molecules confined in CNTs modified by carboxylic acid functional groups. Similarly, Dezfoli et al.<sup>47-49</sup> studied the ion ( $\text{Zn}^{2+}$ ,  $\text{Cd}^{2+}$  etc.) adsorption on the charged carbon nanotubes and also the effect of temperature, pH of the solution, mass of the nanotube and surface modification of CNT on adsorption. They concluded that layers of water around CNT and the interaction energies play important role in the adsorption process. Moreover, electrostatic force controls the adsorption of ions on the CNT sidewall. Also, the modification of CNT with hydroxyl and carboxyl functional groups led to increase in the rate of adsorption process. Using molecular dynamics simulation, absorption of heavy metal ions ( $\text{Cd}^{2+}$ ,  $\text{Cu}^{2+}$ ,  $\text{Pd}^{2+}$  and  $\text{Hg}^{2+}$ ) from their aqueous solutions by functionalized single-walled CNTs has been investigated.<sup>50</sup> Different functional groups such as  $-\text{COO}^-$ ,  $-\text{OH}$ ,  $-\text{CONH}_2$  anchored on the side walls of the CNT have been tested for their relative ability to adsorb the bivalent heavy metal ions. It is observed that the adsorption capacity increases with increase in metal ion concentration or on surface modification using above mentioned functional groups, effect being the strongest with  $-\text{COO}^-$  group. Uranyl ion being a radiotoxic ion and used extensively in nuclear industry, its separation from its aqueous solution using functionalized CNTs will be an important step in nuclear fuel cycle as well as in water decontamination. This is a field of research which has not been investigated thoroughly. Therefore, in the present study we

intend to investigate the characteristics of aqueous solution of uranyl ions in the vicinity of pristine/bare or functionalized CNT using atomistic MD simulations. Two different functionalized nanotubes namely carboxylated ( $-\text{COO}^-$ ) and hydroxylated ( $-\text{OH}$ ) CNTs have been studied here. In each of the functionalized CNTs, two, four and six number of the carbon atoms of the CNT have been functionalized using functional groups (either  $-\text{COO}^-$  or  $-\text{OH}$ ). The impact of the nature and number of functional groups is analyzed on the various properties of the aqueous solution such as the extent of uranyl ion adsorption on the CNT, radial arrangement of uranyl ions with respect to the CNT etc. and these are compared with the same for a bare CNT system. We have also investigated how the change in uranyl ion concentration in the aqueous solution affects the adsorption behavior and other characteristics of the species present in the solution.

## 6.2 Models and Simulation Details

In the present investigation, we have prepared aqueous solutions with different concentrations of divalent uranyl ions,  $\text{UO}_2^{2+}$ , by solvating respectively 20, 30 and 40 uranyl ions in a cubic box containing 2988 water molecules with a bulk water density of around 0.98 g/cc. The corresponding concentrations of the aqueous solutions of uranyl ions are 0.36 M, 0.55 M and 0.73 M respectively. Such concentrations of uranyl ion solutions may be encountered during the reprocessing of the spent fuel from uranium fueled reactors.<sup>51,52</sup> The electrical neutrality of the system was maintained by introducing required number of negative ions (nitrate,  $\text{NO}_3^-$ ) in the system. A carbon nanotube (CNT) of length 25.8 Å with chirality (6,6) is prepared using Gabedit 2.4.8 software.<sup>53</sup> Using the same software, two, four or six number of the carbon atoms of the CNT are functionalized with different functional groups such as carboxylate group ( $-\text{COO}^-$ ) and hydroxyl group ( $-\text{OH}$ ). In case of  $\text{COO}^-$  group, the negative charge on the functional group is balanced by introducing required number of

positive sodium ions ( $\text{Na}^+$ ) in the aqueous solution of uranyl ions. The preparation of cubic water box, and the solvation of ions (uranyl, nitrate, sodium) and the functionalized CNT into the cubic box of water is carried out using PACKMOL program.<sup>54</sup> The various systems studied in present work along with their abbreviations are given in Table 6.1. Simulations were performed in canonical (NVT) ensemble with molecular dynamics extended system approach of Nose.<sup>55</sup> All the simulations were carried out at a target temperature of 298 K using periodic boundary conditions and minimum image convention in all three directions. We have used atomistic model with one uranium and two oxygen sites for the uranyl ion and one nitrogen and three oxygen sites for the nitrate ion whereas SPC/E model<sup>56</sup> for water was used in all the cases. Non-bonded site-site inter-molecular interaction is modeled with Lennard–Jones plus Coulomb interactions and intra-molecular interaction for uranyl and nitrate ions consist of bond and angle terms. The potential energy of such a system is described by Eq. 1.5 given in Chapter 1 of this thesis.

**Table 6.1: Details of the systems considered in present study**

S. No.	Functional group	Number of functional groups	System abbreviation
<b>Uranyl concentration 0.36 M</b>			
1	bare	---	B11
2	$\text{COO}^-$	2	CA21
3	$\text{COO}^-$	4	CA41
4	$\text{COO}^-$	6	CA61
5	OH	2	HY21
6	OH	4	HY41
7	OH	6	HY61

<b>Uranyl concentration 0.55 M</b>			
8	bare	---	B22
9	COO <sup>-</sup>	2	CA22
10	COO <sup>-</sup>	4	CA42
11	COO <sup>-</sup>	6	CA62
12	OH	2	HY22
13	OH	4	HY42
14	OH	6	HY62
<b>Uranyl concentration 0.73 M</b>			
15	bare	---	B33
16	COO <sup>-</sup>	2	CA23
17	COO <sup>-</sup>	4	CA43
18	COO <sup>-</sup>	6	CA63
19	OH	2	HY23
20	OH	4	HY43
21	OH	6	HY63

The values of the potential parameters for both inter- and intra-molecular interactions are given in Table 6.2.<sup>43,45,56,57,58</sup> The LJ parameters and the bonded parameters reported by Pomogaev et al.<sup>43</sup> for solvated uranyl ion are used whereas those reported by Berendsen et al.<sup>56</sup> for SPC/E water molecules are taken. The parameters related to bonded interactions and the LJ parameters for the nitrate ion are taken as reported by Guilbaud et al.<sup>45</sup> The LJ parameters for CNT carbon atoms and the atoms of the functional groups are used from AMBER96 force-field parameters<sup>58</sup> and OPLS force-field as given by Jorgensen et al.<sup>57</sup> respectively. The cross parameters for the LJ potential are estimated by using Lorentz–



Berthelot mixing rule. For each system, the production run was for 20 ns after equilibration for 5 ns and the trajectories were saved at every 0.1 ps.

**Table 6.2: Force Field Parameters**

**Non-bonded Parameters**

Atom Type	$\sigma$ (nm)	$\varepsilon$ (kJ/mol)	$q/e$
<b>Uranyl ions</b>			
U	0.295	0.5299	+2.500
O <sub>U</sub> (Uranyl oxygen)	0.383	0.0567	-0.250
<b>Nitrate ions</b>			
N	0.312	0.6694	+0.626
O <sub>N</sub> (Nitrate oxygen)	0.294	0.6276	-0.542
<b>Water</b>			
O <sub>W</sub> (SPC/E)	0.317	0.6502	-0.8476
H <sub>W</sub> (SPC/E)	-	-	+0.4238
<b>Sodium ions</b>			
Na	0.216	1.4754	+1.000
<b>CNT</b>			
C	0.340	0.3598	0.000
<b>Carboxylate ion</b>			
C (COO <sup>-</sup> )	0.375	0.4393	+0.700
O (COO <sup>-</sup> )	0.296	0.8786	-0.850
<b>Hydroxyl group</b>			
O (OH)	0.307	0.7113	-0.585
H (OH)	0.000	0.000	+0.435

$C_f$ (CNT)	0.340	0.3598	+0.15
-------------	-------	--------	-------

$C_f$  = Functionalized carbon of CNT

### Bonded Parameters

Bond Type	$r_{eq}$ (nm)	$K_r$ (kJ mol <sup>-1</sup> nm <sup>-2</sup> )
<b>Uranyl ions</b>		
U-O <sub>U</sub>	0.176	622300
<b>Nitrate ions</b>		
N-O <sub>N</sub>	0.126	251040
Angle Type	$\theta_{eq}$ (°)	$K_\theta$ (kJ mol <sup>-1</sup> rad <sup>-2</sup> )
<b>Uranyl ions</b>		
O <sub>U</sub> -U-O <sub>U</sub>	180	198
<b>Nitrate ions</b>		
O <sub>N</sub> -N-O <sub>N</sub>	120	1255.2

## 6.3 Results and Discussion

Molecular dynamics simulations are employed to study the structural features of uranyl ions in aqueous solutions of varying concentrations in the presence of bare and functionalized CNTs. The radial density distributions showing the arrangement of uranyl ions with respect to the CNT axis are estimated and discussed in subsection 6.3.1. The number of uranyl ions within the first coordination shell defined by a cylindrical region at a radial distance equal to the first minimum of the RDFs around the CNT is calculated. This gives an idea about the extent of adsorption of uranyl ions on the bare as well as functionalized CNT. The trajectories of uranyl ions are followed to check the time elapsed before the ions come within the adsorption distance around CNT in the presence of different types of functional

groups. The phenomenon of adsorption is discussed in subsection 6.3.2. The transport characteristics of the various species in terms of their diffusion coefficients estimated from the mean squared displacement (MSD) functions are discussed in the subsection 6.3.3.

### 6.3.1 Radial Density Distribution Functions of Uranyl Ions

The normalized density profiles of uranyl ions as a function of distance  $r$  from the axis of the CNT with origin at its centre are estimated in order to analyze the distribution of uranyl ions with respect to the CNT. Figure 6.1 shows the radial density distributions of uranyl ions at different uranyl concentrations for bare CNT and CNT with two functional groups (either both are carboxylate ions or  $-OH$  groups). From Figure 6.1, it is observed that in all the cases presented here, the closest (radial) distance of approach of the uranyl ion from the nanotube axis is more than or equal to around  $7.8 \text{ \AA}$ , signifying that the probability of entering the uranyl ions inside the CNT (of radius  $4.05 \text{ \AA}$ ) is practically nil. Moreover, the peaks of the RDFs are much higher when the CNT is functionalized with  $-COO^-$  ions as compared to those in case of  $-OH$  groups or bare CNT. In other words, the distribution of uranyl ions is much more structured/ordered around the carboxylate ion functionalized CNT. This is more so in case of lower concentrations of uranyl ions (Figure 6.1a).

As the concentration of uranyl ions in the aqueous solution is increased, the peak heights for bare and  $-OH$  functionalized CNT become higher than those at lower concentration, whereas no such pattern is observed for  $-COO^-$  functional group (Figure 6.1(b), (c)). Also, it is seen that for  $-COO^-$  functionalized CNT, the broad peak consists of two peaks at around  $8.2$  and  $8.35 \text{ \AA}$  such that the first peak is higher for uranyl concentrations of  $0.36 \text{ M}$  and  $0.73 \text{ M}$  whereas second peak is higher for  $0.55 \text{ M}$ . Moreover, at higher uranyl ion concentrations, although the peak height for  $-COO^-$  functional group still remains higher, the difference between peak heights for  $-COO^-$  and  $-OH$  functional groups reduces. The

higher peak intensities in case of  $\text{--COO}^-$  functionalized CNT as compared to bare and CNT functionalized with  $\text{--OH}$  functional group at all the uranyl ion concentrations suggest greater capability of  $\text{--COO}^-$  functionalized CNT for adsorption of uranyl ions from the aqueous solution. Similar observation was reported in an earlier investigation<sup>50</sup> for common heavy metal ions such as  $\text{Cd}^{2+}$ ,  $\text{Cu}^{2+}$ ,  $\text{Pb}^{2+}$  and  $\text{Hg}^{2+}$ . The peak heights for these heavy metal ions are higher than those obtained here for the uranyl ion corresponding to similar concentrations.

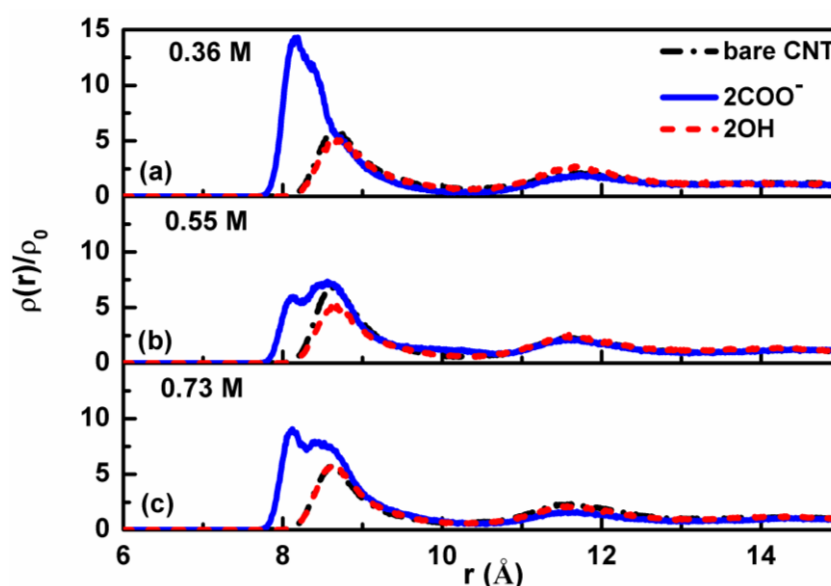


**Figure 6.1:** Normalized density profile,  $\rho(r)/\rho_0$ , of uranyl ions as a function of radial distance,  $r$  measured from the axis of the nanotube functionalized at two carbon atoms at a concentration (a) 0.36 M, (b) 0.55 M and (c) 0.73 M of uranyl ions.

Moreover, the increasing peak height and reducing peak width on moving from CNTs with two to four to six number of functional groups indicates higher ordering of the structural arrangement of uranyl ions with increase in the number of  $\text{COO}^-$  functional groups (Figure 6.2). However, the increase in number of  $\text{--OH}$  functional groups (not shown) on the CNT does not show much effect on the structural distribution of uranyl ions around CNT.

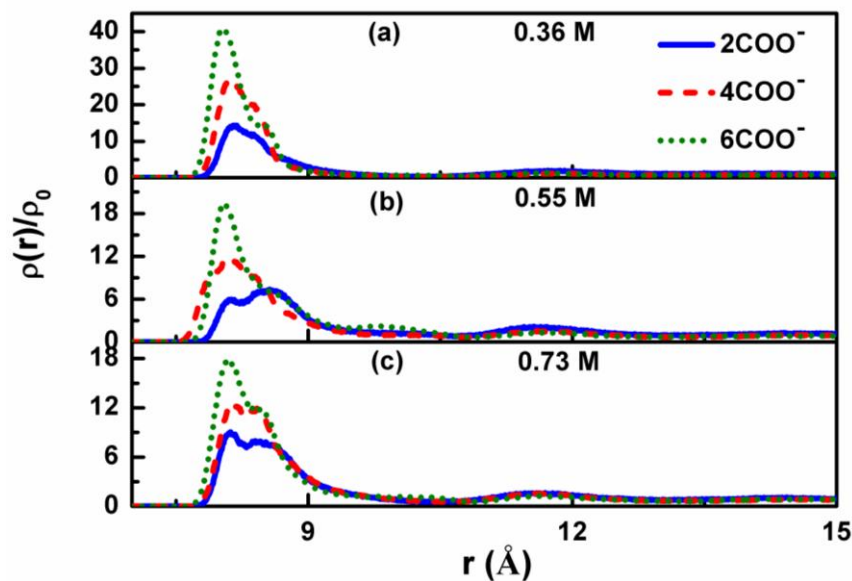


**Figure 6.2:** Normalized density profile,  $\rho(r)/\rho_0$ , of uranyl ions as a function of radial distance,  $r$  measured from the axis of the nanotube functionalized with carboxylate ions at two (blue solid line), four (red dashed line) and six (green dotted line) carbon atoms at a concentration (a) 0.36 M, (b) 0.55 M and (c) 0.73 M of uranyl ions.

### 6.3.2 Adsorption of Uranyl Ions on the Functionalized CNT

The adsorption of uranyl ions from aqueous solutions by bare and CNTs functionalized at two carbon atoms is quantified in terms of the quantity  $q_e$  (in mmol)<sup>50</sup> of uranyl ions adsorbed on the CNT per unit mass (in gm) of the CNT at various concentrations of uranyl ions in the solution (Figure 6.3). The uranyl ion is considered as adsorbed when its radial distance from the CNT axis is within 10.3 Å i.e. within the first coordination shell around CNT (as specified by the position of first trough in the density profile in Figure 6.1). It is observed that the adsorption behavior of uranyl ions is similar for bare and –OH functionalized CNTs, however, it is markedly different for –COO<sup>-</sup> functionalized CNTs. Adsorption of uranyl ions is much more significant in the presence of carboxylate functional group at all uranyl ion concentrations. Moreover, as the concentration of uranyl ions in the

solution increases, the magnitude of adsorption on the CNT also increases in all cases discussed here.

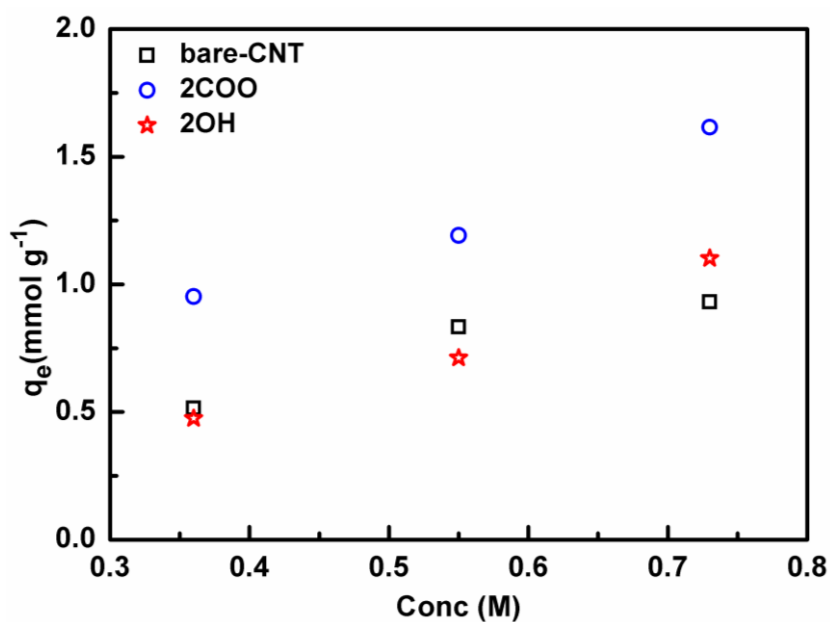


**Figure 6.3:** Adsorption of uranyl ions per unit CNT mass for bare as well as functionalized CNTs as a function of uranyl ion concentration.

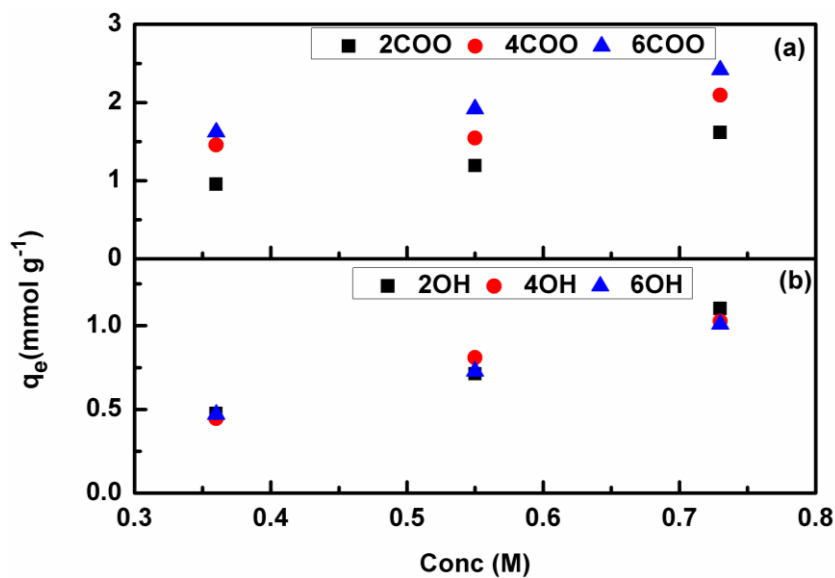


**Figure 6.4:** Number of uranyl ions adsorbed to nanotube functionalized at different number of carbon atoms with (a) carboxylate ion and (b) hydroxyl group as a function of uranyl ion concentration.

Also, the extent of adsorption increases with increase in the number of carboxylate ion functional groups present on the CNT at all concentrations of the uranyl ions studied here (Figure 6.4). This is consistent with the earlier observation of more structured arrangement of uranyl ions with increase in the number of carboxylate ion functional groups. Actually it is seen in case of carboxylate ion functionalized CNT that due to the negative charge on the functional group, the overall positively charged uranyl ion gets attracted towards it and gets adsorbed/attached to it through uranium atom of the uranyl ion and the oxygen atom of the carboxylate anion as shown in Figure 6.5.

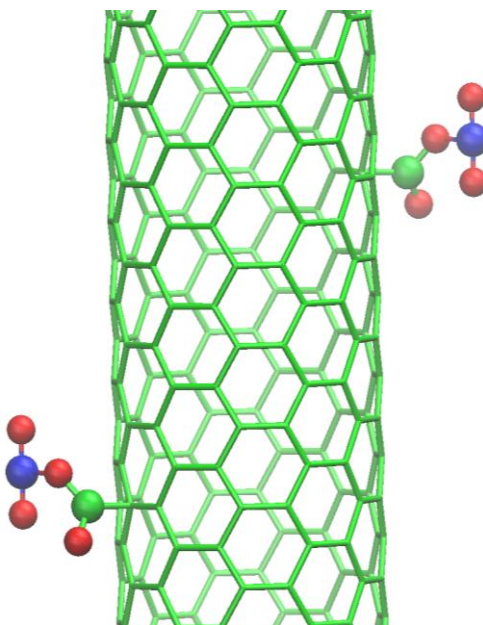


**Figure 6.5: Snapshot of bonding of uranyl ions to the carboxylate oxygen atom, here blue ball = uranium of uranyl ion, red ball = oxygen, green ball = carbon of carboxylate ion.**

For getting further insight, we have analyzed the time profile of number of uranyl ions adsorbed on the CNT functionalized at two positions with  $\text{COO}^-$  for the three concentrations of uranyl ions considered here (Figure 6.6). Figure 6.6 again confirms that the average number of uranyl ions adsorbed on the functionalized CNT increases with increase in the concentration of uranyl ions in the aqueous solution. Also, it is worth noticing that once the

uranyl ion gets attached to the carboxylate functional group, it seems it remains attached to it throughout the remaining simulation period. For instance in Figure 6.6a at 0.36 M uranyl ion concentration, it can be seen that the minimum number of uranyl ions adsorbed during the simulation period of 20 ns is one. It implies that one of the carboxylate ions have already been linked to the uranyl ion during the equilibrium simulation of 5 ns. Moreover, after around 0.6 ns of production run, the number of adsorbed uranyl ions remain more than or equal to two. It shows the linking of another uranyl ion to the second remaining carboxylate ion. Similarly, for the uranyl ion concentration of 0.55 M, after around 6 ns of production run, both the carboxylate ions on the CNT are linked to the uranyl ions as the minimum number of adsorbed uranyl ions is two after that. For the concentration of 0.73 M, both the carboxylate functional groups have already been linked to the uranyl ions in equilibrium simulation of 5 ns as the minimum number of adsorbed uranyl ions is two throughout the 20 ns production run.

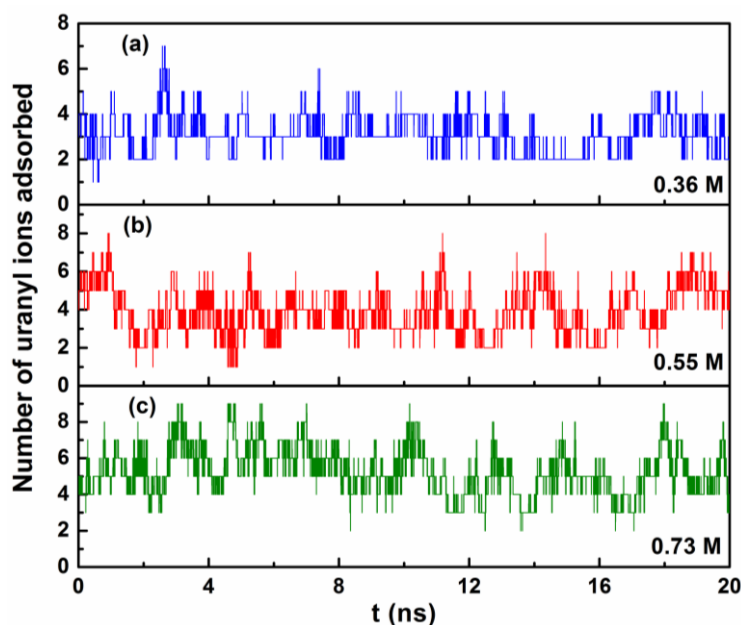


**Figure 6.6:** Number of uranyl ions adsorbed on COO<sup>-</sup> functionalized CNT as a function of simulation time for uranyl ion concentration of (a) 0.36 M, (b) 0.55 M and (c) 0.73 M.



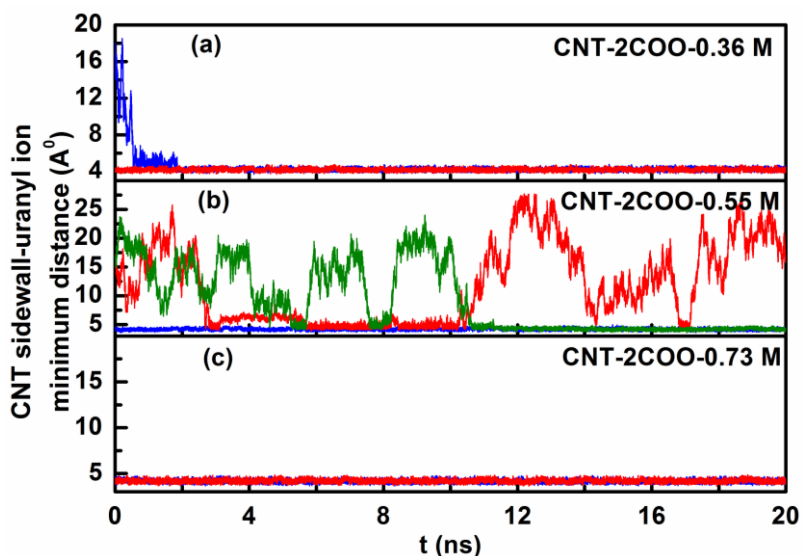


**Figure 6.7:** The minimum distance between uranyl ions and  $\text{-COO}^-$  functionalized CNT-sidewall as a function of simulation time for uranyl ion concentration of (a) 0.36 M, (b) 0.55 M and (c) 0.73 M.

These conclusions are further supported by the plots of time evolution of minimum distance between the linked uranyl ions and the CNT wall for the three concentrations (Figure 6.7). Careful observation of the plots at initial time in Figure 6.7 reveals that for uranyl ion concentrations of 0.36 M and 0.55 M, there is only one uranyl ion (red line in Figure 6.7(a) and blue line in Figure 6.7(b)) which has a distance of  $\sim 4$  Å and it remains so throughout the simulation time of 20 ns. However, another uranyl ion gets attached to the other carboxylate functional group of the CNT after around 0.6 ns and 6 ns of production run for uranyl ion concentration of 0.36 M and 0.55 M (see blue line in Figure 6.7(a) and red line in Figure 6.7(b)) respectively as indicated by the constant distance of  $\sim 4$  Å between the second uranyl ion and CNT sidewall after these time periods. Here it is interesting to note that for uranyl ion concentration of 0.55 M, there is an exchange of uranyl ion linked to one of the carboxylate functional group as shown by the increase in the distance of the CNT sidewall from the initially attached uranyl ion (red line) and reduction in the distance with another uranyl ion (green line) after around 11 ns of production run. On further analysis, it was observed that

although the second uranyl ion comes within the adsorption distance of  $10.3 \text{ \AA}$  after 6 ns of production run, but it does not get attached to the carboxylate ion. The actual linkage occurs with other uranyl ion only after around 10.5 ns of the production run (shown by green line in Figure 6.7b) and the uranyl ion continues to be attached to carboxylate ion of the CNT ever after during the period of simulation. At the uranyl concentration of 0.73 M (see Figure 6.7(c)), at initial time (after equilibration) the number of uranyl ions already linked to the carboxylate functional groups is two (red and blue lines in Figure 6.7(c)), and both these ions maintain a constant minimum distance of  $\sim 4 \text{ \AA}$  with the CNT sidewall throughout the simulation period.

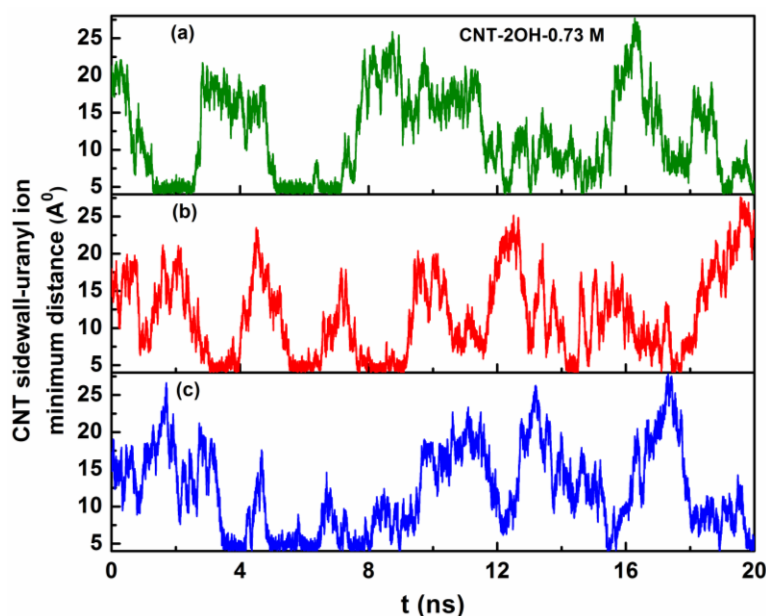


**Figure 6.8: The minimum distance between uranyl ions and –OH functionalized CNT-sidewall as a function of simulation time for three uranyl ions in a solution with uranyl ion concentration of 0.73 M.**

The bonding between the uranyl ion and functional group is not observed in case of –OH functionalized CNTs. Figure 6.8 represents the uranyl ion- CNT sidewall distances for some of the uranyl ions in case of CNTs functionalized with two –OH groups (at 0.73 M uranyl concentration). It can be seen that the uranyl ions closer to CNT-sidewall does not

remain closer for too long and it is replaced by some other uranyl ion. Similar pattern is observed in case of systems with –OH functionalized CNTs at other uranyl ion concentrations too.

### 6.3.3 Diffusion characteristics of various species in the solution

The diffusion characteristics of various species in the solution are analyzed in terms of their mean squared displacement (MSD) functions. The effect of the change in functional group on the functionalized CNT and of the change in the uranyl ion concentration in the solution on the diffusive behavior of various species is investigated. The self-diffusion coefficient ( $D$ ) of the fluid is related to the slope of the linear fitting to the MSD by Eq. 1.19 given in Chapter 1 of this thesis. The dependence of diffusion coefficient ( $D_{\text{PBC}}$ ) on the system size is incorporated by estimating the system size corrected diffusion coefficient using Eq. 1.20 of Chapter 1 where the shear viscosity value for SPC/E<sup>59</sup> water is utilized.

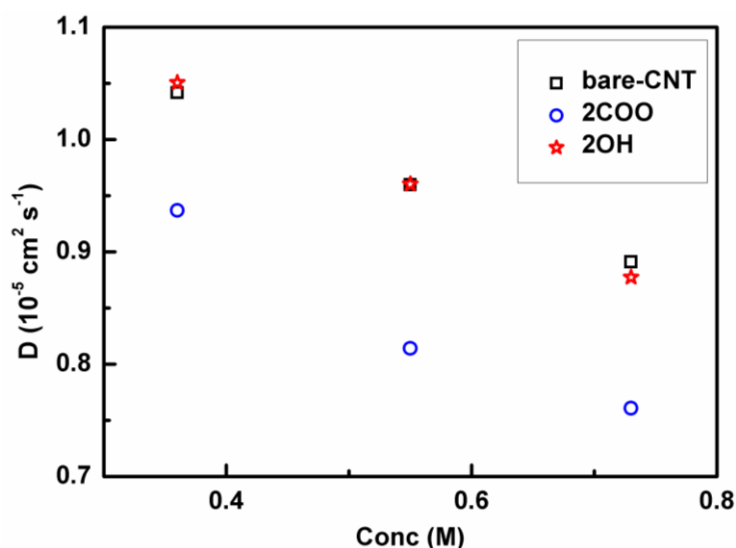


**Figure 6.9: Diffusion constants of uranium atom of uranyl ions as a function of concentration of uranyl ions in presence of bare and functionalized CNTs.**

Figure 6.9 shows the corrected diffusion coefficients of uranyl ions in aqueous solutions as a function of concentration of uranyl ions in the presence of CNT functionalized

at two carbon atoms with different functional groups. It can be seen that the diffusivity of uranyl ions in any of the systems reduces with increase in uranyl ion concentration. This observation is consistent with the results of our earlier works (Chapter 3) related to aqueous solutions of uranyl ions. Moreover, the diffusivity of uranyl ions is much reduced in the presence of CNT functionalized with  $\text{COO}^-$  functional group (blue open circles) as compared to bare CNT (black open squares) or CNT functionalized with OH functional group (red stars), however it is more or less the same for bare CNT and CNT functionalized with OH functional group. This lowering of diffusivity of the uranyl ions in presence of  $\text{COO}^-$  functionalized CNT can be attributed to some of the almost static uranyl ions that are linked directly to the  $\text{COO}^-$  group of the CNT. These results on diffusivity are consistent with more or less similar adsorption pattern for uranyl ions in the presence of bare and OH functionalized CNT which was much lower than that in the presence of  $\text{COO}^-$  functionalized CNT.

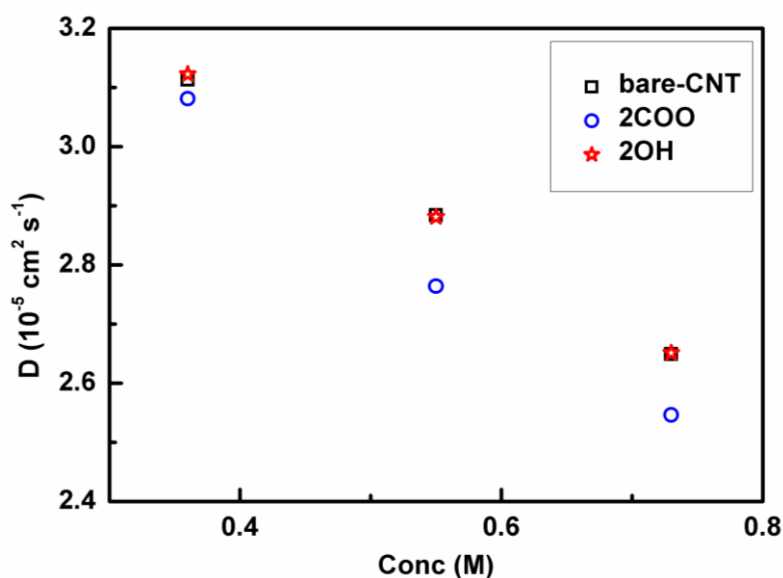


**Figure 6.10: Diffusion constants of oxygen atom of water molecules as a function of concentration of uranyl ions in presence of bare and functionalized CNTs.**

Similar pattern is observed in case of diffusion coefficients of oxygen atom of water molecules as well as nitrogen atom of the nitrate ions in the various systems studied here

(Figures 6.10 and 6.11). The order of diffusion coefficients i.e. water > nitrate > uranyl, is also consistent with that reported in Chapter 2. The comparison of trend of diffusion coefficients as discussed above and the absolute values of diffusion coefficients for SPC/E model with the reported values in Chapter 3 validates the results of this study.

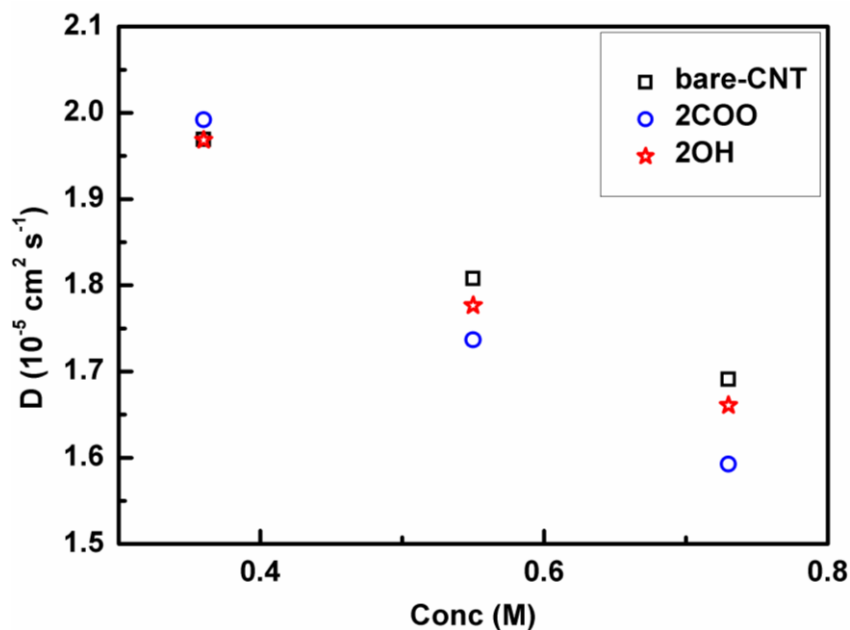


**Figure 6.11: Diffusion constants of nitrogen atom of nitrate ions as a function of concentration of uranyl ions in presence of bare and functionalized CNTs.**

## 6.4 Conclusions

In summary, behavior of aqueous solutions of uranyl ions in the presence of bare and functionalized CNTs is studied by analyzing both structural and dynamical aspects. The motive is to analyze the effect of concentration of the uranyl nitrate, functionalization of CNT, number and the nature of the functional group on the extent of adsorption of uranyl ions on the CNT. The various structural and transport characteristics of the system are studied to quantify the adsorption of uranyl ions on the CNT. The more structured arrangement of uranyl ions in the presence of carboxylate ion functionalized CNT as shown by the radial density distribution of uranyl ions around the CNT implies that the presence of carboxylate

ions on CNT favors the uranyl ion adsorption process as compared to bare CNT and CNT functionalized with hydroxyl group. The same was confirmed by calculating the amount of adsorption of uranyl ions in terms of mmol of uranyl ion adsorbed per unit mass of the CNT. The formation of a linkage between the negatively charged carboxylate ion and positively charged uranyl ion is the basis for higher adsorption of uranyl ions on the CNT. The time history of uranyl trajectories corroborate the existence of such linkage which once formed, remains for the entire simulation time of 20 ns. No such linkage was observed in case of bare CNT or CNT functionalized with hydroxyl group. Also, the adsorption of uranyl ions on CNT is found to increase with increase in uranyl ion concentration in the solution or the number of carboxylate functional groups on the CNT. The lower diffusion coefficients of uranyl ions in the presence of carboxylate ion functionalized CNT further supports the greater extent of adsorption of the uranyl ions and almost static configuration of some of the uranyl ions in this case.

## References

- (1) E. A. Vogler, *Adv. Colloid Interface Sci.*, **1998**, 74, 69.
- (2) K. Ataka, T. Yotsuyanagi and M. Osawa, *J. Phys. Chem.*, **1996**, 100, 10664.
- (3) N. Choudhury, *J. Phys. Chem. B*, **2008**, 112, 6296.
- (4) N. Choudhury and B. M. Pettitt, *J. Am. Chem. Soc.*, **2005**, 127, 3556.
- (5) N. Choudhury, *J. Chem. Phys.*, **2009**, 131, 014507.
- (6) N. Choudhury, *Chem. Phys.*, **2013**, 421, 68.
- (7) J. J. Howard, J. S. Perkyns, N. Choudhury and B. M. Pettitt, *J. Chem. Theory Comput.*, **2008**, 4, 1928.
- (8) N. Choudhury, *Chem. Phys.*, **2010**, 133, 154515.
- (9) D. Bandyopadhyay and N. Choudhury, *Chem. Phys.*, **2012**, 136, 224505.

- (10) Choudhury, *J. Phys. Chem. B*, **2007**, *111*, 10474.
- (11) N. Choudhury, *J. Chem. Phys.*, **2006**, *125*, 034502.
- (12) Y. Saito and S. Bandow, *Introduction to Carbon Nanotubes*; Corona Publishing, Tokyo, 1998. (in Japanese)
- (13) M. J. O'Connell, *Carbon Nanotubes: Properties and Applications*; CRC Press: Boca Raton, FL, 2006.
- (14) S. Iijima, *Nature*, **1991**, *354*, 56.
- (15) O. Beckstein, P. C. Biggin and M. S. P. Sansom, *J. Phys. Chem. B*, 2001, *105*, 12902.
- (16) G. C. Zuo, R. Shen, S. J. Ma, and W. L. Guo, *ACS Nano*, **2010**, *4*, 205.
- (17) J. Kofinger, G. Hummer and C. Dellago, *Proc. Natl. Acad. Sci. U.S.A.*, **2008**, *105*, 13218.
- (18) A. Alexiadis and S. Kassinos, *Chem. Rev.*, **2008**, *108*, 5014.
- (19) A. Kalra, S. Garde and G. Hummer, *Proc. Natl. Acad. Sci. U.S.A.*, **2003**, *100*, 10175.
- (20) S. Ghosh, A. K. Sood and N. Kumar, *Science*, **2003**, *299*, 1042.
- (21) R. Das, M. E. Ali, S. B. A. Hamid, S. Ramakrishna and Z. Z. Chowdhury, *Desalination*, **2014**, *336*, 97.
- (22) P. S. Goh, A. F. Ismail and B. C. Ng, *Desalination*, **2013**, *308*, 2.
- (23) S. Kar, R. C. Bindal and P. K. Tewari, *Nanotoday*, **2012**, *7*, 385.
- (24) A. T. Nasrabadi and M. Foroutan, *Desalination*, **2011**, *277*, 236.
- (25) N. W. S. Kam, M. O'Connell, J. A. Wisdom and H. Dai, *Proc. Natl. Acad. Sci. U.S.A.*, **2005**, *102*, 11600.
- (26) N. Floquet, J. P. Coulomb, N. Dufau and G. Andre, *J. Phys. Chem. B*, **2004**, *108*, 13107.
- (27) D. Y. Lu, A. Aksimentiev, A. Y. Shih, E. Cruz-Chu, P.L. Freddolino, A. Arkhipov and K. Schulten, *Phys. Biol.*, **2006**, *3*, 40.

- (28) X. Qin, Q. Yuan, Y. Zhao, S. Xie and Z. Liu, *Nano Lett.*, **2011**, *11*, 2173.
- (29) J. A. Thomas and A. J. H. McGaughey, *Nano Lett.*, **2008**, *8*, 2788.
- (30) S. Majumder, N. Choudhury and S. K. Ghosh, *J. Chem. Phys.*, **2007**, *127*, 054706.
- (31) H. Y. Yang, Z. J. Han, S. F. Yu, K. L. Pey, K. Ostrikov and R. Karnik, *Nature Commun.*, **2013**, *4*, 2220.
- (32) E. V. Hooijdonk, C. Bittencourt, R. Snyders and J. Colomer, *Beilstein J. Nanotechnol.*, **2013**, *4*, 129.
- (33) B. Corry, *Energy Environ. Sci.*, **2011**, *4*, 715.
- (34) A. K. Mishra and S. Ramaprabhu, *Desalination*, **2011**, *282*, 39.
- (35) X. Ye, S. Cui, V. de Almeida and B. Khomami, *J. Phys. Chem. B*, **2009**, *113*, 9852.
- (36) G. R. Choppin and M. K. Khankhasayev, *Chemical separation technologies and related methods of nuclear waste management: Applications, problems, and research needs*, 1st ed.; Springer: New York, 1999; p 320.
- (37) G. R. Choppin, M. K. Khankhasayev and H. S. Plendl, *Chemical separations in nuclear waste management: The state of the art and a look to the future*; Battelle Press: Columbus, OH, 2002; p 96.
- (38) A. L. Mills and W. R. Logan, *SolVent extraction chemistry*; North- Holland: Amsterdam, The Netherlands, 1967; p 322.
- (39) V. Glezakou and W. A. deJong, *J. Phys. Chem. A*, **2011**, *115*, 257.
- (40) J. A. Greathouse, R. J. O'Brien, G. Bemis and R. T. Pabalan, *J. Phys. Chem. B*, **2002**, *106*, 1646.
- (41) Robert J. Frick, Thomas S. Hofer, Andreas B. Pribil, Bernhard R. Randolph and Bernd M. Rode. *Phys. Chem. Chem. Phys.*, **2010**, *12*, 11736.
- (42) T. Nguyen, M. Duvail, A. Villard, J. J. Molina, P. Guilbaud and J. Dufrêche, *J. Chem. Phys.*, **2015**, *142*, 024501.



- (43) V. Pomogaev, S. P. Tiwari, N. Rai, G. S. Goff, W. Runde, W. F. Schneider and E. J. Maginn, *Phys. Chem. Chem. Phys.*, **2013**, *15*, 15954.
- (44) S. P. Tiwari, N. Rai and E. J. Maginn, *Phys. Chem. Chem. Phys.*, **2014**, *16*, 8060.
- (45) P. Guilbaud and G. Wipff, *J. Phys. Chem.*, **1993**, *97*, 5685.
- (46) L. Huang, Q. Shao, L. Lu, X. Lu, L. Zhang, J. Wang and S. Jiang, *Phys. Chem. Chem. Phys.*, **2006**, *8*, 3836.
- (47) A. Ansari, M. A. Mehrabian and H. Hashemipour, *Pol. J. Chem. Tech.*, **2012**, *14*, 29.
- (48) A. R. A. Dezfoli, M. A. Mehrabian and H. Hashemipour, *J. Comput. Theor. Nanosci.*, **2013**, *10*, 2411.
- (49) A. R. A. Dezfoli, M. A. Mehrabian and H. Hashemipour, *Adsorption*, **2013**, *19*, 1253.
- (50) K. Anitha, S. Namsani and J. K. Singh, *J. Phys. Chem. A*, **2015**, *119*, 8349.
- (51) A. P. Karande, G. K. Mallik, J. P. Panakkal, H. S. Kamath, V. K. Bhargava and J. N. Mathur, *J. Radioanal. Nucl. Chem.*, **2003**, *256*, 185.
- (52) NEA. *Spent Nuclear Fuel Reprocessing Flowsheet*; Nuclear Science, NEA/NSC/WPFC/DOC, Nuclear Energy Agency, Organization for Economic Co-operation and Development, 2012.
- (53) A. R. Allouche, *J. Comput. Chem.*, **2011**, *32*, 174.
- (54) L. Martínez, R. Andrade, E. G. Birgin and J. M. Martínez, *J. Comput. Chem.*, **2009**, *30*, 2157.
- (55) M. P. Allen and D. J. Tildesley, *Computer Simulation of Liquids*; Oxford University, New York, 2004.
- (56) H. J. C. Berendsen, J. R. Grigera and T. P. Straatsma, *J. Phys. Chem.*, **1987**, *91*, 6269.
- (57) W. L. Jorgensen, D. S. Maxwell and J. Tirado-Rives, *J. Am. Chem. Soc.*, **1996**, *118*, 11225.
- (58) G. Hummer, J. C. Rasaiah and J. P. Noworyta, *Nature (London)*, 2001, *414*, 188.

- (59) I. Yeh and G. Hummer, *J. Phys. Chem. B*, **2004**, *108*, 15873.

# *Chapter 7*

## **Summary and Future Directions**



## 7.1 Summary and Conclusions

The ever-growing expansion of nuclear power as a source of energy has generated a lot of interest about radiotoxic actinyl ions in the scientific community. Although actinides are very useful as fuel in the nuclear reactions, their presence in the generated waste becomes a cause of concern due to their long half-lives. Procedures are being developed to minimize the waste by extracting the reusable material from it and also to safely dispose the remaining radioactive waste. Uranium makes the fuel of the majority of the nuclear reactors operating all over the world due to fissile/fertile nature of its isotopes. During the course of this work, we have utilized molecular dynamics (MD) simulations as a tool to analyze the structural and transport characteristics of aqueous solutions of uranyl ions both at ambient and supercritical conditions and these properties are compared with those of bulk water under the respective conditions. After providing the necessary introduction to the topic and computational methodology in Chapter 1, we have simulated bulk water system under ambient conditions to get acquainted with the tool of MD simulations. Further, MD simulations are carried out for aqueous solutions of uranyl ions and the structural and transport characteristics of various species in the aqueous solutions are discussed in Chapter 2 of the thesis. A comparison of the diffusivities of uranyl ions, water and nitrate ions indicates that uranyl ions diffuse slower than nitrate ions as well as water in this order as per the sequence of their masses. The results of analysis of orientational dynamics of water molecules about their different molecular axes showed a little anisotropy among different vectors of water. Moreover, the angular distributions of water within the first coordination shell of uranium atoms have demonstrated that dipole moment vectors of water molecules are oriented along  $\text{U-O}_w$  distance vector and water molecule stays in a plane perpendicular to  $\text{O}_U\text{-U-O}_U$  line of  $\text{UO}_2$ .

Most of the studies in literature related to the uranyl ions involve only one uranyl ion in a box of water. The presence of large number of uranyl ions in aqueous solution may

perturb the tetrahedral structure of water and in effect may modify the structure and dynamics of the aqueous uranyl solution. Similarly, the temperature of the system may also affect the characteristics of the aqueous solution. Therefore, the effect of concentration of uranyl ions as well as of the temperature of the system on the structural and dynamical characteristics of water as well as uranyl and other co-ions is investigated and the results are presented in Chapter 3. With increase in uranyl ion concentration, a slight reduction in the coordination number of uranyl ion with respect to water molecules is observed. The peaks of RDFs reduce slightly with increase in temperature of the system, keeping area under the curve more or less the same. Further, the distribution of nitrate ions (negative ions present in the aqueous solution of uranyl nitrate) with respect to uranyl ions in aqueous solutions showed that the oxygen atom of water and that of nitrate ion compete with each other to occupy the first coordination shell of the uranyl ion. In case of solutions with very low uranyl ion concentration, the diffusivity of water molecules remain more or less same as that in bulk water. However, significant changes in diffusivities of ions as well as water are observed at higher concentrations of uranyl ions. The absolute values of diffusivities of uranyl ions for two different models of water (viz. TIP3P and SPC/E) were found to be quite different. However, the diffusivity values normalized with respect to corresponding water diffusivities compare fairly well with each other and with experimental as well as other theoretical results. The comparison of diffusivities of water molecules within and outside the first coordination shell of uranyl ions showed that the water within the solvation shell of uranyl ions is retarded much more than that present outside the solvation shell. However, the fraction of solvation water is too small to result in the reduction in the overall diffusivity. Thus it was concluded that the reduction in overall water diffusivity is a consequence of the long range effect of the uranyl ions on the water beyond solvation shells. Also, the rise in temperature of the system resulted in the increase in the diffusivities of the various species present in the solution. The

distributions of various angles between vectors of water and uranyl ions were observed to be independent of uranyl ion concentration, however, a slight reduction in the peak intensity values with increase in temperature is observed, angles corresponding to the peaks in the distributions being the same. Orientational mobility of water molecules about different molecular axes of water was observed to remain more or less the same whether all the water molecules in the aqueous solution or only the solvation shell water molecules are considered. However, an increase in temperature makes the relaxation of these vectors much faster.

Further, due to immense scope of supercritical fluids (SCF) for applications in the various stages of the nuclear fuel cycle, knowledge of hydration and transport properties of the actinyl ions in supercritical water generates a lot of interest. Not much literature is available on aqueous solutions of uranyl ions under supercritical conditions. Hence, the behavior of aqueous solution of uranyl ions under supercritical conditions is studied using molecular dynamics simulations and the results are discussed in Chapter 4 of the thesis. The results of this Chapter are divided into two parts: Part A and Part B. Part A deals with the analysis of infinitely dilute aqueous solutions of uranyl ions in comparison to bulk water under supercritical conditions. Part B includes the discussion on dissecting the effect of uranyl ion concentration from that of solvent density on the characteristics of the aqueous solutions of uranyl ions in supercritical water. Systems of three different water densities with varying concentration of uranyl ions were studied to analyze and compare the hydration structure and dynamical properties of different species present in aqueous solution of uranyl ions with those of bulk water. The radial distribution function of water molecules around central water molecule or the uranyl ion is found to be more ordered at low density than at higher densities. However, the coordination number of uranyl ions (or central water molecule in case of bulk water) increases with increase in the density of water or with reduction in the uranyl ion concentration. The coordination/hydration number of water is found to be higher

under supercritical conditions as compared to that under normal conditions. The angular distributions of water within the first coordination/hydration shell of uranium atoms under supercritical conditions are observed to be similar to those under ambient conditions and more or less independent of uranyl ion concentration and water density. The diffusion coefficients of uranyl ions and water molecules get reduced with the increase in density of water or the uranyl ion concentration, the percentage reduction with concentration being less for more dense solutions. The diffusion coefficient values estimated for water molecules in bulk supercritical water of different densities compare fairly well with those reported in literature from theoretical as well as experimental studies. The orientational relaxation of water molecules is found to be slower as the density of water is increased, however it is independent of change in uranyl ion concentration. The translational and rotational dynamics of the species in the aqueous solution becomes much faster under supercritical conditions as compared to those under normal conditions.

Water is known to exhibit interesting properties in the presence of interfaces. Many of the interesting phenomena originate from the mysterious interfacial waters. Hence, our main focus in this thesis was to understand the manifestation of various properties of bulk water or aqueous solutions of uranyl ions in different systems, namely (i) bulk water and aqueous solutions of uranyl ions under ambient conditions (Chapters 2 and 3) (ii) bulk water and aqueous solutions of uranyl ions under supercritical conditions (Chapter 4), and (iii) water and aqueous solutions of uranyl ions at nanoscopic interfaces. Hence, after analyzing the bulk behavior of water and aqueous solutions of uranyl ions, the behaviour of water at interface i.e. carbon nanotube (CNT) was investigated. While studying the literature related to molecular dynamics studies of water in different systems, we understood that in spite of a large number of investigations on the behavior of water in and around carbon nanotubes, many pertinent questions remain unanswered. Hence, molecular dynamic simulations are



carried out to check whether the features such as pulse-like transmission, empty-filled transition and rapid diffusion are specific only to hydrogen bonded fluid or the non-hydrogen bonded non-polar fluid can also exhibit similar properties when transported through the single-file CNT. The structure and dynamics of a polar, hydrogen bonded fluid such as water is compared with those of a non-polar (non-hydrogen bonded) fluid like methane in and around the hydrophobic CNT with chirality (6,6) and the results are presented in Chapter 5. The methane molecules were observed to form a linear chain at the centre of the CNT whereas water molecules were arranged in a zig-zag manner around the nanotube centre. With change in energy interaction parameter, the transitions between filled and empty states were observed in case of water but not in case of methane. Methane molecules were found to diffuse faster through the CNT as compared to water molecules. Higher probability of translocation for methane, lower residence time inside CNT, lower activation energy for diffusion through the nanotube and lower value of force imposed by the nanotube atoms on methane molecules as compared to those of water molecules further supported their faster transport. Interestingly, the pulse-like transmission (so called conduction burst) was observed in case of methane too, indicating that the pulse-like conduction of fluid molecules does not have any relation with the polarity or hydrogen bond forming ability of the fluid molecules. The effect of nanotube diameter on the various features of water-CNT system is also demonstrated by simulating water molecules in the presence of nanotubes of varying diameter. The distribution of water molecules inside the CNT is observed to depend upon the size characteristics of the CNT i.e. the space available for water molecules within the CNT. Moreover, considerable changes in the short timescale behaviors of velocity autocorrelation functions (VCFs) in case of different water-CNT systems were observed, indicating interesting changes in the collective vibrations of water in various environments. The power spectra as obtained from VCFs indicate that the behavior of water molecules within CNT(6,6)

deviate significantly from bulk behavior, with trend converging to bulk behavior for higher diameter CNTs. The translational movement of water molecules along the axis of the nanotube is observed to become faster and faster as the diameter of the nanotube is increased.

The modifications in the properties of fluids under nano-confinement as discussed above led us to study the behavior of aqueous solutions of uranyl ions in the presence of CNT and the results are discussed in Chapter 6. We have also simulated aqueous solutions of varying concentrations of uranyl ions in the presence of CNTs functionalized with different types such as  $\text{--COO}^-$  and  $\text{--OH}$  and different number (two, four or six) of functional groups, which may find their utility for specific applications. It was observed that the adsorption capacity of CNT gets enhanced in the presence of negatively charged carboxylate ion functional group due to its linking to positively charged uranyl ion. Due to absence of any such linkage with the uranyl ions, the adsorption capacity of bare and hydroxyl group functionalized CNT was more or less the same and much lesser than that of the carboxylate ion functionalized CNT. Moreover, the adsorption capacity shows an increasing trend with increase in the uranyl ion concentration in the solution or with increase in number of carboxylate ion functional groups on the CNT.

## 7.2 Future Scope

The work reported in this thesis provides the much needed basis related to the characteristics of solutions of uranyl ions as not much literature is available for such radioactive ions. Since the nuclear fuel cycle involves a lot of variation in system temperature as well as uranyl ion concentration in various solutions, the results of this work will help in better understanding of these systems and to use this knowledge for betterment of the various processes involved in the nuclear fuel cycle. Also, the interesting variations in the behavior of aqueous solutions of uranyl ions as we move from normal to supercritical conditions suggests

that the tuning of the conditions of the aqueous solutions may help in better implementation of new strategies in the nuclear industry. Moreover, the results related to behavior of water and uranyl ions at interfaces will provide the opening for research related to advancement of nanomembrane technologies for various applications. The key features which can be explored further include: (i) the long range effect of change in uranyl ion concentration as concluded in this thesis can be studied in detail to get an exact idea about the mechanism by which uranyl ions affect the characteristics of water molecules present in the aqueous solution. (ii) More specific experimental or computational work can be taken up to understand why the change in uranyl ion concentration has significant affect on the transport characteristics of the aqueous solutions, although structural features remain more or less un-affected. (iii) The concentrations considered in this thesis are of higher order as these are related to the back end of the nuclear fuel cycle, it will be interesting to study the characteristics of aqueous solutions of uranyl ions at much lower concentrations encountered in the groundwater system. It will help in better understanding of the migration mechanisms of uranyl ions along with groundwater which may prove useful for better management of radioactive waste in geological matrices. (iv) Due to the occurrence of pulse like transmission, both in case of polar and non-polar fluids as reported in this thesis, it will be important to analyze the exact reason of this conduction burst. (v) The thesis demonstrated the enhanced uranyl ion adsorption capacity of CNTs functionalized with carboxylate ion functional group. This observation may open a new field of studying CNTs functionalized with specific functional groups for different actinyl ions which may ultimately find application in better management of radioactive waste.